THE DYNAMICS OF MINE HOIST CATENARIES

Charles Peter Constancon

A Thesis Submitted to the Faculty of Engineering,
University of the Witwatersrand, Johannesburg, South Africa
for the Degree of Doctor of Philosophy.

Johannesburg 1993

Abstract

The dynamic analysis of catenary vibration of mine hoist ropes on South African mines is examined. This research has been preceded by studies in the mining industry, which have laid the foundation for the definition of design guidelines of hoist systems to avoid catenary vibrations or *rope whip*. These guidelines are based on a classical linear analysis of a taut string, and in essence rely on ensuring that the frequency of excitation at the winder drum due to the coiling mechanism, does not coincide with the linear transverse natural frequency of the taut catenary. Such an approach neglects the nonlinear coupling between the lateral catenary motion and the longitudinal system response. Although previous research suggested the possibility of autoparametric coupling between the catenary and vertical rope, this was not developed further on a theoretical level. The possibility of such behaviour is defined by considering the equations of motion of the coupled system.

A design methodology is developed for determining the parameters of a mine hoist system so as to avoid rope whip. The methodology accounts for the nonlinear coupling between the catenary and longitudinal system. In order to implement the proposed methodology, two phases of the analysis are developed. In the first phase the stability of the linear steady state motion is examined in the context of the nonlinear equations of motion, by applying a harmonic balance method. The stability analysis defines regions of secondary resonance, where it is shown that such regions may arise at sum and difference combinations of the linear lateral and longitudinal natural frequencies due to autoparametric excitation. Prior to this research, this phenomenon had not been appreciated in the context of the mine hoist system. A laboratory experiment was conducted to confirm the existence of these regions experimentally. In reality, the system is non-stationary since the dynamic characteristics of the system change during the winding cycle, and hence the steady state stability analysis can only describe potential regions of nonlinear interaction on a qualitative basis. The second phase of the analysis deals with a non-linear numerical simulation of the hoist system, which accounts for the non-stationary nature of the systems dynamic characteristics, and includes transient excitations induced during the wind.

The methodology developed is assessed by considering the Kloof mine rope system, where rope whip was observed. This study demonstrates that although an appreciation of the steady state system characteristics is useful, the stability analysis alone is not sufficient. It is necessary to account for the non-stationary aspects of the winding cycle if a realistic interpretation of the observed behaviour is to be achieved. To compliment this study, a motion analysis system was developed to record catenary response on an existing mine hoist installation. Such data has not been recorded before. This data provides direct evidence of the autoparametric nature of the coupled catenary/vertical rope system.

DEC ARATION BY THE CANDIDATE

I, Charles Peter Constancon, declare that this thesis is my own work, that its substance neither in whole nor part has been submitted to, or is to be submitted to, any institution other than the University of the Witwatersrand, Johannesburg.

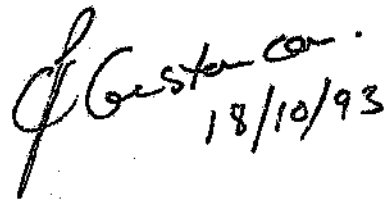

A man breaking his journey between one place and another at a third place of no name, character, population or significance, sees a unicorn cross his path and disappear. That in itself is startling, but there are precedents for mystical encounters of various kinds, or to be less extreme, a choice of persuasions to put it down to fancy; until - "My God," says a second man, "I must be dreaming, I thought I saw a unicorn." At which point a dimension is added that makes the experience as alarming as it will ever be. A third witness, you understand, adds no further dimension but only spreads it thinner, and a fourth thinner still, and the more witnesses there are the thinner it gets and the more reasonable it becomes until it is as thin as reality, the name we give to the common experience.... "Look, look!" recites the crowd. "A horse with an arrow in its forehead! It must have been mistaken for a deer."

Tom Stoppard.

ACKNOWLEDGEMENTS

Professor B W Skews, who has provided support and advice concerning the development and execution of this thesis.

Dr M E Greenway, who provided a forum for discussion concerning the direction in the thesis, as well as access to data captured by his department on Elandsrand Gold Mine.

The Chamber of Mines for the grant which provided funds for the purchase of the motion analysis equipment.

Professor C Dimitriou, who has acted as a mentor throughout my undergraduate and graduate career.

Professor E Dokumaci, who during his visit to the University in October 1990, both stimulated and provided theoretical support for the study.

D Massey, a colleague, who has consistently availed himself to lengthy discussions regarding the thesis and given unfailing encouragement and moral support throughout the thesis.

R A Backeberg, a former colleague, who has consistently availed himself to lengthy discussions regarding the thesis and given unfailing encouragement and moral support throughout the thesis.

M J Howell for the unenviable task of proof reading the script.

To family and friends for their patience and support.

Outline of the Thesis

The topic of catenary vibration or rope whip in hoisting systems on South African mines was examined in the early 70's by Dimitriou and Whillier[1973], and Mankowski, Whillier and Louw[1974]. This research resulted in the development of design guidelines for the avoidance of rope whip, based on classical taut string theory. The possibility of autoparametric response of the system was intuitively described by Dimitriou and Whillier[1973], but not formalised. Mankowski[1982] researched the forced nonlinear response of the system numerically, culminating in a Ph.D. thesis submitted to this University. His thesis examined, and alluded to, the difficulty associated with modelling nonlinear aspects of the Kloof mine hoist system, and consequently of nonlinear hyperbolic partial differential equations. Numerical results defined the forced response of the modelled system. Unfortunately, the simulation exhibited numerical instability, and a complete simulation of the winding cycle of Kloof Mine was not achieved. Nevertheless, Mankowski's contribution provided invaluable information concerning the behaviour of the mine hoist system, as well as the application of dynamic simulation techniques employing Bergeron's[1961] impedance method. However, this effort did not clarify or extend the existing design guidelines.

The current thesis intends to compliment previous research, by developing a methodology pertaining to the avoidance of catenary whip on mine hoist systems. In this regard, during the initial design phase, the nonlinear forced resonance of the system is not of primary concern. It is the definition of system parameters likely to reduce the potential for rope whip, and hence the avoidance of significant nonlinear interactions, which is of primary importance. Hence the nonlinear equations of motion of the catenary are linearised about the steady state first order solution of the system, and the stability of this motion to small disturbances is examined. The philosophy of this approach is to capture the fundamental nature of mechanisms relating to the growth of the catenary response, in such a manner that a routine approach may be employed during the design phase of a shaft head layout to avoid such regions. This approach may appear to discard the reservations apparent in recent literature regarding the study of nonlinear systems, specifically with respect to the discovery of chaotic behaviour and consequently the importance of retaining the integrity of the nonlinear nature of the system. This is particularly important in terms of the final validation of the system parameters selected, since transient excitation, as well as the non-stationary nature of the system may lead to unexpected behaviour. To address this, a numerical simulation retaining nonlinear terms as well as transient excitation was developed. The simulation is computationally intensive, and is intended to be used as the final validation of the design parameters.

In Chapter 1 of this thesis, a description and definition of the scope of the work and its context in the South African mining industry is presented. The components of the mine hoist system are examined and sources of excitation are identified. Relevant research pertaining to studies of the dynamics of the general system are reviewed. A detailed account of past research concerning catenary dynamics of mine hoist systems, and the current guideline employed for the design of a system in order to avoid catenary whip is presented.

In Chapter 2 a discussion relating to research conducted in the literature concerning the dynamics of strings and cables is presented. The purpose of this chapter is to establish a perspective on the types of nonlinear behaviour associated with taut strings and cables. These studies consider strings and cables fixed at each end. Such boundary conditions are relevant to most cable systems, where in practice the longitudinal wave speed is significantly larger than the lateral wave speed; this permits simplification of the equations of motion by neglecting the longitudinal inertia of the system, thereby introducing a quasi-static definition for the longitudinal response. This represents the point of departure between studies presented in the literature, and the mine hoist system, where due to the coupling between the catenary and vertical cable across the sheave, retention of the longitudinal system inertia is essential.

In Chapter 3 the derivation of the equations of motion of the coupled catenary and longitudinal system is presented. The equations are derived by applying Hamilton's principle. In the most general form, the equations of motion include rope curvature, axial transport velocity of the rope, and utilise a nonlinear strain definition relating the axial tension in the cable to motion in three orthogonal directions. These equations form the basis for further development.

In Chapter 4 the theoretical basis for the first phase of the proposed methodology is presented. The equations of motion developed in chapter 3 are simplified. A *datum* solution is then formulated. This solution is only valid in the absence of primary or secondary resonance conditions. The variational form of the solution is developed by substitution of this solution into the nonlinear equations of motion followed by linearisation, and normal mode orthogonalisation. This results in a set of coupled Hill type ordinary differential equations with periodic coefficients. The stability of the system is firstly examined by applying a harmonic balance method. The harmonic balance method was applied, since it is possible to prepare a general numerical code for assessing the stability of the system. Although the definition of regions of stability may be achieved in closed form, by applying a perturbation method such as multiple scales, it is likely that a number of regions may occur simultaneously, resulting in anomalous regions requiring special attention. In addition, perturbation methods require the concept of a small parameter, as well as a higher level

of skill from the designer. However, a multiple scales method is applied to substantiate the regions determined, as well as to define conditions of tuning which could lead to internal resonance. The results from a simple laboratory experiment are presented to further validate the numerical programme developed, as well as to illustrate the significance of the secondary resonance regions at an additive combination of the longitudinal and lateral natural frequency. Finally the stability analysis of the Kloof Mine rope system is presented and discussed.

Chapter 5 presents the numerical simulation developed as the second phase of the methodology. The simulation accounts for the non-stationary nature of the system, and transient excitations. These effects could not be accounted for in the steady state stability analysis. An important aspect of a numerical simulation concerns the damping mechanism applied. Experimental results relating to a definition of a damping mechanism applicable to mine hoist cables are scarce. The damping mechanism applied in the simulation is discussed and motivated. A numerical simulation of the Kloof Mine rope system is presented for both the ascending and descending wind. The results confirm the observations of Dimitriou and Whillier[1973], where severe rope whip occurred on the ascending cycle but not on the descending cycle.

Chapter 6 concludes the study, where a critical appraisal of the work is presented, and suggestions for further research are discussed.

Contents

List of Figures

List of Tables

Nomenclature

c	Longitudinal wave speed.
$\bar{c}$	Lateral wave speed.
E	Youngs Modulus.
J	Mass moment of inertia of the sheave wheel.
l_c	Catenary length.
l_v	Vertical rope length.
M	Conveyance mass.
m	Linear rope mass.
p_i	i^{th} longitudinal normal mode.
q_i	i^{th} lateral in-plane normal mode.
r_i	i^{th} lateral out-of-plane normal mode.
s	Arc length co-ordinate.
u	Longitudinal displacement in the catenary.
v	Lateral in-plane displacement.
w	Lateral out-of-plane displacement.
$\overline{u}$	Longitudinal displacement of the vertical rope.
u_1	Longitudinal displacement at the sheave.
u_2	Longitudinal skip displacement.
$\phi_i(s)$	i^{th} longitudinal mode shape of the longitudinal system.
$\Phi_i(s)$	i^{th} lateral mode shape of the catenary.
ω_i	i^{th} Longitudinal natural frequency.
$\overline{\omega}_i$	i^{th} Lateral natural frequency.

Chapter 1

Introduction

The development of the mining industry in South Africa has stimulated both technical and social change. The primary function of the industry is the extraction of mineral rich ore from natural reserves. During the early stages of development, this necessitated ore extraction from depths measurable in hundreds of meters. Currently the local gold mining industry is internationally distinguished for developing mines to depths of thousands of meters. The need for such depth has dictated the development of high speed hoisting equipment to accommodate production requirements. Due to the capital cost and stringent safety criteria defined by legislation, an active area of research concerning the technical aspects of hoisting has emerged. Research has been pursued under the auspices of The Chamber of Mines Research Organisation (COMRO), which supports research in the *Shafts* programme. Backeberg[1990] states that this programme was established to solve problems associated with access to the reef, and incorporates two main areas of investigation within conventional hoisting, namely, winding ropes and shaft steelwork/conveyances.

The *Shafts* programme can be broadly divided into four main projects which are pertinent to this study

- Winder Ropes - Factors of Safety
- Rope Degradation Mechanisms
- Shaft Steelwork Design
- Conveyances and Guide Rollers

Each of these projects are pertinent to current and future production, safety and maintenance costs associated with the hoisting process. The projects are interrelated and generally pursue one main theme: the extension of the safe operating envelope of single hoist winding systems. Naturally, benefits will be derived by systems operating at shallower depths. The rope factors project examines the extent to which the legal factor of safety can be lowered, thus easing the current depth constraint. Consequently, rope selection strategy, and the aspect of compensating the reduction in overall rope factor of safety by reducing dynamic loads through more stringent winder control, have been considered.

The *Rope Degradation Mechanism* programme examines wear and damage mechanisms related to the winding process and hence is not only concerned with the reduction rope strength, but also with extending the operating life of the rope. With regard to this programme, Chaplin[1989] has identified several deterioration mechanisms, namely plastic and frictional wear due to high contact stresses generated during coiling, followed by axial slipback during the unwinding process. Fatigue loading, due to the combined effect of fluctuating tension and bending over the sheave or underlying coil layer on the winder drum surface, is also identified as a damage mechanism. An experimental programme has been suggested to study such mechanisms and the feasibility of commissioning an experimental facility is currently being considered by the Council for Scientific and Industrial Research (CSIR).

The production constraint of deep level mining will dictate higher winding speeds. Current winding speeds of 18 m/s will be extended to 25-30 m/s. Harvey[1973] attributed the cautious approach to winding speed to *"present limitations in shaft steelwork and conveyance design"* - which *"lead to problems in conveyance oscillations"*. The *Shaft Steelwork Design* programme essentially addressed this problem. The Structural Dynamics Research Corporation (SDRC) was commissioned by COMRO[1990] to investigate the mechanism of slamming behaviour of the conveyance between the guides. Slamming occurs

when the conveyance is excited between the guides to the extent that the guide rollers become inoperative, resulting in steel to steel contact between the skip and guide. Through numerical simulation, SDRC identified significant parameters leading to slamming and hence derived design guidelines. The results of the study demonstrated that slamming is influenced by guide alignment, conveyance speed, guide length and the ratio of mid span guide stiffness to support stiffness. Although this work was carried out independently by SDRC, Tondl (see Schmidt and Tondl[1986]) investigated a similar problem for the German mining industry. Tondl showed that by incorporating rotational and translational degrees of freedom , as well as the effect of periodic guide stiffness, the coupled conveyance/guide system linearised to one with periodic coefficients. He thus concluded that the system was parametrically excited and derived approximate solutions to the stability intervals. These intervals are related to the same parameters subsequently identified by SDRC. The aspect of guide alignment, which was identified as a contributory factor to slamming, has received attention, and two devices capable of measuring alignment have been designed and developed. Since it will not be possible to guarantee perfect guide alignment, the *Conveyances and Guide Rollers* Project was initiated. This project compliments the former in that it focusses on the design of conveyances and lateral conveyance suspension systems, to accommodate and minimise dynamic loads induced by the alignment of the shaft steelwork.

It is evident that the mining industry is involved in significant research. Hoisting technology is a complex field, continually under assessment and revision. The industry employs current technology, as well as investing in international research and development. The study presented in the current thesis covers a small aspect of the global effort. It was stimulated through assessing past research carried out at the University, the aim being to refine and re-initiate research into phenomena associated with catenary dynamics, in preparation for current and future application.

1.1 The Mine Hoist System

The mine hoist system consists of a headgear, vertical shaft and winding house. The headgear is necessary to elevate the conveyance above ground level to effect the dumping of the conveyance load. Thus the design necessitates the existence of an inclined catenary passing over a sheave in the headgear to the conveyance in the vertical shaft. During the design stage, parameters such as rope diameter, sheave diameter, winder drum diameter and power are determined. It is at this critical stage that the dynamic behaviour of the overall system is addressed. Every attempt should be made to ensure that the design speed of the system and the production rate of the shaft is attainable in practice, as little can be done subsequently to correct a system for adverse dynamic behaviour.

In essence three different configurations of the hoist system exist, and are illustrated in figure 1.1.

a) A single drum hoisting system.

b) A Koepe winding system.

c) A Blair multi rope hoisting system.

The single drum winder configuration is the simplest design. It consists of a single drum, single cable and conveyance. This system is generally limited to shallower winds, or lower payloads.

The Koepe system is based on a bollard type friction principle. Each conveyance is attached between a head and tail rope. The system is counter balanced, where a differential torque is supplied by the winder to accommodate the difference in mass between the full ascending conveyance and the empty descending conveyance. No storage facility for the rope on the winder drum is required. Generally the Koepe winding system is used for shallower winds ($< 1000m$). The Koepe winding configuration is not addressed in this study. However tail whip is a consideration on these systems, and is viewed as a potential area for future research.

The Blair multi-rope winder is an extension of the single drum winder configuration, in that two ropes support the conveyance, driven by two single drum winders. The rope between the two winders is continuous, the winders are mechanically coupled, and a compensating sheave on the conveyance facilitates

equal load sharing between the two ropes. If it is assumed that the compensating sheave perfectly isolates the cables from one another, then this system could be approximated as two single drum winders.

This study addresses single drum and Blair multi-rope double drum winders. Although these basic systems differ in physical appearance, for the purpose of dynamic studies they may be reduced to, and treated as a single drum winding system. Thus the particular layout of the mine hoist system studied is in fact that of a single drum winder, where design parameters determined for this system would be readily applicable to either configuration.

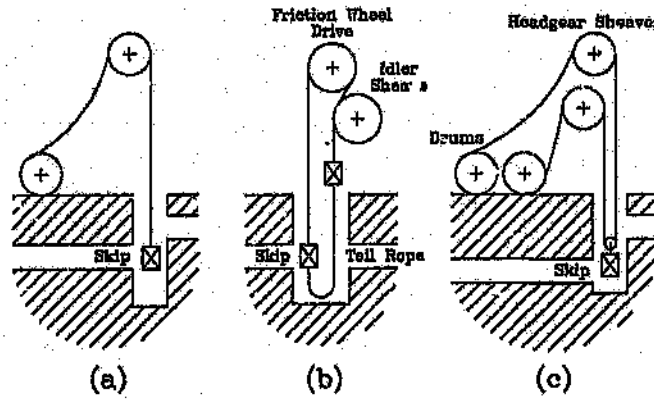

Figure 1.1: Hoisting system configurations

a) Single Drum Winder. b) Koepe Winder. c) Blair Multi-rope Winder.

1.1.1 Excitation Sources

Winder technology developed with the mining industry's need to mine to greater depths. As shaft depth increased, the cost of wire ropes increased due to a higher strength requirement. In order to maximise the life of the rope, mechanisms causing rope damage were minimised. During winding, rope damage may occur at the winder drum due to miscoiling, gaps or pull-through, which may result in crushing or even failure of the rope due to the high contact pressures developed. In order to minimise this damage, coiling mechanisms were designed to ensure a uniform controlled coiling pattern on the winder surface and on subsequent layers.

In the late 1950's, an invention by Frank Lebus (Dimitriou and Whillier [1973]) resolved these problems, and resulted in a system where controlled coiling at high speed could be achieved. This system achieved a neat multi-layer coiling pattern enabling the storage of cable on the drum without the damaging effects of miscoiling. This consisted of grooving the drum as illustrated in figure 1.2. The cross-over points on the Lebus drum are diametrically opposed, and as the cable passes through a cross-over, it is shifted one half of its diameter on one side of the drum, and one half on the other. When the cable reaches a drum flange, a filler guides the layer change, and spooling continues in the opposite direction. A cross section of the typical coiling pattern is illustrated in figure 1.3.

Previous research by Dimitriou and Whillier [1973][1] identified various excitation sources, the major excitation being that due to the coiling mechanism employed on the winder drum surface in order to achieve a uniform coiling pattern. In their analysis, it was shown that the longitudinal and lateral excitation due to the Lebus device forms the primary source of excitation to the system. The excitation is defined with reference to the co-ordinate system illustrated in figure 1.4. The x axis is parallel to the drum axis, whilst the y,z directions represent the normal and tangential co-ordinate directions of the drum surface.

Consider a rope being coiled onto the drum and taking up successive positions as illustrated in figures 1.3, 1.4.

- A pulse in the x direction occurs at each coil cross-over until a layer change, and then the direction of the pulse reverses.

[1]Other sources of excitation, neglected in this study, may arise due to ovality of the winder drum or head sheave, and shaft steelwork misalignment.

- While the cable is winding onto the drum surface. there will be no pulse in the y direction, as the cable remains at constant radius. When a layer change occurs at position 3-4, a strong y pulse occurs. Thereafter a smaller y pulse occurs at each successive coil crossover as the cable mounts over the underlying coil layer.
- A pulse in the z direction occurs at each coil crossover, as the coiling rate is momentarily increased as the cable rises over and across the Lebus surface or lower coil layer. This pulse is accentuated at a layer change.

The various pulses occurring in the rope are illustrated in relation to the rope position in figure 1.4. The frequency at which the pulses occur is directly related to the drum winding speed. Since there is a coil cross-over every half revolution of the drum, the excitation frequency is twice that of the drum rotational frequency, for a 180° Lebus sleeve.

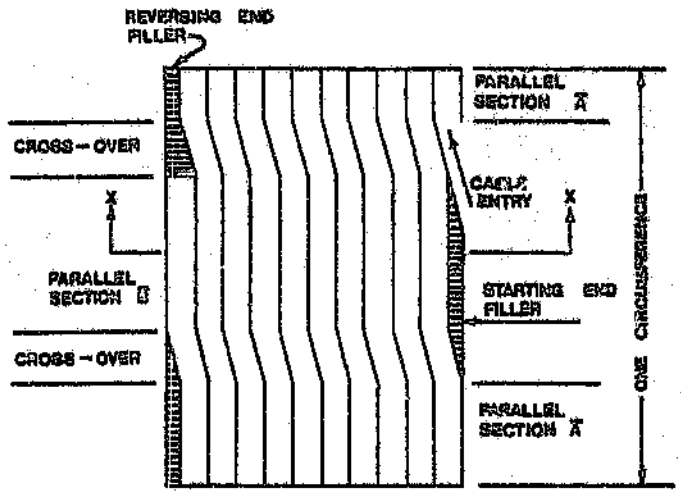

Figure 1.2: Mankowski[1982], Figure 2.4(a): Winder drum fitted with a Lebus liner

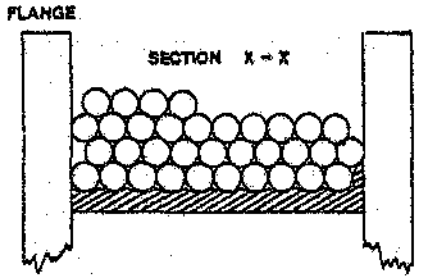

Figure 1.3: Mankowski[1982], Figure 2.4(b): Rope coiling pattern

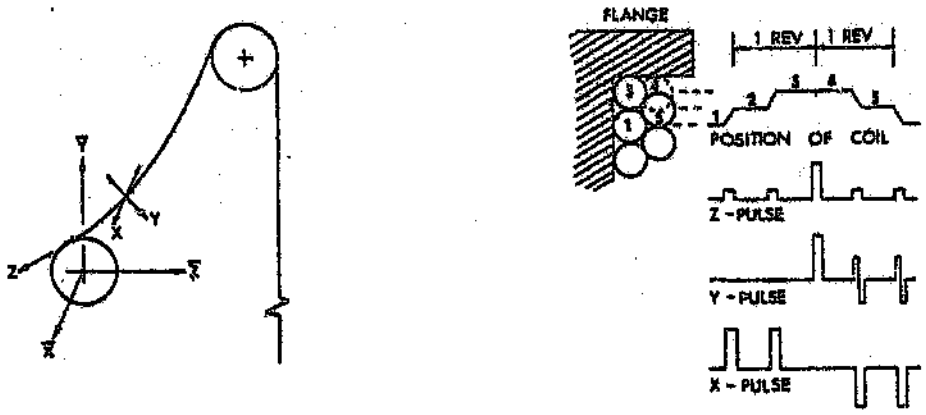

Figure 1.4: Dimitriou & Whillier[1973], Figure 8: Pulse initiation by coil cross-overs at the drum

1.2 The Study of Dynamics in the Industry

1.2.1 Longitudinal Dynamic Studies

Various aspects of hoisting technology have been examined in the past. Initially the industry was concerned with adequate rope factors of safety. This stimulated research into the longitudinal behaviour of a cable supporting an end mass under emergency braking. This aspect was first investigated by Vaughan[1903], where a lumped parameter model of the rope was employed to simulate a descending cable with a suspended mass at its end, suddenly stopped at the top support. Vaughan's [1903] analysis demonstrated that a critical depth exists, where, due to kinetic shocks, the cable is more severely stressed than that at greater depth. Perry[1906] solved a similar problem utilising the solution to the wave equation, however his analysis concentrated on the waveform and frequency of subsequent stress oscillations. These analyses assumed idealised instantaneous deceleration and thus simulated extreme loading conditions. Perry and Smith[1932] assessed the influence of mechanical breaking on winding equipment. Part of their study focused on the calculation of kinetic tension in the rope due to acceleration/deceleration or emergency breaking. They illustrated that if a ramp acceleration/deceleration profile was applied with a period equal to that of the fundamental longitudinal mode, minimum dynamic response would occur. Pollock and Alexander[1951], extended this work, refining the analysis by including higher order terms in the solution, and examining the residual response of the rope after the acceleration/deceleration had ended. Harvey and Laubscher[1965] examined the longitudinal behaviour of the hoist system, including the inertial effects of winder motor/drum and sheave, for the purpose of developing a control system capable of reducing residual response amplitudes during emergency braking. The control system developed imposed an emergency deceleration profile consisting of a ramp change until a predetermined maximum value had been obtained, holding this value constant until the end of the braking cycle. Active winder control is currently being assessed, with respect to the initial acceleration and deceleration profiles imposed during normal winding (Backeberg[1990]). This will result in lower residual response during normal operation, thus improving the fatigue life of ropes currently in use.

More recently, with the discovery of significant ore reserves between 3000-5000m levels, the aspect of rope factor of safety has been re-examined. The rationale being that a reduction in this factor may extend current hoisting technology to accommodate mining to greater depth without the use of multiple hoist systems. Naturally this would also benefit existing installations in

terms of the allowable rope life, or increased payload and production rate.

Greenway[1989] re-addressed the problem as studied by Vaughan[1903], Perry [1906], Perry and Smith[1932], Pollock and Alexander[1951], deriving a model of the longitudinal response of the rope with a suspended end mass under various acceleration/deceleration profiles. This study was primarily intended to be a parametric study to assess the influence of physical parameters on the dynamic response. By utilising a non-dimensional approach, it was demonstrated that the peak response of the upper end dynamic force, and hence the ratio of dynamic to static factor of safety, is a weak function of the ratio of rope mass to attached mass. Also, the dynamic factor of safety is a weak function of shaft depth and of rope selection strategy. The aspect of reduced dynamic response with an acceleration profile of period equal to the fundamental longitudinal mode was confirmed. This study established that scope exists for reducing the rope factor of safety, through controlled ramp acceleration and deceleration profiles. In a similar vein, Greenway[1990a] evaluated the limits of hoisting from great depth. As noted, the cost of developing main and subshaft hoist systems provides strong motivation for deep single lift winding systems. Greenway[1990a] concludes that the factor of safety of the rope, and to a lesser extent, winding speed are primary parameters influencing depth and production constraints.

The static and dynamic characteristics of wire rope has received concerted attention by Costello et al[1983]. The models developed are accordingly complex and non-linear, and are summarised by Costello[1983]. An important aspect of the rope construction is its torsional response due to axial load. Butson[1981] examined this problem in the context of deep level mining. A result of his thesis confirmed that in the case of *long* wire cables rotationally restrained at the ends, the rotational coupling can be discarded, reducing the problem to an *uncoupled* wave equation. Greenway[1990b], re-examined this problem, since triangular strand rope construction, which exhibits torsional coupling is currently utilised in the South African mining industry. Greenway's analysis included an investigation of the lay length changes which occur as a consequence of the torsional response. It was concluded that the lay length change is more strongly influenced by the total rope mass, rather than the end load. Consequently, the application of such cables to deep level mining may be problematic.

1.2.2 Coupled Dynamic Studies

In the early 70's, it was realised by the mining industry that further research concerning the dynamic behaviour of the catenary system, including both lateral as well as longitudinal behaviour was required. Dimitriou and Whillier [1973] initiated research in this direction. Their analysis concentrated on the quasi-static description of the linear transverse and longitudinal natural frequencies of the catenary and vertical cable, as a function of shaft depth. It was considered that the main source of excitation was due to periodic impulses applied to the drum end of the rope as a result of coil cross-overs. Consequently an analysis of the rope movement during coiling on to the drum was conducted, resulting in a description of pulse frequency and displacement magnitudes. They demonstrated that a 180° Lebus liner would impart even harmonics of the drum rotational frequency, whilst a single groove Lebus liner would impart all harmonics of the drum rotation frequency. Furthermore, the magnitudes of the first three harmonics of the excitation would be similar. Subsequently graphical plots consisting of the natural frequencies and excitation frequency versus shaft depth were prepared[2], as illustrated in figure 1.5. It was hoped that this information would explain the phenomenon of rope whip.

Kloof Mine in Carltonville South Africa, was experiencing rope whip, and was utilised as a case study. Figure 1.5 is based on the Kloof Mine system parameters. Catenaries A,D which were of similar length exhibited the most severe vibrations. It was observed that the rope whip was more severe with a full skip ascending than an empty skip descending. With reference to figure 1.5, severe vibration began at phase 1 during ascent, continuing up until the end of the cycle. It was observed from the frequency plots that this condition came about as a result of the coil cross-over frequency coinciding with the second lateral mode of the cable. Furthermore, the fourth longitudinal mode of the system crosses the second harmonic of the coil cross-over excitation frequency line at the start of phase 1. Hence, the frequency of the longitudinal oscillation matches the frequency of the tension fluctuations induced by the amplitude of the second lateral mode of the catenary. Thus it may be expected that longitudinal and lateral oscillations would interact, perhaps mutually exciting one another.

[2]Dimitriou and Whillier, and Mankowski employed the notation $FTCn$ for the n^{th} lateral mode of the catenary, and $FLVn$ for the n^{th} longitudinal mode of the vertical cable, where the vertical cable was treated as fixed at the sheave end. Four catenaries are represented this figure namely A-D; catenaries A,B represent the overlay winder, whilst B,D represent the underlay winder.

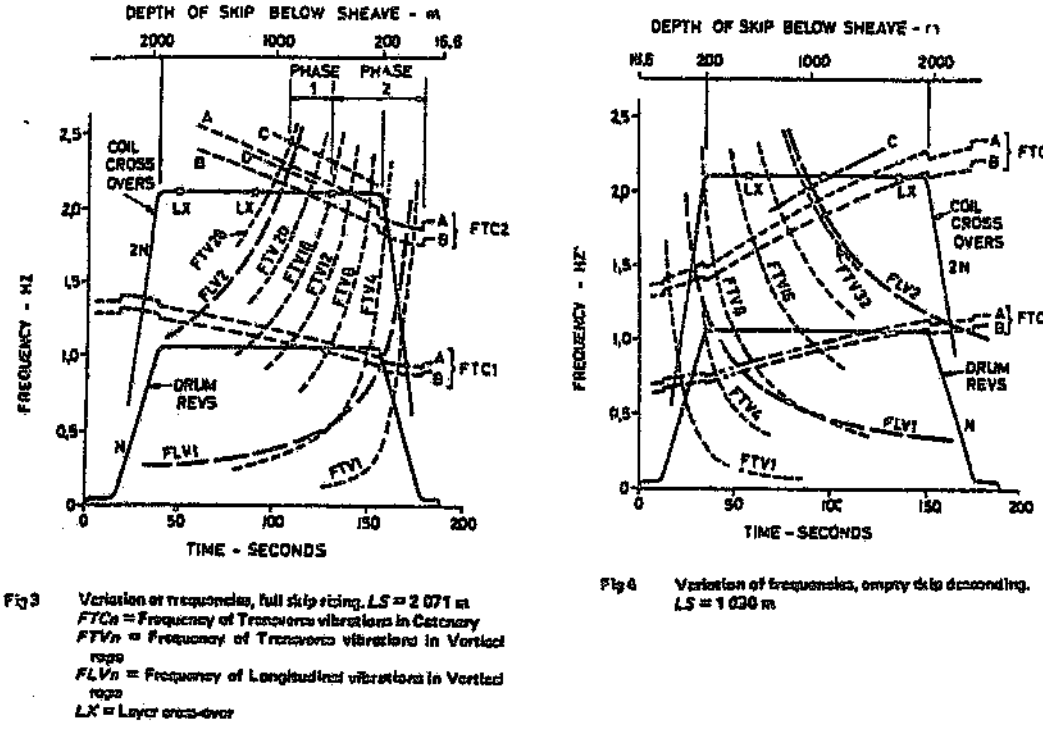

Fig 3 Variation of frequencies, full skip rising. $LS = 2\,071$ m
FTCn = Frequency of Transverse vibrations in Catenary
FTVn = Frequency of Transverse vibrations in Vertical rope
FLVn = Frequency of Longitudinal vibrations in Vertical rope
LX = Layer cross-over

Fig 4 Variation of frequencies, empty skip descending. $LS = 1\,030$ m

Figure 1.5: Dimitriou & Whillier[1973]: Linear frequency map

The catenary lengths for the Kloof underlay and overlay winders were:
$A = 74.4m,\ B = 79.6m,\ C = 69.8m,\ D = 75.3m.$

The passage to phase 2 coincides with a layer cross-over, and a significant axial pulse would be introduced to the system, promoting higher amplitudes. Observations of the lateral response of the vertical cable confirmed that amplitudes rose at the start of phase 1 and were approximately of equal wavelength to that of the catenary.

Dimitriou and Whillier [1973] were aware of the limitations of a linear analysis. This prompted a discussion on aspects of nonlinear system dynamics, providing a plausible description of the observed behaviour. In this discussion, the concept of both the jump phenomenon and of subharmonic resonance of the vertical rope was described. The latter referred to the occurrence of a lateral response of the vertical rope, at half the frequency of longitudinal harmonic tension fluctuations. It was stated that this is a natural consequence of string vibration, as lateral response is a subharmonic of tension fluctuation. This discussion led to a brief description of primary stability intervals associated with parametrically excited systems, and hence the importance of considering

the possible influence of longitudinal tension fluctuations with respect to the lateral response of the catenary and vertical rope. The observed lateral response of the vertical rope was attributed to this effect, with regard to tension fluctuations induced by the lateral motion of the catenary. The concept of mutual excitation of the catenary by the lateral response of the vertical rope, and visa versa was briefly discussed. The possibility of an amplitude dependent natural frequency relationship pertaining to the catenary was presented as one explanation for the different behaviour between the ascending and descending cycles. Although these concepts were discussed, no formal mathematical treatment was pursued, and thus the discussion led to an intuitively described relationship between the lateral natural frequency of the catenary and the longitudinal natural frequency of the vertical rope system. On reflection, these relationships in essence described the possibility of autoparametric coupling between the vertical rope and the catenary, as well as the condition of internal resonance.

Dimitriou and Whillier [1973] concluded that a more detailed study including the non-linear aspects of the system would be required to interpret the forced nonlinear response observed at Kloof Gold Mine. However, provided care was exercised during the design stage, so as to avoid the coincidence of an excitation frequency with any linear lateral natural frequency, then to some degree, later problems could possibly be reduced or avoided. This unfortunately discards the observations concerning the parametric nature of the system, and reverts to a purely linear classical approach. This approach has been adopted by the industry in simplified form. Boshoff[1977] prepared a document for The Anglo American Corporation, describing a hoist system design methodology for the avoidance of rope whip, which still stands today. This document considers only the first mode of the catenary and the first harmonic of the coil cross-over frequency, and neglects the longitudinal modes of the coupled system. Cognisance was taken of the possible effect of transient excitations which occur at the layer change, in that these may cause miscoiling problems. For this reason, the layer change location was specifically chosen not to occur simultaneously with a catenary resonance. However, since the phase of the transverse excitation changes by 180° at a layer change, the transverse excitation may be used to precipitate the build up of a resonant condition. Usually it is not possible to wind to a great depth without inducing resonance in the catenary on either the ascending or descending cycle. It was sugested that it is preferable to accept a resonant condition on the down wind as opposed to the upwind as a design strategy.

Mankowski[1982] extended the study of the the Kloof Mine system by developing a digital computer program, capable of simulating the forced response of the system. This followed the suggestion by Dimitriou and Whillier [1973] that

a comprehensive analysis was required which included nonlinear effects, as well as accounting for the coupling between the catenary and vertical rope. In this study, Mankowski[1982] investigated three different programming strategies.

Firstly, a lumped mass model of the system was employed. The model retained three translational degrees of freedom for each mass element in the catenary, whilst only considering the longitudinal motion of the vertical rope. The effect of gravity on the catenary was accounted for, as well as nonlinear geometric deformation of the cable elements. Thus the analysis was not limited to small deflection theory. The displacement function induced by the coil cross-over was simulated accurately, in the three orthogonal directions. The analysis did not account for the velocity of the cable, as this was considered a secondary effect. A simulation was performed on a system where the conveyance was close to the sheave, and the performance of the programme assessed. It was found that the formulation required substantial computational effort in order to attain accuracy and numerical stability and thus an alternative formulation based on the method of characteristics was implemented. Once again computational effort was a limiting factor, and finally a method based on Bergeron's [1961] impedance technique was employed. Expertise with the impedance method was gleaned by applying it firstly to simulate the longitudinal response of the system under harmonic excitation. Subsequently, the nonlinear lateral response of a rope with a clamped/pinned boundary condition, excited by a harmonic displacement at the clamped end, was successfully simulated. Both simulations performed satisfactorily and consequently, a final model attempting to accommodate both longitudinal and lateral behaviour was developed. In this process, the catenary was simplified to assume a parabolic shape symmetrical with respect to the span, where the axial variation in tension due to gravity was discarded. This was justified on the basis that the catenary was taut and had a sag to span ratio of less than 1:20. Only lateral response of the catenary was modelled as stated *"..each lumped mass is constrained to move in an x-y plane perpendicular to the span .."*, whilst the vertical rope was constrained to exhibit only longitudinal motion. T catenary tension was calculated on the basis of the rope stretch, and coupled to the vertical rope through an inertial balance across the sheave. The excitation at the drum was modelled as a displacement function of time, accounting for the lateral and longitudinal pulses applied to the system. The longitudinal pulse was accommodated by increasing or reducing the unstretched length of the catenary, hence directly influencing the calculation of the average tension. The axial travelling velocity was not modelled as it was considered to be unimportant, however the system parameters were varied according to the drum velocity and hence the vertical rope length, as a function of time. This model exhibited numerical difficulties in that high frequency modulations in the output occurred. As a result, a numerical damping function was employed to smooth the data.

Even though care was taken to construct the digital simulation algorithm, and detailed simulations of the lateral and longitudinal behaviour tested the robustness of each algorithm independently, the coupled system simulation became unstable at approximately 800 m during the raising cycle. *"The reason for the termination of the graphical output at 45 s, is primarily, the breakdown of the relation governing the speed of transverse disturbances in the inclined cable.... and the simulation becomes unstable"*. Thus the simulated amplitude of the inclined cable was so severe that the system approached a slack rope condition. Due to this, further discussion concerning the simulated behaviour of the coupled system was restricted to the region between shaft bottom and 800 m. Mankowski[1982] attributed the instability of the simulation to the neglect of rope slip at the sheave, *"..slip at the headsheave would occur as soon as the tension in the inclined cable drops sufficiently and that slip would prevent further reduction in tension"*.

With regard to the stability of the system, Mankowski[1982] states *"As a resonant condition is approached and the amplitudes increase, a form of auto-parametric excitation sets in with the result that growing amplitudes reinforce higher tension fluctuation and visa-versa. Taking into account the almost exponential rise in the velocity and tension amplitudes exhibited in the simulation results beyond 1000m, it is possible that auto-parametric excitation is one cause for the breakdown of the simulation model during resonance"*.

A simulation of the Kloof winding cycle was thus performed between the depths of 1300-800 m only. Mankowski[1982] discussed the results of the simulation at length. Concerning the longitudinal motion of the skip he states: *"One puzzling aspect ... is the appearance of the fourth longitudinal mode. The fourth mode appears in all the computer output ... and is seen to be present before the completion of the acceleration profile and persists until a depth of approximately 900m where it locks in on* $2 \times FTC2$ *(the second transverse mode of the catenary)"*. Mankowski[1982] detailed the dominant frequency content of the skip response versus shaft depth in figure 11.28 of his thesis[3]. This is reproduced in figure 1.6. The unshaded circles indicate the variation in the skip velocity during the simulation. The solid lines in this figure reflect the natural frequencies of the longitudinal system. These lines were calculated from a theoretical model of the longitudinal system, where the sheave inertia and skip mass were accounted for as lumped masses. The longitudinal modes are indicated in braces, where the sign indicates the relative phase between the sheave and skip motion. The dotted line indicates the relative amplitude

[3]Figures of this form were constructed by counting the cycles of the output records manually, and not by employing a Fourier analysis. Hence no indication is presented concerning the amplitudes associated with the frequency content, and in essence only the dominant modes of the wave form were extracted.

ratio between the sheave and skip, where the numerical ratios are presented on the upper ordinate of the figure. This amplitude ratio is defined as the ratio of the skip motion to the sheave motion, and hence the relative minimum at 3.75 Hz indicates a larger sheave motion than skip motion. The figure clearly indicates the presence of the fourth longitudinal mode in the simulation. Mankowski[1982] could find no plausible explanation for the persistence of the fourth longitudinal mode and states : *"... the propensity of the model to exhibit a fourth mode appears to be an inherent feature of the computer simulation model : until a precise mathematical closed-form solution to the non-linear problem can be formulated, the phenomenon remains intractable to explanation"*.

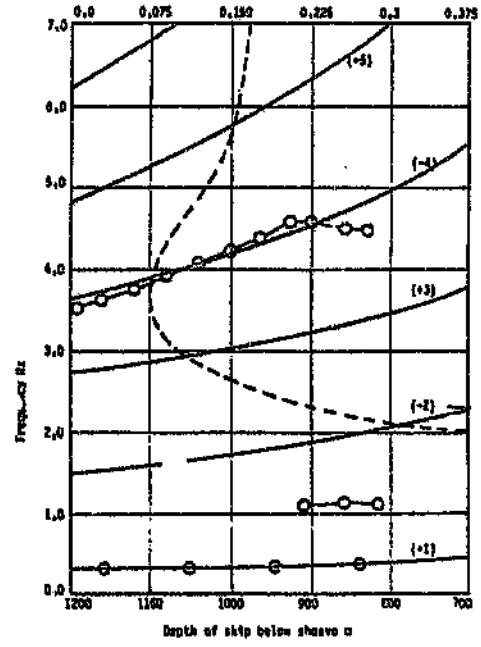

Figure 1.6: Mankowski[1982], Figure 11.28: Longitudinal frequency content of skip velocity - simulation model and theoretical modes of double mass model.

The frequency content of the response depicted in figure 1.6 was described by Mankowski[1982] as follows:

- The first longitudinal mode is excited by the acceleration profile. In practice, the first longitudinal mode may be excited by either the acceleration profile, or by the large axial pulse introduced by a layer change.

- Longitudinal response at $2 \times FTC2$ is due to the lateral response of the catenary at $FTC2$.
- The response of the skip at $FTC1$ is due to tension fluctuations in the inclined cable at frequency $FTC1$. This is associated with lateral subharmonic response of the inclined cable at frequency $\frac{1}{2}FTC1$ due to the cable rising above its equilibrium configuration.

Figure 11.29 and 11.30 of Mankowski's thesis are reproduced in figure 1.7. The first figure (figure 11.29) contains the dominant frequencies present in both the inclined cable tension and the skip velocity records from the numerical simulation. In Figure 1.7, the shaded circles serve two purposes, they indicate both the frequency of the tension variation occurring in the inclined cable and the variation in the skips velocity. The second figure (figure 11.30) presents possible excitation frequencies of the longitudinal rope, namely that at the drum revolution frequency, coil cross-over and $2\times$ coil cross-over, and the autoparametric excitation frequencies due to the transverse motion of the catenary, namely at $FTC1$, $FTC2$, $2 \times FTC2$. Mankowski[1982] attempted to describe the presence of the fourth longitudinal mode, by examining the steady state longitudinal response as a function of shaft depth, due to an excitation at these frequencies ie at $FTC1$, $FTC2$, $2 \times FTC2$. This did not prove fruitful.

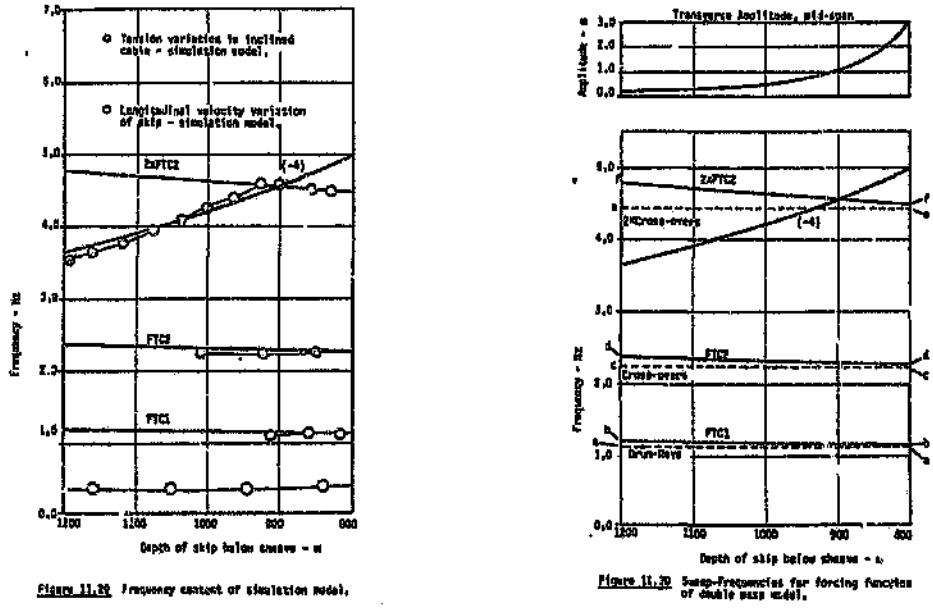

Figure 1.7: Mankowski[1982]:Frequency content of the simulation and the double mass model.

The autoparametric coupling between the catenary and vertical rope is evident in the simulation, especially in the region where the second transverse mode clearly causes longitudinal response in the vertical rope. This occurs at approximately 925m, after which the longitudinal response is dominated by the lateral response of the catenary at $2 \times FTC2$. It is interesting to note that with respect to the coupling between the longitudinal and lateral catenary motion, two conditions of internal resonance are approached whereby the longitudinal natural frequency tunes to twice the lateral frequency of the catenary. Namely at approximately 925m $FLV4 = 2 \times FTC2$, where frequency locking occurs, and towards the end of the simulation $FLV2 = 2 \times FTC1$ at 700m.

The concluding chapter of Mankowski's thesis draws attention to the correlation achieved between the simulation and observed results. Dimitriou and Whillier[1973] observed that the amplitude of lateral motion began to grow at approximately 900m. The motion settled into a clearly defined second mode, where the out of plane amplitude was largest and of the order of 1m. On occasions these vibrations continued to the end of the wind with a gradual change in mode but no perceptible change in amplitude. On other occasions severe rope whip occurred at the beginning of phase 2 (indicated in figure 1.5, at approximately 550m), following a layer change, where the in-plane amplitude reached amplitudes in excess of 2m. Mankowski's simulation predicts large am-

plitude catenary motion (greater than 1m amplitude) at approximately 900m. On this basis, it was judged that a fair correlation between the simulation and observed behaviour was achieved. Unfortunately a simulation of the descending skip was not presented. This would have been a useful validation of the simulation, as rope whip was not observed for the descending cycle.

Although the aspect of autoparametric excitation was identified as a mechanism affecting the stability of the simulation, the question as to whether this was representative of the system was left for future experimental and theoretical validation. As stated *".. until further improvements in the simulation model are made to accommodate slack tensile conditions and cable slip at the headsheave, the question of parametric excitation occurring in practice cannot be answered definitely"*.

Mankowski[1982] suggested that further experimental work was necessary to fully appreciate the complexities of the system, and to validate the digital simulation. In this regard rotational acceleration measurements of the headsheave would be essential. Experimental activity on operating shafts is limited due to production restraints. In light of this, Backeberg[198] constructed a laboratory model of the system for further experimental assessment. The model consisted of an hydraulic actuator which provided axial excitation to a wire rope passing over a sheave to a suspended end mass. Figure 1.8 illustrates the laboratory model. The purpose of this work clearly stemmed from Mankowski's thesis in that it was intended to complement the simulation through correlation with experimental observation. The configuration of the model focussed the experimental results on the parametric behaviour of the system. Unfortunately a dimensional analysis tuning the laboratory model to simulate even approximately the parameters of an actual installation was not performed. In particular, the tuning of the first longitudinal mode was substantially higher than the lateral catenary modes excited during the test. Thus any possible interaction between the longitudinal and lateral catenary modes was not marked. Nevertheless, the results indicated that a relatively small axial parametric excitation was sufficient to excite the lateral modes of the catenary. The aspect of nonlinear response, namely the jump phenomenon was observed to a degree. The headsheave was observed to rotate when large amplitude catenary motion occurred, accentuating the coupling between the the catenary and vertical rope. This illustrated that slip at the sheave could arise. The scope of the investigation did not extend to the determination of the regions of parametric stability of the system, and thus these were not identified.

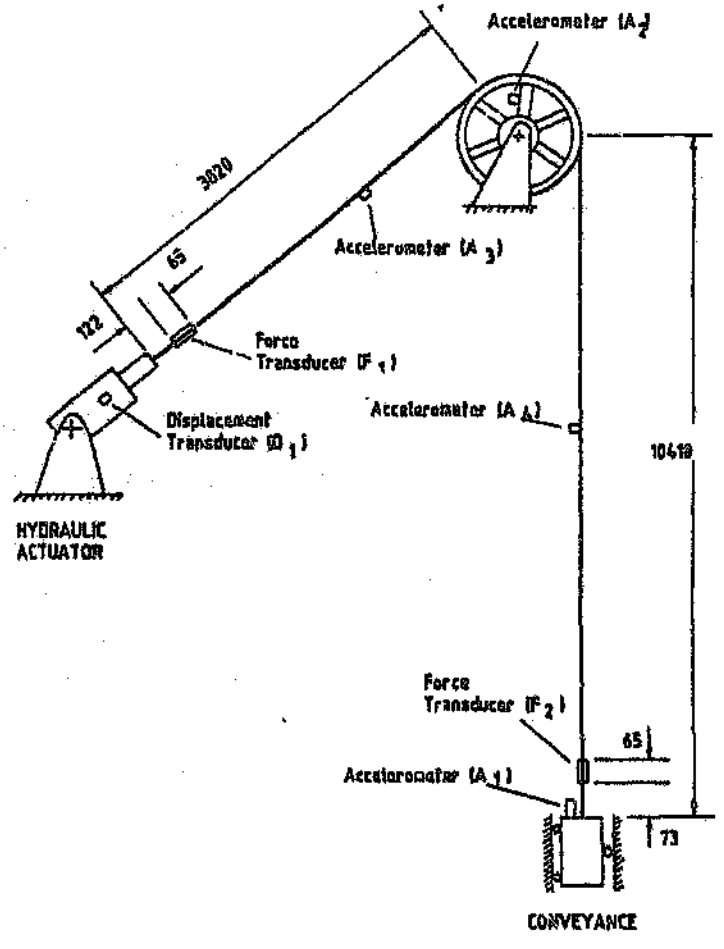

Figure 1.8: Backeberg[1984], Figure 4.1: Mine rope model

1.3 Scope for Analytical Research

As is evident from previous research, adverse catenary motion is a phenomenon which is cause for concern in the mining industry. Such motion is commonly referred to as *rope whip*. The fundamental parameters governing rope whip have not been clearly defined, and thus the dynamic integrity of hoisting systems has depended on the experience and intuition developed in the mining industry.

Mankowski[1982] identified a number of features of the hoist system which contribute to the complexity of the system behaviour. It is evident that these aspects motivated his research, and that emphasis was placed on modelling the nonlinear aspects of the system and its response numerically. Features of the system identified in the modelling process were:

- The geometrically complex nature of the cable construction.
- The inclination and sag of the catenary.
- Geometric stiffening and the associated tension variations in the catenary during large amplitude transverse motion.
- The complex boundary conditions applied to the rope at the conveyance end and at the winding drum.
- Intermediate boundary conditions at the headsheave, coupling the catenary to the vertical rope.
- Friction and slip of the cable at the headsheave.

The scope for analytical research within the context of those items identified by Mankowski[1982] is substantial. Mankowski[1982] chose to develop a digital programme modelling the effect of gravity as well as geometric stiffening, and thereby investigated the dynamic behaviour of the system.

In contrast, it is proposed here that an approach which develops the nonlinear partial differential equations of motion for the mine hoist system prior to numerical implementation, enhances the scope for describing the dynamic nature of the system. This is inferred from studies presented in the literature concerning the dynamic analyses of nonlinear taut strings and cables with pinned end conditions. These studies provide excellent paradigms for advanced studies in nonlinear dynamics. Although the techniques applied in this study are

not novel, the unique characteristics of the mine hoist system, which arise due to the boundary condition at the sheave, and hence the coupling between the lateral catenary and longitudinal system response, presents a novel extension to current knowledge regarding mine hoist catenary dynamics, and perhaps a practical vehicle for further analytical development. This aspect of the coupling between longitudinal and lateral motion in the mine hoist system necessitates the retention of the longitudinal system inertia, which is commonly neglected in analyses of taut strings and cables with pinned end conditions. Furthermore the system is excited periodically, and has a nonstationary nature due to the transport velocity necessary to complete a winding cycle. The inclination of the catenary and its curvature introduce a further dimension for study.

It is likely that a comprehensive treatment including all the former aspects will lead to a situation intractable to analysis. In this context, it is necessary to capture the fundamental nonlinear aspects of the system, which promote rope whip. The autoparametric nature of the system was identified in previous studies as a potential mechanism promoting rope whip and thus warranted further research. Although literature is available on the parametric, autoparametric and internal resonance of dynamic systems, the mine hoist system provides a vehicle for a practical investigation novel to the literature. In this regard, the system has peculiar features in that the lateral natural frequencies of the catenary and vertical rope are related to higher modes by integer multiples. Specific tuning between the lateral modes and the longitudinal system modes may result in commensurate frequency relationships. Thus it is possible for the system to exhibit regions where not only parametric response, but autoparametric as well as internal resonance occurs simultaneously in the presence of external excitation. Furthermore, since the excitation is periodic, it is possible that more than one internal resonance can be stimulated simultaneously by different harmonics of the excitation frequency. If one considers that in addition to this, the dynamic characteristics of the system are non-stationary, a recipe exists for sustained research beyond the scope of this thesis. It is proposed that these features alone justify sufficient scope for an analytical study.

1.4 Scope of the Study

The autoparametric behaviour of the mine hoist system has been addressed superficially in previous research, thus this aspect of the system behaviour forms the initial focus of the study. The linear stability of the stationary system is governed by the relationship between parametric and autoparametrically induced excitation frequencies, and the tuning of the natural frequencies of the system. It is the definition of such relationships which is considered central to developing an understanding of the potential effect of adverse tuning conditions on the system response. In order to account for transient excitations and the nonstationary nature of the dynamic characteristics of the system, a nonlinear numerical simulation of the system is developed. The specific aims of the thesis are thus:

- The development of the non-linear equations of motion of the mine hoist system.
- The investigation of the autoparametric nature of the system, leading to the definition of the steady state stability of the first order response of the system.
- The development of a numerical simulation of the system which accounts for transient excitation and the non-stationary nature of the system.
- The development of a design methodology for selecting the mine hoist parameters so as to avoid rope whip.

In conclusion, the goal of the research involves proposing a strategy for selecting the system parameters so as to avoid rope whip. Conversely, this is viewed as ascertaining the hoist system dynamic characteristics which contribute to the onset of rope whip. Although the description of the large amplitude response occurring during rope whip is of secondary importance when compared to the definition of the system characteristics required to avoid rope whip, this is a necessary aspect of the study and is addressed through the development of a numerical simulation in the later part of the thesis. This gives further insight into the behaviour of existing systems exhibiting rope whip, leading to design strategies concerning the influence of transient excitation on the overall system behaviour.

Chapter 2

The Dynamics of Strings and Cables

2.1 Introduction

Cables are utilised as structural elements in many situations, a few being ship mooring cables, guy towers, suspension bridges, overhead power lines, and hoisting equipment. The specific configuration of the cable may permit a linear approximation of its behaviour, however in general, a cable exhibits nonlinear behaviour; the degree of nonlinearity being dependent on the configuration and loading to which the cable is subjected. The analysis of dynamic systems can be similarly divided into studies where a linear or a nonlinear approach is adopted. The latter may be imperative for an understanding of the phenomena associated with the observed behaviour. Prior to pursuing a particular analysis strategy with respect to the mine hoist system, it is necessary to examine the broader aspects of the possible behaviour of strings and cables.

Although this thesis is concerned with the dynamic aspects of cables, it is pertinent to briefly consider the static response of a suspended cable. This will provide an insight into the possible nonlinear nature of the problem, as well as facilitating a description of the terminology employed. Thereafter, a brief development of the linear dynamic theory, leading to nonlinear dynamic studies of cables and strings is presented.

2.2 Static Response of Cables

Irvine and Sinclair[1976], present a static analysis of an elastic cable for an arbitrary sag to span ratio, subjected to vertical point loads. Pugsley[1983] presented a review of an analysis by Pipard and Chitty, which considers an approximate method for a shallow sag cable subjected to vertical point loads. The method reduces to that presented by Irvine[1981] for shallow sag cables, which is briefly described below.

As stated by Irvine[1981], the word *catenary* derives from the Latin word for chain, meaning the profile of a chain hanging between two points, under its self weight. The mathematical description of this profile is obtained by solving the differential equations of equilibrium associated with a differential element of the chain. Figure 2.1 illustrates a cable supported at equal height, with initial sag due to its self weight. A free body diagram of a differential element of the cable is presented in the lower part of the figure . The span of the cable is defined as the chord length between the supports, whilst the sag represents the displacement of the profile from the chord. A Lagrangian co-ordinate s is employed, and is aligned along the arc length or equilibrium profile of the cable. In the theoretical development which follows, it is assumed that the element supports tensile loads only, and that the flexural rigidity is zero.

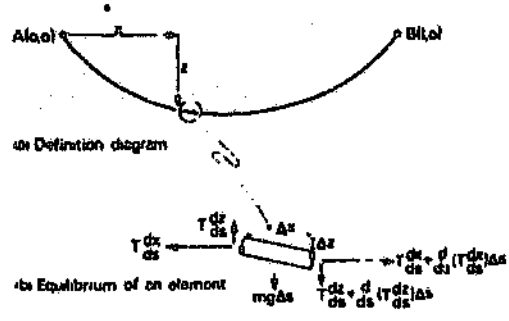

Figure 2.1: Irvine (1981): Equilibrium of an element of cable

On application of a force balance to the differential element in figure 2.1, the equations of equilibrium are obtained as :

$$\frac{d}{ds}(T\frac{dz}{ds}) = -mg$$

$$\frac{d}{ds}(T\frac{dx}{ds}) = 0$$

Where T, m refer to the tension and mass per unit length of the cable respectively. Integration of the second equation, and solving for the integration coefficient yields:

$$T\frac{dx}{ds} = H$$

Where H represents the horizontal component of the tension at the supports. Since no horizontal loads are applied to the cable, H is constant everywhere. The above equations may be manipulated into the form:

$$H(\frac{d^2z}{dx^2}) = -mg\frac{ds}{dx}$$

Under the condition of inextensiblity, $(\frac{dx}{ds})^2 + (\frac{dz}{ds})^2 = 1$, the above equation yields:

$$H\frac{d^2z}{dx^2} = -mg[1 + (\frac{dz}{dx})^2]^{\frac{1}{2}} \qquad (2.1,$$

Solving this equation, subject to the boundary conditions, results in the mathematical description of the profile as a function of the span x:

$$z(x) = \frac{H}{mg}[cosh(\frac{mgl}{2H}) - cosh\frac{mg}{2H}(\frac{l}{2} - x)]$$

Although this represents the correct solution for the profile of an inextensible cable, supported at equal elevation under its self weight, significant simplifications may be made when the cable is taut, and its sag to span ratio is small.

Although Irvine [1981] advises that such an analysis is appropriate for sag to span ratios less than 1:8, Pugsley [1983] states that the results should be applicable with considerable accuracy to cables with larger sag to span ratios.

In the case where the sag to span ratio is small, $\frac{ds}{dx} \approx 1$, the cable equation (2.1) reduces to:

$$H\frac{d^2z}{dx^2} = -mg$$

$$\mathbf{z} = \frac{\mathbf{x}}{2}(1-\mathbf{x})$$

Where $\mathbf{z} = \frac{z}{mgl^2/H}$ and $\mathbf{x} = \frac{x}{l}$. It is evident that the profile is symmetric[1] with respect to the mid-plane of the span line. The sag to span ratio δ is defined as the ratio of the cable sag at mid span, to the span length:

$$\delta = \frac{mgl}{8H}$$

Thus far, the equilibrium profile of a cable due to its self weight has been considered. The analysis can be generalised to include the case of concentrated point loads, however, in preparation for the discussion of the dynamic behaviour of a sagged cable, consideration of the mechanism by which the cable supports additional load through deformation from its equilibrium profile is pertinent. Simply stated, additional tension may be generated in the cable to first order through geometric adjustment of the profile, and to second order through stretch. Both mechanisms contribute to the nonlinear response of a sagged cable. The first mechanism dominates the response of a deep sag cable, where the axial stiffness of the cable is much greater than the geometric catenary stiffness, and thus inextensible cable behaviour dominates the response. The latter mechanism dominates the load deflection response when the cable is taut, and additional tension is generated through axial cable strain. These mechanisms may be investigated by formulating the additional tension generated in the cable when its profile changes from its equilibrium condition, under the action of external load. This load may be a consequence of direct static forces, or inertia forces. The problem is considered below.

[1]Irvine[1981] extends this analysis to include the case of an inclined cable under its self weight, and demonstrates that an approximate profile may be obtained. This profile is no longer symmetric with respect to the span or the mid point of the chord joining the supports.

Consider a cable in equilibrium, where its profile due to self weight is z. If the cable is loaded further, additional deflection w occurs. The deflection w, induces additional tension τ in the cable, and the profile changes to $z + w$. Employing a Lagrangian strain measure, it can be shown that the additional tension generated is related to the displacement of the element through Hooke's Law, and is given as:

$$\frac{\tau}{EA} = \epsilon = \frac{du}{ds}(\frac{dx}{ds}) + \frac{dz}{ds}(\frac{dw}{ds}) + \frac{1}{2}(\frac{dw}{ds})^2$$

Where u, z, w represent the longitudinal displacement, the equilibrium profile, and the additional vertical displacement induced by the load respectively.

Since the [illegible] component of the additional tension generated during the de[illegible] [illegible] tra[illegible] $h = \tau\frac{ds}{dx}$, the previous equation may be manipulated

$$\frac{h(\frac{ds}{dx})^3}{EA} = \frac{du}{dx} + \frac{dz}{dx}\frac{dw}{dx} + \frac{1}{2}(\frac{dw}{dx})^2$$

In the absence of longitudinal loads, h is constant, and this equation may be integrated with respect to x to obtain[2]:

$$\frac{hL_e}{EA} = u(l) - u(0) + \frac{mg}{H}\int_0^l w dx + \int_0^l \frac{1}{2}(\frac{dw}{dx})^2 dx \qquad (2.2)$$

Important observations may be made regarding the form of equation (2.2). Firstly, the cable may be influenced by the support movement, in which case $u(0), u(l)$ would not necessarily be zero. Secondly, it is influenced by the final cable profile via the term $\int_0^l w dx$. It is important to note that this term will be zero if an antisymmetric change w in the profile occurs. The third term $\int_0^l \frac{1}{2}(\frac{\partial w}{\partial x})^2 dx$ is a measure of the change in arc length of the cable, and is thus a second order effect due to cable stretch. The dominance of these two terms is related to the cable parameter λ^2. The derivation and discussion of the cable parameter will be considered further in the section regarding the dynamics of sagged cables.

[2] Where $L_e = \int_0^l (\frac{ds}{dx})^3 dx \approx l(1 + 8\delta^2)$, and w, z vanish at the limits of the integration, and the relationship $\frac{d^2z}{dx^2} = -\frac{mg}{H}$ has been employed in the reduction.

2.3 Dynamics of Strings and Cables

The development of the wave equation for a taut flat string is associated with many of the eminent personalities in the historical development of dynamics and mathematical physics. Lindsay traced the historical development of the subject in the introduction to the second revised edition of Rayleigh's "The Theory of Sound" [1945], where it is evident that numerous people have applied themselves to the study of string dynamics, for instance Pythagoras, Galileo Galilei, Hooke, Taylor, Bernoulli, D'Alembert, Euler and Lagrange. These analyses resulted in the wave equation, which is commonly presented in the literature as representative of a taut flat string undergoing small amplitude longitudinal or lateral motion. This equation may be derived on application of Newton's Second Law of motion to a differential element of the string. If small amplitude motion is assumed such that only first order terms are retained, then the equations of motion describing the longitudinal and lateral motion of the string decouple and are given as:

$$\frac{\partial^2 w}{\partial t^2} = c_t^2 \frac{\partial^2 w}{\partial x^2}$$

$$\frac{\partial^2 u}{\partial t^2} = c_l^2 \frac{\partial^2 u}{\partial x^2}$$

$$c_t = \sqrt{\frac{T}{\rho A}}$$

$$c_l = \sqrt{\frac{E}{\rho}}$$

$$\frac{c_l}{c_t} = \sqrt{EA/T}$$

where c_t, c_l represent the lateral and longitudinal wave propagation speeds respectively, and w and u represent the lateral and longitudinal displacements respectively.

Note that T/EA is the longitudinal strain under the initial tension T, and in typical applications with steel cables, this value is small, thus the ratio

$c_t/c_l << 1$, and the longitudinal disturbances have a significantly higher propagation speed than the transverse disturbances. For a fixed length of string, the propagation speed of the longitudinal disturbance is thus sufficiently high compared to that of the lateral propagation speed to view the tension as being spatially uniform along the length of the string (Oplinger[1960]). This leads to the concept of spatially uniform but temporally variable tension. Although, when the string satisfies this condition, a state of constant tension may exist along the length of the string, additional tension change may occur during the motion due to changes in the arc length of the string. Accounting for the variation of tension due to the stretch of the string leads to the nonlinear description of the taut flat string. Thus this approach accentuates the nonlinear behaviour of a string where the catenary approaches that of a flat profile. On the other hand, the nonlinearity may be introduced via initial curvature, in which case the string is commonly referred to as a cable. In this case, additional tension may be generated during the motion due to geometric changes in the unstretched profile of the cable. In combination, these effects define the nonlinear nature of cable dynamics, and in the special case where the curvature approaches zero, and the amplitude of vibration is small, the wave equations evolve. A brief discussion outlining the salient features of string and cable dynamics follows. In this discussion, a string is defined as the limiting configuration of a cable, where the curvature is by definition zero.

2.4 Taut String Analyses

2.4.1 Nonlinear Taut String Analyses

Carrier[1945] investigated the nonlinear frequency response of a stretched string. In this analysis, the equations of motion accounted for both longitudinal and lateral inertia. A solution for the in-plane motion of the string due to an initial in-plane sinusoidal deformation was obtained by applying a perturbation method. This analysis indicated that to first order in the perturbation, the nonlinearity induces a stiffening response with increasing lateral amplitude. The nonlinear period is thus amplitude dependent, and decreases with respect to the linear period, as the lateral amplitude of motion increases. Carrier [1945] also considered the coupled out-of-plane problem, and the condition whereby the string describes a quasi-elliptic orbit. Oplinger[1960] investigated the in-plane frequency response of a nonlinear taut string, and derived equations of motion on the basis of spatially uniform but temporarily variable tension. Thus longitudinal inertia was not regarded as significant in his solution. The nonlinear nature of the system was introduced by relating the change in arc length due to the amplitude of the motion, to the additional tension generated via Hooke's Law. Application of the method of variable separation resulted in trigonometric functions for the spatial domain, and periodic elliptic functions for the temporal domain. This analysis confirmed the presence of the jump phenomenon, as well as a frequency-amplitude relationship common to nonlinear systems. Experimental correlation was achieved by constraining the string to planar motion, confirming the validity of the analysis and of the hypothesis of temporally variable but spatially uniform tension. The analysis however did not include the case of nonplanar or whirling motion. Murthy and Ramakrishna[1965], and Miles[1965] examined the nonplanar motion of the nonlinear stretched string. Murthy and Ramakrishna[1965] derived their equations by formulating the potential and kinetic energies of the system and applying Hamilton's principle. Their analysis neglected the longitudinal motion and hence longitudinal inertia, resulting in equations defining the nonlinear motion of a string where all particles of the string were constrained to move in planes perpendicular to the equilibrium chord. Although the equations provided nonlinear terms coupling the in- and out-of-plane motion, which provided a plausible mechanism describing the transition from planar to nonplanar motion, the equations developed were inconsistent with regard to the longitudinal response of the string. Anand[1966] adopted the equations defined by Murthy and Ramakrishna[1965], including a viscous damping term, and extending their analysis to examine the nonlinear forced response of the string in the presence of damping. Anand's[1966] analysis examined both the in- and

out-of-plane response of the string resulting from an in-plane distributed driving force, and it was demonstrated that the stability of the planar motion, and the occurrence of the jump phenomenon was a function of the magnitude of the driving force and the degree of damping. The analysis also demonstrated that under constant damping action and excitation, the degree of *non-linearity* was described by a dimensionless parameter $\eta = (nc_l/c_t)^2$, where c_l, c_t, n refer to the longitudinal wave speed, the lateral wave speed and the mode number respectively. Since the longitudinal wave speed is fixed by the material properties, whilst the lateral wave speed is dependent on the initial tension, η is directly proportional to the square of the mode number, and inversely proportional to the initial tension. Thus a decrease in the initial tension accentuates the nonlinear behaviour. This parameter is related to the ratio of the peak additional tension generated during an oscillation, τ_p, to the equilibrium tension in the string, which directly effects the nonlinear natural period, as demonstrated by Carrier [1945]. Although this parameter may be reduced by increasing the initial tension, the neglect of the possibility of modal interaction between the longitudinal and lateral modes limits the degree to which such an approach would apply without invalidating the premise of the analysis. Anand[1969a] rederived the equations of motion, whilst examining the free response of a damped nonlinear string, due to sinusoidal initial conditions, showing that in general coupling exists between the longitudinal and transverse modes. This coupling was not accounted for in the previous analyses of Oplinger [1960], Murthy and Ramakrishna [1965] and Miles[1965]. Anand [1969a] showed that by neglecting the inertia term in the longitudinal equation of motion, a static compatibility relationship between the longitudinal and lateral response could be determined. Inclusion of this relationship in the transverse equations of motion, resulted in transverse equations of motion identical to those employed by Oplinger [1960]. Thus although the equations of motion developed by Murthy and Ramakrishna[1965] qualitatively described experimentally observed behaviour, Anand[1969a] showed these to be incorrect, and thereby confirmed the consistency of the equations formulated by Oplinger[1960] which were based on the concept of spatially uniform but temporally variable tension. Although Anand [1969a] did not employ this concept in deriving his equations of motion, it was effectively introduced by neglecting the longitudinal inertia term. Specifically, Anand's [1969a] approximation requires that the longitudinal natural frequency of the string be much higher than the lateral natural frequency and the frequency of excitation. Thus modal interaction between the longitudinal and lateral modes could be neglected. Anand[1969a] showed that with regard to the decay of the free response of the nonlinear damped string with nonplanar initial conditions, the nonlinearity and coupling between the equations of motion induces an oscillatory energy transfer between the two planes of vibration, which results in the string describing an elliptic orbit, where the axes precess during the free decay. Anand[1969b] pursued this analysis further

by investigating the stability of damped forced and undamped free vibrations of the nonlinear stretched string. This was accomplished by examining the stability of the variational form of the in-plane and out-of-plane equations of motion. In the variational form, these equations reduce to coupled Hill-type equations, and the stability map was constructed by considering the roots of the characteristic equation. This analysis confirmed experimental observations, in that the in-plane oscillation becomes unstable in particular regions of the parameter space, resulting in non-planar motion. Thus the analysis demonstrated the potential complexity of the response of the non-linear taut string. Anand[1969b] also proved that in the case of free undamped vibration, planar motion is unstable and circular motion results, whilst planar motion is stable in the presence of damping. Eller[1972] provided experimental validation to Anand's [1969b] theoretical predictions. Gough[1984] related the perturbation in the orbital angular frequency and the frequency of precession of the orbital motion during free vibration decay of a nonlinear damped string to the mean square radius and area of the orbital motion respectively. The planar and nonplanar motion of a taut string due to in-plane excitation is well summarised by Nafeh and Mook[1983]. Their discussion details the locus of the in-plane and out-of-plane response amplitudes due to a constant excitation level and variable frequency, and with respect to a variable excitation amplitude at a frequency close to the in-plane natural frequency. Legge and Fletcher[1984] compare the free response of a taut string between rigid supports with that observed when one support has a mechanical impedance associated with it. They show that due to the mechanical impedance, and the nonlinear coupling between the modes, response occurs in modes not normally excited by the initial disturbance. Watzky[1992] derives the equations of motion for the large amplitude response of a stiff elastic stretched string, where both bending stiffness and torsional coupling are included. Although this study appears to be motivated primarily for assessing the vibration of musical instruments, the concept of torsional coupling is certainly relevant to mine hoist ropes. Whereas in Watzky's derivation, torsional coupling is introduced as a consequence of material torsion, in the context of mine hoist ropes, torsional response is a consequence of rope construction, where coupling exists between longitudinal and torsional motion. Such coupling has been examined by Butson[1981], Greenway[1990b] in the context of linear longitudinal models only, and provides an interesting incentive for examining the nonlinear lateral motion of such a rope.

Tagata[1977, 1983] examined the lateral nonlinear response of a taut string subjected to a longitudinal parametric excitation. This study was preceded by Lubkin and Stoker[1943] who considered the conditions governing the linear stability of a taut string to a longitudinal excitation, Tagata's[1977, 1983] analysis examined the nonlinear large amplitude response due to an axial exci-

tation, for the first, second and third parametric instability regions of the first lateral mode.

In summary, the previous studies considered the nonlinear response of a taut string of fixed length, where longitudinal inertia is not dominant, and the lateral motion of the string is consequently governed by an equation of motion having the general form:

$$w_{tt} + 2Rw_t - (c_t^2 - \frac{c_l^2}{2l}\int_0^l (v_x^2 + w_x^2)dx)w_{xx} = f \tag{2.3}$$

where v, w represent the motion of the string orthogonal to its axis, and R represents the damping action. This equation has become synonymous with the nonlinear dynamic response of a taut string. The integral term represents the change in arc length of the string, and accounts for the nonlinear stiffening/amplitude dependence of the dynamic characteristics.

2.4.2 Travelling Taut Strings

The analysis of travelling strings initially addressed processes in the textile and related industries. According to Sack[1954], Skutsch[1897] first investigated the linear transverse vibration of axially travelling strings. Sack [1954] presented a linear analysis of the lateral response of a travelling string subjected to a lateral excitation at one support. This analysis demonstrates that the natural frequency of a travelling string decreases with increasing transport velocity, and that the related mode shapes are complex, representative of travelling waves as opposed to the real normal modes associated with stationary strings. This behaviour is attributed to the gyroscopic or Coriolis term associated with a travelling medium. The equation of motion of a travelling string undergoing small amplitude lateral motion is commonly referred to as the *threadline* equation and is given as:

$$\frac{\partial^2 w}{\partial t^2} + 2V_a\frac{\partial^2 w}{\partial t \partial x} + (V_a^2 - c_t^2)\frac{\partial^2 w}{\partial x^2} = 0 \tag{2.4}$$

The ratio of the first linear natural frequency of a string travelling axially at velocity V_a to that of a stationary string is shown to be $1 - (V_a/c_t)^2$. In hoisting applications on South African mines, $(V_a/c_t) \approx 0.14 - 0.075$, thus the

error induced by neglecting the axial velocity would be of the order of 2%.[3] Mote[1966b] presented a nonlinear analysis of a flat axially moving string. This analysis indicated that in the presence of axial velocity, the nonlinear stretch behaviour of the string can contribute significantly to changes in the fundamental period. Mote [1966b] varied the parameters of a string undergoing periodic motion with an amplitude equivalent to $\frac{1}{2}$% of it's span. The results generated by Mote[1966b] are illustrated in figure 2.2, where $\beta = V_a/c_t$, $w_{max} = v/l$ and v represents the midspan deflection, P represents the initial tension, and $\tau = 2/(1-\beta^2)$ represents the nondimensional period of the fundamental. The shaded region represents cable parameters employed on South African mines. Although this result may be valid in the case of a travelling string, axially restrained to maintain a constant unstretched length of string between the supports, is not directly applicable to the mine hoist system as the sheave end does not fulfill such a restraint. However the result is of interest as it emphasises the differing mechanisms governing the system response.

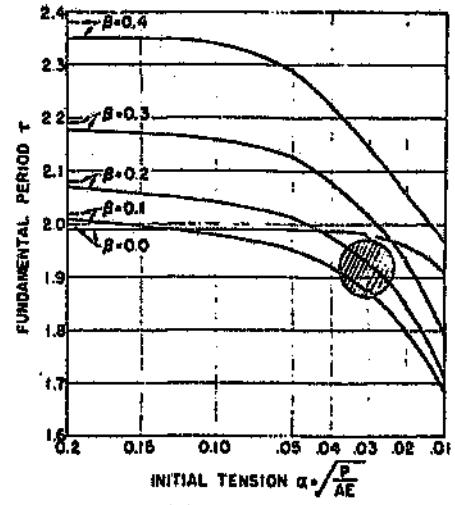

Fig. 1 Fundamental period of oscillation for $w_{max} = 0.005$ as a function of nondimensional initial tension α. (Period predicted by linear theory is indicated by a tick on the ordinate at the particular string velocity β.)

Figure 2.2: Mote (1966): Nonlinear fundamental period of an axially translating string

[3]This prompted Mankowski [1982] to discard axial velocity in his simulation of the mine hoist system.

Kim and Taborrok[1972] presented a derivation of the nonlinear equations of motion of a travelling string by considering the momentum and continuity equations of the string, as well as a mass tension constitutive law. The equations were solved by employing the method of characteristics, and applied to simulate the response of a taut flat travelling string, plucked at its mid span. Shih[1971, 1975] examined the three dimensional nature of the equations developed by Ames et al [1968], examining the phenomenon of elliptic ballooning, which is associated with a moving string under boundary excitation, where the major axis of the elliptic envelope is aligned with the direction of the excitation. It was proved that circular ballooning was unstable, a result observed experimentally by Ames et al[1968], where the motion became unstable once a circular envelope was approached, followed by a jump to second mode planar motion.

In a similar vein, Mote and Naguleswaran[1966a] investigated the linear vibrations of travelling bandsaw blades due to tension changes induced in the band by the axial velocity. Their analysis considered the flexural stiffness of the band and presented an approximate formula for determining the band natural frequency as a function of the axial velocity. The theoretical results were validated experimentally. Naguleswaran and Williams[1968] examined the parametric nature of a pulley belt or band saw blade, due to tension changes caused by eccentricities in the pulley wheels, or flaws in the blade. It was confirmed experimentally that primary parametric resonance occurred when the frequency of the tension fluctuations approached twice that of the lateral natural frequency of the travelling band. This application has been pursued further recently, Mote and Wu[1985], Wu and Mote[1986], Wang and Mote[1986, 1987].

2.5 Small Amplitude Vibration of Sagged Cables

2.5.1 Stationary Sagged Cables

Irvine and Caughey[1974], Irvine[1981] trace the historical development of sagged cables, and conclude that by the early 1800's correct solutions had been achieved for the limiting cases of catenaries, namely taut strings and vertically hanging cables. However, the intermediate condition had not been solved. The symmetric modes of flat sagged cables where the sag to span ratio was neither zero nor infinite was analysed initially by Rohrs(1851)[1851] and Routh(1868)[1884]. Both authors assumed inextensible cable behaviour, thus solving the wave equation subject to a constraint condition. The resulting solutions applied essentially to situations where the catenary stiffness associated with its geometric profile is low compared to the axial stiffness of the cable element. Although solutions for the limiting conditions of the cable were established, no single theory could describe the transition continuously between deep sag cable behaviour and the limiting case of the taut string. Specifically, the modal characteristics of the symmetric modes of flat sag and deep sag cables were at that stage known to be governed by the roots of the frequency equations, cited respectively as:

$$cos(\frac{1}{2}\beta l) = 0$$

$$tan(\frac{1}{2}\beta l) = \frac{1}{2}\beta l$$

Where $\beta = (m\omega^2/H)^{\frac{1}{2}}$. The roots of the above equations are vastly different, where the first root of each equation is π and 2.86π respectively. This difference reflects the fact that in the limiting condition of a flat sag cable, the taut string, the fundamental mode is symmetric with respect to the midspan, whilst in the case of the deep sag cable, the fundamental is antisymmetric with respect to the midspan. Irvine and Caughey[1974] note that the assumption of inextensible cable behaviour is unrealistic when considering a cable where the sag tends to zero, since any deformation would necessitate elastic stretch. By allowing for elastic stretch, Irvine and Caughey[1974] demonstrated that a consistent theory could be developed describing the transition from deep sag to taut string behaviour.

The aerodynamic failure of Tacoma Narrows bridge in 1940 prompted further research into cable dynamics. Pugsley[1949], Saxon and Cahn[1953], Goodey[1961], developed the deep sag inextensible cable theory further. However, it was only when cable elasticity was accounted for that the dynamic behaviour of a cable could adequately be described in the transition region between that of the taut flat string to the deep sag profile. Laasonen[1959] and later Soler[1970] presented an analysis whereby cable elasticity was accounted for, and identified a dimensionless parameter, which Irvine and Caughey [4][1974] later termed the cable parameter, λ^2. Irvine and Caughey [1974] demonstrated that this single parameter was sufficient to describe the transition between taut string and deep sag cable behaviour. A brief development of the theory pertaining to the dynamic characteristics of small amplitude sagged cables is presented below.

Irvine and Caughey [1974] demonstrated that by considering small amplitude oscillations w from the equilibrium profile of the cable z, and accounting only for first order terms, the in-plane equation of motion of a shallow sag cable reduced to:

$$H\frac{\partial^2 w}{\partial x^2} + h\frac{\partial^2 z}{\partial x^2} = m\frac{\partial^2 w}{\partial t^2} \tag{2.5}$$

Where m represents the mass per unit length, and h represents the additional component of the horizontal tension generated during the motion, which is given to first order as:

$$\frac{hL_e}{EA} = \frac{mg}{H}\int_0^l w dx \tag{2.6}$$

It is pertinent to note that the term $\frac{\partial^2 z}{\partial x^2}$ in equation (2.5) represents to first order the curvature of the cable in its equilibrium configuration. Employing the argument introduced previously, equation (2.6) confirms that no additional tension is generated in the cable during the oscillation, if the mode shape, or displacement w from the equilibrium profile is antisymmetric about the midplane of the span. Thus it is clear, that the equation of motion (2.5) reduces to that of the wave equation for antisymmetric modes, and consequently, to first order the curvature of the cable does not influence the natural frequency.

[4]Laasonen's[1959] results are equivalent to those of Irvine and Caughey[1974], however the latter formulated the problem in a more physical sense, which perhaps explains why so little reference is made to Laasonen.

Conversely, symmetric mode shapes introduce tension changes due to geometric adjustment during the oscillation, and consequently cable curvature can significantly affect the natural frequency of symmetric modes.

Since the cable profile was assumed shallow, an approximate quadratic cable profile for z may be utilised and substituted into equation (2.5). In this instance the curvature is constant, and the equation of motion may be solved to obtain w as a function of h. Substituting the solution for w into equation (2.6), results in a transcendental characteristic equation, the roots of which represent the linear natural frequencies of the cable, spanning all configurations from a taut string to a deep sag cable[5].

$$tan\frac{\overline{\omega}}{2} = \frac{\overline{\omega}}{2} - \frac{4}{\lambda^2}(\frac{\overline{\omega}}{2})^3 \tag{2.7}$$

Where $\overline{\omega} = \omega l/(H/m)^{\frac{1}{2}}$, and $\lambda^2 = (mgl/H)^2 l/(HL_e/EA)$. The dependence of the characteristic equation on the cable parameter λ^2 is clearly demonstrated. The limiting configurations of $\lambda^2 \approx 0, \infty$ represent the taut string and deep sag cable respectively. The dependence of the natural frequencies on λ^2 is illustrated in figure 2.3.

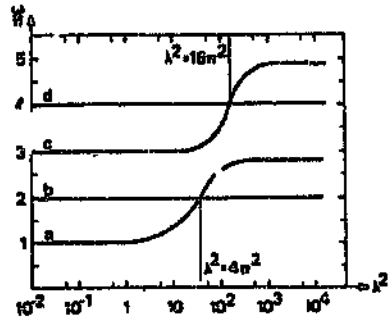

3.3 General dimensionless curves for the first four natural frequencies of a flat-sag suspended cable: (a) first symmetric in-plane mode, (b) first antisymmetric in-plane mode, (c) second symmetric in-plane mode, (d) second antisymmetric in-plane mode.

Figure 2.3: Irvine (1981): In-plane natural frequencies of a cable.

With reference to figure 2.3, it is evident that the antisymmetric modes are independent of λ, and equivalent to those of a taut string. The symmetric modes however change significantly as λ increases with increasing sag or cable

[5]This frequency equation is identical to that derived by Laasonen [1959].

curvature, resulting in a modal cross-over or mode reversion, after which the antisymmetric mode becomes the fundamental in-plane mode of a deep sag cable. Irvine[1981] also considered the case of a cable inclined at an angle θ to the horizontal plane, and concluded that if the cable parameter were modified to account for the angle of inclination, $\lambda_*^2 = (mglcos\theta/H)^2 l/(HL_e/EA)$, then the results presented in figure 2.3 would apply. This result is not strictly correct, since the asymmetry of the mode shapes associated with inclined cables causes frequency veering as opposed to modal cross-over.

Iyengar and Rao[1988] presented a study of the natural frequencies of a sagged cable under a constant lateral load. In this case the equilibrium profile is non-planar, and hence curvature coupling exists between the in- and out-of-plane equations of motion. The stability of the cable due to an additional periodic lateral load was considered. The emphasis of this analysis was clearly directed at power transmission lines. Rao and Iyengar[1991] extended this analysis to examine the response of a shallow sag cable in its first symmetric in-plane and out-of-plane mode, due to forced harmonic excitation in the in-plane and a uniform static load in the out-of-plane directions. A special case of tuning was chosen such that the first symmetric in-plane mode tuned to twice the first symmetric out-of-plane mode, and hence an internal resonance of 2:1 existed, coupling the response between the in-plane and out-of-plane symmetric modes. Simultaneously an in-plane external resonance was induced. The tuning of the internal resonance was dependent on the cable curvature, and hence the quadratic nonlinearities present in the system. By comparing the response of the system due to an external resonance, with and without internal resonance, it was concluded that cable curvature and hence the quadratic nonlinearity has a significant effect on the system response. The stability analysis of the system confirmed that regions existed where steady state periodic motion did not exist.

In a similar fashion to the analyses of Lubkin and Stoker[1943], Tagata[1977, 1983], Takahashi[1991] examined the stability of flat-sag cables to periodic axial excitation. The sag to span ratio was varied to span the first modal cross-over region. It was demonstrated that the widths of the unstable regions were affected by the sag to span ratio in the regions of modal cross-over, and that combination parametric resonances arose. Perkins[1992b] showed that the equations of motion applied by Takahaskhi[1991] were inconsistent, leading to erroneous conclusions. Perkins[1992b] showed that such a configuration resulted in parametric as well as external excitation, and that combination parametric resonances did not arise.

2.5.2 Travelling Sagged Cables

Simpson[1972] investigated the in-plane free vibration of a horizontal travelling elastic catenary. The equations of motion were derived by generalising the equations of a static catenary. Simpson's[1972] analysis considered a catenary with a sag to span ratio of 1:20. Through a process of linearisation of the nonlinear equations of motion, Simpson [1972] confirmed previous results pertaining to flat travelling strings, and demonstrated the influence of cable curvature on the natural frequencies. Simpson's [1972] results indicated that frequency coalescence between modes may occur, as well as mode reversion, whereby a higher order mode reverts to the shape of a lower order mode for certain axial velocities.

More recent analyses by Triantafyllou[1985], Perkins and Mote[1987] have reconsidered the problem of cables with initial sag translating between arbitrarily inclined eyelets. Triantafyllou[1985] presented an analysis which considered the case of small sag and large sag translating cables. His analysis confirmed the results of Simpson[1972], and provided further explanation to the occurrence of mode reversion and frequency coalescence. The results indicated that for small sag horizontal cables, the phenomenon of mode reversion and frequency coalescence occurred, whereas when the cable was inclined, frequency coalescence was replaced by frequency avoidance or veering, where the frequencies approach closely but are distinct. Also, only partial mode reversion occurs, where the mode shapes become hybrid combinations of symmetric and antisymmetric modes. Perkins and Mote [1987] derived the three dimensional equations of motion for an arbitrarily sagged translating cable based on a finite strain approach and conservation of cable mass. On linearising the equations of motion, they demonstrated that the phenomenon of frequency coalescence is conditional on the symmetry of the mode shapes, and thus frequency veering as opposed to coalescence occurs for both translating cables and inclined cables, as the mode shapes become asymmetrical. The results of the analysis were compared with those of Simpson [1972] for a horizontal small sag translating cable, and with those of Irvine and Caughey [1974] for stationary cables. It was demonstrated that the results confirmed those of Simpson [1972], except that frequency crossings were replaced by veerings, and those of Irvine and Caughey[1974], except at extreme values of the cable parameter λ^2. The large difference at small values λ^2 was attributed to the modal interaction of longitudinal modes with lateral modes, not accommodated by Irvine and Caughey's[1974] derivation which assumed quasi-static stretch in the longitudinal direction. The divergence of the behaviour was accentuated by varying the cable elasticity, thus in practice with steel wire ropes, this behaviour is associated with higher transverse modes, where longitudinal/ lateral

modal interaction is more significant. Perkins and Mote [1987] noted in this study that a second stable equilibrium profile could exist, after the divergence and buckling of the stable catenary at speeds greater than the lateral wave speed. This concept was developed further, Perkins and Mote[1989], and confirmed experimentally. Burges and Triantafyllou[1988] investigated the aspect of longitudinal and lateral modal interaction further. They examined stationary small sag horizontal and inclined cables. Modal interaction between the first elastic or longitudinal mode and the higher (18-22) transverse modes was considered. It was demonstrated that longitudinal interaction promoted the phenomena of frequency coalescence and avoidance in the horizontal case, whereas only avoidance occurred in the inclined case.

The results obtained by Perkins and Mote are presented in figure 2.4, and figure 2.5., where a comparison between those of Irvine and Caughey[1974] for a stationary sagged cable, and those of Simpson[1972] for a translating cable with a sag to span ratio of 1:20, is presented respectively.

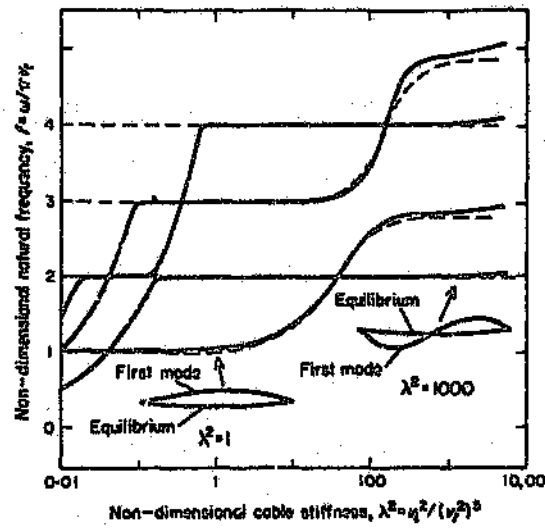

Figure 4. Comparison with Irvine's theory for the case $v_f^2 = 5$. Irvine's results are reproduced from reference [6] and reported in the units used in references [3, 6]. The first mode shape is shown for $\lambda^2 = 1$ and 1000. ——, Cable model; - - -, Irvine.

Figure 2.4: Perkins and Mote (1987): In-plane natural frequencies of a cable - Comparison with Irvine's theory.

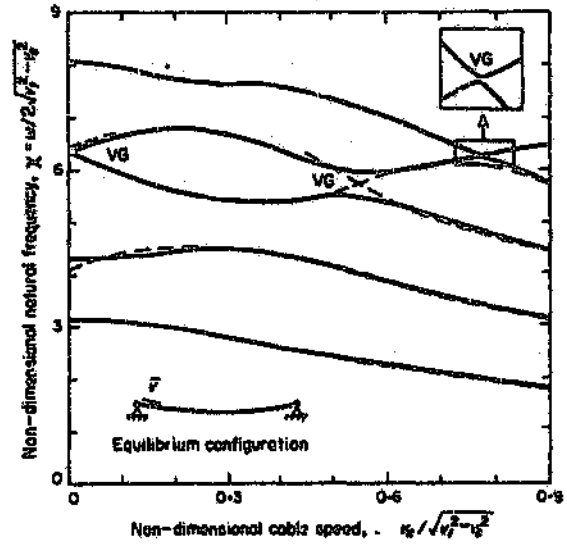

Figure 8. Comparison with Simpson's theory. In-plane frequencies for a travelling cable having horizontal eyelets and equilibrium sag to span ratio 0·050. Simpson's results are reproduced from reference [14] and based on Simpson's parameters: $\varepsilon = 0{\cdot}1 = 1/4(v_i^2 - v_c^2)$ and $\mu = 0{\cdot}001 = (v_i^2 - v_c^2)/v_i^2$. ——, Cable model; - - -, Simpson; VG, veering.

Figure 2.5: Perkins and Mote (1987): In-plane natural frequencies of a translating cable - Comparison with Simpson's theory.

2.6 Large Amplitude Vibration of Sagged Cables

Luogno, Rega and Vestroni[1982] defined a simplified two degree of freedom model for transverse in-plane and out-of-plane motion of a sagged cable. The purpose of the study was to demonstrate monofrequent in-plane and out-of-plane oscillation. As defined by Luogno et al[1982], monofrequent oscillations occur when one of the normal displacement co-ordinates prevails over the others, and all points move with a frequency that is equal to or a multiple of the nonlinear frequency of that co-ordinate. Thus monofrequent oscillations reduce to the modal oscillations of the linear system, as the nonlinearity vanishes. This provides a convenient basis for ascertaining the influence of system parameters on the nonlinear frequency amplitude relationship. The equations of motion developed contained both quadratic and cubic nonlinearities, associated with the curvature and stretch of the cable respectively. The initial conditions required to induce in-plane (extensional) and out-of-plane (pendulum type) monofrequent oscillations were determined. It was shown that in-plane or extensional monofrequent oscillations could be induced for any tuning of the in- and out-of-plane modes, conversely out-of-plane monofrequent oscillations could only be induced in the absence of internal resonance. With regard to the in-plane motion, it was demonstrated that the nonlinearities, and the amplitude of the induced motion strongly influenced the nonlinear frequencies of the cable. Drift of the midpoint of the in-plane oscillations occurred due to the quadratic nature of the nonlinearity related to cable curvature. The variation of the nonlinear frequency from the linear frequency depended strongly on the cable parameters, where a softening behaviour was observed as the cable curvature increased, whilst hardening behaviour occurred as the cable approached a taut string. The importance of internal resonance was demonstrated with respect to the out-of-plane or pendulum type monofrequent oscillations, which depended strongly on the degree of tuning between the symmetric in- and out-of-plane modes. The internal resonance condition (where the first symmetric in-plane mode tunes to twice the first symmetric out-of-plane mode at a modal cross-over as defined by Irvine and Caughey[1974]) divided the system behaviour between a hardening or softening type.

Rega, Vestroni and Benedettini[1984], examined the planar response of a sagged cable with sag to span ratios of less than 1/8, where the amplitude of response was sufficiently large to necessitate the inclusion of higher order nonlinearities. The spatial variable was eliminated from the partial differential equations of motion by using the linear eigenfunctions of a shallow sag cable, and applying an integral formulation. The resulting equations of motion reflected both quadratic and cubic nonlinearities; the quadratic nonlinearity is induced by

the cable curvature and thus the ability of the cable to absorb additional tension by geometric adjustment of the profile. The cubic nonlinearity reflects the additional tension generated via second order stretch of the cable. These terms are related to the first and second integral on the right hand side of equation 2.2. The equation pertinent to the temporal domain was thus cast in the form:

$$\ddot{q} + q + c_2 q^2 + c_3 q^3 = Q(t)$$

Since the quadratic coefficient is a consequence of the cables ability to absorb additional tension through geometric adjustment of the profile, which vanishes with respect to the antisymmetric modes of a suspended cable, the antisymmetric modes exhibit hardening behaviour only. Quadratic nonlinearities do however influence symmetric modes, where a softening-hardening behaviour results, as demonstrated by Luogno et al [1982], depending on the cable parameters. The nonlinear frequency amplitude relationship was developed and indicated that the point of modal cross-over where the first symmetric and antisymmetric modes coalesce became dependent on the amplitude of motion. Al-Noury and Ali[1985] presented a similar analysis, focussing on cables with small sag to span ratios. Their study included the out-of-plane co-ordinate in the equations of motion. This study concentrated on describing the resulting nonlinear behaviour due to excitation in the horizontal plane, excitation in the vertical plane, and excitation in the horizontal plane such that primary resonance occurred, when the transverse and vertical linear natural frequencies are closely spaced. Similar observations were made concerning the dependence of the softening, hardening behaviour on the cable parameters. The last case studied indicated the presence of strong coupling between the in-plane and out-of-plane modes, and the potential complexity of the ensuing response. Takahashi and Konishi[1987a] examined this problem further, and extended the analysis to include the three dimensional behaviour of arbitrarily inclined cables with arbitrary sag to span ratios. A Galerkin approach was adopted for the spatial domain, whilst the method of harmonic balance accounted for the temporal domain. The analysis investigated the free response of the cable, and hence defined the nonlinear frequency of vibration as a function of the amplitude of in-plane and out-of-plane initial deformations. The analysis confirmed that the in-plane behaviour exhibited a generally hardening response, although softening behaviour could be achieved depending on the system parameters. Due to the nonlinear coupling between the in-plane and out-of-plane equations of motion, where in-plane terms behave as coefficients in the out-of-plane equation of motion, out of plane response due to an in-plane excitation would result from bifurcation or parametric instability. Conversely, out-of-plane terms occur independently in the in-plane equation of motion, thus providing direct

excitation of the in-plane response due to out-of-plane excitation. This is confirmed by the analysis of Luogno et al [1982], where out-of-plane monofrequent oscillations were strongly coupled to in-plane motion. Consequently, out-of-plane excitation of a cable results in three dimensional motion, and thus the nonlinear out of plane behaviour is influenced by the in-plane response. In the second part of the study, Takahashi and Konishi[1987b], the stability of the out-of-plane response due to in-plane excitation was examined. It was demonstrated that the stability regions associated with the out-of-plane vibrations, occurred due to parametric excitation via the nonlinear coupling terms. Thus this analysis examined the parametric stability of the out-of-plane motion and concluded that in the general case both simple and sum type combination parametric resonances occurred[6]. The existence of the stability regions was shown to be dependent on the cable parameters, and on the symmetry of the excitation, which dictates the symmetry of the response and hence the importance of the cable curvature. In this regard it was demonstrated that in the case of a horizontally supported sagged cable subjected to a symmetric excitation (quadratic nonlinearities included), as opposed to an antisymmetric excitation (quadratic nonlinearities excluded), the stability chart could be significantly different. In the latter, principal simple parametric resonances of symmetric modes do not arise. In the case of an inclined cable, the asymmetry of the profile resulted in the occurrence of all types of instability regions, irrespective of the forcing function. Benedettini and Rega[1987] presented a further study, employing a perturbation method, to investigate the planar behaviour of a horizontal cable with initial sag to in-plane primary resonance. It was concluded that the cable was most sensitive to cubic nonlinearities when its parameters conformed to those of a taut string, and thus hardening behaviour was observed, with one unstable and two stable periodic solutions. When a sagged configuration was analysed, it was evident that the quadratic nonlinearities lead to a softening-hardening behaviour, and consequently up to five periodic solutions may exist close to resonance. The sensitivity of the system to initial conditions was demonstrated by a numerical simulation of the equations of motion. Rega and Benedettini[1989a, 1989b], pursued their study further, by examining the superharmonic and subharmonic behaviour[7] of a cable to in-plane excitation, for cables with various sag to span ratios. The studies demonstrated that the second order superharmonic produces notably stronger effects generally. This behaviour is accentuated by increased curvature or more

[6]Simple parametric resonances occur at intervals $2\omega_i/n$, where ω_i represents the linear natural frequency. A principal region is defined by $n = 1$, and secondary and tertiary regions follow $n = 2, 3$ respectively. A sum type combination resonance occurs in the intervals $(\omega_i + \omega_j)/n$, $n = 1, 2, 3, ...$

[7]In this context, subharmonic refers to the situation where the response frequency is a subharmonic of the excitation frequency, the converse applying for the superharmonic case. A second order and third order subharmonic would arise when response occurs at $\Omega/2$ or $\Omega/3$ respectively, where Ω represents the excitation frequency.

dominant quadratic nonlinearity in the equations of motion.

Perkins[1992a] presents a study of the nonlinear modal interactions in a sagged cable when it is excited tangentially to the equilibrium profile, at one support. This study examines the condition whereby the first symmetric in-plane mode tunes to twice the first symmetric out of plane mode, and consequently an internal resonance exists. The longitudinal excitation was tuned to excite a principal parametric resonance of the out-of-plane mode, and due to the internal resonance, this excitation could simultaneously excite primary external resonance of the in-plane mode. Perkins[1992a] demonstrated that the cable response was either planar or highly coupled. A two degree of freedom model was applied to examine the stability of the planar and nonplanar motions[8]. The bifurcation condition governing planar stability indicated that the presence of the internal resonance greatly reduces the planar stability and enhances nonplanar response. It was also found that the principal parametric resonance disrupted the saturation phenomenon that would normally occur in the case of primary external resonance alone. The theoretical model provided a good qualitative description of the experimental behaviour observed in a laboratory exercise. It was demonstrated that a small support motion could induce substantial out-of-plane motion. Perhaps it is pertinent to note that the mine hoist system lends itself to combinations of tuning of a similar nature, with respect to the longitudinal and lateral modes, and the excitation. This aspect will be elaborated further in later chapters.

[8]Perkins notes that this condition of tuning coincides with the modal cross-over, and therefore the first in-plane symmetric and antisymmetric modes, and the second out-of-plane mode occur simultaneously. If the system was excited to induce principal parametric resonance of these modes, a truncated two degree of freedom model would not apply.

2.7 Conclusion

The purpose of this chapter was to establish an overall perspective of various aspects of the nonlinear dynamic nature of a suspended cable or taut string, and thereby reflect the depth and diversity of the subject. It is clear on reviewing the literature that a structural cable provides a remarkably good vehicle for the study of nonlinear dynamics. Recent research (Molteno [1990], O'Reilly and Holmes [1992]) confirms that chaotic motion has been observed in a taut stationary string, and this will no doubt stimulate further research. The particular studies reviewed were applied to a cable or string fixed at its extremities, and for this reason the results are not directly applicable to a mine hoist system. Many other studies exist concerning aspects of taut string and cable vibrations which are not considered pertinent to this thesis. For instance studies regarding the response of a taut string to travelling loads (Rodeman[1976], Sagartz[1975], Schultz[1968]), or where the string or cable supports a discrete mass (Rosenthal[1981], Smith[1964], Wickert[1988]). An interesting application regarding the effect of Coriolis coupling on a moving string resulted in a vibrating string being considered as a basis for the development of an angular motion sensor (Quick [1964]), and consequently the consideration of nonlinear effects and methods to quench these (Dimeff et al. [1966]).

Issues pertinent to the mine hoist system, namely the potential importance of cable curvature, transport velocity, nonlinear cable stretch and longitudinal inertia, require assessment in light of the literature reviewed.

Considering the Kloof Mine system, which is typical of many shafts in South Africa, the sag to span ratio[9] varies between 1:100 and 1:500, whilst the non-dimensional cable stiffness parameter [10] λ_*^2 varies between $\lambda_*^2 \approx 4$ to $\lambda_*^2 \approx 0.03$ for an empty skip at shaft head to a fully laden skip at shaft bottom respectively. The small sag to span ratios typically encountered on mine hoist systems justifies Mankowski's treatment of the catenary as a horizontally supported truncated catenary symmetrical about its mid point. This approximation will be applied in this thesis. In terms of the cable parameter, and with reference to Irvine's results [1981], the natural frequency of the first in-plane mode at shaft head, with an empty skip will be in error by approximately 15%, whilst the higher frequencies will be unaffected. On the ascending cycle, when the skip is at shaft head, this ratio is of the order of $\lambda^2 \approx 0.3$ and thus the in-plane natural frequencies of the cable will be well predicted by classical

[9] The sag to span ratio is given as $(d : l) = \frac{mgl\cos(\theta)}{8H}$, where H is the horizontal component of tension, m the mass per unit length, l the span length, and θ the angle of inclination.

[10] Kloof Mine system parameters are $H = 80 - 340kN, m = 8.5kg/m, l = 75m, E = 1.1 \times 10^{11}, A = 1.02 \times 10^{-3}, \theta = 50°$

taut string theory. Since the dominant lateral excitation is in the out-of-plane direction, avoidance of a directly excited mode could be assessed by considering the linear lateral natural frequencies of the catenary. However, since cable curvature provides coupling between the in-plane and out-of-plane motion, as demonstrated by Luongo et al[1982], Takahashi and Konishi [1987a],[1987b], Perkins [1992a], curvature is an important parameter to include in a numerical simulation.

With regard to the transport velocity of the cable, the effect on the linear natural frequencies is small, causing frequency changes of less than 2%. For this reason, it has been neglected in previous analyses (Dimitriou and Whillier [1973], Mankowski [1982]) of mine hoist systems. Although the lateral natural frequencies of the catenary are not strongly influenced by the Coriolis force developed, it is noted that if a real normal mode method is applied for the purpose of a numerical simulation, then a realistic simulation would dictate the inclusion of this effect. This occurs since the actual mode shapes associated with a travelling medium are complex, and consequently in the context of a real normal mode solution, implies that the Coriolis force couples and excites the higher modes resulting in a nonsynchronous behaviour.

A number of the studies presented regarding strings and cables with pinned end conditions neglected the longitudinal inertia, due to the large difference between the longitudinal and lateral wave speeds. In the context of the mine hoist system, the longitudinal wave speed is far greater than the lateral wave speed, however the longitudinal response is dictated by the modal response of the coupled system, and thus modal interaction between the transverse and longitudinal modes of the system must be accommodated.

Since the intention of this study is to examine the steady state stability of the stationary system as well as to develop a numerical simulation to account for the nonstationary nature of the system, the equations should be developed to account for transport velocity, catenary curvature and nonlinear stretch of the cable. These equations can then be simplified where appropriate as the thesis develops.

Chapter 3

Equations of Motion

3.1 Introduction

The purpose of this chapter is to develop the equations of motion of the coupled system. The coupled system refers to the catenary, headsheave, conveyance, and the coupling which exists between the catenary and the vertical rope. Mankowski[1982] attempted a lumped parameter numerical simulation of the mine hoist system by accounting for curvature and nonlinear rope stretch in the catenary, and coupling the catenary motion inertially through the headsheave to longitudinal motion in the vertical rope. It is preferred to achieve the description of the system in a more theoretical manner, by applying a continuum mechanics approach as developed by Luogno et al[1984], and later applied by Perkins and Mote[1987]. In this approach, the Lagrangian function of the system is formulated, and Hamilton's principle is applied to define the nonlinear equations of motion of the system. Since the definition of the Lagrangian function depends on the strain measure adopted, and the boundary conditions assumed, simplifications introduced are clearly evident in the theoretical development. This is considered to provide an advantage over a purely numerical approach as developed by Mankowski[1982], as it allows for an appreciation of the resulting equations of motion in terms of conventional techniques applied in nonlinear dynamics. To facilitate the development, the methodology applied by Perkins and Mote[1987] in deriving the equations of motion applicable to a sagged travelling cable, is presented. This approach is then extended to the mine hoist system, where the appropriate boundary conditions are accounted for. The full nonlinear equations of motion, consistent with the strain measure adopted are presented, where further truncation is applied as appropriate in later chapters.

3.2 The Sagged Travelling Catenary

3.2.1 Equations of Motion

A sagged, travelling elastic cable passing between two fixed eyelets is illustrated in figure (3.1). The cable is treated as a one dimensional continuum, located in the vertical $X_1 - X_2$ plane with gravity, g, aligned with the $-\underline{e}_2$ direction. The cable passes from the static equilibrium configuration χ^i to a final configuration χ^f during the motion. The unstretched or natural state is defined by χ^o[1].The cable has a cross sectional area and transport velocity of A^o and c^o in the natural state χ^o, a modulus of elasticity E, and a mass density of ρ. The equilibrium configuration is defined by the position vector $\underline{R}^i(S^i,t)$ where S^i is the arc length co-ordinate referenced to the equilibrium configuration. Unit vectors in the equilibrium configuration are $\underline{t}^i, \underline{n}^i, \underline{b}^i$ in the tangential, normal and bi-normal directions respectively. The final configuration is defined by $\underline{R}^f(S^i,t) = \underline{R}^i(S^i,t) + \underline{U}(S^i,t)$ where $\underline{U}(S^i,t)$ represents the three dimensional motion of the final configuration, with respect to the equilibrium profile. The motion of a cable particle which includes the particle transport velocity $c^f\underline{t}^f$ is illustrated in figure 3.1. Thus:

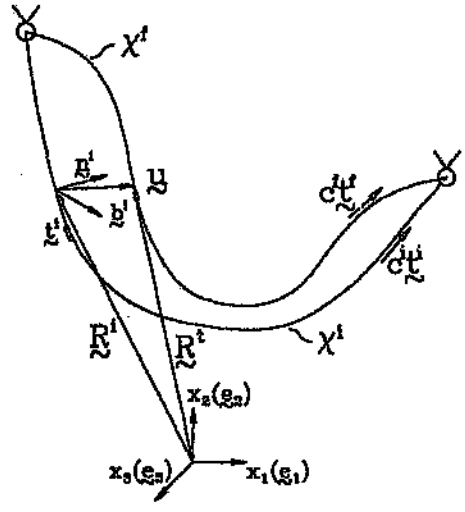

Figure 3.1: Catenary configuration

[1]The purpose of introducing the natural or unstressed state, facilitates the extraction of the equations describing the equilibrium profile of the catenary from the equations of motion.

$$\underline{R}^f(S^i,t) = \underline{R}^i(S^i,t) + \underline{U}(S^i,t) \tag{3.1}$$

The motion $\underline{U}(S^i,t)$ is defined in the tangential, normal and bi-normal directions of the equilibrium configuration as:

$$\underline{U}(S^i,t) = u\underline{t}^i + v\underline{n}^i + w\underline{b}^i$$

The cable is considered as a one dimensional continuum in the $\underline{t}^i$ direction. Second order deformation effects are accounted for by utilising the $\underline{t}^i$ component of the Green-Lagrange strain tensor. Luogno et al[1984], Perkins and Mote[1987] define the Lagrangian strain in the final configuration as:

$$e^f = \frac{1}{2}\left[\left\{\frac{\partial}{\partial S^o}R^f(S^i,t)\right\}^T \cdot \left\{\frac{\partial}{\partial S^o}R^f(S^i,t)\right\} - 1\right]$$

where S^o denotes the arc length of the unstressed cable configuration. The Lagrangian strain in terms of the initial differential element dS^o and the final element dS^f is defined as $e^f = \frac{1}{2}[\frac{(dS^f)^2-(dS^o)^2}{(dS^o)^2}]$. Introducing an intermediate equilibrium state, dS^i results in the strain measure e^f:

$$e^f = e^i + (\frac{dS^i}{dS^o})^2)\epsilon$$

The Lagrangian strain resulting from a deformation from the equilibrium configuration χ^i to the final configuration χ^f is defined as ϵ: [2]:

$$\epsilon = u_{,s} - \kappa v + \frac{1}{2}\{u_{,s}^2 + v_{,s}^2 + w_{,s}^2\} + \kappa\{uv_{,s} - vu_{,s} + \frac{1}{2}\kappa(u^2+v^2)\}$$

[2]The following manipulation is required:

$$e^f = e^i + \frac{1}{2}\left[\left\{\frac{\partial}{\partial S^i}\underline{U}(S^i,t)\right\}^T \cdot \left\{\frac{\partial}{\partial S^i}\underline{U}(S^i,t)\right\} + 2\left\{\frac{\partial}{\partial S^i}\underline{U}(S^i,t)\right\}^T \cdot \underline{t}^i\right](\frac{dS^i}{dS^o})^2$$

where: $\underline{U}(S^i,t) = u\underline{t}^i + v\underline{n}^i + w\underline{b}^i$
and : $\frac{\partial \underline{t}^i}{\partial S^i} = \kappa\underline{n}^i$ $\quad$ $\frac{\partial \underline{n}^i}{\partial S^i} = -\kappa\underline{t}^i$ $\quad$ $\frac{\partial}{\partial S^i}R^i(S^i,t) = \underline{t}^i$
$\frac{\partial}{\partial S^i}\underline{U}(S^i,t) = (u_{,s} - \kappa v)\underline{t}^i + (v_{,s} + \kappa u)\underline{n}^i + w_{,s}\underline{b}^i$

in which $(\quad)_{,s}$ denotes partial differentiation with respect to S^i and κ refers to the curvature of the equilibrium configuration χ^i.

The Lagrangian strain may be formulated in a more direct manner by considering the deformation associated with a differential element in χ^f, referenced to a differential element in χ^i. Figure 3.2 presents a differential element of the cable in the $u-w$ and $u-v$ plane, with curvature κ, deformed from the equilibrium profile χ^i to the final profile χ^f. The differential length of the element in the final configuration can be calculated by considering the projection of the element onto the three orthogonal cartesian planes defined by X_1, X_2, X_3:

$$(dS^f)^2 = [dS^i + u_{,s}dS^i - (v + v_{,s}dS^i)d\theta]^2 + [v_{,s}dS^i + (u + u_{,s}dS^i)d\theta]^2 + (w_{,s}dS^i)^2$$

Since $d\theta = \kappa dS^i$, and $\epsilon = \frac{1}{2}\frac{(dS^f)^2-(dS^i)^2}{(dS^i)^2}$, and neglecting the differential products $v_{,s}dS^i d\theta, u_{,s}dS^i d\theta$ which vanish in the limit $dS^i \to 0$, the Green-Lagrange strain ϵ can be derived.

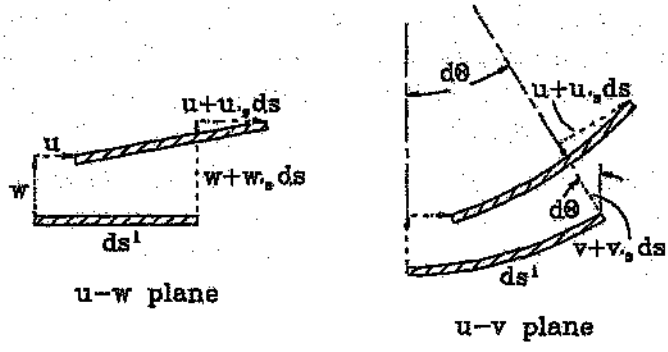

Figure 3.2: Displacement of a differential element of cable from χ^i to χ^f

3.2.2 Hamilton's Principle

In order to apply Hamilton's principle, the action integral is formulated as a combination of the kinetic energy π_V^f, the strain energy π_e^f, and the gravitational potential energy π_g^f of the system. The action integral is stated as:

$$I = \int_{t_0}^{t_1} (\pi_V^f - \pi_e^f - \pi_g^f) dt$$

The strain energy of the cable π_e^f in the final configuration χ^f formulated in terms of the equilibrium strain energy π_e^i of the cable in the equilibrium configuration χ^i is:

$$\pi_e^f = \pi_e^i + \int_0^{l^i} (P^i + \frac{1}{2} A^i E \epsilon) \epsilon dS^i$$

where P^i represents the tension in the cable in the static equilibrium state χ^i. This represents a reduced form applied by Perkins and Mote[1987] to the more complete derivation provided by Luogno et al[1984]. It implies that $\frac{dS^i}{dS^o} \approx 1$, and thus the deformation of the cable from its unstretched length to the static equilibrium profile is in-elastic. This assumption is well justified for practical cables as can be ascertained by considering the constitutive law for a uniaxial cable: $P^i = EA^o e^i$, where $e^i = \frac{1}{2}[\frac{(dS^i)^2 - (dS^o)^2}{(dS^o)^2}]$, $\frac{dS^i}{dS^o} = [1 + \frac{2P^i}{EA^o}]^{\frac{1}{2}}$. For practical cables $\frac{P^i}{EA^o} << 1$, and consequently the approximation $\frac{dS^i}{dS^o} \approx 1$ is justified. Since conservation of momentum and mass requires that $c^i A^i = c^o A^o$ and $A^i dS^i = A^o dS^o$ it follows that by the same argument A^i and c^i may be treated as constants.

The kinetic energy of the cable in the final configuration χ_V^f, referenced to the equilibrium configuration χ_V^i, is formulated as:

$$\pi_V^f = \int_o^{l^i} \frac{1}{2} \rho A^i \underline{V}^f \cdot \underline{V}^f dS^i$$

The velocity of the cable $\underline{V}^f$ in the final configuration χ^f, may be obtained in terms of the equilibrium configuration χ^i, as follows:

$$\underline{V}^f(S^i, t) = \frac{d}{dt}[\underline{U}(S^i, t)] + c^f \underline{t}^f$$

$$\underline{t}^f = \frac{\partial}{\partial S^f}[\underline{R}^f(S^i,t)] = \frac{\partial}{\partial S^i}[\underline{R}^i(S^i,t) + \underline{U}(S^i,t)]\frac{dS^i}{dS^f}$$

$$\underline{t}^f = [\underline{t}^i + \frac{\partial}{\partial S^i}\underline{U}(S^i,t)]\frac{dS^i}{dS^f}$$

The term $\frac{dS^i}{dS^f}$ is defined by considering the conservation of mass and momentum of a cable element:

$$A^i dS^i = A^f dS^f$$

$$A^i c^i = A^f c^f$$

$$\longrightarrow \frac{dS^i}{dS^f} = \frac{c^i}{c^f}$$

Thus the velocity of the cable, referenced to the equilibrium profile may be formulated as:

$$\longrightarrow \underline{V}^f(S^i,t) = c^i\underline{t}^i + c^i\frac{\partial}{\partial S^i}\underline{U}(S^i,t) + \frac{d}{dt}\underline{U}(S^i,t)$$

The gravitational potential energy π_g^f of the cable in its final configuration χ^f, written in terms of the gravitational potential energy π_g^i of the cable in the equilibrium configuration χ^i is:

$$\pi_g^f = \pi_g^i + \int_0^{l^i}(ul_t + vl_n)\rho g A^i dS^i$$

where l_t, l_n are the components of the normal and tangential unit vectors projected on the vertical cartesian unit vector $\underline{e}_2$, $\underline{e}_2 = l_t\underline{t}^i + l_n\underline{\tau}_\perp^i$.

The equations of motion are determined by applying Hamilton's Principle, which requires stationarity of the action integral for arbitrary variations $\delta\underline{U}(S^i,t)$, vanishing at the limits t_o, t_1.

$$\delta\left\{\int_{t_0}^{t_1}(\pi_V^f - \pi_e^f - \pi_g^f)dt\right\} = 0 \qquad (3.2)$$

On applying the condition of stationarity with respect to arbitrary variations $\delta\underline{U}(S^i,t)$, the above equation reduces to:

$$\delta I = \int_{t_0}^{t_1}\int_0^{l^i}[\frac{\partial\mathcal{L}}{\partial\underline{U}}\delta\underline{U} - (\frac{\partial\mathcal{L}}{\partial\dot{\underline{U}}})\frac{\partial}{\partial t}(\delta\underline{U}) - \frac{\partial\mathcal{L}}{\partial\underline{U}'}\frac{\partial}{\partial S^i}(\delta\underline{U})]dS^i dt$$

where:

$$\mathcal{L}(\underline{U},\underline{U}',\dot{\underline{U}}) = \frac{1}{2}\rho A^i\underline{V}^f\cdot\underline{V}^f - (P^i + \frac{1}{2}A^iE\epsilon)\epsilon - \rho g A^i(ul_t + vl_n)$$

Integration by parts with respect to t in the second term and S^i in the third, leads to:

$$\delta I = \int_{t_0}^{t_1}\left[\int_0^{l^i}[\frac{\partial\mathcal{L}}{\partial\underline{U}} - \frac{\partial}{\partial t}(\frac{\partial\mathcal{L}}{\partial\dot{\underline{U}}}) - \frac{\partial}{\partial S^i}(\frac{\partial\mathcal{L}}{\partial\underline{U}'})]\delta\underline{U}dS^i\right] + (\frac{\partial\mathcal{L}}{\partial\underline{U}'}\delta\underline{U}|_0^{l^i})dt$$

If the cable passes through fixed eyelets, as in the analysis of Perkins and Mote[1987], then $\delta\underline{U}|_0^{l^i}$ vanishes at the eyelets and consequently the last term in the above equation vanishes. Thus the equations of motion are obtained by satisfying Hamilton's principle by setting the integrand identically to zero. Perkins and Mote[1987] obtained the following equations of motion.

u Component

$$\left[(P^i + A^iE\epsilon)a_1\right]_{,s} - \left[(P^i + A^iE\epsilon)\kappa a_2\right] - \rho g l_t = \left[\rho A^i(u_{,t} + c^i a_1)\right]_{,t} + \left[\rho A^i c^i(u_{,t} + c^i a_1)\right]_{,s} - \rho A^i c^i\kappa\left[v_{,t} + c^i a_2\right]$$

v Component

$$\left[(P^i + A^iE\epsilon)a_2\right]_{,s} + \left[(P^i + A^iE\epsilon)\kappa a_1\right] - \rho g l_n = \left[\rho A^i(v_{,t} + c^i a_2)\right]_{,t} + \left[\rho A^i c^i(v_{,t} + c^i a_2)\right]_{,s} - \rho A^i c^i\kappa\left[u_{,t} + c^i a_1\right]$$

w Component

$$\left[(P^i + A^iE\epsilon)a_3\right]_{,s} = \left[\rho A^i(w_{,t} + c^i a_3)\right]_{,t} + \left[\rho A^i c^i(w_{,t} + c^i a_3\right]_{,s}$$

where $a_1 = 1 + u_{,s} - \kappa v$, $a_2 = v_{,s} + \kappa u$ and $a_3 = w_{,s}$.

The equations of static equilibrium are extracted by setting the time derivatives and displacement components u, v, w to zero. Thus the equations governing the static equilibrium profile are:

$$-[(\rho A^i c^i)c^i]_{,s} + P^i_{,s} = \rho g A^i l_t$$

$$-\rho A^i \kappa (c^i)^2 + \kappa P^i = \rho g A^i l_n$$

Perkins and Mote[1987] show that by considering a momentum balance between the natural configuration χ^o and the equilibrium configuration χ^i, when the cable is stationary, a description of the equilibrium configuration results which is identical to that of the inelastic catenary solution in elementary statics. On linearising the equations of motion about the equilibrium profile, and retaining only first order terms in the displacements, Perkins and Mote[1987] determined the natural frequencies of a shallow sag, inclined travelling cable.

3.3 The Mine Hoist System

In the case of the mine hoist system, the boundary conditions differ from those applied to cables pinned at each end. Figure 3.3 represents the model of the mine hoist system analysed. In this figure, the catenary refers to the section of rope between the winder drum and sheave wheel. In practice, the static tension in the catenary is high, and consequently the asymmetry due to the cable inclination is small. The catenary profile is flat and lies close to the chord between the drum and sheave. The sag to span ratio at the mid point of the chord, where the sag is measured perpendicular to the chord, is of the order of 1:100 or less. In this regard it is acceptable to treat the cable as a flat sag cable, by neglecting variations in the tension and treating the curvature as constant. This results in a symmetric parabolic cable equilibrium profile, where the inclination of the cable is accounted for by modifying the gravitational constant to $gcos(\theta)$, where θ represents the angle of inclination of the chord from the horizontal axis[3]. Initially the equations of motion are developed to account for the general case of an inclined sagged catenary as illustrated in figure 3.3. Subsequent simplification of the equations of motion is introduced, on the basis of assuming constant tension and curvature, leading to the equilibrium profile of a flat sag parabolic cable.

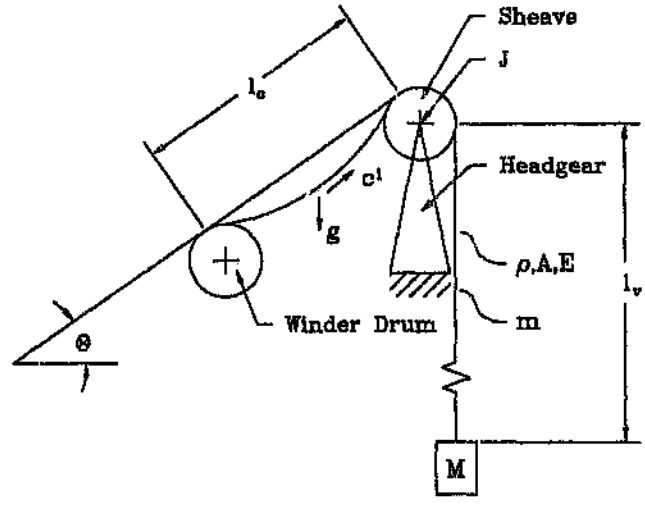

Figure 3.3: Mine hoist configuration

[3]Mankowski[1982] made a similar simplification, justified on the basis that the variation in axial tension due to the inclination of the cable is small in comparison to the static tension, hence a symmetric parabolic catenary was employed in his analysis.

The system parameters are the catenary length l_c, the total rope length l_v, the material density of the cable ρ, the linear mass density of the cable m, the cross-sectional area of the cable A, the elastic modulus of the cable E, the sheave wheel mass moment of inertia J, the mass of the skip and pay load M, and the transport velocity c^i.

The boundary condition at the drum end is treated as pinned. Thus the winder is considered as a perfect power source, and dynamic interaction between the winder and hoist system is neglected[4]. The sheave end boundary condition represents the fundamental difference between studies regarding strings and cables and the mine hoist system. In this study the coupling between the catenary motion and the vertical rope is accommodated. To simplify the analysis, it is assumed that the catenary-sheave-vertical rope interface is accounted for by a rigid band passing over the sheave. The catenary is attached to this band, which admits motion tangential to the equilibrium profile. Thus the catenary is effectively supported by frictionless rollers at the sheave, such that lateral motion at the point of attachment to the band is eliminated, as illustrated in figure 3.4. This effectively couples the sheave inertially to the longitudinal system response[5]. Although lateral movement of the vertical rope occurs in practice through autoparametric excitation due to the catenary motion, only longitudinal motion of the vertical rope is admitted. Thus the model proposed is ultimately identical to that implemented numerically by Mankowski[1982]. The aspect of including lateral motion of the vertical rope is viewed as a future research incentive.

The definition of the dynamic response of this model requires equations of motion describing the three dimensional motion of the catenary, the motion of the sheave wheel, and the longitudinal motion of the vertical rope and skip. Figure 3.4 illustrates the variables $u(s,t), v(s,t), w(s,t)$ which represent the motion at a station along the catenary in the tangential, normal and bi-normal direction of the equilibrium profile respectively, where s refers to the arc length co-ordinate measured along the equilibrium configuration. The co-ordinates u_1, $\overline{u}(s,t)$,u_2 represent the tangential motion at the sheave, the longitudinal motion of the vertical rope, and the motion at the skip respectively. Continuity of motion across the sheave requires $u(l_c,t) = u_1 = \overline{u}(l_c,t)$.

[4]This is a significant assumption which was introduced to simplify the analysis at this stage of the research. Kaczmarczyk[1993] is considering the effect of including the electrical characteristics of the winder motor.

[5]Appendix M presents an alternative formulation, where the kinematics of the cable sheave contact are defined through geometric considerations, resulting in constraint relationships governing the motion of the cable at the sheave end.

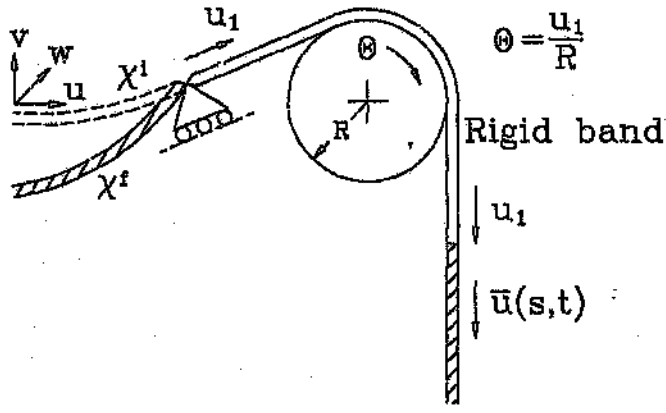

Figure 3.4: Catenary - sheave interface

3.3.1 Equations of Motion and Equilibrium

The equations of motion are developed for the system described, by following a similar development to that of Perkins and Mote[1987]. The kinetic, elastic and gravitational potential energy of the system is defined in terms of the equilibrium state of the system. The equations of motion are extracted via Hamilton's principle. By setting displacements and time derivatives to zero the equations defining the equilibrium state of the system result.

In this analysis the Lagrangian strain ϵ defines the strain measure in the catenary:

$$\epsilon = u_{,s} - \kappa v + \frac{1}{2}\{u_{,s}^2 + v_{,s}^2 + w_{,s}^2\} + \kappa\{uv_{,s} - vu_{,s} + \frac{1}{2}\kappa(u^2 + v^2)\}$$

Since lateral motion is not permitted in the vertical rope, the strain measure applied in the vertical rope $\bar{\epsilon}$ is defined as:

$$\bar{\epsilon} = \bar{u}_{,s}$$

The strain energy of the cable π_ϵ^f in the final configuration, formulated in terms

of the equilibrium strain energy π_e^i of the cable in the equilibrium configuration is:

$$\pi_e^f = \pi_e^i + \int_0^{l_c}(P^i + \frac{1}{2}AE\epsilon)\epsilon ds + \int_{l_c}^{l^v}(\overline{P}^i + \frac{1}{2}AE\overline{\epsilon})\overline{\epsilon}ds$$

where P^i,$\overline{P}^i$ represent the tension in the catenary and vertical rope in the static equilibrium state respectively.

The kinetic energy of the cable in the final configuration, referenced to the equilibrium configuration is formulated as:

$$\pi_V^f = \int_o^{l_c}\frac{1}{2}\rho A^i\underline{V}^f\cdot\underline{V}^f ds + \int_{l_c}^{l^v}\frac{1}{2}\rho A^i\overline{V}^f\cdot\overline{V}^f ds + \frac{1}{2}\frac{I}{R^2}(\dot{u}_1 + c^i)^2 + \frac{1}{2}M(\dot{u}_2 + c^i)^2$$

where V^f,$\overline{V}^f$ represents the particle velocity of the rope in the catenary and vertical section respectively; $(\dot{u}_1 + c^i)$, $(\dot{u}_2 + c^i)$ represent the tangential velocity at the sheave and skip respectively.

The velocity of the catenary $\underline{V}^f$ in the final configuration is obtained as:

$$\underline{V}^f = \{c^i a_1 + u_{,t}\}\underline{t}^i + \{c^i a_2 + v_{,t}\}\underline{n}^i + \{c^i a_3 + w_{,t}\}\underline{b}^i$$

where: $a_1 = 1 + u_{,s} - \kappa v$, $a_2 = v_{,s} + \kappa u$, $a_3 = w_{,s}$.

The velocity of the vertical rope $\overline{V}^f$ in the final configuration is obtained as:

$$\overline{V}^f = \{c^i(1 + \overline{u}_{,s}) + \overline{u}_{,t}\}\overline{t}^i$$

The gravitational potential energy π_g^f of the cable in the final configuration, written in terms of the gravitational potential energy π_g^i of the cable in the equilibrium configuration is:

$$\pi_g^f = \pi_g^i + \int_0^{l_c}(ul_t + vl_n)\rho g A^i ds - \int_{l_c}^{l^v}\rho g A^i\overline{u}ds - Mgu_2$$

where l_t, l_n are the components of the normal and tangential unit vectors projected on the vertical cartesian unit vector $\underline{e}_2$, $\underline{e}_2 = l_t\underline{t}^i + l_n\underline{n}^i$.

The Lagrangian of the system is thus:

$$\mathcal{L}(s,t,u,v,w,u_1,u_2,u_{,s},v_{,s},w_{,s},\overline{u}_{,s},u_{,t},\dot{v}_{,t},w_{,t},\dot{u}_1,\dot{u}_2,\overline{u}_{,t}) = \pi_k^f - \pi_e^f - \pi_g^f$$

The Lagrangian is split into discrete and continuous components for convenience:

$$\begin{aligned}\mathcal{L}(s,t,u,v,w,u_{,s},v_{,s},w_{,s},u_{,t},v_{,t},w_{,t},\overline{u},\overline{u}_{,s},\overline{u}_{,t},u_1,\dot{u}_1,u_2,\dot{u}_2) = \\ \mathcal{L}_1(s,t,u,v,w,u_{,s},v_{,s},w_{,s},u_{,t},v_{,t},w_{,t}) \\ +\mathcal{L}_2(s,t,\overline{u},\overline{u}_{,s},\overline{u}_{,t}) + \mathcal{L}_3(t,u_1,\dot{u}_1) + \mathcal{L}_4(t,u_2,\dot{u}_2)\end{aligned}$$

where:

$$\mathcal{L}_1 = \int_0^{l_e}[$$

$$\int_{l_e}^{l_v}[\frac{1}{2}\rho A^i\underline{\overline{V}}^f\cdot\underline{\overline{V}}^f - (\overline{P}^i + \frac{1}{2}A^iE\overline{\epsilon})\overline{\epsilon} + mg\overline{u}]ds$$

$$\mathcal{L}_3 = \frac{1}{2}\frac{I}{R^2}(\dot{u}_1 + c^i)^2$$

$$\mathcal{L}_4 = \frac{1}{2}M(\dot{u}_2 + c^i)^2 + Mgu_2$$

The equations of motion are determined by applying Hamilton's principle, which requires stationarity of the action integral for arbitrary variations in the dependent co-ordinates, compatible with the boundary conditions, which vanish at t_o, t_1.

$$\delta\left\{\int_{t_0}^{t_1}(\pi_V^f - \pi_e^f - \pi_g^f)dt\right\} = 0 \qquad (3.3)$$

Applying the condition of stationarity with respect to arbitrary variations in the co-ordinates $\delta\underline{U}(s,t)$,$\delta\overline{u}(s,t)$,δu_1,δu_2, leads to the requirement that:

$$\int_{t_0}^{t_1}\left[\int_0^{l_c}\left\{\frac{\partial\mathcal{L}_1}{\partial\underline{U}}-\frac{\partial}{\partial t}(\frac{\partial\mathcal{L}_1}{\partial\dot{\underline{U}}})-\frac{\partial}{\partial s}(\frac{\partial\mathcal{L}_1}{\partial\underline{U}'})\right\}\delta\underline{U}ds+\frac{\partial\mathcal{L}_1}{\partial\underline{U}'}\delta\underline{U}|_0^{l_c}\right.$$
$$+\int_{l_c}^{l^*}\left\{\frac{\partial\mathcal{L}_2}{\partial\overline{u}}-\frac{\partial}{\partial t}(\frac{\partial\mathcal{L}_2}{\partial\dot{\overline{u}}})-\frac{\partial}{\partial s}(\frac{\partial\mathcal{L}_2}{\partial\overline{u}'})\right\}\delta\overline{u}ds+\frac{\partial\mathcal{L}_2}{\partial\overline{u}'}\delta\overline{u}|_{l_c}^{l^*}$$
$$\left.+\left\{\frac{\partial\mathcal{L}_3}{\partial u_1}-\frac{\partial}{\partial t}(\frac{\partial\mathcal{L}_3}{\partial\dot{u}_1})\right\}\delta u_1+\left\{\frac{\partial\mathcal{L}_4}{\partial u_2}-\frac{\partial}{\partial t}(\frac{\partial\mathcal{L}_4}{\partial\dot{u}_2})\right\}\delta u_2\right]dt=0$$

where:

$$\underline{U}^T(s,t)=\{u(s,t),v(s,t),w(s,t)\}$$

$$\delta\underline{U}^T(0,t)=\{0,0,0\}$$

$$\delta\underline{U}^T(l_c,t)=\{\delta u_1,0,0\}$$

$$\delta\overline{u}(l_c,t)=\delta u_1$$

$$\delta\overline{u}(l_v,t)=\delta u_2$$

Applying these conditions, the equations of motion result as:

$$\begin{aligned}
\frac{\partial\mathcal{L}_1}{\partial\underline{U}}-\frac{\partial}{\partial t}(\frac{\partial\mathcal{L}_1}{\partial\dot{\underline{U}}})-\frac{\partial}{\partial s}(\frac{\partial\mathcal{L}_1}{\partial\underline{U}'}) &= 0\\
\frac{\partial\mathcal{L}_2}{\partial\overline{u}}-\frac{\partial}{\partial t}(\frac{\partial\mathcal{L}_2}{\partial\dot{\overline{u}}})-\frac{\partial}{\partial s}(\frac{\partial\mathcal{L}_2}{\partial\overline{u}'}) &= 0\\
\frac{\partial\mathcal{L}_3}{\partial u_1}-\frac{\partial}{\partial t}(\frac{\partial\mathcal{L}_3}{\partial\dot{u}_1})+\frac{\partial\mathcal{L}_1}{\partial u'}|_{l_c}-\frac{\partial\mathcal{L}_2}{\partial\overline{u}'}|_{l_c} &= 0\\
\frac{\partial\mathcal{L}_4}{\partial u_2}-\frac{\partial}{\partial t}(\frac{\partial\mathcal{L}_4}{\partial\dot{u}_2})+\frac{\partial\mathcal{L}_2}{\partial\overline{u}'}|_{l_v} &= 0
\end{aligned}$$

Performing the necessary manipulations results in a set of six nonlinear differential equations defining the motion of the mine hoist system.

$$\left[(P^i + A^i E\epsilon)c^i\right]_{,s} - \left[(P^i + A^i E\epsilon)\kappa a_2\right] - \rho g A^i l_t = \left[\rho A^i(u_{,t} + c^i a_1)\right]_{,t} + \left[\rho A^i c^i(u_{,t} + c^i a_1)\right]_{,s} - \rho A^i c^i \kappa \left[v_{,t} + c^i a_2\right]$$

$$\left[(P^i + A^i E\epsilon)a_2\right]_{,s} + \left[(P^i + A^i E\epsilon)\kappa a_1\right] - \rho g l_n = \left[\rho A^i(v_{,t} + c^i a_2)\right]_{,t} + \left[\rho A^i \quad _{,t} + c^i a_2)\right]_{,s} - \rho A^i c^i \kappa \left[u_{,t} + c^i a_1\right]$$

$$\left[(P^i + A^i E\epsilon)a_3\right]_{,s} = \left[\rho A^i(w_{,t} + c^i a_3)\right]_{,t} + \left[\rho A^i c^i(w_{,t} + c^i a_3)\right]_{,s}$$

$$[(\overline{P}^i + A^i E\overline{\epsilon})]_{,s} + mg = [\rho A^i(c^i a_4 + \overline{v}_{,t})]_{,t} + [\rho A^i c^i(c^i a_4 + \overline{v}_{,t})]_{,s}$$

$$\left[(\overline{P}^i + A^i E\overline{\epsilon}) - (P^i + A^i E\epsilon)a_1\right]|_{l_c} - \rho A^i (c^i)^2(\overline{v}_{,s} - v_{,s})|_{l_c} = [\frac{I}{R^2}(\dot{u}_1 + c^i)]_{,t}$$

$$M g + \rho A^i (c^i)^2 - \overline{P}^i(l_u) - [A^i E\overline{\epsilon}]|_{l_u} = [M(\dot{u}_2 + c^i)]_t - \rho A^i c^i \dot{u}_2$$

where $a_1 = 1 + u_{,s} - \kappa v$, $a_2 = v_{,s} + \kappa u$ $a_3 = w_{,s}$, $a_4 = 1 + \overline{v}_{,s}$.

The first three equations are identical to those derived by Perkins and Mote[1987]. The fourth equation describes the longitudinal motion of the vertical rope. The fifth and sixth equations describe the inertial balance across the sheave, coupling the catenary to the vertical rope, and the boundary condition required to achieve dynamic equilibrium between the skip and the tail of the vertical rope, respectively.

The equations of static equilibrium, for a constant velocity state $c^i_{,t} = 0$, are extracted by setting the time derivatives and displacement components to zero. Thus the equations governing the static equilibrium profile are:

$$-[(\rho A^i c^i)c^i]_{,s} + P^i_{,s} = \rho g A^i l_t \tag{3.4}$$

$$-\rho A^i \kappa (c^i)^2 + \kappa P^i = \rho g A^i l_n \tag{3.5}$$

$$\overline{P}^i_{,s} + mg = 0 \tag{3.6}$$

$$P^i(l_c) - \overline{P}^i(l_c) = 0 \tag{3.7}$$

$$Mg + \rho A^i (c^i)^2 - \overline{P}^i(l_o) = 0 \tag{3.8}$$

Perkins and Mote[1987] solved the equilibrium equations governing the profile of a cable with arbitrary inclination and sag. This was accomplished by introducing a momentum balance across a segment of arc length S^i, extending from the the lowest point on the profile where the tension is P_o, to any other station along the arc length where the tension is P^i[6]. Referring to figure 3.5, the momentum balance yields:

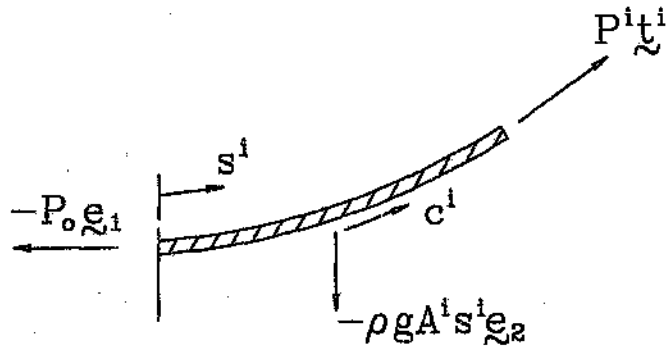

Figure 3.5: Control volume of segment of cable.

$$[P^i - \rho A^i c^{i^2}]\underline{t}^i = [P_o - \rho A^i c^{i^2}]\underline{e}_1 + \rho A^i g S^i \underline{e}_2$$

Since $\underline{t}^i = l_2 \underline{e}_1 + l_1 \underline{e}_2$, l_1, l_2 can be defined. Together with the first two equilibrium equations, the tension distribution and curvature can be defined as:

$$P^i(S^i) = [(P_0 - \rho A^i c^{i^2})^2 + (\rho g A^i S^i)^2]^{\frac{1}{2}} + \rho A^i c^{i^2}$$

$$\kappa^i(S^i) = \rho g A^i (P_0 - \rho A^i c^{i^2}) / [(P_0 - \rho A^i c^{i^2})^2 + (\rho A^i S^i)^2]$$

Integration of the cable curvature leads to:

$$X_2^i(X_1^i) = M^2 cosh(X_1^i / M^2)$$

[6]The approximation $A^o \approx A^i$ and $c^o \approx c^i$ is introduced on the basis that $P^i / EA^o << 1$.

and the arc length co-ordinate:

$$S^i = \int_0^{X_1^i} (1 + (\frac{dX_2^i}{dX_1^i})^2)^{\frac{1}{2}} dX_1 = M^2 sinh(X_1^i/M^2)$$

where $M^2 = (P_o - \rho A^i c^{i^2})/\rho g A^i$. The equation for the catenary profile $X_2^i(X_1^i)$ and the arc length S^i are used to define the tension P_o and the position of the catenary in the X_1, X_2 plane, given c^i, and the initial cable length L^i. Although this approach accurately accounts for the tension and curvature distribution in the equilibrium configuration, as noted previously, substantial simplification can be made in the context of the mine hoist system by treating the catenary as a flat sag cable.

3.3.2 Flat Sag Cable Approximation

In the mine hoist system, the catenary is inclined. However, due to the high tension in the catenary as a result of the payload and mass of the vertical rope, the cable profile lies close to the chord between the drum and sheave. Irvine[1981] derived the profile of a static inclined cable, under sufficient tension such that the profile lies close to the chord, as illustrated in figure 3.6. The approximate profile with respect to the chord is defined as:

$$\mathbf{z} = \frac{1}{2}\mathbf{x}(1 - \mathbf{x})[1 - \frac{\epsilon}{3}(1 - 2\mathbf{x})]$$

where $\mathbf{z} = z/(mgl^2 cos(\theta)/H)$, $\mathbf{x} = x/l$, $\epsilon = mglsin(\theta)/H$; z represents the perpendicular distance between the profile and the chord, x represents the distance from the upper support along the chord length, and H represents the component of the cable tension projected onto the chord at the upper support. This profile is asymmetric with respect to the mid span, where the asymmetry is dictated by the magnitude of ϵ. If $\epsilon << 1$, the variation of the tension is considered to be negligible with respect to the static tension, and the profile may be approximated by a symmetric parabola with respect to its mid span[7]. By assuming such a profile, Irvine[1981] suggests that the natural frequencies of an inclined cable can be determined from the frequency equation of a flat sag horizontal cable, where the cable parameter is corrected

[7]The same solution is obtained by considering the cable to be supported at equal elevation, and correcting the gravitational constant to $gcos(\theta)$.

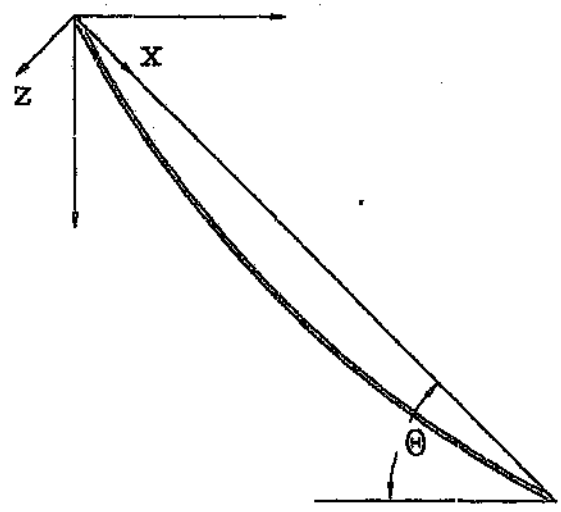

Figure 3.6: Flat sag inclined cable

to $\lambda^2 = (mglcos(\theta)/H)/(HL_e/EA)$. Perkins and Mote[1987] demonstrated that the loss of symmetry of the profile of an inclined cable, leads to frequency veering as opposed to coalescence in the proximity of a modal cross-over.

In the context of mine hoist systems, the cable tension is sufficiently high such that the assumption of a flat sag cable profile symmetrical with respect to the span is reasonable[8]. Mankowski[1982] introduced this approximation by treating the catenary as being horizontally supported, symmetric with respect to the mid-span, and correcting the gravitational constant to $gcos(\theta)$. Although the equations derived account correctly for the tension and curvature distribution in the catenary, this approximation will be introduced, and consequently the system analysed is presented in figure 3.7.

Considering the equations of static equilibrium of the catenary, the variation of tension along the cable due to its self weight is negligible, and the cable tension and curvature are constant. Thus $P^i, s \approx 0$, c^i is constant and $l_t \approx 0$ and $l_n \approx 1$. Equation 3.4 is trivial, whilst equation 3.5 results in a description of the equilibrium curvature where g has been corrected to $gcos(\theta)$. Applying these approximations to equations 3.4,3.5 results in:

$$P^i(s) = P^i$$

[8]In typical mine hoist systems, $0.01 < \epsilon < 0.05$, $\lambda^2 < 2$

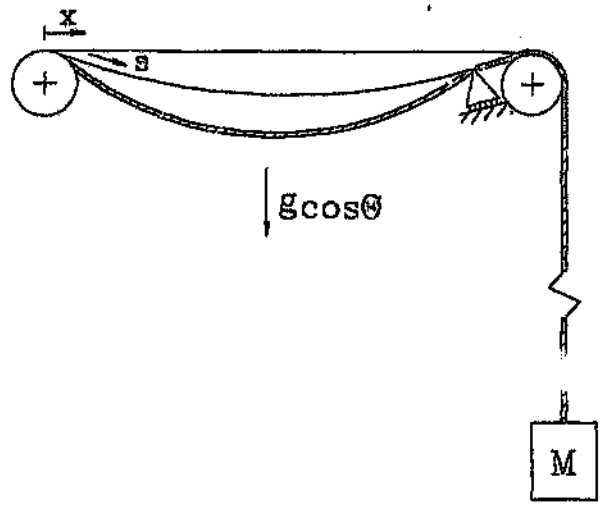

Figure 3.7: Mine hoist model

$$\kappa = \frac{\rho A^i g cos\theta}{P^i - \rho A^i (c^i)^2}$$

Equations 3.6-3.8 define the static tension distribution in the rope, which give:

$$\overline{F}^i(l_c) = P^i = M^i g + \rho A^i[(c^i)^2 + l_v g]$$

Thus the equilibrium curvature of the catenary is determined by:

$$\kappa = \frac{\rho A^i cos\theta}{M + \rho A^i l_v}$$

The equilibrium profile is defined by:

$$\mathbf{z} = \frac{1}{2}\mathbf{x}(1 - \mathbf{x})$$

where $\mathbf{z} = z/(mgl^2 cos(\theta)/H)$, $\mathbf{x} = x/l$; z represents the perpendicular distance between the profile and the chord, x represents the distance along the chord between the drum and sheave.

The equations of motion are simplified further by treating $u = O(v^2) = O(w^2)$, and retaining terms up to $O(v^3), O(w^3)$, and terms to $O(v^2), O(w^2)$ which have curvature κ as a coefficient[9]. Thus the equations of motion applied to analyse the mine hoist system are defined as:

$$u_{,tt} + 2c^i u_{t,s} - c^i\kappa\{v_{,t} + 2c^i v_{,s} + c^i\kappa u\} + c^i_{,t}\{1 + u_{,s} - \kappa v\} = (c_l^2 - c^{i^2})u_{,ss} + c_l^2\{v_{,s}v_{,ss} + w_{,s}w_{,ss} - \kappa v_{,s}\} \tag{3.9}$$

$$v_{,tt} + 2c^i v_{t,s} - c^i\kappa\{u_{,t} - c^i\kappa v\} + c^i_{,t}\{v_{,s} + \kappa u\} = (c_v^2 - c^{i^2})v_{,ss} + c_l^2\{(u_{,s}v_{,s})_{,s} + \frac{3}{2}v_{,s}^2 v_{,ss} + \frac{1}{2}w_{,s}^2 v_{,ss} + v_{,s}w_{,s}w_{,ss}\} - \kappa c_l^2\{vv_{,ss} - u_{,s} + \kappa v + \frac{1}{2}v_{,s}^2 - \frac{1}{2}w_{,s}^2\} \tag{3.10}$$

$$w_{,tt} + 2c^i w_{t,s} + c^i_{,t}w_{,s} = (c_v^2 - c^{i^2})w_{,ss} + c_l^2\{(u_{,s}w_{,s})_{,s} + \frac{3}{2}w_{,s}^2 w_{,ss} + \frac{1}{2}v_{,s}^2 w_{,ss} + w_{,s}v_{,s}v_{,ss}\} - \kappa c_l^2\{vw_{,ss} + w_{,s}v_{,s}\} \tag{3.11}$$

$$\overline{u}_{,tt} + 2c^i\overline{u}_{t,s} + c^i_{,t}\{1 + \overline{u}_{,s}\} = (c_l^2 - c^{i^2})\overline{u}_{,ss}$$

$$\left[A^i E\{\overline{\epsilon} - \epsilon a_1\}\right]|_{l_c} - \rho A^i(c^i)^2(\overline{u}_{,s} - u_{,s})|_{l_c} = [\frac{I}{R^2}(\dot{u}_1 + c^i)]_{,t}$$

$$-[A^i E\overline{\epsilon}]|_{l_v} = [M(\dot{u}_2 + c^i)]_t - \rho A^i c^i \dot{u}_2$$

where $c_l = E/\rho$, $c_v = P^i/\rho A^i$, represent the longitudinal and lateral wave speed respectively. c^i, c^i_t represent the transport velocity and acceleration of the rope respectively.

[9]The same equations result if the strain measure is defined as: $\epsilon = u_{,s} - \kappa v + \frac{1}{2}(v_{,s}^2 + w_{,s}^2)$

The displacements u, v, w are referenced to the local tangential, normal and bi-normal directions of the catenary profile respectively. In the limit where $\kappa = 0$, the unit vectors $\underline{t}^i, \underline{n}^i, \underline{b}^i$ align with the cartesian unit vectors $\underline{e}_1, \underline{e}_2, \underline{e}_3$, and the arc length co-ordinate s is replaced by the cord length co-ordinate x. The displacements in the cartesian plane u_c, v_c, w_c may be found by applying a transformation of axes $u_c = u + z_x v, v_c = v - z_x u, w_c = w$[10].

3.4 Conclusion

This chapter has developed the equations of motion applicable to the mine hoist system. However, further development is required to account for the excitation mechanism. In this regard, the excitation can be defined broadly as comprising of inertial loading of the system due to the acceleration/deceleration profile employed to accelerate the system to, or decelerate the system from the nominal winding velocity, and periodic boundary excitation at the drum due to the coil cross-over mechanism. The latter excitation comprises of periodic pulses normal, transverse and tangential to the drum radius. Once the rope has traversed the full drum width, a layer change occurs, which induces a significant axial and radial pulse to the rope at the drum end. Following the layer change, the traverse direction of the rope changes, and consequently the lateral component of the periodic excitation due to the coil cross-over profile changes phase by 180°. To complicate matters further, during the wind the system parameters are changing due to the decreasing or increasing length of the suspended vertical cable. Thus both the system parameters and the excitation are strictly non-stationary. This aspect introduces a substantial complication to a purely theoretical analysis of the system. Mankowski[1982] appreciated that a theoretical analysis of the system, which accounted for the complex excitation induced by the coil cross-over, as well as the nonlinear nature of the system would lead to a situation intractable to analysis, and thus proposed a numerical analysis of the system. Although ultimately a numerical simulation of the system would be essential, in the current study where the equations of motion have been developed, it is possible to examine the stationary nature of the system to stationary periodic excitation at the drum, prior to a numerical simulation. Achieving desirable stationary system characteristics would extend the current linear design approach, thus providing an initial selection of

[10]The equations of motion could have been derived to reflect displacements in a cartesian reference frame directly (Luogno et al [1984]), however it was decided to use a Lagrangian reference, since it results in a more concise presentation for the general equations. The strain measure applied by Luogno et al[1984], $\epsilon = u_{,x} + y_{,x}v_{,x} + \frac{1}{2}v_{,x}^2$ can be obtained by applying the co-ordinate transformations $u_c = u + z_x v$ $v_c = v - z_x u$ to the equivalent strain measure $\epsilon = u_{,s} - kv + \frac{1}{2}v_{,s}^2$ in the Lagrangian reference frame, and ordering terms appropriately.

system parameters for assessment in a numerical simulation. Since the excitation definition is dependent on whether a stationary or nonstationary analysis is pursued, it will be presented where appropriate in later chapters.

Chapter 4

Stationary Analysis of the Mine Hoist System

The purpose of this study is to identify conditions leading to, or promoting the occurrence of rope whip on mine hoist systems. Although the analysis of the large non-linear motion the system may present a challenging problem, it is not the initial focus of this study. Ideally, the analysis of the system should evolve in a consistent manner, supporting further more complex studies. This philosophy has been applied, where the current analysis of the mine hoist system consists of two phases. This chapter considers the first phase, which examines the steady state behaviour of the system in the absence of rope curvature and transport velocity. The rationale of this phase grows from the approach presented by Dimitriou and Whillier[1973], where the linear natural frequencies of the system were examined as a function of the shaft depth. Dimitriou and Whillier[1973] proposed their quasi-static linear analysis to identify regions where primary external resonance of the system could be expected. This analysis did not provide information regarding the severity of the interaction of the longitudinal and lateral modes, and hence the significance of the system tuning. Since the lateral excitation induced by the Lebus coiling motion is more significant than the longitudinal excitation, it is usual to attempt to avoid lateral catenary resonance, whilst neglecting the longitudinal system behaviour. This strategy is often not successful, particularly with respect to deep shafts. In fact it would be unusual to find a mine hoist system in practice, where primary external resonance of the system does not occur at some stage during the ascending or descending cycle. Although catenary resonance generally occurs, some systems exhibit more severe behaviour than others. This supports the notion that the overall system tuning may be an important feature influencing the system behaviour. This is a pertinent observation, since it is possible for

the lateral catenary motion to induce autoparametric system response due to the non-linear coupling between the lateral and longitudinal modes. Dimitriou and Whillier[1973] discussed this possibility qualitatively, and proposed that an autoparametric excitation mechanism was probably responsible for the observed lateral motion of the vertical section of the rope. Although the results presented by Dimitriou and Whillier[1973] provide a basis for a qualitative discussion, in practice they are only useful to define conditions of primary external resonance of the system. In order for an analysis to be practical, a quantitative analysis, accounting for the degree of excitation, damping, and the system tuning is required.

In the context of Industry, such an analysis should present the results in an unambiguous and simple manner. Ideally the analysis should identify regions of avoidance regarding the system parameters, rather than presenting the design engineer with a thorough non-linear steady state solution of the modal amplitudes, which may be multi-valued and even non-periodic. Linear dynamic characteristics of a system are generally well understood by graduate engineers, however this is not the case with regard to non-linear studies. It is for this reason that the concept of avoidance of non-linear interaction is proposed as a basis for assessing the dynamic behaviour of the system. Thus the method presented considers the avoidance of significant non-linear behaviour as a criterion for designing a mine hoist system. This criterion is based on the formulation of a datum steady state solution. The datum solution is chosen as the *linear* solution in the absence of primary external resonance.

Regions of non-linear interaction, where the response will deviate from the datum solution due to non-linear effects are identified by considering the stability of the motion in the context of the non-linear equations of motion. The linear stability analysis is defined by considering the stability of a system of equations with periodic coefficients, and consequently regions of avoidance are identified by constructing a stability chart which is synonymous with the Strutt stability chart. This represents the first phase of the analysis, where system parameters satisfying this criterion are selected. The non-stationary nature of the system, as well as transient excitation induced during a layer change requires a more advanced analysis. Chapter 5 presents a complete non-linear numerical simulation of the system, which accounts for the non-stationary system characteristics, transient excitations, rope curvature and winding velocity.

4.1 The Steady State Analysis

The non-linear equations of motion of the system developed in Chapter 3, are considered in the absence of catenary curvature and axial transport velocity. Initially, the lateral stability of the catenary was investigated under the influence of stationary periodic axial excitation. In this case the trivial condition $v(s,t) = w(s,t) = 0$ for the lateral motion represents a possible solution, where non-trivial lateral motion results as a consequence of dynamic instability. By applying the trivial condition, $v(s,t) = w(s,t) = 0$, to the equations of motion, an independent linear wave equation describes the forced steady state longitudinal system response This equation can be solved in closed form. Conversely the non-linear lateral equations of motion represent variational equations, which describe the stability of the trivial state of the lateral modes to small disturbances. Since the longitudinal steady state response may be defined in closed form, terms which couple the lateral variational equations to the longitudinal motion may be eliminated by direct substitution. Consequently the linear stability of the lateral variational modes is described by a set of Hill type equations with periodic coefficients. This analysis is presented in detail in Appendix B, where a perturbation technique and a harmonic balance method are applied to define regions of linear instability of the trivial lateral motion of the catenary to small disturbances. The stability analysis confirms that the lateral stability of the trivial state of the catenary is disrupted when conditions of simple and additive combination parametric resonance arise. Such conditions are related to the proximity of the axial excitation frequency to a condition of parametric resonance, and the amplitude of the parametric excitation, which is governed by the steady state longitudinal motion. Although the longitudinal excitation is small, this motion is amplified at longitudinal resonance, enhancing regions of lateral instability. Consequently narrow regions of parametric instability may result when the system is tuned to a condition of longitudinal resonance, even when the system is not closely tuned to a parametric resonance. The amplitude of the forced longitudinal response is sensitive to dissipation, and consequently these regions are quickly eroded by the inclusion of longitudinal damping.

Since the external longitudinal excitation of the system is small in comparison to the lateral excitation, the longitudinal response induced by the forced lateral motion is significant. Accounting for the lateral motion enhances the autoparametric nature of the system, whereby lateral catenary motion causes forced longitudinal system response. Autoparametric response is enhanced when the system tunes to an internal resonance, for instance where a longitudinal mode is tuned to twice the frequency of the lateral mode. In such a case, lateral motion may induce significant longitudinal reponse. In addi-

tion, due to the coupling between the lateral and longitudinal motion, regions of secondary resonance may arise when the excitation tunes to additive and difference combinations of the longitudinal and lateral modes.

As the most significant excitation to the system occurs axially, and in the out-of-plane lateral direction parallel to the winder drum surface, in-plane excitation and consequently in-plane response due to the drum excitation is assumed negligible. In the absence of catenary curvature direct excitation of lateral in-plane motion, due to curvature coupling with the longitudinal motion does not arise. Products coupling the in-plane and longitudinal motion exist in the in-plane equation of motion, thus the in-plane modes are parametrically excited, and consequently non-trivial response arises through instability or bifurcation. Thus the *linear* steady state out-of-plane response due to longitudinal and lateral out-of-plane excitation forms the basis for constructing a datum solution. Three dimensional motion, or rope whip followed by further intermodal energy exchanges between the longitudinal and lateral modes is initiated as a consequence of bifurcation of the planar steady state motion.

Longitudinal and lateral damping is accounted for in the steady state datum solution. The particular form of the damping model assumed is of significance, particularly with regard to the longitudinal response. In the past, Industry has assumed that a relative proportional viscous damping mechanism[1] applied to the longitudinal dissipation. Rudimentary tests performed by industry (Thomas et al.[1987], Greenway[1989]) approximate the dimensionless modal damping ratio of the fundamental longitudinal mode at $\approx 2-3\%$ of critical. Further experimental tests were performed at Elandsrand Gold Mine (Constancon [1992]) in an attempt to determine an appropriate damping mechanism. A detailed discussion regarding the longitudinal damping estimates extracted from the experimental results is presented in Appendix G. These results indicate that the first mode is more highly damped than higher modes, a result which is inconsistent with a relative proportional viscous damping mechanism. A general proportional damping model[2] appears to characterise the longitudinal dissipation characteristics of the mine hoist rope adequately. This model is applied for convenience, and is not considered to represent the true nature of the damping mechanism. With regard to the lateral damping characteristics of a mine hoist rope, Mankowski[1986] presents dissipation factors extracted from a laboratory experiment. Based on Mankowski's dissipation factors, it appears

[1] A relative proportional damping mechanism considers the material dissipation characteristics to be distributed in a manner which is proportional to the stiffness properties of the rope.

[2] A general proportional damping mechanism considers the material dissipation characteristics to be distributed in a manner which is proportional to both the stiffness and mass properties of the rope.

that aerodynamic drag may represent a more significant lateral damping effect than the inherent properties of the hoist rope. This is discussed further in Appendix H. In the context of the stationary steady state analysis, a proportional lateral damping mechanism will be assumed, where the damping in the fundamental mode is of the order of 0.05% of critical.

4.2 The Linear *Datum* Solution

In order to pursue the strategy proposed, it is necessary to formulate the datum solution to provide a basis for the stability analysis, and the comparative study of the system tuning. In the absence of axial transport velocity and catenary curvature, the undamped non-linear equations of motion for the catenary, as developed in chapter 3, reduce to:

$$u_{,tt} = c^2 u_{,ss} + c\{v_{,s}v_{,ss} + w_{,s}w_{,ss}\} \tag{4.1}$$

$$v_{,tt} = \bar{c}v_{,ss} + c^2\{(u_{,s}v_{,s})_{,s} + \frac{3}{2}v_{,s}^2 v_{,ss} + \frac{1}{2}w_{,s}^2 v_{,ss} + v_{,s}w_{,s}w_{,ss}\} \tag{4.2}$$

$$w_{,tt} = \bar{c}w_{,ss} + c^2\{(u_{,s}w_{,s})_{,s} + \frac{3}{2}w_{,s}^2 w_{,ss} + \frac{1}{2}v_{,s}^2 w_{,ss} + w_{,s}v_{,s}v_{,ss}\} \tag{4.3}$$

where c, $\bar{c}$ represents the longitudinal and lateral wave speed respectively. The three dimensional motion of the catenary is described by the displacements $u(s,t)$, $v(s,t)$, $w(s,t)$, which represent the longitudinal, in-plane lateral and out-of-plane lateral motion respectively. In the absence of in-plane lateral excitation, a trivial solution is assumed for the in-plane lateral displacement, ie. $v(s,t) = 0$. Since the in-plane motion is assumed trivial, the in-plane equation of motion may be discarded at this stage. Thus the equations of motion describing the planar response of the catenary due to out-of-plane lateral and axial boundary excitation reduce to:

$$u_{,tt} = c^2 u_{,ss} + c\{w_{,s}w_{,ss}\} \tag{4.4}$$

$$w_{,tt} = \bar{c}w_{,ss} + c^2\{(u_{,s}w_{,s})_{,s} + \frac{3}{2}w_{,s}^2 w_{,ss}\} \tag{4.5}$$

The solution of equations (4.4),(4.5) leads to the definition of the non-linear planar steady state response of the system. A consistent non-linear analysis would address these equations by approximating the solution via a harmonic balance or alternative method. Although this was an attractive analytical route to follow, it is important to consider the significance of such complexity in terms of a practical industrial solution, and particularly in the context of defining a simple design criterion. It is for this reason, that a linearised solution to equations (4.4),(4.5) is sought, which reflects single valued response and provides a datum for approximating the degree of non-linear interaction which could be expected.

Primary external resonance of the catenary represents a principal consideration in the assessment of the mine hoist system. In general such a condition is unavoidable. However in these regions it would be advantageous to assess the system parameters, so that further non-linear coupling could be minimised. From a practical perspective it is accepted that mine hoist ropes will reflect dynamic behaviour, thus at this stage the knowledge of the steady state non-linear amplitude is of secondary importance with regard to the achievement of the best possible condition of tuning to minimise or avoid such behaviour.

Secondary conditions of resonance have not received attention in the context of the mine hoist system. Here the linear solution approximates a possible branch of the non-linear motion. Secondary resonance arises when this solution branch is unstable, and the response is attracted to an alternative dynamic state. In the context of this discussion, a linearised form of equations (4.4),(4.5) is proposed for the datum solution as:

$$u_{,tt} = c^2 u_{,ss} + c\{w_{,s}w_{,ss}\} \tag{4.6}$$

$$w_{,tt} = \bar{c}w_{,ss} \tag{4.7}$$

These equations reflect the coupling between the lateral and longitudinal motion, where the lateral steady state motion provides direct excitation to the

longitudinal system. Retaining the non-linear lateral coupling term in the longitudinal equation of motion is consistent with the ordering $uo(w^2)$. Conversely, the counter coupling of the longitudinal response on the lateral motion is discarded, since if $uo(w^2)$, then the quadratic term $(u_{,s}v_{,s})_{,s}\, o(w^3)$. This implies that the lateral motion is small, and hence excludes the condition of primary external resonance of the catenary. Away from regions of primary external resonance of the catenary, the cubic term $w_g^2 w_{,ss}$ may be neglected. Thus the datum solution proposed is valid for identifying regions of secondary resonance, however due to the neglect of cubic terms, it is not valid close to a condition of primary external resonance. However, it is the boundary of stability which is sought, which may be close to, but not exactly tuned to a condition of primary external resonance. Since the solution essentially describes the lower branch of the response on either side of the resonant condition, it cannot predict regions of subcritical stability, where a higher amplitude stable solution branch may exist, which may be reached through initial conditions due to transient forces. The intention of the analysis is to identify regions where non-linear interaction is likely, and even under conditions of primary external resonance of the catenary, the datum solution will reflect the compliance of the longitudinal to lateral tuning, and it is proposed that the exponent of growth associated with the unstable datum solution in this region provides a comparative basis for assessment. Thus the stability analysis of the datum solution requires both the definition of the region of instability as well as the exponent of growth. This is a normal consequence of the stability technique chosen to examine the stability of the datum solution to small disturbances.

In conclusion, the datum solution is defined to provide a basis for a comparative assessment of the system tuning with regard to system parameters, and is not intended to represent the global non-linear steady state solution. Since the datum solution is valid in the absence of primary external resonance, regions of secondary resonance may be identified confidently. In light of the non-stationary nature of the system, an extensive study of the non-linear planar stationary motion would be counter productive, since numerical simulation would ultimately be required. It is emphasised that the datum solution was primarily motivated to illustrate the existence of secondary resonance conditions, which are less obvious to a designer. It is expected that further research will refine the datum solution, to account for primary external resonance of the catenary. Appendix J presents a further discussion of the stationary steady state behaviour in the context of non-linear studies presented in the literature, and with regard to the existence of secondary and internal resonance conditions which are defined via the method of multiple scales. Appendices C,D,E present the closed form datum solution in the presence of general proportional damping, and axial and lateral out-of-plane boundary excitation at the winder drum, due to the first two harmonics of the Lebus groove excitation.

4.3 Stability of the *Datum* Solution

The steady state planar response, which is referred to as the datum solution, and represents the closed form continuous solution to equations (4.6),(4.7), is considered in the context of the non-linear equations (4.4),(4.5) of motion of the catenary. Variational equations of motion are constructed by considering small perturbations around the steady state datum solution. This is represented by:

$$\begin{aligned} u(s,t) &= \overline{u}(s,t) + u_D(s,t) \\ v(s,t) &= \overline{v}(s,t) \\ w(s,t) &= \overline{w}(s,t) + w_D(s,t) \end{aligned} \tag{4.8}$$

where $\overline{u}(s,t)$, $\overline{v}(s,t)$, $\overline{w}(s,t)$ represent small variations in the longitudinal, in-plane lateral and out-of-plane lateral motion with respect to the steady state datum solution $u_D(s,t)$, $v_D(s,t)$, $w_D(s,t)$. Substituting equations (4.8) into equations (4.4),(4.5), and considering the homogeneous[3] component of the linearised equations leads to[4]:

$$[1+\zeta\delta(s-l_1)+\eta(s-l_2)]\overline{u}_{tt} = \mu\overline{u}_{t,ss}+c^2\overline{u}_{,ss}+c^2\{w_{,s}\overline{w}_{,s}\}_{,s}[H(s)-H(s-l_1)] \tag{4.9}$$

$$\overline{v}_{,tt} = \mu_l\overline{v}_{t,ss} + \overline{c}^2\overline{v}_{,ss} + c^2\{(\overline{v}_{,s}u_{,s})_{,s} + \frac{1}{2}(w^2_{,s}\overline{v}_{,s})_{,s}\} \tag{4.10}$$

$$\overline{w}_{,tt} = \mu_l\overline{w}_{t,ss} + \overline{c}^2\overline{w}_{,ss} + c^2\{(\overline{w}_{,s}u_{,s})_{,s} + (w_{,s}\overline{u}_{,s})_{,s} + \frac{3}{2}(w^2_{,s}\overline{w}_{,s})_{,s}\} \tag{4.11}$$

$\zeta = I/\rho AR^2, \quad \eta = M/\rho A$

where l_1 represents the catenary length, whilst l_2 represents the total cable length. The longitudinal equation (4.9) is defined over the entire length of the

[3]Non-Homogeneous terms arise in the lateral variational equations. These terms represent a *residue* related to the neglect of the non-linear terms in the datum solution. In the presence of small steady state lateral motion ie. away from regions of primary external catenary resonance, the residue is considered small and is neglected.

[4]The boundary conditions at the sheave, and the skip are introduced via the use of the Dirac delta and Heaviside step functions. Thus the equations (4.9,4.10,4.11) represent the overall system equations rather than just those pertaining to the catenary.

rope $0 \leq s \leq l_2$, whilst the lateral equations (4.10),(4.11) are defined only over the catenary length $0 \leq s \leq l_1$.

The variational equations of motion may be reduced to ordinary differential form by applying a normal mode expansion for the continuous variables ie.

$$\overline{u} = \sum \phi_i(s) p_i(t)$$

$$\overline{v} = \sum \Phi_i(s) q_i(t)$$

$$\overline{w} = \sum \Phi_i(s) r_i(t) \tag{4.12}$$

where $\phi(s)$, $\Phi(s)$ represent the longitudinal and lateral eigen functions of the linear system. These are defined in Appendix C, D. Performing the orthogonalisation, leads to a set of coupled linear parametrically excited ordinary differential equations of the form:

$$[I]\{\ddot{y}\} + [2\zeta_n\omega_n]\{\dot{y}\} + \left[[\omega_n^2] + [A_d] + \sum_{n=1}^{4}[P(n\Omega t)]\right]\{y\} = 0 \tag{4.13}$$

where:

$$\{y\}^T = (p_i, q_i, r_i)$$

$$\sum_{n=1}^{4}[P(n\Omega t)] = \begin{bmatrix} 0 & 0 & U_{uw}(\Omega t, 2\Omega t) \\ 0 & V_{vv}(\Omega t, 2\Omega t, 3\Omega t, 4\Omega t) & 0 \\ W_{uw}(\Omega t, 2\Omega t) & 0 & W_{ww}(\Omega t, 2\Omega t, 3\Omega t, 4\Omega t) \end{bmatrix}$$

Where $[A_d]$ represents an initial stress matrix which represents the change in the variational natural frequencies due to a change in the average dynamic tension in the catenary. $[A_d]$ is defined in Appendix F.3.

The parametric coupling matrix $[P(n\Omega t)]$ and its constituent submatrices are defined in Appendix (F). It is pertinent to note that although modal truncation may occur with respect to the variational equations of motion, due to the application of the normal mode expansion, the datum solution is obtained

as a continuous solution and is not truncated. Periodic components in the parametric coupling matrix are generated up to the fourth harmonic of the Lebus coil cross-over frequency as a result of the first and second harmonic of the Lebus groove excitation. The parametric excitation matrix contains submatrices coupling the longitudinal and lateral modes. It is well established that regions of simple parametric resonance are dependent on the diagonal terms in the parametric excitation matrix (Hsu[1963]). Conversely regions of combination parametric resonance are dependent on the off diagonal terms. Thus simple parametric resonance does not arise with regard to the longitudinal modes alone. However, since the submatrices $[U_{uw}]$, $[W_{uw}]$ exist, regions of combination parametric resonance arise with respect to the longitudinal and lateral out-of-plane modes. Since the submatrices $[U_{uw}]$, $[W_{uw}]$ are not identical, it is possible that both additive and difference regions of combination resonance may arise, depending on the system parameters. Since the submatrices $[V_{vv}]$, $[W_{ww}]$ are symmetric, both simple and additive combination parametric resonance can occur with regard to the lateral in- and out-of-plane modes.

4.3.1 Stability of the Variational Equations

The criterion proposed as a design strategy for the mine hoist system amounts to an examination of the stability of the datum solution to small disturbances. The stability of the motion is dependent on the stability of equation (4.13). Linear systems with periodic coefficients have received much attention in the literature. A general discussion regarding parametric excitation is presented in Appendix K. A number of techniques can be applied to define the boundary of stability, for instance direct numerical integration combined with Floquet theory, perturbation techniques and the harmonic balance method. The first is numerically intensive, whilst the second is limited to the existence of small excitation and requires special attention for anomalous conditions of tuning (Hsu[1963]). Since a general approach is required which is capable of providing a stability chart regardless of the state of tuning, or the amplitude of excitation, a harmonic balance technique was applied. Takahashi[1981b] described an algorithm for determining regions of simple and combination parametric resonance of a parametrically excited system. This technique was applied in this study. A discussion of the method proposed by Takahashi[1981b] is presented in Appendix K.

The method is based on assuming an harmonic expansion for the response in

the form:

$$\{y(t)\} = e^{\lambda t}\{\frac{1}{2}\mathbf{b}_o + \sum_{n=1}^{\infty}(\mathbf{a}_n sin\ n\Omega t + \mathbf{b}_n cos\ n\Omega t)\} \tag{4.14}$$

Direct substitution of the assumed expansion (4.14) into equation (4.13), and applying the harmonic balance method leads to a relationship defining the response of the system in terms of the exponent λ, and the coefficients $\mathbf{b}_o, \mathbf{a}_n, \mathbf{b}_n$. Takahashi[1981b] demonstrated that this relationship could be formulated conveniently in matrix form. As a result, the method reduces to an eigenvalue extraction for the exponent λ. The stability of the system is thus dependent on $Re(\lambda) < 0$. In regions of instability, the exponent $Re(\lambda)$ reflects the initial exponential rate of growth of a disturbance away from the steady state solution. This exponent is extracted as a normal consequence of the solution, and is valuable in terms of the comparative study, since it is applied to assess the severity of a region of instability.

4.3.2 Experimental Validation

The method proposed to examine the stability of the steady state lateral motion of the catenary was confirmed experimentally. An experiment was conducted on a laboratory model of the mine hoist system. A photographic illustration of the experimental model is presented in figure 4.1. The model comprises of a guitar string, a pulley and a dead weight. The guitar string passes from a steel slider at one end, over a pulley wheel to a dead weight at the other end. An electro-dynamic shaker was applied to excite a single frequency sinusoidal lateral motion in the catenary[5]. The model was constructed so as to enable easy adjustment of the catenary length, and hence tuning of the lateral natural frequencies. It was found that the longitudinal system exhibited a single natural frequency in the test bandwidth, which could be tuned to some degree by changing the mass of the dead weight[6]. The free length between the pulley and dead weight was kept as short as possible to prevent lateral parametric excitation of this section[7]. The parameters of the model

[5]Since position feedback control was not applied to the shaker, the motion of the slider was monitored to ascertain that the system response did not affect the excitation wave form.

[6]The higher longitudinal modes fell well beyond the the test bandwidth of 0-100Hz. The first longitudinal mode occurred at approximately 20Hz, whilst the second occurred at $\approx$ 1.2 kHz.

[7]When a longer free length was accommodated, at certain tuning conditions, violent interactions between the catenary and free length section were evident. This presents an interesting condition of practical importance which is currently being considered.

Table 4.1: Laboratory model parameters

Parameter		1	2	3
Catenary Length	$l_c(m)$	0.479	0.485	0.790
Dead Weight	M (kg)	1.95	1.45	1.9
Pulley Inertia	J (kgm^2)	1.56×10^{-5}	1.56×10^{-5}	1.56×10^{-5}
Linear String Density	m (kg/m)	0.00745	0.00745	0.0268
Longitudinal Wave Speed	c (m/s)	1512.6	1512.6	845
Longitudinal Damping Factor	ζ (%)	0.2	0.2	0.8
Lateral Damping Factor	$\bar{\zeta}$ (%)	0.125	0.125	0.35

were accurately measured, and are tabulated in table 4.1. The most difficult parameter to measure was the longitudinal and lateral damping factor. These factors were approximated by impulsively exciting the system and determining the modal bandwidth of each mode.

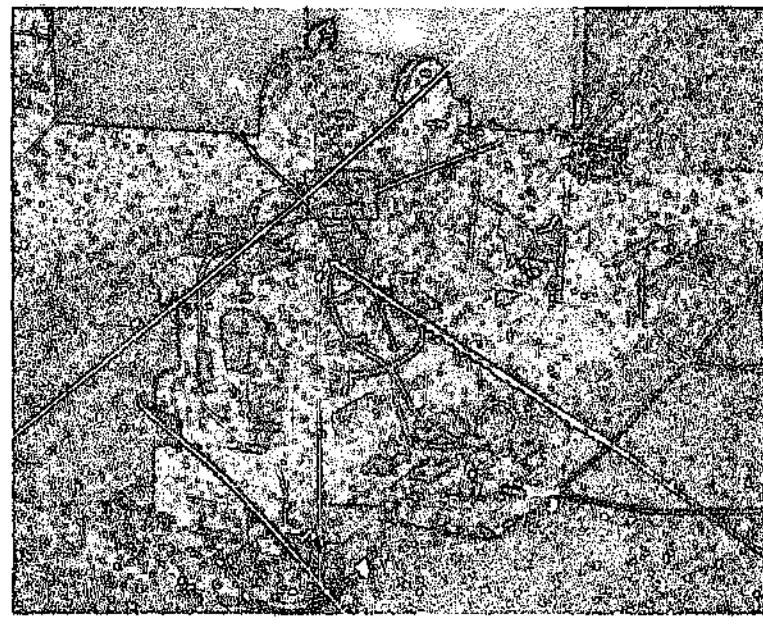

Figure 4.1: Laboratory model of the mine hoist system

The lateral amplitude of the excitation applied to the slider was monitored with an LVDT. The motion of the catenary in the lateral in- and out-of-plane direction was monitored with proximity probes. Since the range of the

Table 4.2: Tuning conditions of the laboratory model

Case	ω	$\overline{\omega}_1$	Resonance Condition
1	20.34 Hz	52.89 Hz	$\Omega \approx \overline{\omega}_1, \Omega \approx \overline{\omega}_2$ $\Omega \approx \omega + \overline{\omega}_1 \approx 73.23 Hz$ $\Omega \approx \frac{1}{2}(\overline{\omega}_1 + \overline{\omega}_2) = \frac{1}{2}\overline{\omega}_3 \approx 79.33 Hz$
2	22.5 Hz	45 Hz	$\Omega \approx \overline{\omega}_1, \Omega \approx \overline{\omega}_2$ $\Omega \approx \omega + \overline{\omega}_1 \approx 67.5 Hz$ $\Omega \approx \frac{1}{2}(\overline{\omega}_1 + \overline{\omega}_2) \approx 67.5 Hz$
3	16.55 Hz	16.69 Hz	$\Omega \approx \overline{\omega}_1, \Omega \approx \overline{\omega}_2, \Omega \approx \overline{\omega}_3$ $\Omega \approx \frac{1}{2}(\omega + \overline{\omega}_1) \approx \overline{\omega}_1 \approx 16.62 Hz$ $\Omega \approx \omega + \overline{\omega}_1 \approx \overline{\omega}_2 \approx 33.24 Hz$ $\Omega \approx \omega + \overline{\omega}_2 \approx \overline{\omega}_3 \approx 50 Hz$

proximity probes was limited to $\pm 0.5mm$, they were positioned close to the pulley wheel where the lateral amplitudes remained small. The motion of the dead mass was monitored with a piezo crystal accelerometer. The transducer signals were analysed continuously by constructing the autospectra of each transducer signal on a Genrad 2515 analyser.

The purpose of the experiment was to confirm the existence of secondary regions of resonance related to combination parametric resonance of the out-of-plane lateral and longitudinal modes, as well as additive combination parametric resonance involving either the in-plane or out-of-plane lateral modes only. Three cases of system tuning were considered as presented in table 4.2, where Ω, ω, $\overline{\omega}_i$ represent the excitation frequency, and the longitudinal and lateral natural frequency respectively.

The first case represents a general state of tuning, where the combination resonance involving the longitudinal and first lateral mode is distinct from other combination resonances involving the lateral modes only. The second case considers the condition where a region of combination resonance involving the longitudinal and first lateral mode overlaps with the second region of combination resonance of the first and second lateral modes, as well as the second region of primary resonance of the third lateral mode etc. The third case considers the condition where the longitudinal and first lateral mode are closely tuned to one another. In this case, regions of combination parametric resonance occur simultaneously with conditions of primary external resonance of the lateral modes. The second and third cases coincide with a condition of internal resonance ie. $2\overline{\omega}_1 = \omega$, $\overline{\omega}_1 = \omega$, as defined by the perturbation analysis presented in Appendix J .

The boundary of stability of the planar steady state motion was determined experimentally by adjusting the excitation frequency, and then increasing the excitation amplitude until the response reflected a sudden growth in the motion. This condition was examined by viewing the signals from the proximity probes as a Lissajous plot on an oscilloscope. It was clearly evident that once a region of instability was entered, the steady state forced response was disrupted, indicating a change in the nature of the motion. In the first case, the boundary of stability associated with the longitudinal and lateral combination resonance resulted in unstable planar motion, which remained planar[8]. However, the combination resonance relating to the lateral modes only ie. $\Omega = \frac{1}{2}(\overline{\omega}_1 + \overline{\omega}_2) \approx \frac{1}{2}\overline{\omega}_3 \cdots$ was characterised by non-planar motion[9]. In regions close to primary external resonance of the lateral modes ie.$\Omega = \overline{\omega}_i$, the boundary of stability was characterised by a growth of the in-plane motion, leading to non-planar whirling motion.

With regard to the second and third case, the boundary of stability was characterised by planar and non-planar motion. With regard to the third case, it was found that since the natural frequency of the longitudinal mode was slightly lower than that of the first lateral mode, the left hand side of an unstable region of instability was characterised by a combination resonance involving the lateral and longitudinal modes; On this boundary, the planar steady state motion became unstable and initially remained planar. The right hand side of an unstable region was characterised by a growth of the in-plane motion immediately leading to non-planar motion.

In all cases, for a large enough amplitude, violent non-planar motion was observed. It was also evident that once this motion had evolved, it was difficult to detune the resonance by simply increasing or decreasing the excitation frequency.

The stability chart of the steady state motion constructed from the experimental model was compared with the stability chart obtained via the analytical technique proposed in this chapter. The variational equations were truncated to account for a single longitudinal mode, and three in and out-of-plane lateral modes. The harmonic balance method was applied to determine these regions, where a five term harmonic expansion was employed. The accuracy of the stability chart was verified via direct numerical simulation of the variational equations. The experimental and analytical stability charts pertaining to the

[8]On the boundary of stability, the autospectra of the longitudinal and lateral response indicated dominant response close to the natural frequencies related to the longitudinal and first lateral modes respectively.

[9]The autospectrum of the lateral motion indicated multi-modal response in the lateral modes.

laboratory model are presented in figure 4.2 for the three cases considered. The experimental results are indicated in figure 4.2 by a +, whilst shaded regions indicate the analytically determined regions.

Figure 4.3 illustrates typical stable and unstable motion observed during the experiment. The photographs were obtained by strobing the catenary at a slightly lower frequency than the excitation frequency, and using a time exposure to photograph the motion. These photographic slides illustrate the stable/unstable motion of the catenary on the boundary of stability for the third case of tuning. In this case, the excitation frequency and amplitude were such that the system passed from stable to unstable motion through the left hand boundary of the second and third region of primary external resonance.

Generally, the experimentally determined boundary of stability correlates well with the analytically determined regions of instability. Since the datum solution is representative of the steady state motion away from conditions of primary external resonance, the boundary of stability associated with regions close to primary external resonance are approximate. However, since the condition of primary external resonance is contained within the region of instability, and since the lateral damping factor is small and consequently the modal bandwidth is small, reasonable accuracy was achieved even for this condition. With regard to the first case of tuning, the second region of combination parametric resonance related to the lateral modes ie. $\Omega = \frac{1}{2}(\varpi_1 + \varpi_2) = \frac{1}{3}\varpi_3$ indicates stiffening behaviour, as predicted by the analytical solution. It was difficult to excite this region, since more precise tuning was required, and consequently it was not easy to tune the system to a condition of neutral stability and thus identify the boundary precisely. It is also important to recognise that although the laboratory model is representative of the mine hoist system, the analytical technique models a slider at the pulley end. It is proposed that this contributes to the higher degree of stiffening predicted analytically for the region, in comparison to the experimental results; also as discussed in chapter 5, the application of a normal mode technique contributes to stiffer behaviour.

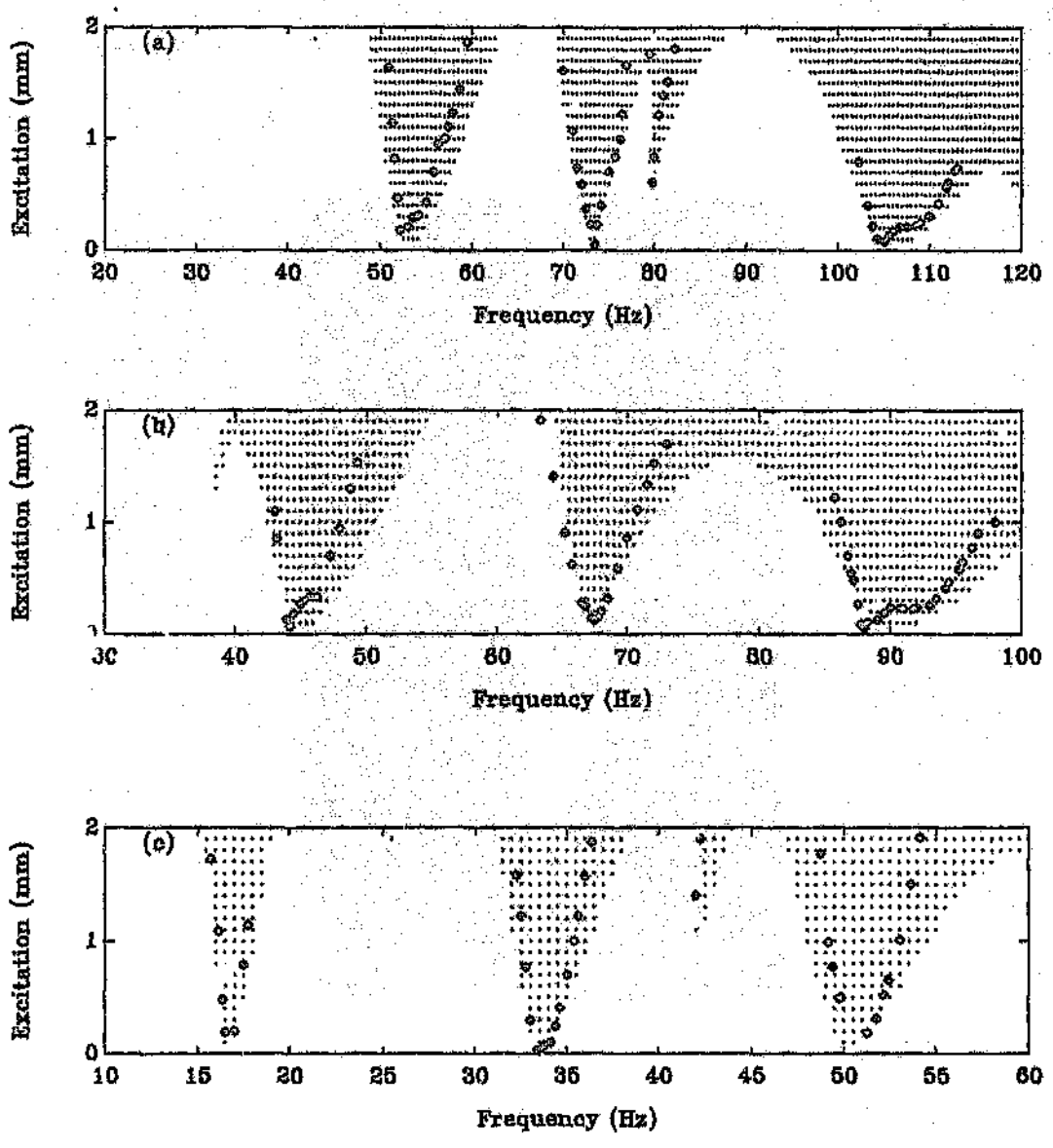

Figure 4.2: Stability chart of the laboratory model
a) Case 1.
b) Case 2.
c) Case 3.
+ Experimental

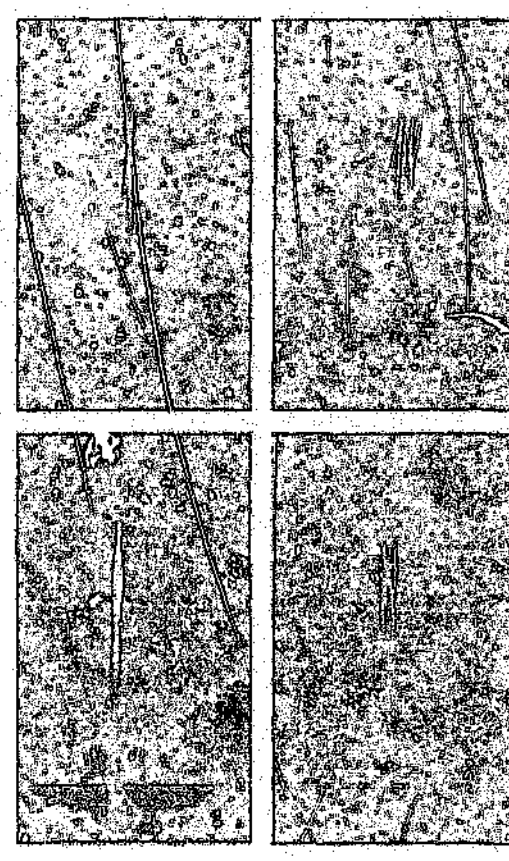

Figure 4.3: Stable/unstable catenary motion - Case 3.

a) Stable motion $\Omega \approx \varpi_2$ b) Unstable motion $\Omega \approx \varpi_2$
c) Stable motion $\Omega \approx \varpi_3$ d) Unstable motion $\Omega \approx \varpi_3$

4.4 The Kloof Mine Hoist System

The stability analysis developed in this chapter is applied to examine the Kloof Mine hoist system. As discussed in chapter 1, this system experienced severe rope whip during the ascending cycle. Dimitriou and Whill[...1973] analysed this system by examining the quasi-static description of the system characteristics. Although this is a useful approach to identify potential regions of primary external resonance, it fails to account for the physical system parameters such as damping, the level of excitation and the potential influence of lateral to longitudinal tuning. The Kloof Mine Hoist system parameters applied in the analysis are presented in table 4.4. Figure 4.4(a,b) presents the linear dynamic characteristics of the system during the descending and ascending cycle respectively. The horizontal lines in figure 4.4(a,b) represent the first and second harmonic of the Lebus excitation frequencies, at a constant nominal winding speed of 15 m/s[10]. The vertical lines reflect the layer change-over locations. It is evident in figure 4.4(b) that during the ascending cycle the second lateral mode of the catenary is resonant at approximately 700m. This occurs simultaneously with the second longitudinal mode. Prior to this condition at approximately 900m, the fourth longitudinal mode is tuned to twice the second lateral catenary mode and hence a condition of internal resonance arises.

The stability chart of the steady state solution was constructed as a function of shaft depth and the nominal winding velocity, whilst the excitation amplitude at the winder drum, as determined from the Lebus groove geometry[11] was held constant. The purpose of this chart is to reflect regions of avoidance of likely non-linear interaction, and hence to determine a viable winding speed for the given system parameters. Only two regions of instability were evident on the ascending cycle, and these were related to direct external resonance of the third and second lateral catenary modes, at the beginning and end of the wind respectively. The eigenvalue exponents associated with these regions did not reflect any local maximum, or special condition of tuning between the lateral and longitudinal system. Figure 4.5 illustrates the stability chart for the ascending cycle[12]. The region of instability is related to primary external resonance of the second and fourth catenary modes. Although the steady state or datum solution accounts for conditions away from primary external

[10]The nominal winding speed reflects the drum surface speed, consequently the rope speed increases as the number of rope layers increase.

[11]Appendix A presents the definition and calculation of the Lebus groove excitations.

[12]The shaded region of the chart represents an unstable solution, where the eigenvalue of exponent λ is greater than zero. The contours on the shaded region represent the magnitude of the exponent λ. The maximum exponent is 110, whilst the countour lines represent an exponent of 0.01,.1,1,10,50,100.

resonance of the catenary, it is clearly evident from the eigenvalue plot that a significant region of interaction is predicted close to 15m/s, which spans approximately 100 m from 650m-750m. This region is characterised by the interaction of two conditions of resonance. The solid lines on this figure reflect various conditions of resonance. The solid line represented by (b) reflects the additive combination resonance of the second catenary and second longitudinal mode. Even though the second catenary mode is resonant away from this winding speed, the eigenvalue plot reflects that the severity of the tuning drops.

In order to accentuate regions of secondary resonance, a similar stability chart was constructed for the ascending and descending cycles, where the winding velocity was maintained at 15 m/s, whilst the amplitude of the excitation and hence of the steady state motion was increased proportionately. These charts are presented in figures 4.6,4.7 respectively. In these charts the nominal Lebus groove excitation is amplified by a factor of ϵ. Secondary regions of resonance are evident in these figures. However substantial steady state excitation would be required to activate such regions. With regard to the ascending wind, presented in figure 4.6, the region at 250m is related to a condition of parametric combination resonance of the first lateral and longitudinal modes, which tune to the first harmonic of the Lebus excitation frequency. The region to the right of the primary resonance ($\approx 900m$) region is related to resonance of the fourth longitudinal mode, combined with the internal resonance between the fourth longitudinal and second lateral modes. The descending cycle exhibits similar regions of secondary resonance. The two most significant regions are related to primary external resonance of the third lateral catenary mode ($\approx 500m$) and of the second lateral mode towards the end of the wind ($\approx 1700m$). The latter condition is larger and more important as it spans a greater section of the wind. This is confirmed by the simulation results presented in Chapter 5.

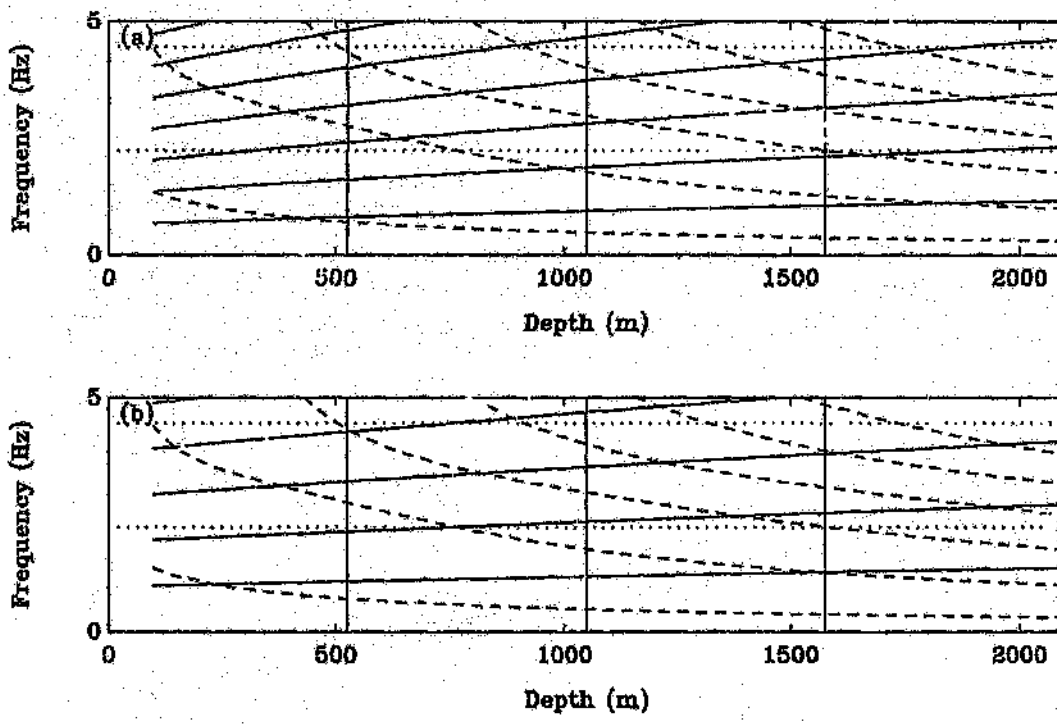

Figure 4.4: .Kloof Mine: Linear dynamic characteristics.

a) Descending cycle	b) Ascending cycle
...	Lebus groove excitation frequency
– –	Longitudinal natural frequencies
——	Lateral natural frequencies

Table 4.3: Kloof Mine - System parameters

J	Sheave Inertia.	15200 kgm^2
M	Skip Mass.	7920 kg
M0	Skip Pay-load.	9664 kg
m	Linear Rope density.	8.4 kg/m
V	Nomina' Winding Speed.	15 m/s
De	Depth of wind.	2100m
Lc	Catenary Length.	74.95 m
E	Effective Youngs Modulus of the rope.	$1.1E^{11}$
Ax	Effective steel area of the rope.	$0.001028m^2$
β	Cross over arc.	0.2 rad
Dd	Drum Diameter.	4.28 m
Ds	Sheave Diameter.	4.26 m
Dr	Rope Diameter.	0.048 m
μ_a	General proportional damping parameter	0.159
$\mu_b(s_2)$	General proportional damping parameter	$10.49s_2$
ζ_1	Lateral proportional modal damping ratio	0.05%

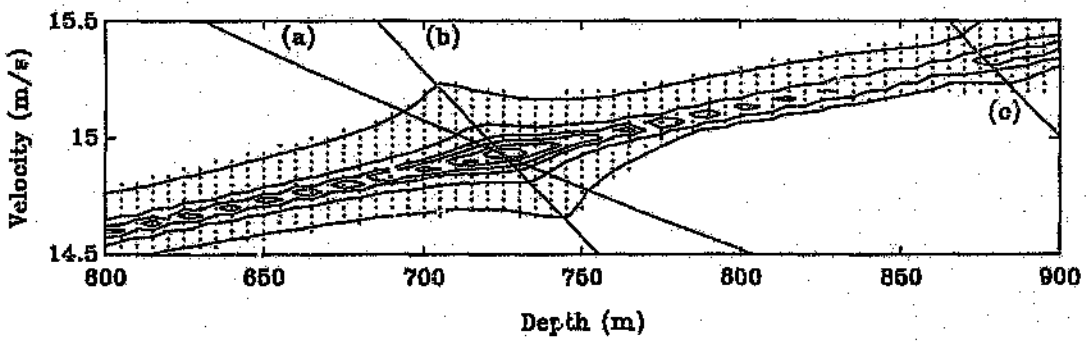

Figure 4.5: Stability chart of the steady state datum solution - Ascending

a) $2\Omega_{Lebus} = w_2 + \varpi_2$
b) $\Omega_{Lebus} = \varpi_2$
c) $\Omega_{Lebus} = \varpi_4$

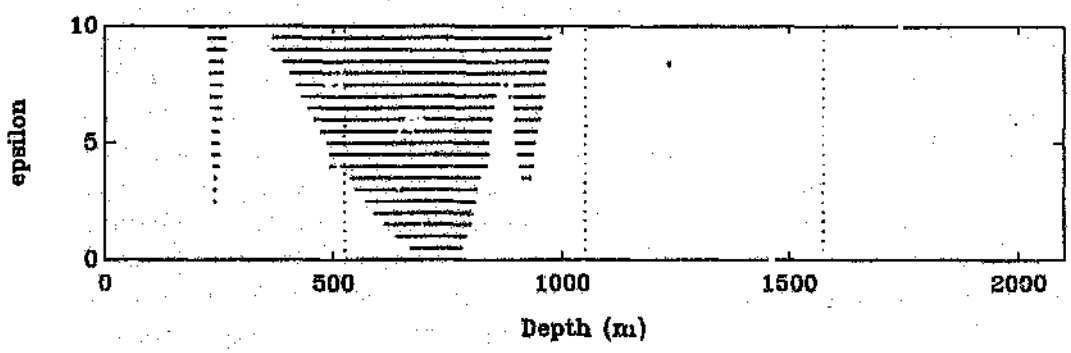

Figure 4.6: Stability chart of the steady state datum solution - Ascending
Increasing amplitude of excitation ϵ, $\zeta_1 = 0.05\%$

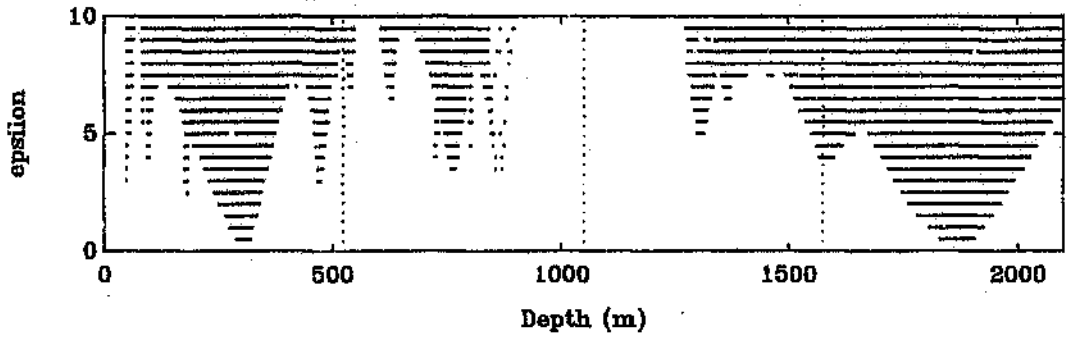

Figure 4.7: Stability chart of the steady state datum solution - Descending
Increasing amplitude of excitation ϵ, $\zeta_1 = 0.05\%$

4.5 Conclusion

The purpose of the steady state analysis was to identify regions where non-linear interaction is likely. The analysis was validated experimentally and then applied to examine the Kloof Mine hoist system characteristics. Satisfactory correlation was achieved with respect to the laboratory experiment. In the context of a hoisting system, the analysis would provide a preliminary assessment of the hoist characteristics. It is important to emphasise that the stationary steady state analysis was intended to compliment the linear approach proposed by Dimitriou and Whillier[1973]. It is limited in that it does not account for the non-stationary behaviour of the system, nor does it account for the transient excitation introduced during the acceleration/deceleration phases or during layer change-overs. In effect, the mine hoist system does not achieve steady state; the effect of the winding velocity is to attenuate and delay the resonant condition. The transient excitations introduced at the layer change, may also significantly influence the dynamic state of the system; the location of layer changes is pertinent, since the phase of the out-of-plane lateral excitation changes by 180° after a layer change. This mechanism can be used to advantage to precipitate resonant amplitudes from developing further. In terms of the stationary analysis of the Kloof Mine hoist system, the analysis serves to confirm to some degree the observation of Dimitriou and Whillier that the lateral motion may induce significant longitudinal interaction at approximately 700m. It is evident from the stability (figure 4.5) plot that this occurs in the vicinity of 15m/s. Hopefully such information would draw attention to this condition of tuning, and such a condition would be avoided. For realistic stationary excitation levels calculated from the drum geometry, significant regions of secondary resonance as observed in the laboratory experiment, do not arise on the Kloof mine hoist system. However, at substantially larger excitation levels such regions may be entered, as is evident in figures 4.6, 4.7. During a winding cycle, the dynamic response never reaches steady state, and consequently the residual response due to the non-stationary nature of the system may activate regions of secondary resonance. In light of these additional features of the system, a numerical simulation is necessary as a final validation of the system design. Such a simulation is presented in the following chapter.

Chapter 5

Nonlinear Numerical Simulation

Chapter 4 presented a stability analysis of the steady state out-of-plane datum solution. The stability of this motion was investigated as a criterion to identify system parameters which reduced the nonlinear coupling between the lateral and longitudinal motion. The analysis confirmed the existence of simple and additive combination parametric resonances of the lateral modes, as well as the possibility of parametric resonance involving additive and difference combinations of the longitudinal and lateral modes. A further discussion regarding the steady state motion is presented in Appendix J, where the existence of these regions of secondary resonance is confirmed by applying the method of multiple time scales to examine the nonlinear equations of motion directly. The perturbation analysis also identifies conditions of tuning which lead to internal resonance. Although an appreciation of the steady state stability of the system may be useful for identifying regions of potential nonlinear interaction, the system is non-stationary, and steady state motion is never attained. In addition the Lebus excitation at the drum was idealised in the stability analysis as a two term Fourier expansion of the groove profile. In reality the Lebus groove profile induces strong pulses at each coil cross-over. Thus modelling the geometry of the cross-over region accurately is essential. For this reason, a numerical simulation capable of approximating the real time response of the system is developed. Since such an analysis is intended to simulate the behaviour of the system as realistically as possible, nonlinear terms consistent with the strain definition, as well as cable curvature and cable transport velocity are included in the analysis.

This chapter progresses through three phases. Firstly the nonlinear partial differential equations of motion as derived in chapter 3 are considered. Thereafter, a numerical simulation of these equations is developed. In the early stages of this study, the normal mode method was applied to transform the partial differential equations of motion to ordinary differential form. An extensive simulation based on this approach was developed. The numerical simulation failed to correlate with measurements extracted from the laboratory model of the system. This exercise demonstrated the limitations of a nonlinear normal mode approach, and resulted in the development of a quasi-static model for the catenary section. Finally a nonlinear simulation of the Kloof Mine hoist system, based on a quasi-static model which includes catenary curvature and transport velocity, is presented. The numerical simulation predicts dynamic interactions on the up-wind, leading to rope whip, as observed by Dimitriou and Whillier[1973], whilst negligible interaction occurs on the down-wind.

5.1 Nonlinear Equations of Motion

5.1.1 Simplifications Applied in the Modelling Process

The nonlinear equations of motion were developed by applying Hamilton's principle. In developing these equations, the Lagrangian strain in the axial direction of the rope was defined as:[1]

$$\epsilon = u_s - \kappa v + \frac{1}{2}(v_s^2 + w_s^2)$$

Since the catenary curvature is small, the catenary is treated as a symmetric horizontally supported cable with constant curvature, where the equilibrium curvature is defined as:

$$\kappa = \frac{mgcos(\theta)}{H}$$

where θ refers to the angle of inclination of the catenary and H is the equilibrium tension. Typically the curvature will vary between $1 \times 10^{-4} < \kappa < 1 \times 10^{-3}$.

[1]Since the correct expression for the strain is: $\epsilon = u_s - \kappa v + \frac{1}{2}((u_s - \kappa v)^2 + w_s^2 + (v_s + \kappa u)^2)$, $uO(v^2), O(w^2), \kappa O(u)$, where u, v, w represent axial, lateral in-plane and out-of-plane motion respectively.

The catenary remains in contact with the sheave, admitting longitudinal motion tangential to the equilibrium profile ie. $\delta v(l_c) = 0, \delta w(l_c) = 0$. No slip occurs across the sheave; finally the lateral motion of the vertical rope is restrained.

The transport velocity of the rope is neglected with respect to longitudinal motion, but is included with respect to the lateral catenary motion[2].

5.1.2 Reduced Equations of Motion

Applying these simplifications, the undamped[3] nonlinear equations of motion of the mine hoist system are defined as.

$$(1 + \zeta\delta(s - l_c) + \eta\delta(s - l_v))u_{tt} = c^2 u_{ss} + c^2(v_s v_{ss} + w_s w_{ss} - \kappa v_s)[H(s) - H(s - l_c)] \tag{5.1}$$

Where $\zeta = \frac{I}{\rho A R^2}, \eta = \frac{M}{\rho A}$, and l_c, l_v refer to the length of the catenary and vertical rope respectively[4].

$$v_{tt} + 2Vv_{s,t} = (\bar{c}^2 - V^2)v_{ss} + c^2\left[v_s\{u_s - \kappa v + \tfrac{1}{2}(v_s^2 + w_s^2)\}\right]_{,s} + \kappa\{u_s - \kappa v + \tfrac{1}{2}(v_s^2 + w_s^2)\} \tag{5.2}$$

$$w_{tt} + 2Vw_{s,t} = (\bar{c}^2 - V^2)w_{ss} + c^2\left[w_s\{u_s - \kappa v + \tfrac{1}{2}(v_s^2 + w_s^2)\}\right]_{,s} \tag{5.3}$$

Where c^2, and $\bar{c}^2$ represent the longitudinal and lateral wave speeds, κ represents the catenary curvature, and V the axial transport velocity of the rope.

---

[2]This follows from the observation that the importance of the Coriolis coupling is dependent on the ratio of the transport velocity to the wave speed. ie $\frac{V}{\bar{c}} \approx 10^{-1}$, where as $\frac{V}{c} \approx 10^{-3}$, where $c, \bar{c}$ represent the longitudinal and lateral wave speed respectively.

[3]Since a proportional damping mechanism is applied, modal damping factors will be introduced at a later stage.

[4]I, R, M, E, A refer to the sheave inertia, sheave radius, conveyance mass, modulus of elasticity, and effective steel area of the rope respectively.

5.2 Normal Mode Model of the Equations of Motion

Initially the normal mode technique was applied to discretise the equations of motion. Although this technique is commonly applied to obtain approximate solutions to weakly nonlinear continuous systems, it was found that the simulation based on this method did not correlate with laboratory measurements. For this reason an alternative technique was ultimately applied. Nevertheless, the normal mode technique applied to model the system is presented and discussed for the purpose of documenting the limitations of this approach.

In applying the normal mode method, trivial boundary conditions are required, such that the spatial variables can be approximated by applying the linear eigenfunctions or normal modes of the system. This can be accomplished by transforming the equations of motion so that the boundary excitation is introduced as distributed inertial forces in the equations of motion.

The following transformation is a valid transformation[5].

$$u(s,t) = u(0,t) - \frac{1}{2l_c}[v(0,t)^2 + w(0,t)^2]\left\{\frac{s}{l_c}[H(s) - H(s-l_c)] + H(s-l_c)\right\} + \frac{\kappa}{2l_c}s(2l_c - s)[H(s) - H(s-l_c)]w(0,t) + \overline{u}(s,t)$$

$$v(s,t) = v(0,t)(1 - \frac{s}{l_c}) + \overline{v}(s,t)$$

$$w(s,t) = w(0,t)(1 - \frac{s}{l_c}) + \overline{w}(s,t)$$

Substituting these co-ordinate transformations into the equations of motion (5.1,5.3,5.2), leads to a set of equations, where the boundary excitation induces an equivalent distributed inertial load. In this reference frame, trivial

[5]This transformation ensures that the longitudinal strain remains unchanged during a static rigid body displacement, in accordance with the tension compensation mechanism induced by the sheave interface ie the equation of motion at the sheave due to a static displacement field reduces to $[u_s - \kappa v + \frac{1}{2}(v_s^2 + w_s^2)]_1 = u_s|_2 = 0$, where 1, 2 refer to stations on the catenary and vertical sides of the sheave respectively. The transformation adopted satisfies this condition.

boundary conditions exist at the winder drum. Since the excitation in the in-plane direction $v(0,t)$ is of the order of 0.5mm, it is included only as a weak source of direct excitation of the in-plane motion. For this reason, it is not carried through the subsequent equations, and results only in defining the direct excitation of the in-plane motion $F_v(s,t)$.

$$\begin{aligned}(1+\zeta\delta(s-l_c)+\eta\delta(s-l_v))\overline{u}_{tt} &= c^2\overline{u}_{ss} \\ +c^2[\overline{v}_s\overline{v}_{ss}+\overline{w}_s w_{ss} &- \frac{1}{l_c}w(0,t)\overline{w}_{ss}-\kappa\overline{v}_s][H(s)-H(s-l_c)] \\ &+F_u(s,t) \end{aligned} \tag{5.4}$$

$$\begin{aligned}\overline{v}_{tt}+2V\overline{v}_{s,t} = \; & (c^2-V^2)\overline{v}_{ss}+c^2\left[(\overline{u}_s\overline{v}_s)_s+\tfrac{3}{2}(\overline{v}_s)^2\overline{v}_{ss}+\tfrac{1}{2}(\overline{w}_s^2\overline{v}_s)_s\right] \\ & -\kappa c^2\left[\overline{v}\;\overline{v}_{ss}-\overline{v}_s+\kappa\overline{v}-\tfrac{1}{2}(\overline{w}_s)^2+\tfrac{1}{2}(\overline{v}_s)^2\right] \\ & -c^2\tfrac{w(o,t)}{l_o}\left[(\overline{w}_s\overline{v}_s)_s+\kappa\overline{w}_s\right]+F_v(s,t)\end{aligned} \tag{5.5}$$

$$\begin{aligned}\overline{w}_{tt}+2V\overline{w}_{s,t} = \; & (c^2-V^2)\overline{w}_{ss}+c^2\left[(\overline{v}_s\overline{w}_s)_s+\tfrac{3}{2}(\overline{w}_s)^2\overline{w}_{ss}+\tfrac{1}{2}(\overline{v}_s^2\overline{w}_s)_s\right] \\ & -\kappa c^2\left[\overline{v}\;\overline{w}_{ss}+\overline{w}_s\overline{v}_s\right] \\ & c^2\tfrac{w(0,t)}{l_o}\left[\tfrac{w(0,t)}{l_o}\overline{w}_{ss}-\overline{u}_{ss}-3\overline{w}_s\overline{w}_{ss}-\overline{v}_s\overline{v}_{ss}+\kappa\overline{v}_s\right] \\ & +F_w(s,t)\end{aligned} \tag{5.6}$$

where

$$\begin{aligned}F_u(s,t) = \; & -[1+\zeta\delta(s-l_c)+\eta\delta(s-l_v)]\times \\ & \left\{\tfrac{\partial^2 u(0,t)}{\partial t^2}-\tfrac{1}{2l_o}\tfrac{\partial^2[v(0,t)]^2}{\partial t^2}\right\}\left[[H(s)-H(s-l_c)]\tfrac{s}{l_c}+H(s-l_c)\right]\end{aligned}$$

$$F_v(s,t) = -(1-\frac{s}{l_c})\frac{\partial^2 v(0,t)}{\partial t^2}+\frac{2V}{l_c}\frac{\partial v(0,t)}{\partial t}$$

$$F_w(s,t) = -(1-\frac{s}{l_c})\frac{\partial^2 w(0,t)}{\partial t^2}+\frac{2V}{l_c}\frac{\partial w(0,t)}{\partial t}$$

$$\overline{v}(0,t)=\overline{w}(o,t)=\overline{u}(0,t)=0$$

$$\overline{v}(l_e, t) = \overline{w}(l_e, t) = 0$$

It is evident that these equations of motion contain spatially distributed forcing functions, as well as terms with periodic coefficients. It is convenient to transform the partial differential equations into a set of ordinary differential equations. Usually this is accomplished by means of the expansion theorem (Meirovitch[1970]), where the solution is expanded in terms of a superposition of the linear eigenfunctions (the normal modes) multiplied by time dependent functions. Since the dynamic characteristics of the mine hoist system are non-stationary due to the changing length of the vertical rope, this approach cannot be applied directly. The normal mode expansion may be applied to approximate the non-stationary spatial domain by assuming the vertical length changes *slowly* with time. In this context, *slowly* means that small changes in the dynamic characteristics occur during a period of the fundamental frequency of the system. This condition applies to the mine hoist system except towards the shaft head, where the longitudinal system characteristics change significantly over a short depth. If the system is treated as one with *slowly varying* parameters, then the change in the vertical length l, which introduces the non-stationary nature to the spatial variables, can be observed on a *slow* time scale $\tau = \epsilon t$, where ϵ is a small parameter. In this case an approximate solution can be found by considering an expansion of the form, $\sum_{n=1}^{\infty} \phi(s,l)_n q_n(t)$, where $\phi_n(s,l)$ represents the eigenfunction of the n^{th} mode, and $l = l(\tau)$. Thus the eigenfunctions can be found as a function of the vertical length $l(\tau)$, and applied to transform the system to ordinary differential form discreetly during the numerical simulation[6]. Since the boundary conditions applicable to the transformed partial differential equations of motion are trivial, a normal mode method is readily applied to convert the partial differential equations into nonlinear ordinary differential form ie.

$$\overline{u}(s,t) = \sum \phi(s) q(t)$$

$$\overline{v}(s,t) = \sum \Phi(s) p(t)$$

$$\overline{w}(s,t) = \sum \Phi(s) r(t)$$

[6]If one Accounts for the *slowly* varying properties of the dynamic characteristics, additional terms are introduced in the equations of motion. This effect is being considered by Kaczmarczyk[1993].

Substituting the normal mode expansions into equations (5.4,5.5,5.6), and orthogonalising these equations with respect to the linear normal modes ϕ_i, Φ_i, a set of nonlinear ordinary differential equations result[7].

$$\ddot{p}_i + 2\zeta_u\omega_i\dot{p}_i + \omega_i^2 p_i + (\frac{v(0,t)}{l_c})U^u_{ij}r_j + K^u_{ij}q_j + \Gamma_{ijk}[r_jr_k + q_jq_k] = P_i(t) \tag{5.7}$$

$$\begin{aligned} \ddot{q}_i + 2(\zeta_w\overline{\omega}_i + VV_{ij})\dot{q}_i + \overline{\omega}_i^2 q_i &+ \Delta_{ijk}p_jq_k \\ +\beta_{ijkl}(\frac{3}{2}q_jq_kq_l + \frac{1}{2}r_jr_kq_l + r_jq_kr_l) &+ \gamma_{ijk}q_jq_k + \\ \epsilon_{ij}p_j + \eta_{ijk}(q_jq_k - r_jr_k) - \kappa K_{ij}q_j &+ \frac{v(0,t)}{l_c}(\zeta_{ijk}r_jq_k + K^w_{ij}r_j) = Q_i(t) \end{aligned} \tag{5.8}$$

$$\begin{aligned} \ddot{r}_i + 2(\zeta_v\overline{\omega}_i + VV_{ij})\dot{r}_i + \overline{\omega}_i^2(1 + (\frac{c}{a_l})^2(\frac{v(0,t)}{l_c})^2)r_i &+ \Delta_{ijk}p_jr_k \\ +\beta_{ijkl}(\frac{3}{2}r_jr_kr_l + \frac{1}{2}q_jq_kr_l + q_jr_kq_l) &+ \alpha_{ijk}q_jr_k + \\ \frac{v(0,t)}{l_c}\left[U^v_{ij}p_j + \delta_{ijk}(3r_jr_k + q_jq_k) + K_{ij}q_j\right] &= R_i(t) \end{aligned} \tag{5.9}$$

Where:

$$\overline{\omega}_i^2 = [1 - (\tfrac{V}{c})^2]^{\frac{1}{2}}\tfrac{i\pi}{l_c}c \qquad U^u_{ij} = \tfrac{c^2}{m^u_{ii}}\left\{\int_0^{l_c}\phi_i(s)\Phi_j''(s)ds - \phi_i(l_c)\Phi_j'(l_c)\right\}$$

$$K^u_{ij} = \tfrac{\kappa c^2}{m^u_{ii}}\int_0^{l_a}\phi_i(s)\Phi_j'(s)ds \qquad \Gamma_{ijk} = -\tfrac{c^2}{m^u_{ii}}\left\{\int_0^{l_c}\phi_i(s)\Phi_j'(s)\Phi_k''(s)ds - \tfrac{1}{2}\phi_i(l_c)\Phi_j'(l_c)\Phi_k'(l_c)\right\}$$

$$V_{ij} = \tfrac{1}{m^v_{ij}}\int_0^{l_a}\Phi_i(s)\Phi_j'(s)ds \qquad \Delta_{ijk} = -\tfrac{c^2}{m^v_{ij}}\int_0^{l_a}\Phi_i(s)\{\phi_j''(s)\Phi_k'(s) + \phi_j'(s)\Phi_k''(s)\}ds$$

$$\delta_{ijk} = \tfrac{c^2}{m^v_{ij}}\int_0^{l_a}\Phi_i(s)\Phi_j'(s)\Phi_k''(s)ds \qquad \beta_{ijkl} = -\tfrac{c^2}{m^v_{ij}}\int_0^{l_a}\Phi_i(s)\Phi_j'(s)\Phi_k'(s)\Phi_l''(s)ds$$

$$U^v_{ij} = \tfrac{c^2}{m^v_{ii}}\int_0^{l_a}\Phi_i(s)\phi_j''(s)ds \qquad \alpha_{ijk} = \tfrac{\kappa c^2}{m^v_{ij}}\int_0^{l_a}\Phi_i(s)\{\Phi_j(s)\Phi_k''(s) + \Phi_j'(s)\Phi_k'(s)\}ds$$

$$K_{ij} = -\tfrac{\kappa c^2}{m^v_{ii}}\int_0^{l_a}\Phi_i(s)\Phi_j(s)ds \qquad \gamma_{ijk} = \tfrac{\kappa c^2}{m^v_{ij}}\int_0^{l_c}\Phi_i(s)\Phi_j(s)\Phi_k''(s)ds$$

$$\epsilon_{ij} = -\tfrac{\kappa c^2}{m^v_{ii}}\int_0^{l_a}\Phi_i(s)\phi_j'(s)ds \qquad \eta_{ijk} = \tfrac{\kappa c^2}{2m^v_{ii}}\int_0^{l_a}\Phi_i(s)\Phi_j'(s)\Phi_k'(s)ds$$

$$K^w_{ij} = \tfrac{\kappa c^2}{m^v_{ii}}\int_0^{l_c}\Phi_i(s)\Phi_j'(s)ds \qquad \zeta_{ijk} = \tfrac{c^2}{m^v_{ij}}\int_0^{l_c}\Phi_i(s)\{\Phi_j'(s)\Phi_k''(s) + \Phi_j''(s)\Phi_k'(s)\}ds$$

$$m^v_{ii} = m^w_{ii} = \int_0^{l_c}[\Phi_i(s)]^2ds \qquad m^u_{ii} = \int_0^{l_c+l_v}[\phi_i(s)]^2ds + \zeta[\phi(l_c)]^2 + \eta[\phi(l_v)]^2$$

$$P_i(t) = \tfrac{1}{m^u_{ii}}\int_0^{l_v}F_u(s,t)ds \qquad Q_i(t) = \tfrac{1}{m^v_{ii}}\int_0^{l_v}F_v(s,t)ds$$

$$R_i(t) = \tfrac{1}{m^w_{ii}}\int_0^{l_v}F_w(s,t)ds$$

[7]Modal damping is added to the equation of motion via $\zeta_{u,v,w}$; where ζ may be defined to account for a general proportional viscous damping mechanism as defined in Appendix G

During the accelerating or decelerating phase of the winding cycle, or at layer change where the rope rises in the in-plane direction by a full rope diameter, transient excitation is applied to the system. This excitation can be accounted for in the equations of motion by introducing additional inertial forces. At a layer change, the reversal in the direction of traverse in the out-of-plane direction can be accounted for by changing the phase of the out-of-plane excitation appropriately. Thus the ordinary differential equations of motion of the mine hoist system are expressed in a concise form, and readily coded in a numerical simulation. Initial simulation trials provided convincing results. In fact the simulation of the Kloof mine hoist system based on the normal mode model correlated well with the observations of Dimitriou and Whillier[1973]. Such a simulation is presented in figure 5.1, for the ascending and descending cycle of the Kloof Hoist system, between the depths of 50-1400 m[8]. In this figure, the in and out-of-plane lateral motion at the quarter point of the catenary, and the longitudinal motion of the sheave and skip are presented. Large lateral catenary motion is evident on the ascending cycle, as well as significant longitudinal oscillation at the sheave. The tension ratio across the sheave is sufficiently high on the ascending cycle, such that frictional slip across the sheave must occur. Such a condition invalidates the simulation, and the simulation was stopped short of the full wind. It is clear from this simulation that significant dynamic effects could be expected on the ascending cycle, as confirmed by Dimitriou and Whillier's observations. The acceleration and deceleration phase of the winding cycle, as well as the transient response induced by a layer change over is clearly marked. Layer change over locations are represented by the vertical lines in the figure. The in-plane motion is referenced to the chord line between the drum and sheave, and consequently the mean position rises with increasing shaft depth in accordance with the decreasing rope curvature due to the increasing vertical rope mass and thus catenary tension.

[8]The Kloof Mine hoist system actually extends over a 2100m shaft depth. The simulation was executed over a 1400m shaft depth to emulate Mankowski's simulation. It is not clear why Mankowski truncated the shaft depth in his simulation; it is presumed that this was to reduce the simulation time.

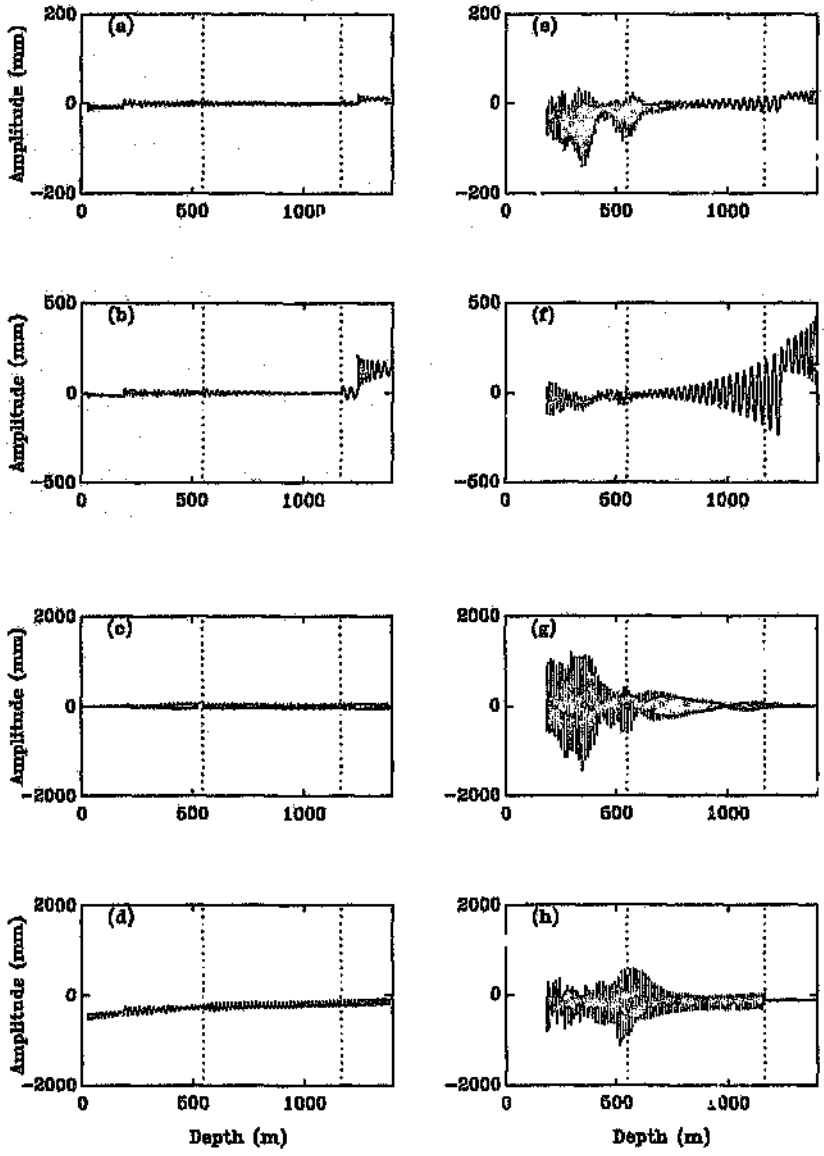

Figure 5.1: Kloof Mine simulation - Normal mode model

(a-d) - Descending Wind.
(a,e) Sheave Displacement.
(c,g) Out-of-plane Lateral Motion - $s = l_c/4$
(e-h) - Ascending Wind.
(b,f) Skip Displacement.
(d,h) In-plane Lateral Motion - $s = l_c/4$

Reservations concerning the applicability of the normal mode method with reference to nonlinear dynamic systems, lead to an examination of the degree of correlation attainable between numerical results, and experimentally extracted measurements. Since an accurate correlation exercise from on site measurements would be difficult to control, the stationary laboratory model was applied. It was clear that although the numerical simulation correctly predicted the onset of in-plane motion, the amplitudes were grossly incorrect within regions of primary and secondary resonance. It is noted that in the laboratory experiment, sinusoidal excitation amplitudes of 1mm were applied for a 475mm catenary length. In the context of the mine hoist system, excitation amplitudes of 7mm are applied to catenary lengths of 70m. Clearly the level of excitation applied in the laboratory experiment was significantly higher; perhaps it could be argued that for lower levels of excitation the system would be weakly nonlinear and hence the normal mode method would be appropriate. Since the transient excitations applied to the mine hoist system during layer changes, and during the acceleration/deceleration profiles are significant, it was decided not to accept the normal mode method. On comparing the numerical results to experimental measurements, it was evident that the numerical simulation predicted substantial stiffening, resulting in a pronounced backbone, whereas the experimental measurements indicated that the laboratory model did not exhibit a backbone.

In applying the normal mode method, it is assumed that the linear normal modes of the system form a spatial basis for the nonlinear motion. This assumption has found acceptance on condition that the system conforms to that of a weakly nonlinear system, where the nonlinear motion remains close to that of the linear motion. Szemplinska-Stupnika [1983] considered the validity of such an assumption, and proposed the nonlinear normal mode method. In this approach, Szemplinska-Stupnika calculated the nonlinear steady state response of a system via the conventional normal mode method, and the nonlinear normal mode method proposed. Since the steady state response was considered, a harmonic temporal response was assumed, and the equations of motion resulted in nonlinear ordinary differential equations describing the spatial domain and boundary conditions of the solution. Significant differences in the response were found. Nayfeh et al[1992] considered this problem, with reference to continuous systems with quadratic and cubic nonlinearities. Nayfeh et al. applied perturbation techniques directly to the Lagrangian of the system, followed by averaging over the fast time scale to obtain the ordinary differential equations that govern the modulation and phase of the response directly. Nayfeh et. al observed that the conventional normal mode technique is based on applying a Galerkin procedure to minimise errors between the assumed and exact spatial distribution, leading to ordinary nonlinear differential equations of motion which minimise this error. By considering a simple non-

linear system with quadratic and cubic nonlinearities for various conditions of tuning, Nayfeh et al. demonstrated that the normal mode technique generally fails to correctly account for the spatial variations of the drift terms, and other harmonics. It also incorrectly predicts the effective nonlinearity and the nonlinear frequency shift.

At the stage of completing the laboratory experiment, a significant effort had been invested in developing the normal mode simulation of the mine hoist system. The significance of the effect of the normal mode approximation on the response was not fully appreciated. Although it would be expected that a simulation model based on a normal mode approach would exhibit modal truncation, it was not expected that the truncation would be so severe that it would drastically alter the dynamic characteristics of the system. In an attempt to investigate the aspect of modal truncation, additional longitudinal modes were included with little success. It became evident that the normal modes related to the linear eigenfunctions of the longitudinal system, could not adequately describe the tension distribution in the catenary, as induced by the lateral motion; in particular the drift term in the longitudinal equation of motion which is produced by the quadratic coupling of the longitudinal co-ordinate to the lateral motion was not correctly accounted for, as supported by Nayfeh et al. This feature of the normal mode model occurs as a result of applying the linear eigenfunctions to the spatial domain, which are not compatible with the nonlinear deformation relationship in the catenary. Thus constraint forces are induced in the system, and the tension compensation normally afforded by the sheave interface is disrupted. As a result the nonlinear nature of the system is aliased by the presumed dynamic motion.

If one considers a quasi-static relationship for the catenary then a constraint equation develops relating the longitudinal to lateral motion, such that the quasi-static strain in the catenary is described by: $g(t) = u_s + \frac{1}{2}(v_s^2 + w_s^2)$. In applying a normal mode method, it is assumed that the lateral motion $v(s) = \Phi(s)q(t), w(s) = \Phi(s)r(t)$, where $\Phi(s) = sin(\frac{\pi s}{l_c})$; as a result, a quasi-static deformation would require that the longitudinal deformation in the catenary permits a longitudinal strain deformation of the form $u_s = g(t) + A + Bcos(\frac{2\pi s}{l_c})$. If a normal mode based on the continuous longitudinal system is applied, such a relationship cannot be accommodated. Furthermore, longitudinal modes with a wavelength of the order of the catenary section would imply short wavelengths in the vertical section. As a result, although the spatial distribution $Bcos(\frac{2\pi s}{l_c})$, may be satisfied in the catenary section by the inclusion of higher longitudinal modes, the normal co-ordinates involved would require elastic deformation of the vertical section, and thus constrain the longitudinal motion. This problem can be overcome by splitting the system at the sheave, and applying fixed free normal modes to the catenary section alone.

The catenary section could then be coupled to the sheave and vertical longitudinal system with independent normal co-ordinates. Thus the vertical system would contain a rigid body mode, enabling the tension to be correctly distributed between the catenary and vertical section. Considering the mine rope system, the catenary is generally shorter than the vertical system, and the natural frequencies of the normal co-ordinates applied to model the catenary section would be significantly higher than the response and excitation frequencies. As a result the retention of longitudinal inertia in the catenary section is unnecessary. A more usual proposition supporting this notion is that since the longitudinal wave speed in the catenary section is far greater than the lateral wave speed, the interaction between longitudinal and lateral motion would occur in a quasi-static manner, wher the tension distribution in the catenary is spatially uniform. Since the retention of longitudinal inertia in the catenary section is thus unlikely to be significant, and would increase the number of co-ordinates required in the simulation model, it is sensible to apply a quasi-static description to the catenary section directly. The implication of a quasi-static constraint is that secondary regions of resonance related to combination parametric resonance involving different lateral modes of the catenary would be eliminated (Perkins[1992b]). However, on the basis of the stability chart extracted from the laboratory experiment, such regions are less significant and more difficult to excite. The more important combinatir esonance involving the lateral and longitudinal system would be accounted for due to the retention of the longitudinal inertia of the vertical section. This observation prompted a reappraisal of the normal mode discretisation technique, leading to the development of a more conventional quasi-static model of the mine hoist system.

5.3 Laboratory Measurements

A validation of the the numerical simulation was achieved by considering the laboratory model introduced in chapter 4. The laboratory model was tuned to the first case presented in tables (4.1),(4.2) of chapter 4. The system was excited with a constant amplitude, and the er .elope of the motion in the in and out-of-plane direction, at the mid point of the string was measured visually. It would have been useful to track the motion of the guitar string, so that polar plots of the steady state motion could be directly compared with the results of th numerical simulation, however suitable measurement transducers were not available. The envelope of the motion was measured with video CCD cameras. A camera was aligned normal to each plane. A screen lined with graph paper was placed behind the guitar string, within the focal depth of the camera, such that the envelope of the steady state motion could be detected visually. The excitation frequency was increased incrementally, and the amplitude of the excitation was adjusted so that it remained constant. This process was repeated for excitation amplitudes of 0.1,0.5 and 1mm, over a bandwidth from 40-80 Hz. The measurement resolution was judged to be of the order of 0.5 mm.

The experimental envelope of the in and out-of-plane motion is presented in figure 5.2 for three sinusoidal excitation amplitudes of 0.1, 0.5 and 1 mm. This figure reflects the in and out-of-plane motion simultaneously, where the positive absolute motion of the out-of-plane and the negative absolute motion of the in-plane response is presented on a single axis. During the experiment, it was found that non-planar motion developed rapidly. It also became evident that the system did not exhibit a *backbone*, and consequently non-planar motion developed at approx.mately the same frequency regardless of whether the the excitation frequency was increased or decreased. An interesting region of motion was observed between approximately 55-57 Hz, where large non-planar motion occurred. The motion was clearly non-periodic, and it was not possible to measure the amplitude of the envelope consistently by using the video camera technique. A beating motion appeared to develop between the in and out-of-plane modes, and the motion appeared to be chaotic. Whereas the region close to primary resonance at 53 Hz resulted in the mass being raised to a new equilibrium level due to the arc length change in the catenary, the region between 54-57 Hz was charac'erised by substantial longitudinal dynamic motion, and a saturation phenomenon appeared to develop with respect to the lateral modes.

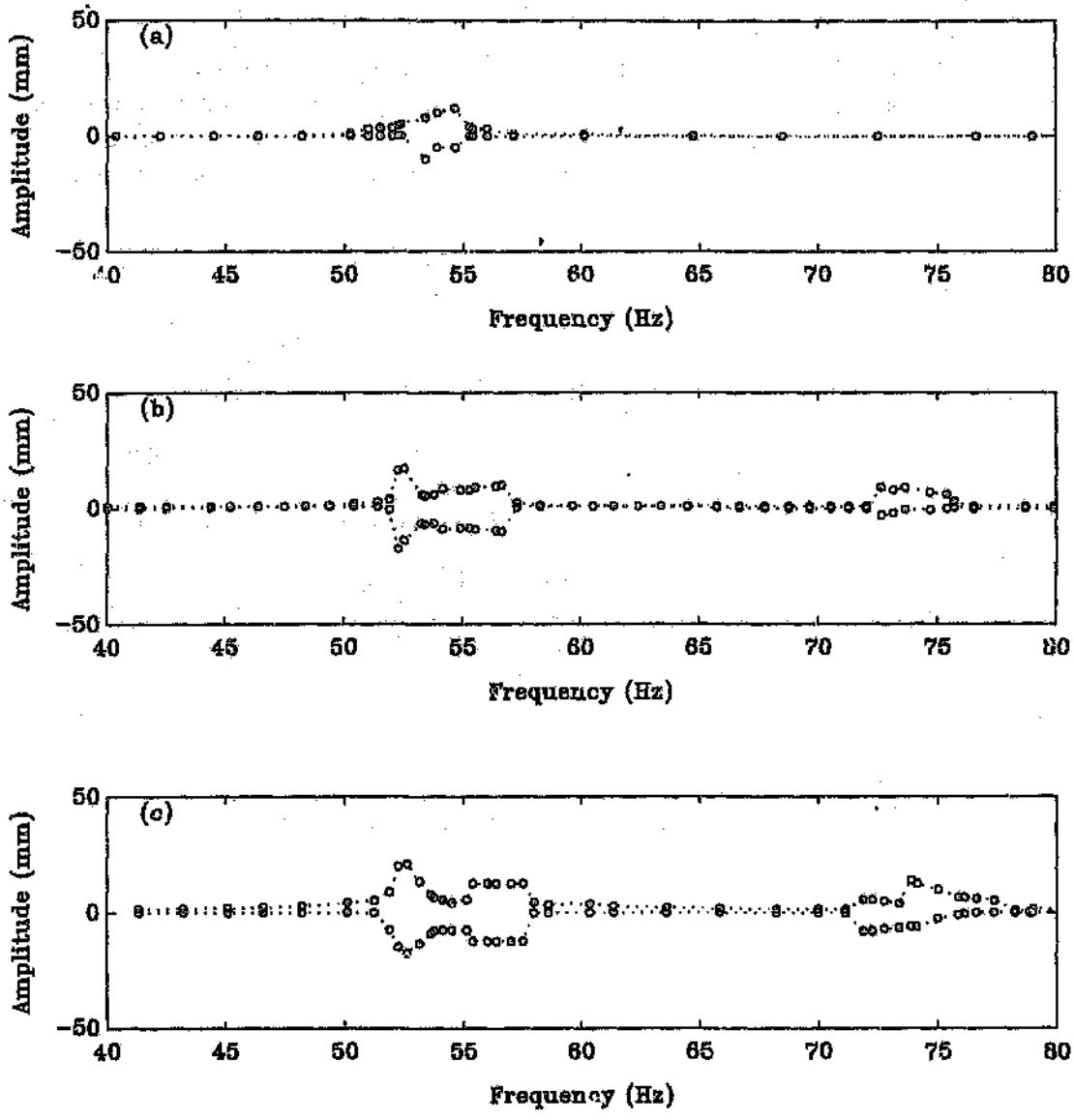

Figure 5.2: Experimental steady state amplitudes

(a) 0.1 mm Excitation amplitude.
(b) 0.5 mm Excitation amplitude.
(c) 1 mm Excitation amplitude.

5.4 Quasi-Static Laboratory Model

A quasi-static model is developed by considering the catenary and vertical section separately and imposing equilibrium and compatibility at the sheave. In the laboratory model, the pulley wheel is light, and is neglected. A schematic of the laboratory model is presented in figure 5.3.

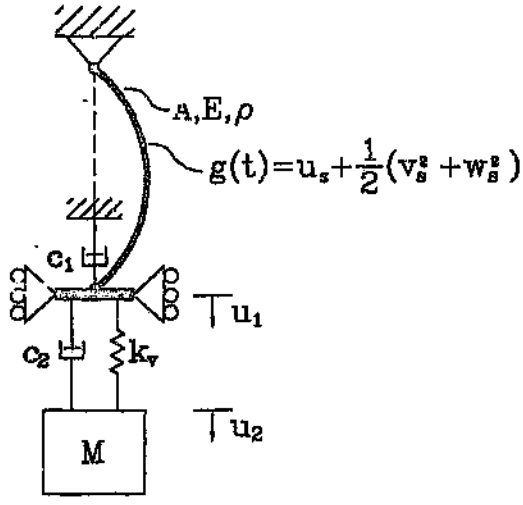

Figure 5.3: Quasi-static laboratory model

The equations of motion of the catenary section are:

$$u_{tt} = c^2[u_s + \frac{1}{2}(v_s^2 + w_s^2]_s \tag{5.10}$$

$$v_{tt} = \bar{c}^2 v_{ss} + c^2 \left\{ [u_s + \frac{1}{2}\{(v_s)^2 + (w_s)^2\}]v_s \right\}_s \tag{5.11}$$

$$w_{tt} = \bar{c}^2 w_{ss} + c^2 \left\{ [u_s + \frac{1}{2}\{(v_s)^2 + (w_s)^2\}]w_s \right\}_s \tag{5.12}$$

By neglecting the longitudinal inertia in equation (5.10), a quasi-static constraint relationship develops whereby:

$$u_s + \frac{1}{2}(v_s^2 + w_s^2) = g(t)$$

$g(t)$ represents the quasi-static strain in the catenary which is spatially uniform. This constraint relationship enables u_s to be formulated as:

$$u_s = g(t) - \frac{1}{2}(v_s^2 + w_s^2) \tag{5.13}$$

Substituting the quasi-static relationship into equations (5.11,5.12) results in the quasi-static description of the lateral equations of motion as:

$$v_{tt} = \bar{c}^2\{1 + (\frac{c}{\bar{c}})^2 g(t)\}v_{ss} \tag{5.14}$$

$$w_{tt} = \bar{c}^2\{1 + (\frac{c}{\bar{c}})^2 g(t)\}w_{ss} \tag{5.15}$$

The quasi-static strain in the catenary can be evaluated by considering the equilibrium of the oscillator which is coupled to the catenary section. With reference to figure 5.3, these equations are developed as:

$$c_1\dot{u}_1 + c_2(\dot{u}_1 - \dot{u}_2) + k(u_1 - u_2) = -AEg(t)$$

$$M\ddot{u}_2 + c_2\dot{u}_2 + ku_2 = ku_1 + c_2\dot{u}_1$$

$$M\ddot{u}_2 = -AEg(t) - c_1\dot{u}_1$$

$$u_1 = g(t)l_c - y_a$$

$$y_a = \frac{1}{2}\int_0^{l_c}(v_s^2 + w_s^2)ds$$

Manipulating these equations, the equation of motion for the suspended mass is obtained as:

$$M[1 + \frac{k_c}{k}]\ddot{u}_2 + c_2\frac{k_c}{k}\dot{u}_2 + k_c u_2 = (c_2\frac{k_c}{k} - c_1)\dot{u}_1 - k_c y_a$$

where $k_c = \frac{AE}{l_c}$, which represents the static stiffness of the catenary section. Thus the equation can be written in standard form as:

$$\ddot{u}_2 + 2\zeta\omega_n\dot{u}_2 + \omega_n^2 u_2 = -\omega_n^2 y_a + \chi\dot{u}_1$$

where $\chi = 2\zeta\omega_n - c_1\frac{\omega_n^2}{k_c}$, and ω_n represents the natural frequency of the longitudinal system.

Since $\dot{u}_1 = \dot{g}(t)l_c - \dot{y}_a$ this equation reduces to:

$$\ddot{u}_2 + 2\zeta\omega_n\dot{u}_2 + \omega_n^2 u_2 = -\omega_n^2 y_a - \chi\dot{y}_a + \chi\dot{g}(t)l_c \tag{5.16}$$

The equation describing $g(t)$ is generated through further manipulation of the previous equations:

$$\dot{g}(t) = \frac{1}{l_c}(\dot{u}_1 + \dot{y}_a)$$

$$\dot{u}_1 = -\frac{AE}{c_1}g(t) - \frac{M}{c_1}\ddot{u}_2$$

This leads to:

$$\dot{g}(t) + \frac{k_c}{c_1}g(t) = -\frac{M}{c_1 l_c}\ddot{u}_2 + \frac{1}{l_c}\dot{y}_a \tag{5.17}$$

The lateral excitation at the slider is introduced by transforming the lateral coordinates such that the boundary conditions become trivial, and the dynamic motion is then referenced to the base motion. This is achieved by applying the transformation:

$$v(s,t) = \overline{v}(s,t) + \frac{v_o}{l_c}(1 - \frac{s}{l_c})$$

Introducing this transformation into equations (5.14,5.15,5.16,5.17) results in the forced equations of motion as:

$$\overline{v}_{tt} = \overline{c}^2\{1 + (\frac{c}{\overline{c}})^2 g(t)\}\overline{v}_{ss} + \frac{d^2}{dt^2}[(1 - \frac{s}{l_c})v_o] \tag{5.18}$$

$$\overline{w}_{tt} = \overline{c}^2\{1 + (\frac{c}{\overline{c}})^2 g(t)\}\overline{w}_{ss} \tag{5.19}$$

$$\ddot{u}_2 + 2\zeta\omega_n\dot{u}_2 + \omega_n^2 u_2 = -\omega_n^2\{y_a + (\frac{v_o^2}{2l_c})\}, \\ -\chi\{\dot{y}_a + \frac{d}{dt}(\frac{v_o^2}{2l_c}) - \dot{g}(t)l_c\} \tag{5.20}$$

$$\dot{g}(t) + \frac{k_c}{c_1}g(t) = -\frac{M}{c_1 l_c}\ddot{u}_2 + \frac{1}{l_c}\dot{y}_a + \frac{1}{l_c}\frac{d}{dt}(\frac{v_o^2}{2l_c}) \tag{5.21}$$

Examining these equations, it is evident that if the average damping effort in the catenary section is equivalent to that in the suspended oscillator, then $\chi = 0$. Additional concentrated damping at the sheave can be accommodated by making $\chi < 0$. Since the longitudinal equation and that for the quasi-static strain are coupled, they may be further reduced to produce a single third order ordinary differential equation of motion for the suspended system.

The equation of motion for the suspended mass, and that for the quasi-static strain $g(t)$ are ordinary differential equations. The equations of motion for the lateral motion of the catenary are converted to ordinary differential form by applying a normal mode expansion:

$$v(s,t) = \sum \Phi_i(s)q_i$$

$$w(s,t) = \sum \Phi_i(s)r_i$$

Applying this expansion to equations (5.18,5.19), and orthogonalising the equations in the usual manner, a set of nonlinear ordinary differential equations result. For the special case where the longitudinal damping ζ, C_1 is zero, the equations can be represented as a set of coupled nonlinear ordinary differential equations, with quadratic and cubic nonlinearities. In the absence of longitudinal damping, the longitudinal equation of motion can be incorporated into the equation describing the quasi-static strain $g(t)$ to give:

$$g(t) = \omega_n^2\frac{M}{AE}\{u_2 + y_a + (\frac{v_o^2}{2l_c})\}$$

Applying the normal mode expansion for the lateral motion $v(s,t), w(s,t)$:

$$y_a = \alpha_i\{q_i^2 + r_i^2\}$$

Thus $g(t)$ can be written as:

$$g(t) = \gamma u_2 + \gamma \sum_{i=1}^{n} \alpha_i\{q_i^2 + r_i^2\} + \gamma(\frac{v_o^2}{2l_c})$$

where $\gamma = \frac{\omega_n^2 M}{AE}$. Applying the normal mode expansion to the lateral equations of motion, the equations of motion of the system are:

$$\ddot{q}_i + \omega_i^2 q_i + \beta(t)q_i + \Lambda_i q_i u_2 + \Gamma_{ij}\{q_i^2 + r_i^2\}q_j = F_q(t)$$

$$\ddot{r}_i + \omega_i^2 r_i + \beta(t)r_i + \Lambda_i r_i u_2 + \Gamma_{ij}\{q_i^2 + r_i^2\}r_j = 0$$

$$\ddot{u}_2 + \omega_n^2 u_2 + \omega_n^2 \alpha_i\{q_i^2 + r_i^2\} = -\omega_n^2(\frac{v_o^2}{2l_c})$$

where $\Gamma_{ij} = (\frac{\alpha\omega_i}{c})^2\alpha_i\gamma$, $\alpha_i = \frac{i^2\pi^2}{4l_c}$, $\Lambda_i = (\frac{\alpha\omega_i}{c})^2\gamma, \beta_i(t) = \gamma(\frac{\alpha\omega_i}{c})^2(\frac{v_o^2}{2l_c})$

It is apparent from these equations of motion, that the longitudinal system is quadratically coupled to the lateral modes. The lateral modes are quadratically coupled to the longitudinal mode, and cubic coupling arises due to the intermodal coupling of the lateral in and out-of-plane modes. In addition, the lateral system is subject to both parametric and external excitation, whilst the longitudinal system is subjected to external excitation only. Nayfeh and Mook[1983] discuss the analysis of ship pitch-roll motion with regard to a two degree of freedom model with quadratic nonlinearities. In the absence of parametric excitation ($\beta_i(t) = 0$) and cubic nonlinearity ($\Gamma_{ij} = 0$), the out-of-plane and longitudinal equations of motion for the laboratory model are similar in form to those analysed by Nayfeh and Mook, which are considered further in Appendix J.

5.4.1 Experimental Correlation

The quasi-static equations of motion developed for the laboratory model were coded with the Matlab-Simulink software programme. An Adams-Gear algorithm was applied with a variable step size and a relative integration error tolerance of 10^{-6}. The numerical simulation accounted for a single longitudinal mode, and two lateral modes in the in and out-of-plane directions. The physical parameters applied in the numerical simulation are tabulated in table 4.1 of chapter 4. It was assumed that the average longitudinal damping effort was equivalent in the catenary and vertical section of the string, and thus χ was set to zero.

For the purpose of the correlation, the numerical simulation was conducted at a series of points in 40-80 Hz range. Each simulation was executed for 40 seconds to allow the steady state motion to evolve. The comparison of the numerically simulated steady state response and the experimental results for an excitation amplitude of 0.5 mm is presented in figure 5.4.

It is evident that excellent correlation was achieved. It is interesting to observe that the plateaux region between 54-56 Hz is not related to the presence of the second lateral mode. In fact similar results are obtained for a single mode model. The plateaux region dissipates as the excitation amplitude reduces; it is characterised by strong longitudinal dynamic motion. An intensive study of the equations of motion would be required to adequately explain the observed behaviour. However, it is sufficient to observe that the equations of motion reflect quadratic coupling between the lateral and longitudinal mode, whilst quadratic and cubic coupling arises in the lateral equations of motion. The observed behaviour is attributed to the accentuated quadratic nature of the system due to the specific physical parameters, and consequently the plateaux region is characterised by a saturation phenomenon where the longitudinal dynamic motion develops at the expense of a saturated lateral motion. A secondary region of resonance occurs between 72-75 Hz. This region is related to the combination resonance of the longitudinal and first lateral mode. Although the out-of-plane measurements correlate well with the experimental measurements, larger in-plane motion is predicted by the simulation, resulting in a symmetrical response envelope. This is partly attributed to the neglect of gravity on the in-plane motion[9], but more likely due to differing boundary conditions in the two planes due to the physical construction of the model.

[9] Accounting for curvature in the in-plane mode introduces direct excitation of the symmetric in-plane modes. Although the curvature is small, a simulation which accounted for curvature of the string illustrated that the response envelope became asymmetrical, where the in-plane motion was ± 2mm less than the out-of-plane motion.

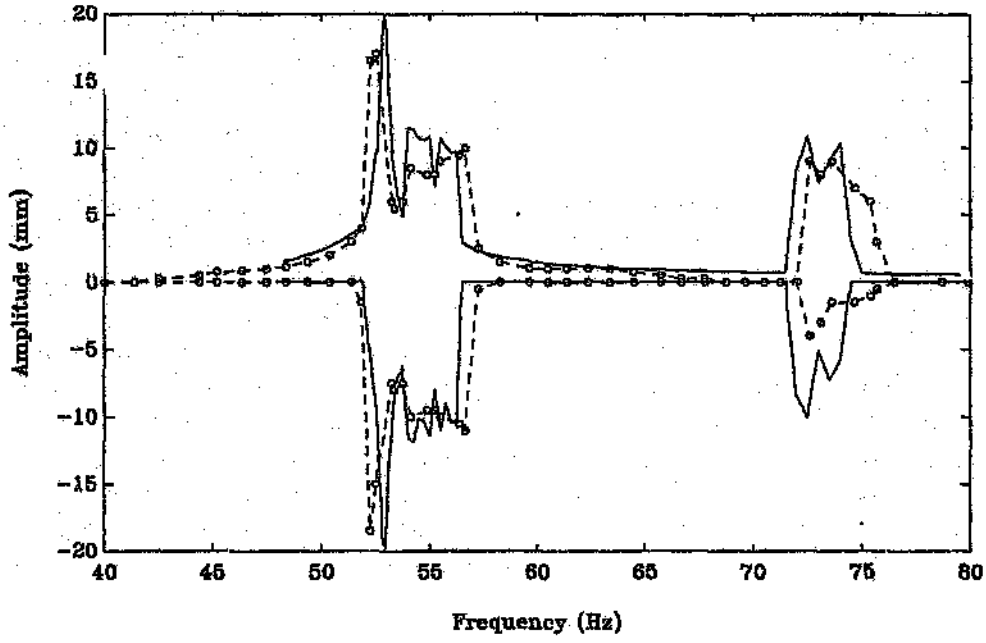

Figure 5.4: Experimental measurements vs simulation results

Steady state mid-plane response amplitudes.
- 0.5 mm excitation, two lateral in and out-of-plane modes.
– – o – – Experimental Measurements. —— Numerical Simulation.

Since the numerical simulation provided satisfactory correlation, the influence of non-stationary system parameters was examined. In the mine hoist system the vertical length of rope changes continuously during the wind, whilst the Lebus excitation frequency remains constant. Although the laboratory model was not necessarily scaled to parameters representative of the mine hoist system, it was decided to numerically assess the influence of a swept sine excitation on the response. Unfortunately measurements could not be made to confirm the numerically simulated results, nevertheless the numerical response presents interesting features. A sinusoidal sweep was applied to the numerical model between 40-60 Hz, and 60-80 Hz with a positive and negative sweep rate of 0.1 Hz/sec. A linear system subjected to a swept sinusoidal excitation reflects a delay in resonance with respect to the location of the steady state resonance. A study by Nayfeh and Asfar[1988], and Neal and Nayfeh[1990] on the non-stationary principal parametric excitation of a cubically nonlinear system demonstrates the passage through resonance for positive and negative sweep rates, illustrating the phenomena of penetration, overshoot and lingering or dragout of the response. Penetration refers to the phenomenon where the trivial response grows only after penetration of the region where the stationary trivial response is unstable; this is followed by an overshoot of the stationary non-trivial response and then convergence with the stationary non-trivial response. Lingering or dragout occurs for negative sweep rates, where the non-stationary response separates from the stationary response after convergence with it, and remains non-trivial after the stationary response is trivial. Surprisingly, in the numerical simulation of the laboratory model, the maximum response occurs as a precursor to the steady state resonance regardless of the direction of the sweep. Figures 5.5,5.6 present the response amplitudes for a positive and negative sweep rate at a 0.5mm excitation amplitude. An appreciable shift in the resonant peak with respect to the steady state response is observed. In addition response develops in regions where the steady state motion is small. A detailed explanation for this behaviour is not ventured. However, it is suggested that this behaviour is a result of the influence of the longitudinal system response on the lateral motion. In the case of the positive sweep rate, as the system approaches resonance, the suspended mass is drawn into the catenary, softening the system[10]. Since steady state motion is never attained, the lateral natural frequency drops promoting further growth. This causes the resonance to occur as a precursor to the steady state resonance. With regard to a negative sweep rate, the phase between the lateral and longitudinal motion is such that the average catenary tension rises due to the acceleration of the suspended mass, raising the catenary tension and once again promoting resonance as a precursor to the steady state resonant location. An explanation for the splitting of the resonance for a negative

[10]Such response was observed in the steady state simulations, where an overshoot in the longitudinal motion occurred prior to the system settling at a steady state amplitude.

sweep rate is not ventured. Clearly this system exhibits peculiar behaviour, and requires experimental and analytical validation in order to consistently explain the observed phenomena. This behaviour may have implications in the context of the mine hoist system, however, the excitation amplitudes and sweep rates are significantly less on the mine hoist system, and without an in-depth analytical study erroneous conclusions may be drawn. Finally, since the system inherently contains both quadratic and cubic coupling terms, it may be expected that the specific system parameters may influence the degree of quadratic and cubic coupling, and thereby the character of the response envelope significantly.

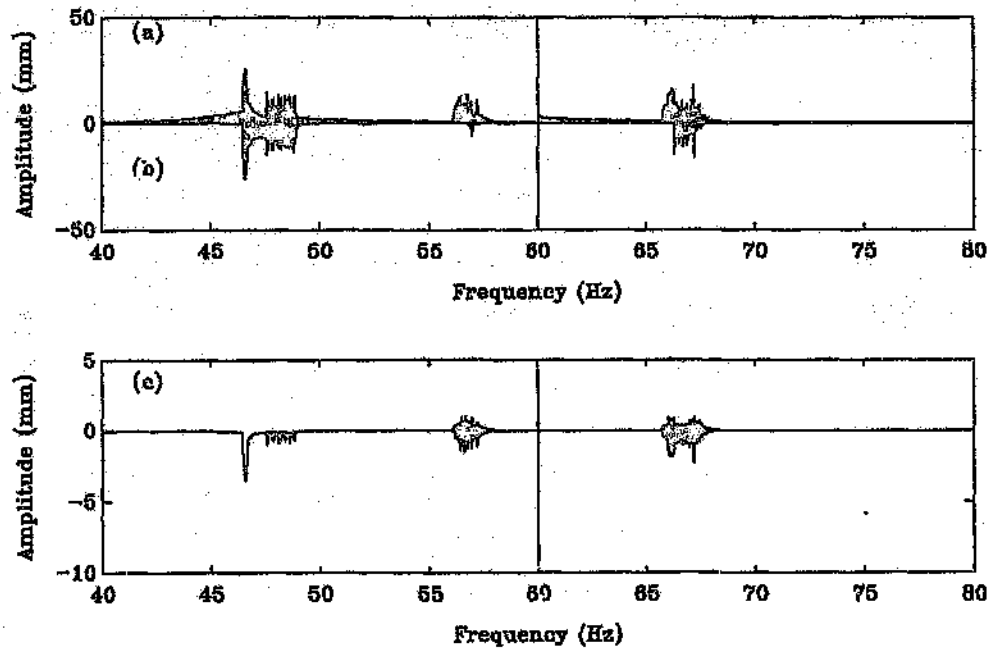

Figure 5.5: Sine sweep simulation - positive sweep rate.

Steady state mid-plane response amplitudes.
- 0.5 mm excitation, two lateral in and out-of-plane modes, 0.1 Hz/sec sweep rate.
(a) Out-of-plane Response.
(b) In-plane Response.
(c) Longitudinal response.

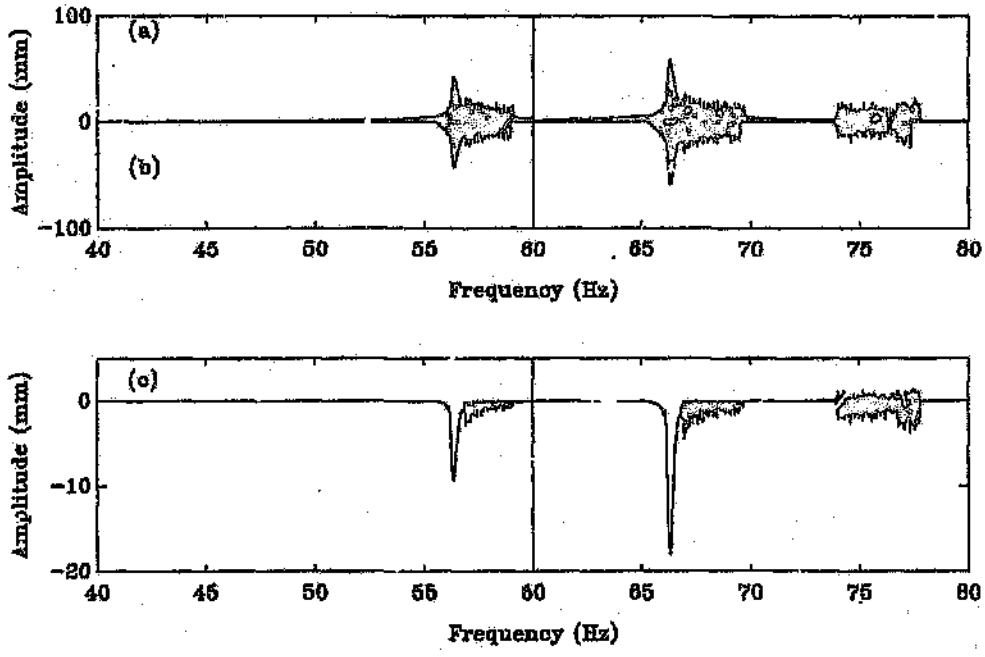

Figure 5.6: Sine sweep simulation - negative sweep rate.

Steady state mid-plane response amplitudes.
- 0.5 mm excitation, two lateral in and out-of-plane modes, -0.1 Hz/sec sweep rate.
(a) Out-of-plane Response.
(b) In-plane Response.
(c) Longitudinal re ponse.

5.5 Quasi-Static Mine Hoist Model

A quasi static version of the mine hoist system was developed by following a similar procedure to that implemented for the laboratory model. This model is illustrated in figure 5.7.

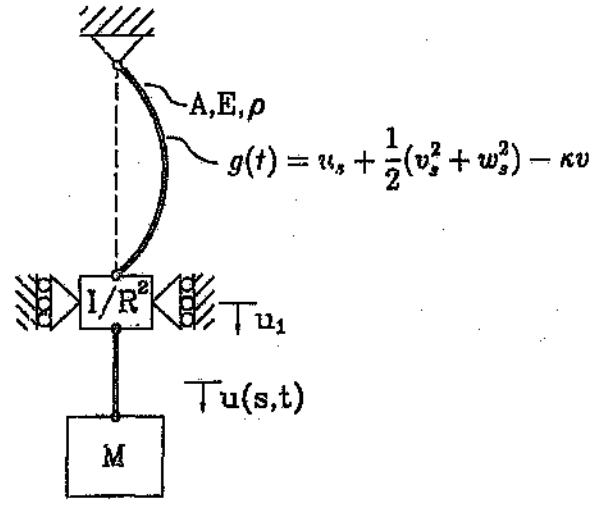

Figure 5.7: Quasi-static mine hoist model

A quasi static relationship is developed for the catenary motion by neglecting the longitudinal inertia u_{tt} in equation 5.1. As a result a constraint relationship arises which defines the quasi-static strain $g(t)$ in the catenary:

$$g(t) = u_s + \frac{1}{2}(v_s^2 + w_s^2) - \kappa v \tag{5.22}$$

Substituting this relationship into the lateral equations of motion (5.2,5.3) results in a quasi static-description for the lateral catenary motion, and the equations of motion reduce to:

$$v_{tt} + 2Vv_{s,t} = (\bar{c}^2 - V^2)v_{ss} + c^2 g(t)v_{ss} + \kappa c^2 g(t) \tag{5.23}$$

$$w_{tt} + 2Vw_{s,t} = (\bar{c}^2 - V^2)w_{ss} + c^2 g(t)w_{ss} \tag{5.24}$$

The vertical system is modelled as an unrestrained system, where the sheave inertia and the suspended mass are accounted for. When this system is attached to the catenary, it is restrained by the dynamic catenary tension, induced by the quasi-static strain $g(t)$.

$$[1+\eta\delta(0)+\zeta\delta(l_v]u_{tt}+\mu_a u_t = c^2 u_{ss}+\mu_i u_{ss,t} \\ -c^2\delta(0)g(t)+F_{I_u}(t) \quad (5.25)$$

where $u(s,t)$ represents the total longitudinal motion in the vertical rope, and $\eta = \frac{I}{mR^2}, \quad \zeta = \frac{M}{m}$. $F_{I_u}(t)$ accounts for the inertial acceleration loading due to a uniform longitudinal acceleration. This is defined subsequently.

The lateral boundary excitation at the winder drum can be accommodated in the equations of motion via a co-ordinate transformation resulting in the forced equations of motion of the system, referenced to the base motion. This is achieved by applying co-ordinate transformations to equations (5.23,5.24,5.25) ie.:

$$\overline{v}(s,t) = v(s,t)+(1-\frac{s}{l_c})v_o(t)$$

$$\overline{w}(s,t) = w(s,t)+(1-\frac{s}{l_c})w_o(t)$$

Thus the forced equations of motion for the system are:

$$\overline{v}_{tt}+2V\overline{v}_{s,t} = (\overline{c}^2-V^2)\overline{v}_{ss}+c^2 g(t)\overline{v}_{ss} \\ +\kappa g(t)+F_v(s,t)+F_{I_v}(s,t) \quad (5.26)$$

$$F_v(s,t) = -(1-\frac{s}{l_c})\frac{d^2 v_o}{dt^2}+2V\frac{d}{dt}(\frac{v_o}{l_c})$$

where $F_{I_v}(s,t)$ represents the additional inertial loading applied to the catenary in the in-plane direction due the radial velocity and acceleration associated with a layer change.

$$\overline{w}_{tt} + 2V\overline{w}_{s,t} = (\overline{c}^2 - V^2)\overline{w}_{ss} + c^2 g(t)\overline{w}_{ss} + F_w(s,t) \tag{5.27}$$

$$F_w(s,t) = -(1 - \frac{s}{l_c})\frac{d^2 w_o}{dt^2} + 2V\frac{d}{dt}(\frac{w_o}{l_c})$$

$$[1 + \eta\delta(0) + \zeta\delta(l_v]u_{tt} + \mu_a u_t = c^2 u_{ss} + \mu_b u_{ss,t} - c^2\delta(o)g(t) \tag{5.28}$$

The quasi-static strain $g(t)$ is defined by integrating equation (5.22), and applying the lateral co-ordinate transformations, and accounting for the longitudinal boundary condition at the winder drum $u_o(t)$. Thus:

$$u_1(t) = g(t)l_c + \int_o^{l_c} \kappa\overline{v} - \frac{1}{2}(\overline{v}_s^2 + \overline{w}_s^2)ds + u_o(t) \tag{5.29}$$
$$-\frac{1}{2l_c}(v_o(t)^2 + w_o(t)^2) + \frac{1}{2}\kappa l_c v_o(t)$$

where $u_1(t)$ represents tLe longitudinal motion at the sheave. This relationship defines the compatibility between the catenary and vertical section, as well as introducing the periodic excitation associated with the Lebus groove profile, and the transient excitation associated with a layer change, to the longitudinal system. These excitations are defined in Appendix A.

During the acceleration or deceleration phase of the winding cycle an additional inertial load is imposed on the longitudinal system. This load is applied by introducing a uniform acceleration to the entire system. Since the catenary is assumed massless, the inertial load generated due to a uniform longitudinal acceleration a_u is:

$$F_{I_u}(t) = -[1 + \eta(0) + \zeta(l_v)]a_u$$

This load is applied appropriately during the simulation. The lateral excitation due to the radial displacement and acceleration v_v and a_v at a layer change is accounted for in similar fashion, where the inertial load applied to the in-plane lateral equation is:

$$F_{I_v}(s,t) = -(1 - \frac{s}{l_c})a_v + 2V\frac{d}{dt}(\frac{v_v}{l_c})$$

The equations of motion for lateral and longitudinal motion can be discretised in the usual manner by applying the normal mode technique, or a Galerkin approximation. Since a quasi-static relationship implicitly satisfies the nonlinear relationship between the lateral and longitudinal motion in the catenary, the limitations evident in the original normal mode model are obviated. However, modal truncation is possible, and sufficient lateral and longitudinal modes would be required to simulate the system response accurately. The normal mode method is applied by assuming a spatial expansion for the lateral and longitudinal motion as:

$$u(s,t) = \sum \phi_i(s) p_i(t)$$

$$v(s,t) = \sum \overline{\Phi}_i(s) q_i(t)$$

$$w(s,t) = \sum \Phi_i(s) r_i(t)$$

where, for the out-of-plane modes, the mode shape is $\Phi_i(s) = sin(\frac{i\pi}{l_c}s)$[11] and the natural frequency is given by $\omega_i = i\pi\overline{c}/l_c$. $\phi_i(s)$ represents the longitudinal mode shapes of the unconstrained linear system, where the longitudinal natural frequencies are calculated via the frequency equation:

$$\Delta(\gamma_i) = \zeta\gamma_i^2\{cos(\gamma_i l_v) - \gamma_i\eta sin(\gamma_i l_v)\} + \gamma_i\{sin(\gamma_i l_v) + \gamma_i\eta cos(\gamma_i l_v)\}$$

where $\gamma_i = \frac{\overline{\omega}_i}{\overline{c}}$, $\overline{\omega}_i$ represents the longitudinal natural frequency, $\eta = \frac{I}{mR^2}$, $\zeta = \frac{M}{m}$ and l_v is the length of the vertical rope. The mode shape, normalised to unity at the sheave end is:

$$\phi_i(s) = cos(\gamma_i s) - \gamma_i\eta sin(\gamma_i s)$$

Since the system is unconstrained, the fundamental frequency $\overline{\omega}_1$ is trivial, reflecting the rigid body mode.

[11] Although it is usual to mass normalise the mode shape, the mode shape is normalised to unity so that the co-ordinate $r_i(t)$ reflects the maximum physical response in that mode.

Catenary curvature is accounted for in the simulation and consequently the in-plane natural frequencies may be calculated directly by applying the linear cable theory developed by Irvine and Caughey[1974], where the in-plane natural frequency for the symmetric modes is calculated from the frequency equation:

$$tan\frac{\omega_i}{2} = \frac{\omega_i}{2} - \frac{4}{\lambda^2}(\frac{\omega_i}{2})^3 \qquad i = 1,3,5\cdots$$

Where $\omega_i = \omega_i l_c/\overline{c}$, and $\lambda^2 = \frac{c^2}{(\overline{c}^2)^3}(gl_c)^2$, where ω_i represents the in-plane natural frequency of the symmetric modes.

and the mass normalised mode shape is given by:

$$\overline{\Phi}_i = \frac{2C_i}{cos(\omega_i/2)} sin\frac{\omega_i s}{2l_c} sin\frac{\omega_i}{2l_c}(s - l_c)$$

where:

$$C_i = \sqrt{\frac{\frac{1}{l_c}[cos\omega_i + 1]}{[2 + cos\omega_i - \frac{3}{\omega_i}sin\omega_i]}}$$

for $i = 1,3,5,\cdots$

To first order, the asymmetric in-plane modes induce no dynamic tension, and are identical to the out of plane modes. Thus for $i = 2,4,6\cdots$, the mass normalised mode shape is given by $\overline{\Phi}_i = \sqrt{\frac{l_c}{2}}sin(\frac{i\pi}{l_c}s)$ and the corresponding natural frequency is given by $\omega_i = i\pi\overline{c}/l_c$.

Because the catenary curvature is small, the effect of curvature on the symmetric in-plane modes is only discernible in the first in-plane mode for the descending cycle, as illustrated in figure 5.8. Since the in-plane motion is approximated via a modal expansion, for simplicity the in-plane symmetric mode shapes equivalent to those of a taut string are applied, hence $\overline{\Phi}_i = sin(\frac{i\pi}{l_c}s)$, and the natural frequencies are $\omega_i = i\pi\overline{c}/l_c$[12].

[12]Perkins[1992a] constructs a single mode in-plane model of a cable with fixed end conditions in the region of the first modal cross-over. Consequently, it is necessary to apply the correct form for the symmetric in-plane mode shape, since it is different to its corresponding out-of-plane mode shape.

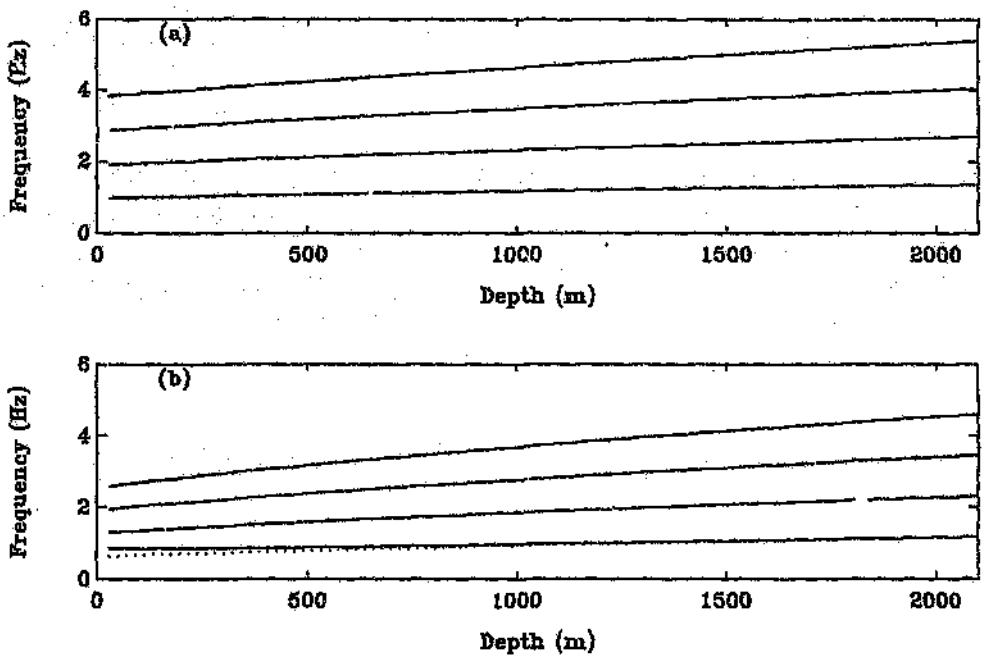

Figure 5.8: Stationary lateral natural frequencies vs shaft depth -Kloof Mine

(a) Ascending Cycle. (b) Descending Cycle.
– - In-plane natural frequencies. · · · · Out-of-plane natural frequencies.

On discretising the equations, a set of ordinary nonlinear differential equations result, where:

$$g(t) = \frac{1}{l_c}\sum_{i=1}^{n_{long}} p_i + \sum_{i=1}^{n_{lat}} \alpha_i q_i + \sum_{i=1}^{n_{lat}} \beta_i \{q_i^2 + r_i^2\} + F_g(t)$$

where:

$F_g(t) = -\frac{1}{l_c}\{u_o - \frac{1}{2l_c}(v_o(t)^2 + w_o(t)^2) + \frac{1}{2}\kappa l_c v_o(\iota)\}$
$\alpha_i = \frac{8}{i\pi}\{(-1)^i - 1\}$
$\beta_i = \frac{1}{4}(\frac{i\pi}{l_c})^2$

It is noted that α_i represents the component of the quasi-static strain due to geometric realignment of the in-plane motion. As expected this component vanishes with respect to anti-symmetric modes. The discretised equations describing the longitudinal (p_i), in-plane lateral (q_i) and out-of-plane lateral (r_i) motion are presented as[13].

$$\ddot{p}_i + 2\overline{\zeta}_i\overline{\omega}_i\dot{p}_i + \overline{\omega}_i^2 p_i + c^2\{\frac{1}{l_c}p_j + \alpha_j q_j + \beta_j\{q_j^2 + r_j^2\}\} = -c^2 F_g(t) \qquad (5.30)$$

$$\ddot{q}_i + 2\zeta_i\omega_i\dot{q}_i + \mathcal{V}_{ij}\dot{q}_j + \omega_i^2\{1 + \eta_i(t)\}q_i + \zeta_i\{\frac{1}{l_c}p_j + \alpha_j q_j + \beta_j\{q_j^2 + r_j^2\}\}q_i + c^2\alpha_i\{\frac{1}{l_c}p_j + \alpha_j q_j + \beta_j\{q_j^2 + r_j^2\}\} = Q_i(t) + c^2\alpha_i F_g(t) \qquad (5.31)$$

$$\ddot{r}_i + 2\zeta_i\omega_i\dot{r}_i + \mathcal{V}_{ij}\dot{r}_j + \omega_i^2\{1 + \eta_i(t)\}r_i + \zeta_i\{\frac{1}{l_c}p_j + \alpha_j q_j + \beta_j\{q_j^2 + r_j^2\}\}q_i = R_i(t) \qquad (5.32)$$

where:

[13]In these equations the summation signs have been left out, and the subscript j refers to summation over the number of modes.

$\eta_i = (\frac{c}{c})^2 \omega_i^2 F_y(t)$
$\zeta_i = (\frac{c}{c})^2 \omega_i^2$
$\mathcal{V}_{i,j} = 8V\{\frac{ij}{(j^2-i^2)l_c}\} \quad i \neq j$
$\mathcal{V}_{i,j} = 0 \quad i = j$

Proportional damping has been added to the longitudinal and lateral equations of motion respectively via $\overline{\zeta}_i, \zeta_i$. The terms $P_i(t), R_i(t), Q_i(t)$ arise due to the direct excitation at the winder drum. These are evaluated as:

$$P_i(t) = \frac{1}{m_{u_{ii}}} \int_0^{l_v} \phi_i(s)\{F_u(s,t) + F_{I_u}(t)\}ds$$

$$Q_i(t) = \frac{1}{m_{v_{ii}}} \int_0^{l_c} \Phi_i(s)\{F_v(s,t) + F_{I_v}(t)\}ds$$

$$R_i(t) = \frac{1}{m_{w_{ii}}} \int_0^{l_c} \Phi_i(s) F_w(s,t)ds$$

where $m_{u_{ii}}, m_{v_{ii}}, m_{w_{ii}}$ represent the modal mass associated with the i^{th} generalised co-ordinate.

Since α_i is zero for the antisymmetric modes, the quadratic nonlinearities introduced by the catenary curvature, and the direct excitation of the in-plane modes due to curvature coupling, vanish with respect to the anti-symmetric lateral modes. However, as with the laboratory model, quadratic coupling between the lateral and longitudinal motion is retained due to the retention of the longitudinal inertia associated with the vertical section.

5.6 Longitudinal and Lateral Damping Mechanisms

The definition of a damping mechanism which is applicable to mine hoist cables has not received a great deal of attention, probably due to the complexity and variation of the rope construction. Mankowski [1986],[1988],[1990] has provided the bulk of the fundamental work in the specific area of mine hoist cables, whilst earlier work by Yu [1952] and Vanderveldt et al [1973] examined some of the parameters influencing the damping characteristics of wire ropes.

5.6.1 Longitudinal Damping

Usually a visco-elastic damping model is applied in the mining industry to study longitudinal oscillations of the mine hoist system. Since these works are concerned primarily with the start up transients, which exhibit dominant first mode response, the damping model is formulated with respect to the measurement of the logarithmic decrement of the first longitudinal mode. Thomas et al.[1987] performed such measurements at Deelkraal Mine with an empty and loaded skip, at $\frac{1}{4}$ and $\frac{3}{4}$ depth. Greenway[1989] analysed these measurements and showed that the logarithmic decrement of the first mode was independent of the total skip mass, but linearly dependent on rope length. The dimensionless damping ratio was of the order of 2.5%. The damping mechanism was not studied further, and proportional damping was assumed in the model. This resulted in strong attenuation of the higher modes. Mankowski [1986] experimentally examined the attenuation of kinetic shock waves travelling along the cable, and also the attenuation of the shock on entering the winder drum. The results of the study indicate that the winder drum may absorb as much as 66% of the energy of an incident kinetic shock. Mankowski notes that this result conflicts with that of Harvey[1965] who reported that "*Tests show that in a typical case, the amplitude of the disturbance is attenuated 0.65 % per 1000 meters of cable and by 1% at each pair of reflections at the drum and at the conveyance combined.*". One surmises that Harvey was referring to low frequency pulses with a large wave-length and longer periods than those applied in Mankowski's experiment, which were due to impact loading where the largest fundamental period of the applied pulse was 11ms. Harvey's results conform more readily with the logarithmic decrement associated with the first mode response, as measured during in-situ drop tests by Thomas et al.[1987].

Due to the potential complexity of the damping mechanism, this study follows the approach adopted by Greenway[1989], in that an equivalent viscous

damping coefficient is sought to model in some way the overall damping effect, without concern for the exact mechanism, which is likely to be highly complex and difficult to include in a simulation. The main concern however is the definition of a convenient and appropriate damping mechanism. Additional drop tests were performed at Elandsrand Gold Mine (Constancon[1992]). In these tests, a man cage was locked between the guides, loaded and suddenly released. The free response was monitored, and processed using standard parameter estimation routines. In order to investigate the higher longitudinal modes, electronic filtering was applied so as to amplify the response of the higher modes. The results of the parameter estimation confirmed that the dimensionless damping coefficient of the first mode was of the order of 3%, whilst the higher modes were were of a lesser value. The results of the drop test are presented in Appendix G. Greenway[1993] analysed these results and proposed a general proportional viscous damping mechanism, which reflects a lower damping effect in the higher modes. This damping mechanism is applied for convenience since an equivalent dimensionless modal damping coefficient can be calculated for each mode during the simulation.

5.6.2 Lateral Damping

Mankowski [1988] presented experimental measurements, defining a model of the lateral damping mechanism in terms of the time rate of change of curvature[14]. This model was considered by Mankowski on the basis that the inter-strand motion induced by an irrotational whirling action of the rope is proportional to the instantaneous curvature of the rope. Mankowski constructed an experimental facility to simulate irrotational whirling action of a typical mine rope. The experimental results presented indicate that the average power dissipation, and hence the equivalent viscous damping coefficients are low in comparison to the potential aerodynamic dissipation of the catenary. A detailed discussion regarding lateral dissipation is presented in Appendix H. Due to the lack of data concerning the lateral dissipation characteristics of mine hoist ropes, a proportional damping mechanism is assumed, where the value of $\zeta_1 = 0.05\%$ of critical damping is applied. This conforms to the order of dissipation determined in Mankowski's tests.

[14]The time rate of change of curvature results in a distributed damping force proportional to the stiffness properties of the rope.

5.7 Simulation of the Equations of Motion

The nonlinear ordinary differential equations of motion developed for the mine hoist system were simulated by applying the Matlab-Simulink programme. Simulink is a powerful simulation package based on the graphical definition of a block diagram description for the system equations. Having developed the block diagram for the system, pertinent physical data pertaining to the installation is supplied to the Simulink package via a definition routine coded and executed in the Matlab environment. A mask of input data required is tabulated in table 5.1.

Since the system characteristics change with time, and consequently depth during the simulation, a look-up table is applied to define the relationship between the angular winding velocity and depth. Additional look-up tables define the longitudinal and lateral natural frequencies, as well as the variation in the longitudinal damping coefficients, and the Lebus drum excitation and layer change excitation as a function of depth. These tables are defined prior to the simulation, and are interpolated during the simulation. This format efficiently accounts for the time dependence of the system parameters during the simulation.

Simulink provides a choice as to the type of integration routine applied. An automatic step size Adams-Gear routine was applied, with a relative error tolerance of 10^{-6}, and a maximum step size of 10^{-3} seconds. The maximum step size tolerance is specified to ensure sufficient accuracy with regard to the excitation look up tables.

In the normal mode simulation introduced in section 5.2, the excitation at the winder drum was accounted for by considering the first two harmonics of the Lebus groove profile, as presented in Appendix A. To better emulate the impulsive nature of the excitation, a look-up table was defined to accurately model the longitudinal and lateral excitation at the drum, as a function of shaft depth. Mankowski approximated the three dimensional displacement imparted to the rope at a coil cross-over as versine functions. This definition is applied, where the periodic displacement in the u, v, w direction at the drum is defined as a function of drum rotation. It is possible to define these displacement functions as a function of shaft depth, and hence drum rotation via a look-up table for the entire winding cycle. Since the lateral excitation is introduced via the lateral acceleration of the the cable, it is a simple manner to construct the appropriate look-up table by differentiating the lateral displacement profile analytically. The lateral excitation induced at a layer change is applied in a similar fashion. The definition of the Lebus coil cross-over excitation, as well

as the layer change excitation is presented in Appendix A.

The periodic longitudinal excitation due to the coil cross-over profile is introduced to the system by $F_g(t)$. The definition of $F_g(t)$ requires that the periodic axial displacement at the drum $u(0,t)$ as well as the gross lateral motion across the drum surface is accounted for. The longitudinal excitation due to a layer change is introduced by adding an additional longitudinal displacement to the periodic axial displacement at the layer change, and holding this value constant until it increases at the next layer change. The direction of the wind influences the longitudinal excitation definition, in that during an ascending wind the periodic pulses due to the coiling profile, and transient pulses induced at a layer change are tensile, whilst during the descending wind they are compressive.

Table 5.1: Simulation variables

N-lat	Number of in and out of plane lateral modes.
N-Long	Number of longitudinal modes.
J	Sheave Inertia.
M	Skip Mass.
M0	Skip Pay-load.
m	Linear Rope density.
a	Acceleration/Deceleration.
V	Nominal Winding Speed.
De	Depth of wind.
Lc	Catenary Length.
E	Effective Youngs Modulus of the rope.
Ax	Effective steel area of the rope.
β	Cross over arc.
Dd	Drum Diameter.
Ds	Sheave Diameter.
Dr	Rope Diameter.
Lx	Layer cross over points.
μ_a, μ_b	Longitudinal proportional material damping factors.
ζ^{lat}	Lateral proportional modal damping factor of the first mode.

5.8 Kloof Mine Simulation

A simulation of the ascending and descending winding cycle on the Kloof mine was conducted. The purpose of the simulation was to assess the degree of correlation achievable via a comparison of the the qualitative observations presented by Dimitriou and Whillier[1973].

The parameters applied in the simulation are presented in table 5.2.

Table 5.2: Simulation variables - Kloof Mine

$N-lat$	Number of in and out-of-plane lateral modes.	4
N-Long	Number of longitudinal modes.	4
J	Sheave Inertia.	15200 kgm^2
M	Skip Mass.	7920 kg
M0	Skip Pay-load.	9664 kg
m	Linear Rope density.	8.4 kg/m
a	Acceleration/Deceleration.	$0.74m/s^2$
V	Nominal Winding Speed.	15 m/s
De	Depth of wind.	2100m
Lc	Catenary Length.	74.95 m
E	Effective Youngs Modulus of the rope.	$1.1 \times 10^{11} N/m^2$
Ax	Effective steel area of the rope.	$0.001028m^2$
β	Cross over arc.	0.2 rad
Dd	Drum Diameter.	4.28 m
Ds	Sheave Diameter.	4.26 m
Dr	Rope Diameter.	0.048 m
Lx	Layer cross over points.	525m, 1050m, 1575m
μ_a	General proportional damping parameter	0.159
$\mu_b(s_2)$	General proportional damping parameter	$10.49s_2$
ζ_1^{lat}	Lateral proportional modal damping ratio	0.05%

Since the physi al parameters of a realistic system are difficult to quantify accurately, and may change during the life of the rope [15], a sensitivity analysis was conducted with respect to the nominal winding speed. In this study,

[15]For instance, the payload mass may vary by 5% from cycle to cycle. Manufacturing tolerances will result in variations in the nominal rope properties. The manufacturers tolerance on the linear mass density is -7%-0%, and -1%-4% on the rope diameter (Haggie Rand [1990]).The layer change locations vary during the life of the rope, since control of rope deterioration at layer and turn cross-overs requires that the *back end* (ie. drum end) be pulled in at short intervals of about six weeks. The front end of the rope is cut and

the winding speed was changed incrementally from 14 m/s to 16 m/s in 0.2 m/s increments, for both the ascending and descending cycle. The results of the sensitivity study are presented in Appendix L. The sensitivity study indicated that the response is sensitive to the winding velocity, in that the amplitude of a resonant condition is sensitive to the layer change location with respect to the resonant condition. On the basis of the sensitivity study, a winding velocity of 14.8 m/s was selected as being representative of the winder condition, since severe dynamic motion occurred on the ascending cycle. This winding condition was judged to be sufficiently close to that considered by Dimitriou and Whillier[1973], and Mankowski[1982], to be representative of the Kloof Mine hoist winder.

The results from the simulation are presented in figures 5.9 -5.12 for the descending cycle, and 5.15 -5.19 for the ascending cycle. Each simulation consists of:

- The lateral in-plane response at the first quarter point of the rope vs. shaft depth.
- The lateral out-of-plane response at the first quarter point of the rope vs. shaft depth.
- The longitudinal elastic response at the sheave vs. shaft depth.
- The longitudinal elastic response at the skip vs. shaft depth.
- The total rope tension on the catenary side of the sheave vs. shaft depth.
- The total rope tension on the shaft side of the sheave vs. shaft depth.
- The rope tension ratio across the sheave vs. shaft depth.
- The lateral in-plane modal amplitudes vs. shaft depth.
- The lateral out-of-plane modal amplitudes vs. shaft depth.

All figures are headed by a linear frequency map of the system. This map illustrates the relationship between the first two harmonics of the Lebus groove excitation frequency, the first four longitudinal and lateral natural frequencies, and the layer change location. The Lebus groove excitation frequency is

tested every six months in accordance with statutory requirements. The ammount cut off the front end, and the ammount of rope lost due to pulling is augmented by using up spare *dead* turns on the drum. A minimum of three *dead* turns is always required on the drum, but additional dead turns are allowed for compensation purposes.

represented by dashed lines; the longitudinal frequencies by dotted lines, and the lateral natural frequencies by solid lines. The layer change locations are represented by vertical lines.

The figures relating to the in-plane lateral motion at the first quarter point of the catenary, are constructed to reflect both the dynamic amplitudes, and the change in rope curvature with depth. This is achieved by referencing the motion to the span line between the end points of the catenary. As the vertical rope length changes, the equilibrium curvature of the cable changes, and hence the mean static position of the cable changes. Thus the in-plane displacement is calculated as[16]:

$$v(\frac{l_c}{4},t) = -\frac{3}{32}\kappa l_c^2 + \sum_{i=1}^{4} \sin(\frac{i\pi}{4}) q_i(t)$$

The tension ratio across the sheave is presented to ascertain if rope slip occurs during the simulation. A simple bollard type friction analysis as presented by Mankowski[1982] indicates that if the tension ratio lies beyond the limits of $0.625 \rightarrow 1.60$ then slip will occur. Since the possibility of slip is not accounted for in the simulation, this condition would invalidate the simulation beyond that time.

The results presented in figures 5.9 -5.12 for the descending cycle should be read from left to right, whilst those presented in figures 5.15 -5.19 for the ascending cycle should be read from right to left.

[16]The equilibrium profile of the rope, measured from the span line is: $Z = \frac{X}{2}(1-X)$, where $Z = -\frac{Hz}{mgl_c^2}$ and $X = \frac{x}{l_c}$, thus $z(\frac{l_c}{4}) = -\frac{3mgl_c^2}{32H}$, and $\kappa = \frac{mg}{H}$, hence $z(\frac{l_c}{4}) = -\frac{3\kappa l_c^2}{32}$

5.9 Simulation Results

5.9.1 Descending Cycle

The simulation results for the descending cycle are presented graphically in figures 5.9-5.14. General observations concerning the simulation of the descending cycle are:

- When the skip accelerates down the shaft, the average rope tension in the catenary drops, and consequently the in-plane motion is off-set in the negative direction. This effect is observed in the odd in-plane modes which are capable of geometric adjustment to account for the change in tension. The reverse effect is noted when the skip is decelerated to rest at the end of the wind.
- The layer change over is evident in the the in-plane lateral response, where it induces transient motion.
- The nonlinear interaction between the lateral and longitudinal modes is evident, where an increase in the catenary motion causes a negative drift in the longitudinal motion at the sheave.
- The motion at the sheave drifts in accordance with the gross lateral motion across the drum. Thus a triangular wave form is perceptible, where the motion drifts in the negative direction between the start of the wind and the first layer change, drifting in the opposite direction during the second layer; this effect repeats itself, and reflects the increase in the rope length due to rope traversing between the drum cheeks.

Specific observations regarding the descending cycle are:

- The in-plane motion remains small through-out the wind.
- The tension ratio across the sheave remains within the no-slip region, and thus slip across the sheave does not occur.
- The out-of-plane motion grows towards the end of the cycle. This occurs since the even (second and fourth etc) catenary modes approach a resonant condition with the Lebus excitation frequency at approximately 1900m.

- At approximately 1700m, the second catenary mode and the third longitudinal mode are equal, promoting coupling between the longitudinal and lateral motion. In effect a condition of combination resonance may occur, where the second lateral and third longitudinal modes are equal to the second Lebus excitation frequency (refer to the stationary stability plot presented in figure 4.7).
- The deceleration cycle begins at approximately 1950 m, and longitudinal transients occur.
- The attenuation of the dynamic tension across the sheave, illustrates a significant filtering action, which tends to isolate the catenary from the vertical section.

The sensitivity of the system to the winding speed is well illustrated by considering the resonant condition towards the end of the wind. Figures 5.13,5.14 present results from the sensitivity study for a winding velocity of 14.6 and 15 m/s respectively. Whilst the lateral out-of-plane motion reduces at a winding velocity of 15 m/s since the passage through resonance is not completed prior to the deceleration cycle, very different conclusions regarding the dynamic integrity of the system would be drawn from the simulation results at 14.6 m/s. In the latter condition of tuning, the resonant condition occurs at approximately 1700m; sufficient time exists for the out-of-plane motion to grow sufficiently to induce in-plane motion, and consequently significant tension fluctuations occur in the catenary from 1600m onwards. Since the lateral frequency lines have a low slope, relatively small changes in the winding speed result in significant shifts in the resonant conditions, and consequently different behaviour.

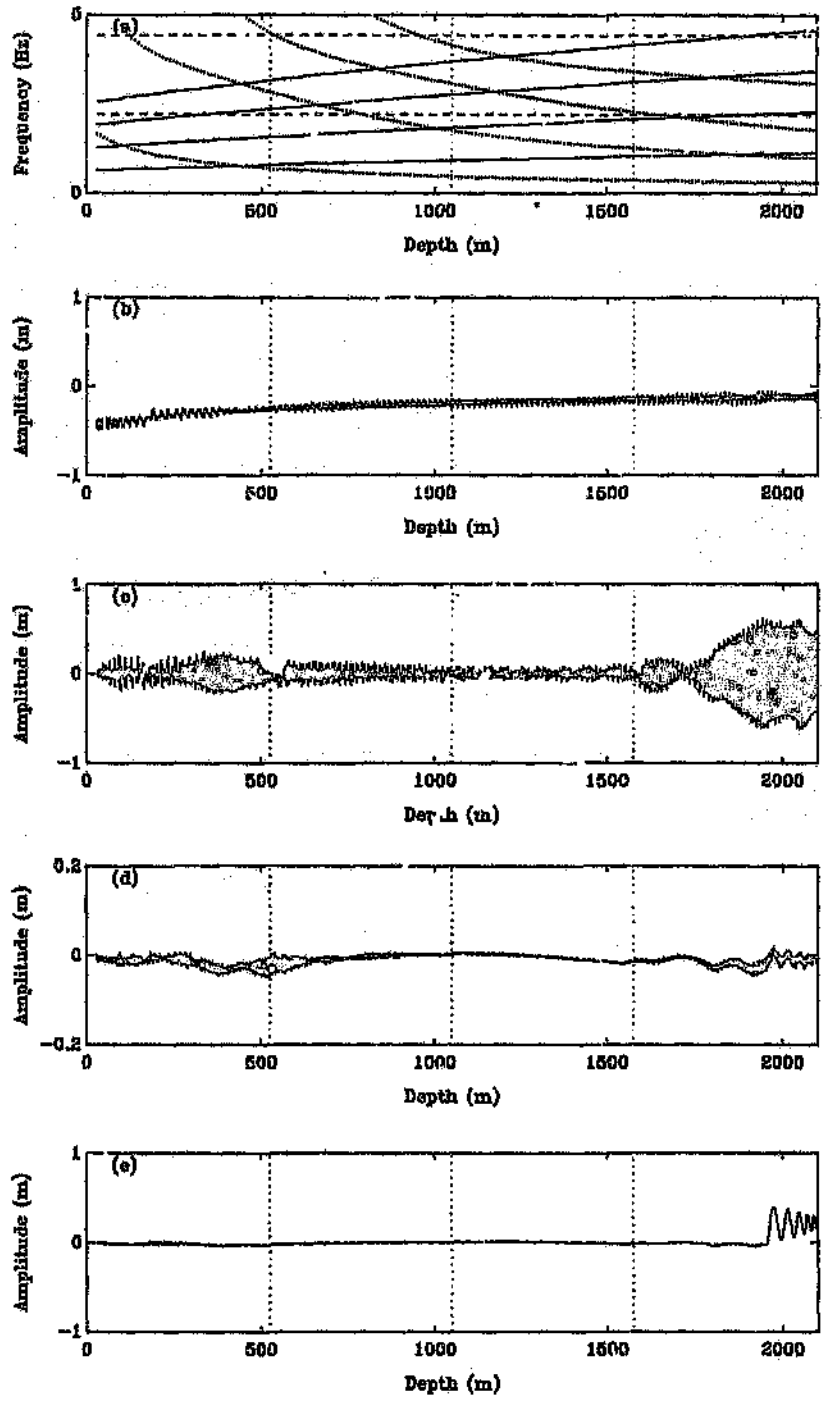

Figure 5.9: Descending cycle: Kloof Mine hoist system: 14.8 m/s

a) Linear Frequency Map
b) In-Plane Response $s = l_c/4$
c) Out-of-Plane Response $s = l_c/4$
d) Sheave Response
e) Skip Response

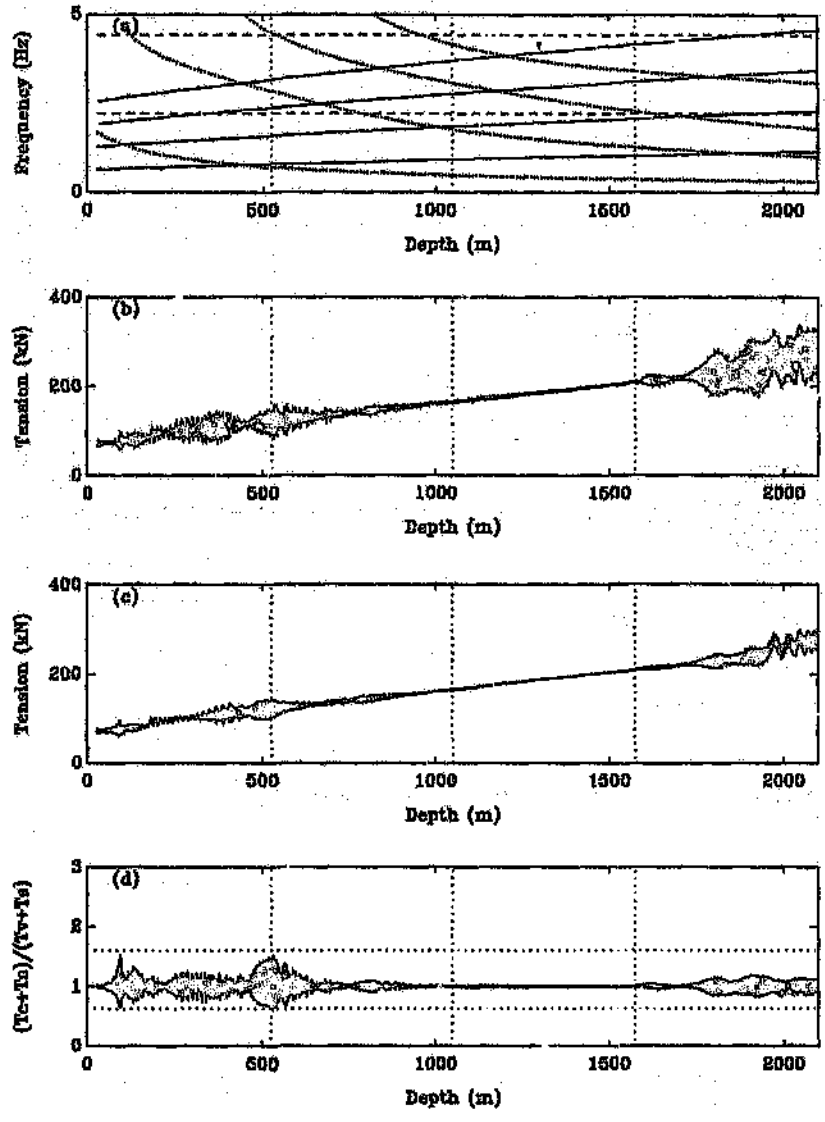

Figure 5.10: Descending cycle: Kloof Mine hoist system: 14.8 m/s

a) Linear Frequency Map
b) Total Catenary Tension
c) Total Vertical Rope Tension $s = l_c$
d) Tension Ratio Across the Sheave $R = \frac{T_{c1}+T_n}{T_v+T_s}$

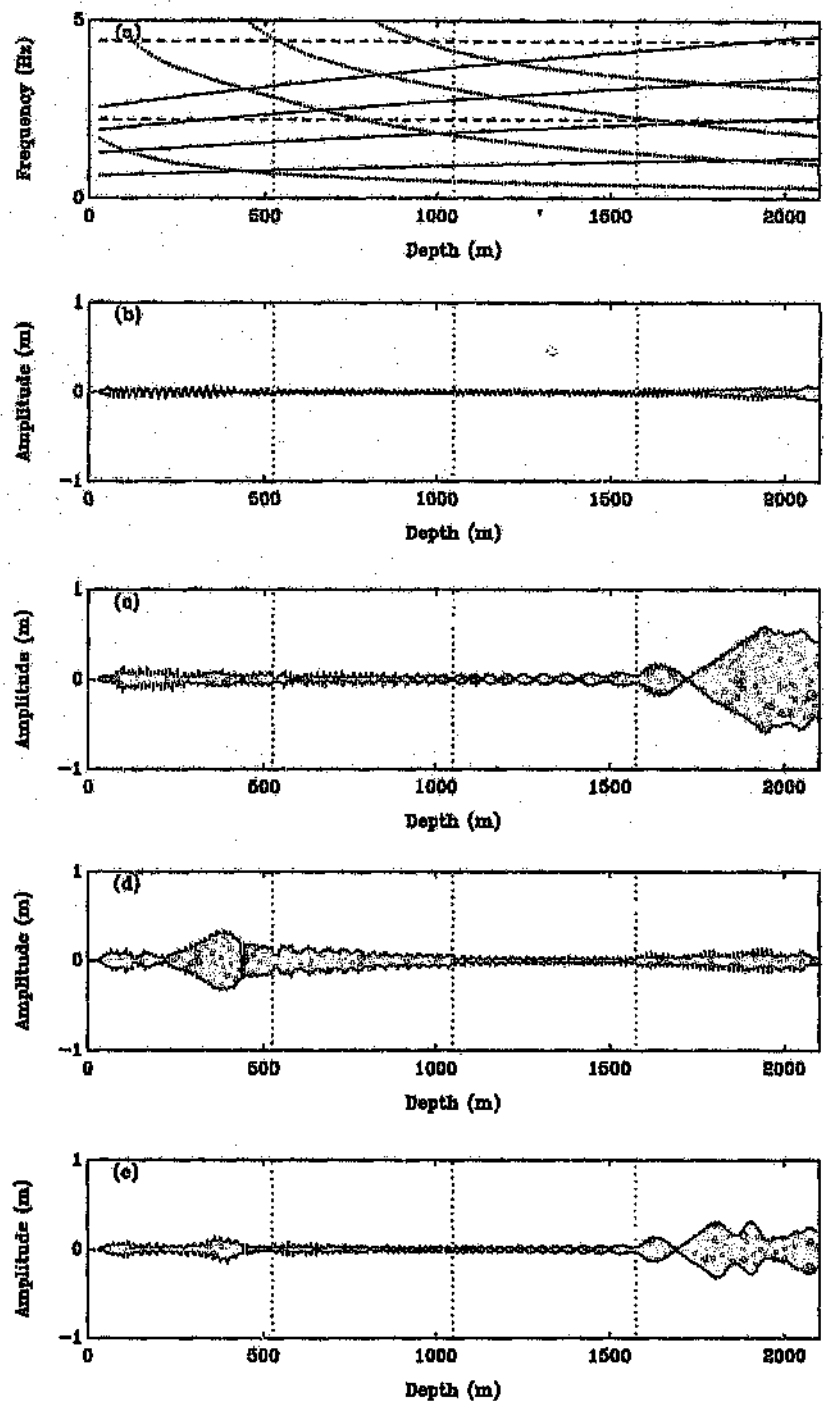

Figure 5.11: Descending cycle: Out-of-plane modal amplitudes: 14.8 m/s

a) Linear Frequency Map, b) $q_1(t)$, c) $q_2(t)$, d) $q_3(t)$, e) $q_4(t)$

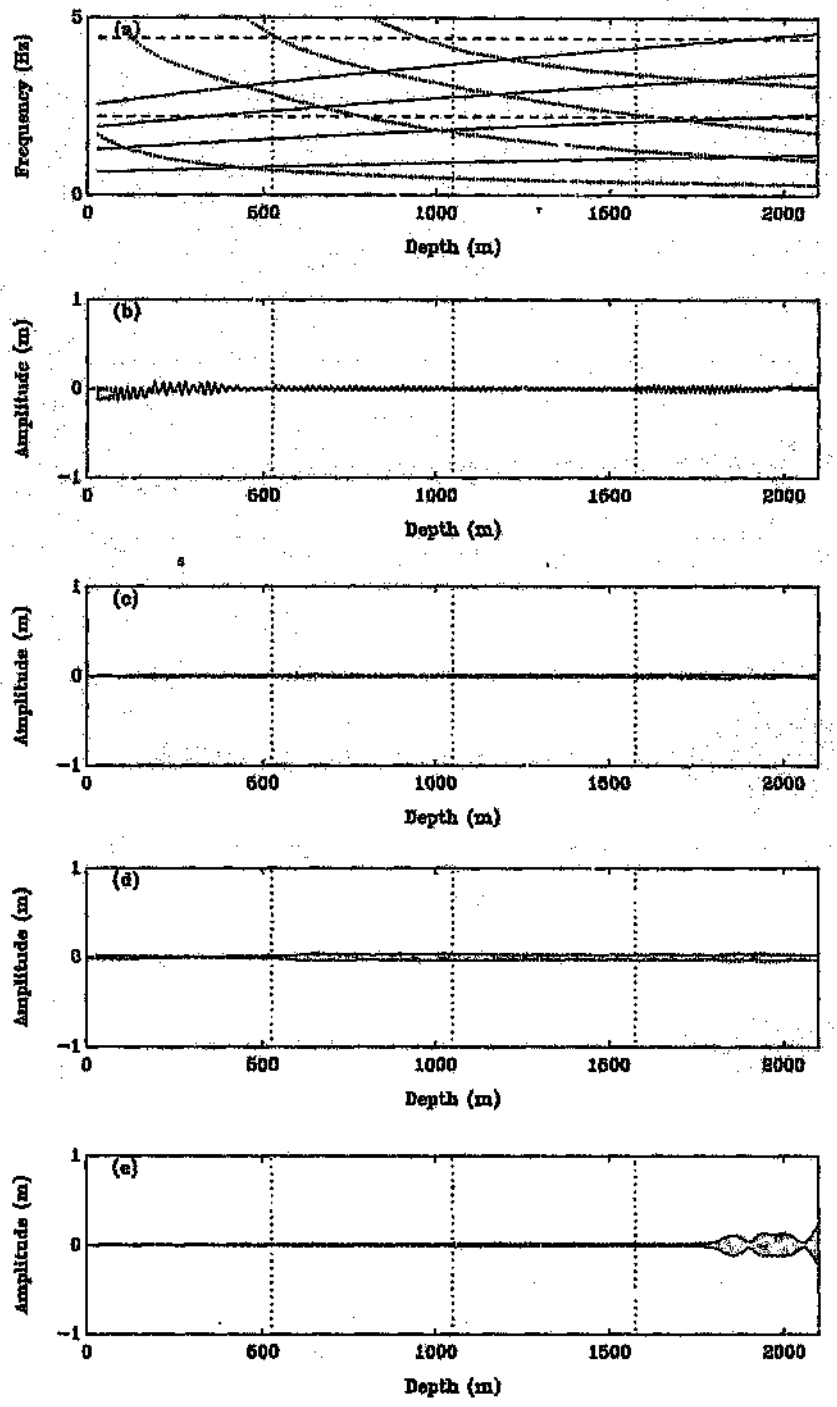

Figure 5.12: Descending cycle: In-plane modal amplitudes: 14.8 m/s

a) Linear Frequency Map, b) $r_1(t)$, c) $r_2(t)$, d) $r_3(t)$, e) $r_4(t)$

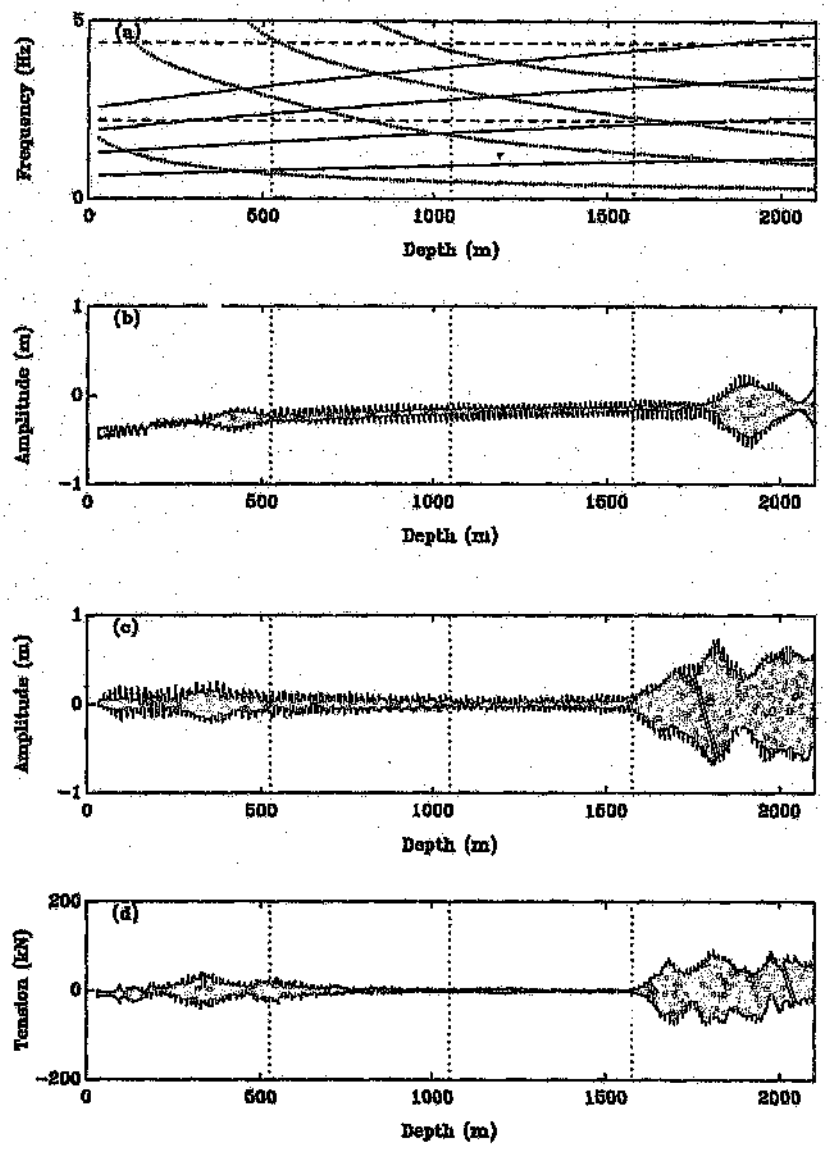

Figure 5.13: Descending cycle: Kloof Mine hoist system: 14.6 m/s

a) Linear Frequency Map.
b) In-Plane Motion - $s = l_c/4$.
c) Out-of-Plane Motion - $s = l_c/4$.
d) Dynamic Catenary Tension.

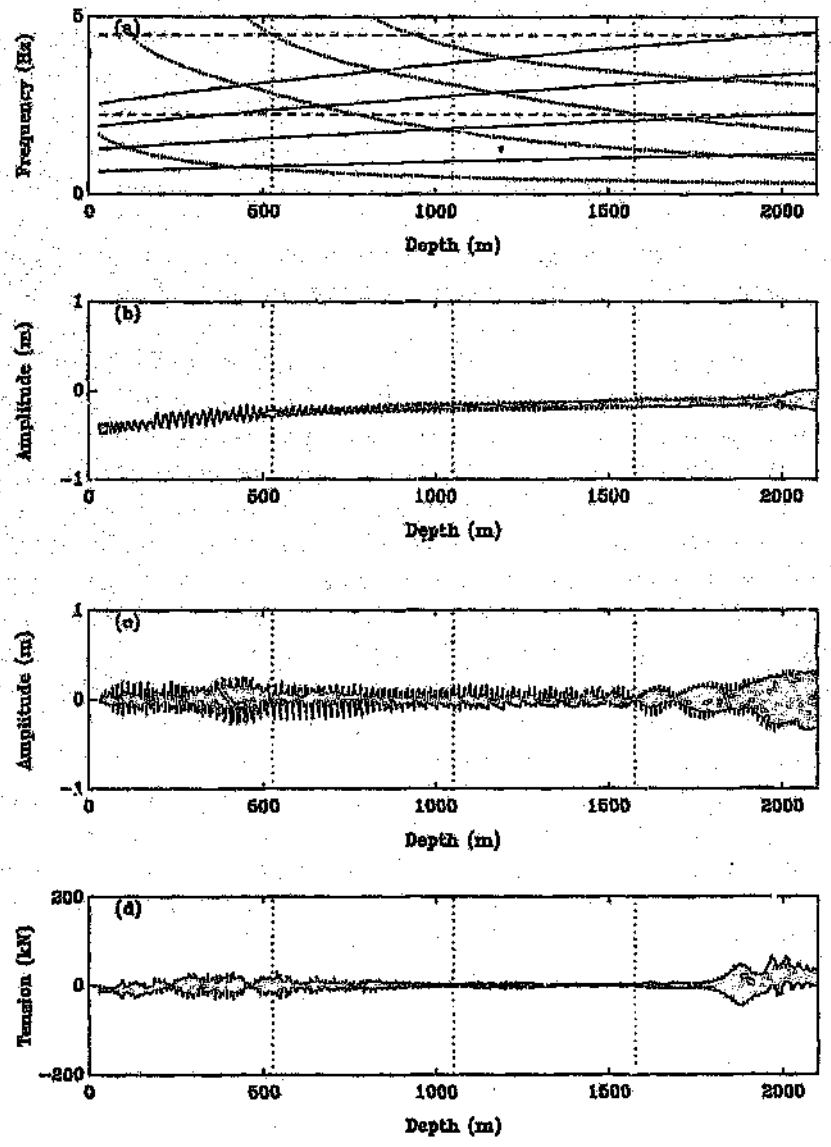

Figure 5.14: Descending cycle: Kloof Mine hoist system: 15 m/s

a) Linear Frequency Map.
b) In-Plane Motion - $s = l_c/4$.
c) Out-of-Plane Motion - $s = l_c/4$.
d) Dynamic Catenary Tension.

5.9.2 Ascending Cycle

The simulated response of the ascending cycle is presented in figures (5.15-5.23). This simulation predicts significant dynamic response, where rope whip occurs and lateral amplitudes of the order of 1m arise in the catenary section. The tension ratio across the sheave exceeds the limits for no slip at approximately 300m, and consequently the simulation would not be realistic above this depth. The rapid growth in the second in-plane mode, reflected in figure 5.18(c), prior to this condition presents convincing evidence of problematic dynamic behaviour. It is noted that according to the stationary linear frequency map, the system is tuned such that the second and fourth out-of-plane modes are directly excited in resonance at approximately 700m. The peak response in the directly excited second and fourth lateral out-of-plane modes occurs in this vicinity. The in-plane response increases after the out-of-plane response has grown. Since the in-plane response is lightly excited, this response is mainly associated with the nonlinear coupling between the in and out-of-plane modes, which is consistent with the autoparametric nature of the system, whereby out-of-plane motion couples to parametrically excite in-plane motion. During the ascending cycle, the Lebus excitation frequency is constant, whilst the lateral natural frequencies reduce with depth. Thus the passage through resonance occurs with the excitation frequency passing from below to above the natural frequency. This is similar to the laboratory model with a positive sweep rate, where as the excitation frequency increased, the lateral out-of-plane motion increased, followed by a bifurcation of the trivial in-plane motion. A plateau region subsequently occurred, where the lateral motion became saturated and significant longitudinal dynamic motion occurred. This behaviour is reflected in the simulation, where the amplitude envelope of the modal response of the even in and out-of-plane lateral modes reflects such a pattern (refer to figures 5.17, 5.18).

The polar response of the catenary is illustrated at four different depths in figures (5.19-5.23); at the start of the wind the motion is essentially planar, becoming almost circular in shape between the depth of 700-500 m. Thereafter, the circular motion gives way to an elliptic orbit, and consequently large fluctuations in the catenary tension arise. It is assumed that the latter region would be termed rope whip by Dimitriou and Whillier[1973]. According to the numerical simulation, the whip is so severe that a slack rope condition is approached during the orbit, which clearly represents very severe dynamic behaviour.

On assessing the overall dynamic response, the auto-parametric nature of the system is evident. An autoparametric mechanism arises when the motion in

a directly excited mode provides parametric excitation leading to response in modes which are not directly excited. This effect is important when conditions of internal resonance exist in the system, as such a condition promotes intermodal response. This situation has been discussed in the literature (Ashworth and Barr[1987], Bux and Roberts[1986],Cartmell and Roberts[1988]), where cascading modal interactions arise, and the directly excited response parametrically excites another mode, which in turn excites a further mode, and so on. Such behaviour occurs with regard to the out-of-plane and in-plane motion, where out-of-plane response parametrically excites in-plane motion. It was expected that the longitudinal system would promote further intermodal response. However, since the sheave tends to isolate the catenary from the vertical system due to its large inertia, such regions of secondary resonance are not clearly evident in the simulated response. It is important to note that in-plane amplitudes of the order of 1m arise, where the direct in-plane excitation is of the order of 0.5 mm. This emphasises the difference between a linear analysis, where in-plane motion would arise purely due to the direct excitation; clearly this amplitude occurs as a result of the nonlinear coupling inherent in the system.

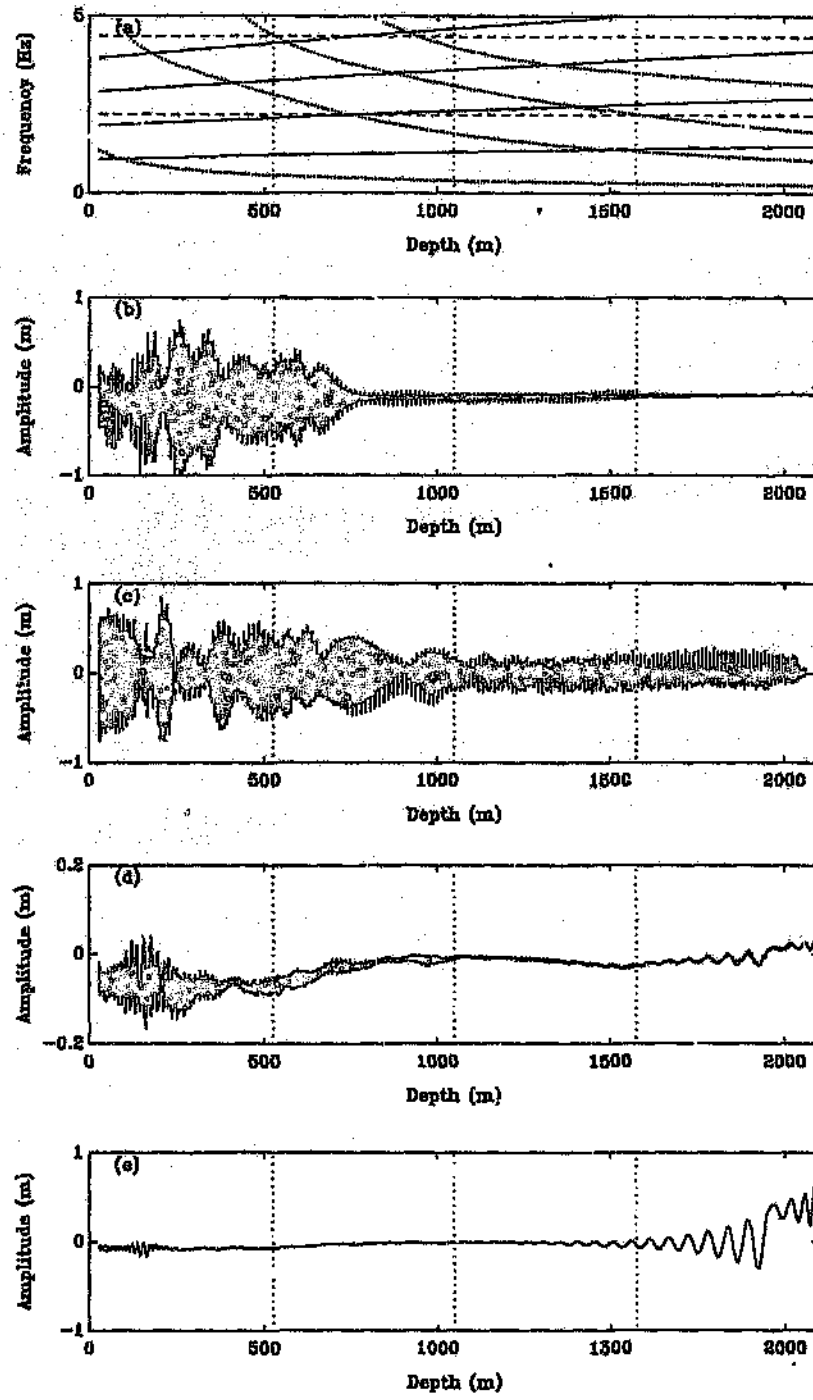

Figure 5.15: Ascending cycle: Kloof Mine hoist system: 14.8 m/s

a) Linear Frequency Map
b) In-Plane Response $s = l_c/4$
c) Out-of-Plane Response $s = l_c/4$
d) Sheave Response
e) Skip Response

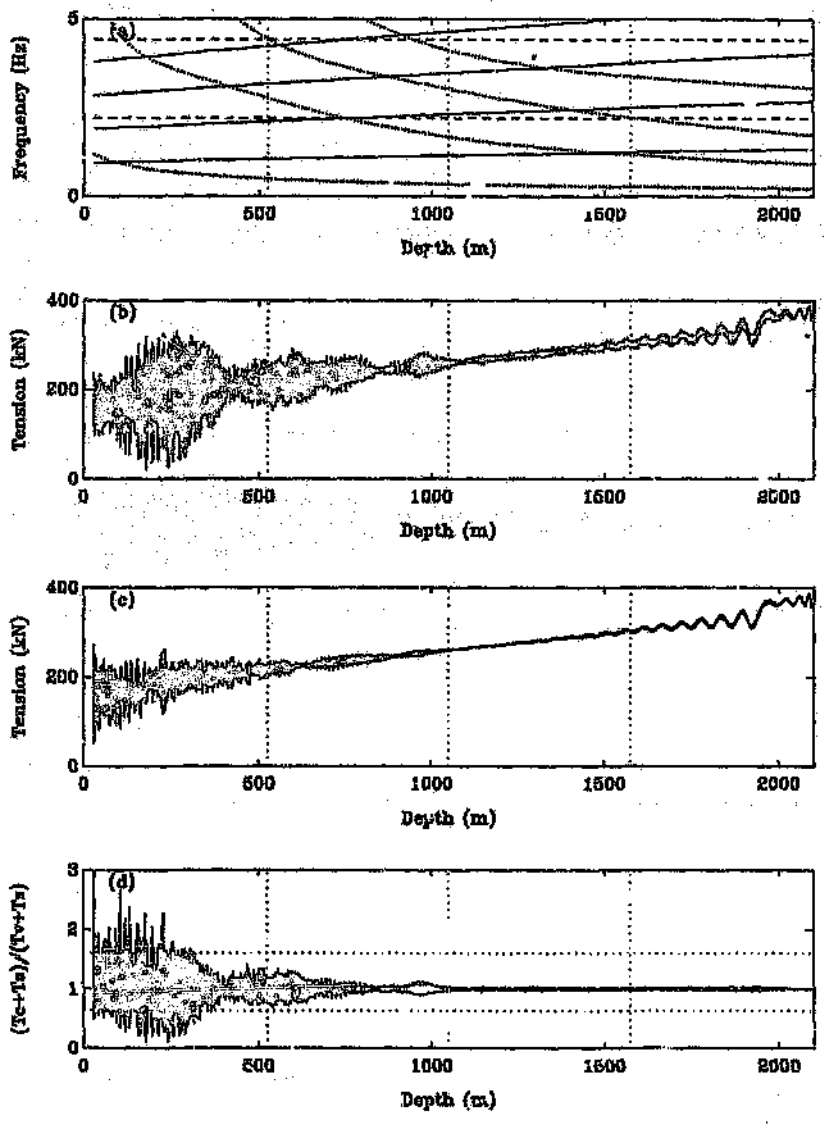

Figure 5.16: Ascending cycle: Kloof Mine hoist system: 14.8 m/s
a) Linear Frequency Map
b) Total Catenary Tension
c) Total Vertical Rope Tension $s = t_c$
d) Tension Ratio Across the Sheave $R = \frac{T_c+T_s}{T_v+T_s}$

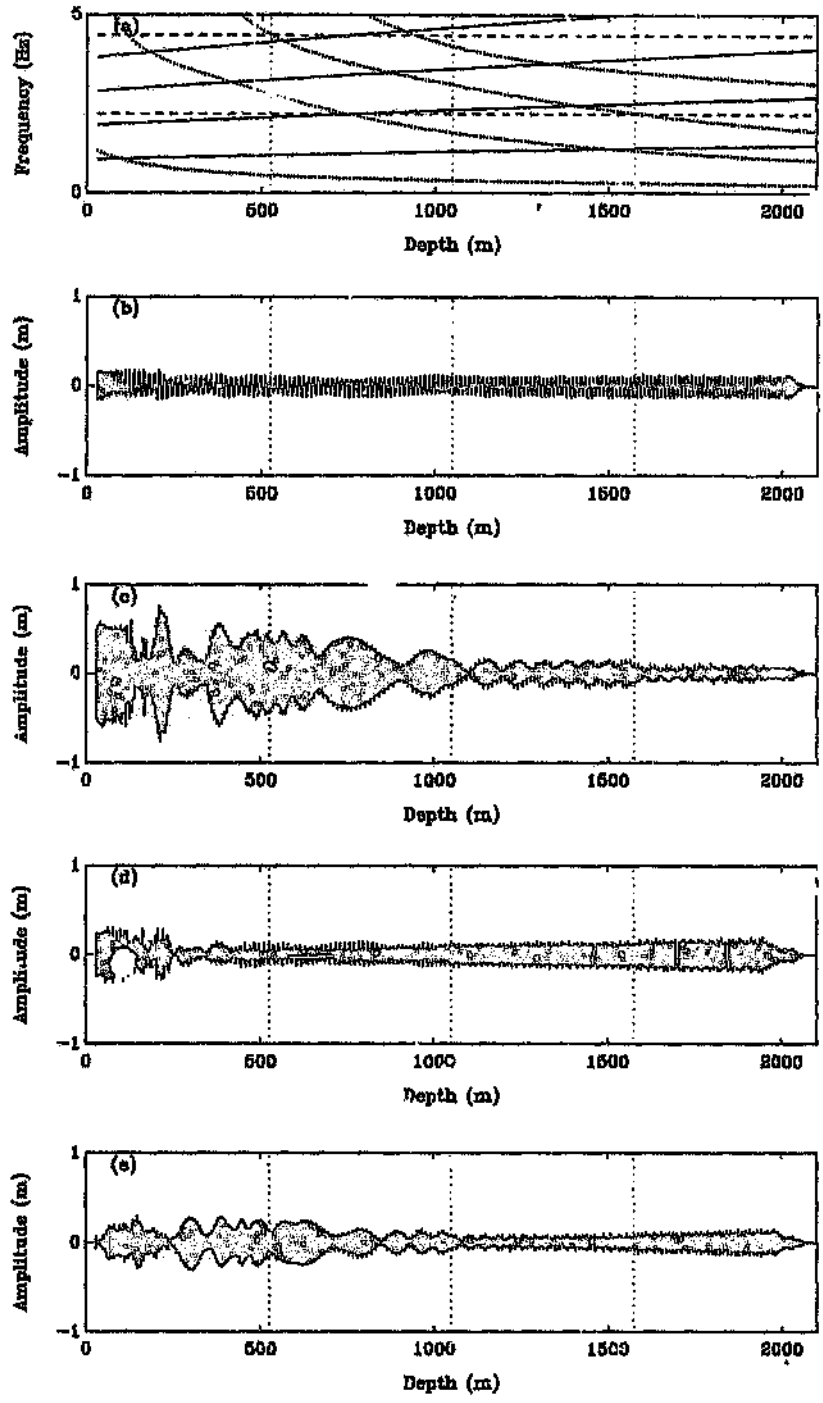

Figure 5.17: Ascending cycle: Out-of-plane modal amplitudes: 14.8 m/s

a) Linear Frequency Map, b) $q_1(t)$, c) $q_2(t)$, d) $q_3(t)$, e) $q_4(t)$

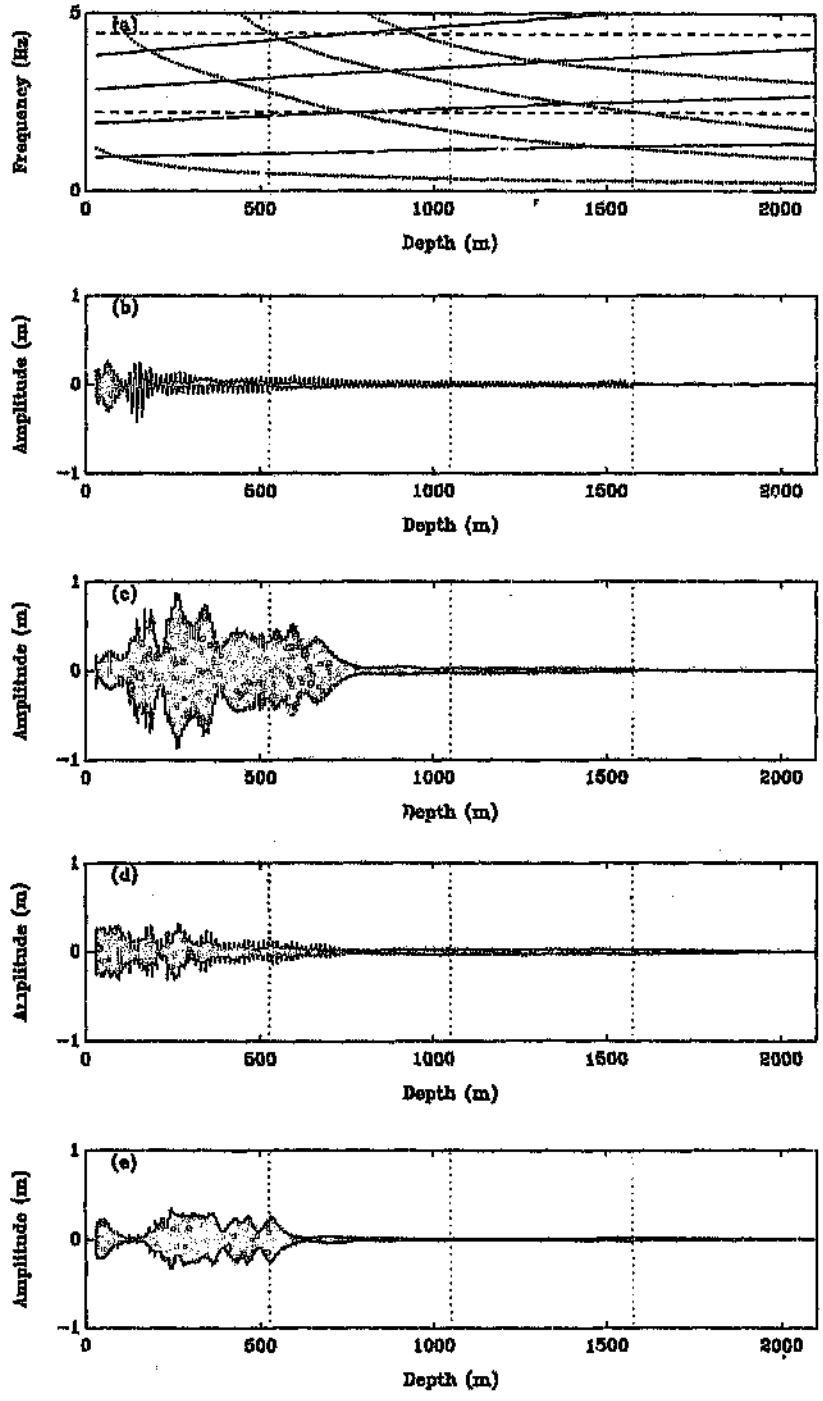

Figure 5.18: Ascending cycle: In-plane modal amplitudes: 14.8 m/s

a) Linear Frequency Map, b) $r_1(t)$, c) $r_2(t)$, d) $r_3(t)$, e) $r_4(t)$

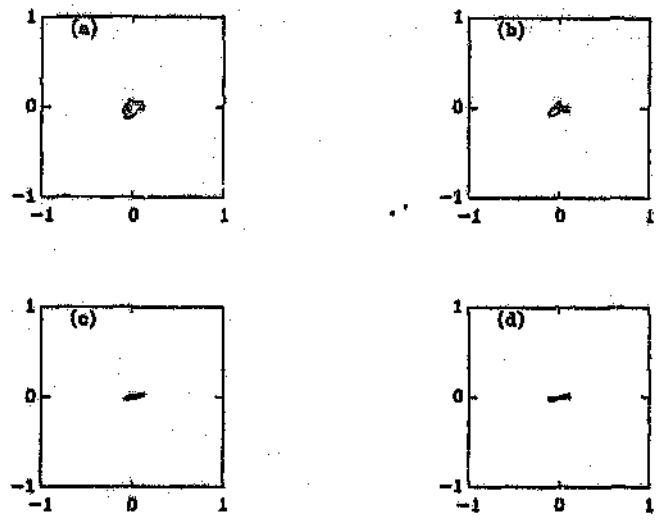

Figure 5.19: Ascending cycle: First mode polar plot
First Mode Polar Plot, Amplitude (m).
a) Depth 300-400 m. b) Depth 500-700 m.
c) Depth 900-1000 m. d) Depth 1500-1600 m.

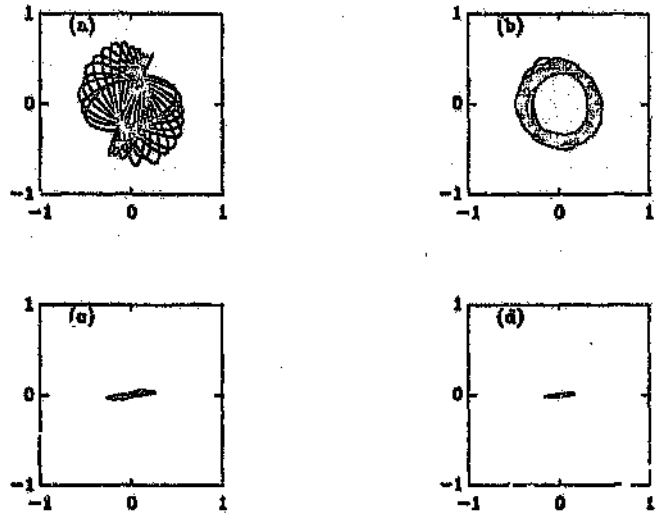

Figure 5.20: Ascending cycle: Second mode polar plot
Second Mode Polar Plot, Amplitude (m).
a) Depth 300-400 m. b) Depth 500-700 m.
c) Depth 900-1000 m. d) Depth 1500-1600 m.

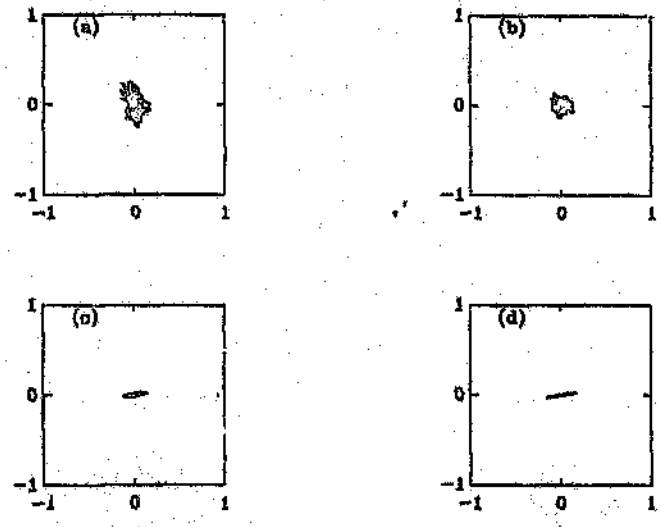

Figure 5.21: Ascending cycle: Third mode polar plot
Third Mode Polar Plot, Amplitude (m).
a) Depth 00-400 m. b) Depth 500-700 m.
c) Depth 900-1000 m. d) Depth 1500-1600 m.

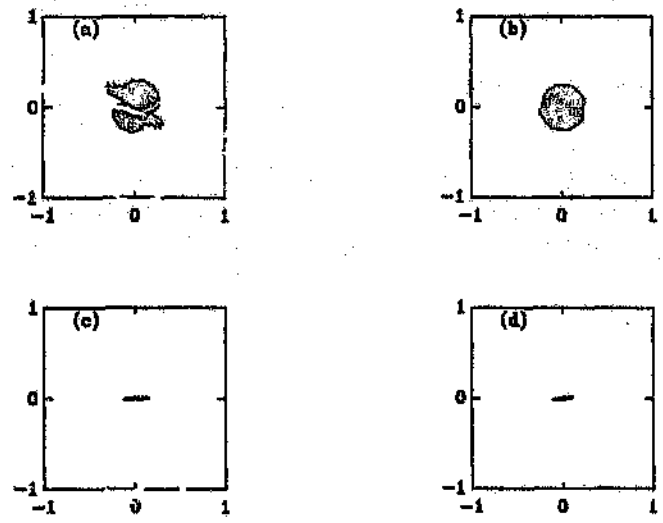

Figure 5.22: Ascending cycle: Fourth mode polar plot
Fourth Mode Polar Plot, Amplitude (m).
a) Depth 300-400 m. b) Depth 500-700 m.
c) Depth 900-1000 m. d) Depth 1500-1600 m.

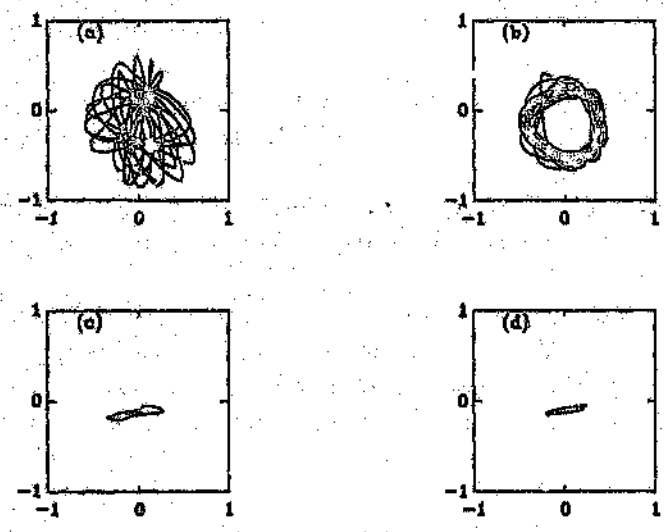

Figure 5.23: Ascending cycle: Polar plot of the response, $s = l_c/4$
Total Response Polar Plot, $s = l_c/4$, Amplitude (m).
a) Depth 300-400 m. b) Depth 500-700 m.
c) Depth 900-1000 m. d) Depth 1500-1600 m.

5.9.3 Dimitriou and Whillier's Observations

Dimitriou and Whillier[1973] considered the Kloof Mine hoist system, and documented observations regarding the motion. These observations are extracted and presented below.

Visual accounts of the dynamic behaviour of the catenaries at Kloof have been recorded over more than a three year period. Some variations have occurred during that time but regular features have been noted and these are numbered below for easy reference. The period of main interest covers the second half of the hoisting cycle, when a full skip is raised, and consists of two distinct phases, marked in figure 1.5.

Phase 1 starts at approximately t=110 s, when the skip is about 900 m below the headsheave, and lasts for about 20 s.

Phase 2 starts at the cross-over from the third to the fourth cable layer on the drum and ends when the skip is at the top of the wind.

Feature 1: All catenaries vibrate to some extent during most of the hoisting cycle, both during raising and lowering of the skips. Except during phases 1 and 2, these vibrations have no clearly defined mode and have small amplitudes. The amplitudes are smaller and the frequencies are higher when the skip is near the bottom of the shaft.

Feature 2: During phase 1, the amplitudes increase and the catenaries settle into a clearly defined second mode for the horizontal and vertical transverse components. The amplitude of the horizontal component is usually larger. Cables A and D[17], in that order, have the greatest amplitude, which is judged to be of the order of 1 m. On occasions, these vibrations continue throughout phase 2 with a gradual change in mode but no perceptible change in amplitude. On other occasions the mode of vibration loses its clear definition at the beginning of phase 2 and the amplitude decreases.

Feature 3: During phase 1 the vertical cables start vibrating transversely. The amplitude, viewed at the collar of the shaft, increases in about 15 s to a maximum of approximately 0.1 m. These vibrations continue, at maximum amplitude throughout phase 2. The vibrations are too rapid for the frequency to be judged by eye. However, a photograph of the vertical cables exhibits an approximate half sine wave of about 40 m length. This indicates that the main wavelength is the same as for the catenaries and the main frequency is ap-

[17]Cables A-D are defined in chapter 1, section 1.2.2.

proximately 2 Hz (but superimposed harmonics give the appearance of a higher frequency to the naked eye.).

Feature 4: On occasions, at the beginning of phase 2, the vibrations of cable A develop a vertical component with an amplitude in excess of 2 m. The cable appears to come down with the speed of a whip. Whenever this occurs the speed of winding is reduced by the operator and this behaviour has not been subjected to regular observation. One observer believes he saw a first mode pattern in the large vertical component of the whip, but this observation has not been corroborated.

Feature 5: None of features 2,3 and 4, is in evidence when the skips are lowered. In particular the vertical cables do not vibrate.

Feature 6: Every six weeks a length of cable is cut at the compensating sheave and the dead coils are pulled over the drum to change the position of the cross-overs. Immediately after this, the vibrations during phases 1 and 2 have their maximum amplitude. The amplitude decreases gradually during the six week interval and the plant can usually be run at full winding speed during the second half of the interval.

Feature 7: An experiment had been tried by the engineering staff at Kloof: the speed of winding was decreased abruptly at the beginning of phase 1. It was found that a drop in speed in this manner from 15 to 14 m/s was sufficient to reduce considerably the amplitude of the vibrations during the remainder of phases 1 and 2.

The simulated behaviour presented in this study largely confirms these observations. The only notable difference is the lack of reported dynamic motion on the descending cycle. It is important to realise that Dimitriou and Whillier's observations were visual, and perhaps they were more sensitive to observations regarding in-plane motion. The lack of in-plane motion in the descending simulation therefor correlates with these observations. Furthermore, the sensitivity of the system to the winding speed is an important consideration. In this regard an increase in winding speed to 14.9 m/s would place this region within the decelerating region, where transverse motion would be viewed as normal. Unfortunately the winder on this system was changed in the late 70's, and further experimental results could not be extracted.

5.10 Conclusion

The simulation exercise conducted has been successful in describing adverse dynamic behaviour at the Kloof mine. It is noted however, that this is a numerical simulation and consequently is constrained by necessary assumptions, for instance the assumption of a proportional lateral and longitudinal damping mechanism, and the neglect of the lateral motion of the vertical rope. It is also important to note that the winder is treated as an ideal energy source, and that no account was made for the flexibility of the headgear structure. Thus any claim that the simulation approaches a precise description of the actual motion would be dubious. Nevertheless, since the equations of motion developed describe the physical nature of the system, it is expected that adverse dynamic behaviour in the simulation would support the notion of adverse dynamic behaviour in reality, and draw attention to this condition of tuning during a design exercise. Thus good engineering judgement would be required to interpret the simulation results.

The assumption in industry that the catenary motion does not generate significant tension fluctuations, and hence any assumption that adverse dynamic catenary motion has no bearing on the fatigue life of the rope is clearly questionable. Significant tension fluctuations were observed in the catenary during the simulated ascending cycle. Although these may be tempered in reality by the support structure flexibility, adverse dynamic catenary motion will result in significant tension fluctuations.

A number of features have been observed during the simulation exercise, which may be used to advantage to improve the dynamic integrity of an existing installation, without changing the geometric parameters of the system. These are itemised below:

- The periodic axial and lateral excitation due to the Lebus cross-over can be reduced, and hence the possibility for whip reduced, by increasing the cross-over arc length, and by profiling the grooves. Since the filler length increases with an increasing cross-over arc-length, the transients induced at a layer change would also reduce. Such an approach has been promoted by industry, and the machining capability is available.
- An important feature, influencing the catenary motion, is the location of a layer change with respect to the linear lateral frequencies of the catenary. It is likely that at some stage of the wind linear resonance of the catenary will arise. Since the phase of the lateral excitation reverses after a layer change, it would be advantageous to position the layer change

close to the occurrence of linear resonance. In this manner, the phase of the excitation may be applied to oppose the residual motion which has developed on approaching resonance, dissipating the motion to some extent. This effect is demonstrated in the sensitivity study presented in Appendix L, where a layer change positioned close to the linear resonance reduced the in-plane amplitudes. Although this may be accomplished on existing installations by including additional dead turns on the drum, to allow for fine tuning of the system with regard to the placement of a layer change, due to pulling the *back* end of the rope, and cutting the front end, these locations would not remain constant throughout the life of the rope. Although the simulation results presented in Appendix L demonstrate the potential advantage of a layer change location close to linear resonance, the response is sensitive to the layer change location. Since the layer change location varies during the life of the rope, in practice this would be an unlikely design strategy. Also, reservations exist regarding miscoiling of the rope at a layer change due to the dynamics of the catenary. For this reason Boshoff suggests that the layer change be located away from a linear resonance.

- Since the periodic longitudinal excitation induces compressive pulses in the catenary on the descending cycle, it is more difficult to excite whip; thus it is recommended that if a resonant condition is unavoidable on either the ascending or descending cycle, then it should be accommodated on the descending cycle.

It is worth considering the response amplitudes in the context of the excitation applied to the catenary at the drum. The harmonic amplitudes comprising the out-of-plane excitation are of the order of 7mm and less, whilst those of the longitudinal and in-plane lateral excitation are of the order of 0.1 mm. The amplitude of the in-plane motion is of the order of 1m. This would represent an amplification of 10 000:1 of the in-plane motion. This clearly highlights the importance of the nonlinear coupling in obtaining a realistic simulation of the response.

With reference to the stability analysis presented in chapter 4, a significant region of instability was predicted in the vicinity of a winding speed of 15 m/s, where nonlinear interaction could be expected with regard to the steady state response. This region occurs at approximately 700m, where the second longitudinal mode tuned to the second lateral mode; thus the additive combination resonance involving the second lateral and longitudinal modes is activated by the second harmonic of the Lebus excitation. Simultaneously, the second lateral mode and the second longitudinal mode are directly excited in resonance by the first harmonic of the Lebus coil cross-over frequency. It would be incor-

rect to attempt to assess the dynamic interactions observed in the simulation in terms of the stationary stability analysis, since the system is non-stationary, and steady state amplitudes are not achieved. Also, the transient excitation due to the start-up and the layer change excitation are not accounted for in the stability analysis. Although good experimental correlation was achieved with the laboratory model, and led to an appreciation of parametric excitation, the neglect of the non-stationary aspect of the system compromises the usefulness of the stationary stability analysis of the system as a single design criterion.

The design strategy proposed is thus to apply the stationary stability analysis to identify conditions of resonance, and to develop an appreciation of the overall system tuning. This would be followed by a sensitivity study based on direct numerical simulation, where an overall appraisal of the system response can be obtained. This is still an involved task, and is perhaps better left to a specialist rather than a design engineer.

Chapter 6

Closure

This study presents a non-linear dynamic analysis of a mine hoist system. During the course of this research, studies concerning the dynamics of strings and cables were reviewed, leading to a critical appraisal of the research conducted by Dimitriou and Whillier[1973], and Mankowski[1982]. At the outset of this study, much emphasis was placed on defining practical criteria to design a mine hoist layout, or to correct the adverse dynamic characteristics of an existing installation. This was initially addressed by considering the stationary dynamic behaviour of the system, where the parametric nature of the system could be confirmed on a laboratory model. It is not surprising that although an appreciation of the stationary system characteristics may provide broad guidelines regarding the avoidance of resonance, since the system is non-linear, the non-stationary aspects of the system ultimately exert an overriding influence on the system behaviour. This feature was apparent in the sensitivity study conducted, where the system response was simulated over a range of winding speeds. Nevertheless, the analytical development was correlated with experimental results measured on a laboratory model, providing confidence in the numerical simulation, and allowing design strategies to be suggested. Ultimately, a comprehensive dynamic analysis of a mine hoist system is a complex task, which requires sound engineering judgement tempered with analytical skills. The techniques developed in this thesis are intended to facilitate the latter, without replacing sound engineering judgement.

It is in the interest of further development that a critical appraisal of the current work is provided. This is important for two reasons. Firstly to examine the limitations of the current analysis and to emphasise that substantial scope exists for further development. Secondly to highlight such issues for the benefit of future researchers pursuing similar studies.

The analytical development pursued by the author is presented in Chapters 4 and 5. With regard to the stationary stability analysis presented in Chapter 4, good experimental correlation was achieved with respect to the laboratory measurements. The definition of the regions of instability of the steady state motion was based on the assumption of a datum solution. The motivation for the datum solution came from a desire to identify regions where the trivial uncoupled lateral *linear* motion was unstable, thus emphasising the importance of the non-linear coupling between the lateral and longitudinal motion and consequently the state of tuning of the system. By applying a harmonic balance method, this approach would directly account for all conditions of tuning obviating the need to consider anomalous or special cases. In light of the experimental results extracted from the laboratory experiment, it would be advantageous to further interrogate the quasi-static equations of motion developed in chapter 5, via a study based on the method of multiple scales. Such a study is currently being pursued at this University (Aligianis[1993]). This study is intended to examine the nonlinear steady state response, and the stability of this response directly for specific tuning conditions of the laboratory model. Further fundamental development is required to examine the system response in the presence of a non-stationary excitation. The simulation of the laboratory model to a swept sine excitation exhibits peculiar behaviour. Such behaviour requires experimental corroboration, as well as fundamental analytical studies in order to assess the implications of such response on the system behaviour with regard to increased winding velocities. This would represent a further extension to the stationary analysis suggested above.

The numerical simulation presented in Chapter 5, illustrated the danger of applying a normal mode technique directly to the equations of motion. This was particularly frustrating, but a worthwhile experience for the author. The initial results from the normal mode simulation were convincing; to the extent that the severity of the problem only became apparent once the laboratory data was available. It is clear from this experience that drawing conclusions based purely on a numerical simulation is a dangerous exercise and should be viewed with skepticism until experimental correlation is achieved. It is in this regard that criticism of the final simulation of the mine hoist system is levelled. The correlation of this system is based on observations provided by Dimitriou and Whillier. Although a video motion analysis system was developed to facilitate such a correlation, and such a study is currently in progress, a number of correlations would be required to convincingly satisfy this criticism. It was decided at this stage to correlate the simulation results broadly with a system which was known by Industry to exhibit adverse dynamic motion, and which had received a great deal of attention in the past, but had not as yet been successfully simulated over the entire ascending and descending winding cycle. Further experimental correlation is clearly necessary, and is currently being

pursued with a major mining house. It is interesting to note that on this particular winder, resonance occurs on the ascending cycle to the extent that the vibration of the headgear superstructure is visible and audible. As a result the winder speed has been reduced from 15 m/s to 13.8 m/s.

The definition of damping mechanisms capable of correctly predicting the lateral and longitudinal dissipation characteristics of mine hoist ropes requires substantial experimental effort. Rudimentary tests were carried out by the author, and a general proportional damping model was applied to model the longitudinal dissipation. Although Mankowski[1988][1990] has examined the lateral dissipation characteristics of a mine hoist rope describing irrotational whirling motion, further studies will be required. The damping mechanism assumed in a dynamic simulation may exert a significant influence on the simulated response, and consequently until accurate data is available, a numerical simulation can be viewed as approximate at best. Conversely, an over ambitious degree of accuracy would be naive.

In the process of developing the analytical model of the mine hoist system, it was assumed that no lateral motion occurs in the vertical rope. Dimitriou and Whillier observed that such motion was related to the adverse catenary motion on the ascending cycle, and hypothesised that it may promote mutual excitation of the catenary via the vertical rope and vice versa. The neglect of the lateral motion in this study was chiefly due to the added complexity associated with accounting for such motion in the discretised model. Such detail would require the incorporation of a substantial number of lateral modes, significantly extending the computational effort. It is the authors' opinion that such detail should be incorporated only after a fundamental appreciation of the system behaviour has been achieved. Simple laboratory tests confirm that violent interactions between the lateral motion on the catenary and vertical section can arise. This represents a further aspect for consideration. Such motion was experimentally monitored on a mine hoist system and is presented in appendix I. A further limitation on the current mine hoist model is that it assumes that the winder is an ideal energy source, and the headgear is rigid. With the advent of advanced winder motors, the electrical winder characteristics are receiving attention in the context of controlling the longitudinal system behaviour due to transients induced during the acceleration and deceleration phase of the winding cycle. This development has been promoted by new legislation which permits the lowering of the rope factor of safety on installations with such control, enabling winding to depths of 4000 m without the use of subshafts. Kaczmarczyk [1993] is currently investigating the simulated response of the hoist system by including the electrical characteristics of the winder motor.

It is natural to question whether an effective strategy exists whereby adverse catenary motion can be corrected or controlled on an existing installation. This is a difficult issue to address, since experience indicates that such strategies ultimately lead to a lowering of the winding velocity, and a consequent loss in production rate. With the advances in control technology and electric motors, it is natural to consider active control strategies. These have not been considered previously. Due to the high drum inertia such strategies cannot be affected directly by the winder. However, it may be possible that if the sheave is energised to equalise the tension between the catenary and vertical system, then an effective strategy may develop to correct such motion. A simulation of the ascending cycle of the Kloof hoist system with a low sheave inertia at 14.8 m/s resulted in a greatly reduced catenary motion. This aspect is currently being investigated with the aid of the laboratory model.

This study has provided a substantial challenge to the candidate. It is natural to be self critical of certain analytical aspects of the work. For instance, it would have been particularly satisfying to complement the simulation of the laboratory model with an analytical study of the steady state motion via the method of multiple scales. The peculiar motion obtained with the non-stationary excitation also represented an attractive avenue of analytical study. In this regard the candidate had to continually redirect the effort towards a practical outcome, even when the analytical aspects of the subject could have been motivated through personal interest. On the otherhand, the experience gained from dealing with a practical system, where it is difficult to obtain physical measurements and quantify the physical parameters accurately, provided valuable experience in that the results achieved required continued critical appraisal.

Clearly further analytical studies are to be pursued in the laboratory and on site to extend this work further. It is hoped that this study will provide support to future researches in the field of mine hoist dynamics, as well as enabling the University to facilitate an informed assessment of existing installations on behalf of the mining industry.

Appendix A

Excitation Definition

This appendix considers the definition of the excitation mechanisms applied in the stationary stability analysis, and in the non-linear numerical simulation of the system. In the stationary stability analysis the excitation accounts for the stationary periodic displacements which occur at the winder drum during constant velocity winding, due to the coiling mechanism. In the numerical simulation, the excitation definition comprises of the former excitation, as well as those excitation mechanisms which give rise to transient system response at various stages of the winding cycle.

During ascent of the conveyance, the winding cycle consists of an initial acceleration to achieve the nominal winding velocity. The conveyance then ascends at a constant winding speed until it decelerates as the conveyance approaches the bank at the head of the shaft. In the process of winding, the rope is coiled onto the drum, and forced displacement excitation occurs at the drum due to the Lebus liner and the resulting coiling pattern. During the constant velocity phase, the excitation imparted to the system via the coiling pattern is periodic and stationary. Since it is not possible to wind the entire length of rope onto the drum in a single layer, multiple layers are required. Typically four layers of rope are wound onto the drum. At the end of a layer, as the rope reaches the drum flange, it changes its traverse direction and rises a full rope diameter to continue coiling on the next layer. The layer change imparts appreciable longitudinal and in-plane lateral transients to the system. Following the layer change, due to the reversal of the traverse direction, the out-of-plane lateral excitation due to the coiling mechanism changes phase by 180° relative to that of the previous layer. Consequently stationary periodic excitation only occurs during the constant velocity phase of the wind, whilst the rope is traversing across the drum surface. Transient excitations occur during the acceleration

and deceleration phases, as well as during a layer change. Thus the excitation applied to the system, and considered in this appendix consists of:

- Longitudinal and lateral in and out of plane stationary periodic excitation due to the Lebus liner coil cross-over profile.
- Longitudinal excitation due to the acceleration/deceleration profile.
- Longitudinal and in-plane lateral excitation due to a layer change.

Other excitation sources not considered in this study may arise due to ovality of the winder drum and head sheave, or due to shaft steelwork misalignment.

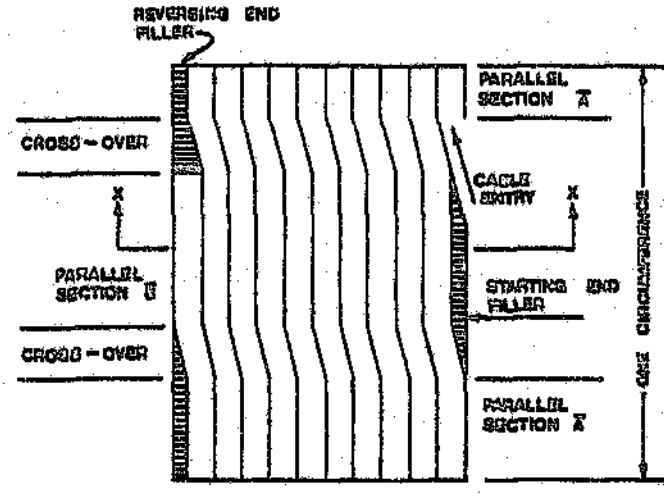

Figure A.1: Mankowski[1982], Figure 2.4(a): Winder drum fitted with a Lebus liner

A.1 Lebus Coil Cross-Over Excitation

Dimitriou and Whillier [1973] identified the Lebus coiling mechanism as the primary source of periodic excitation applied to the system during the constant velocity winding phase. They considered the lateral out-of-plane excitation due to the coiling mechanism to be most significant, and analysed the frequency content of the wave form. In this analysis, they examined a symmetrical 180° Lebus liner, as well as asymmetrical designs with multiple cross over regions. Their analysis demonstrated that in the case of the 180° symmetrical liner, periodic excitation occurred, with a fundamental frequency of twice the angular velocity of the drum. Also the first and second harmonics of the lateral out-of-plane excitation were of a similar order and considered significant. With regard to asymmetrical liners, it was demonstrated that the excitation was periodic with a fundamental excitation at the angular velocity of the drum. The amplitude of the harmonics varied in magnitude with the degree of asymmetry, but no obvious advantage could be found. Since 180° symmetrical Lebus liners are commonly used in the mining industry, the definition of the excitation is based on this configuration.

A 180° lined Lebus drum consists of two parallel grooved circular shells offset from one another by half a rope diameter. The shells are joined at the cross-over insert, which maintains the continuity of the grooves, as illustrated in figure A. Consequently a coil cross-over occurs twice per drum revolution. The cross-over geometry induces excitation in the lateral out of plane w-direction, and in the axial u-direction of the rope. The axial excitation occurs due to the difference in arc length between the diametral arc and that traversed at the cross-over interface. Excitation normal to the drum or in the in-plane v-direction occurs on the second and higher layers as a consequence of the rope rising over underlying coils of the lower layers.

The lateral in-plane displacement of the rope on the second rope layer is calculated from the geometry of the underlying layer as illustrated in figure A.2.

$$v = (1 - \frac{\sqrt{3}}{2})d$$

On the third layer the rope will rise through twice this distance, whilst on the fourth layer it will rise through three times this distance etc. Thus accounting for the layer number, n:

$$v_n = (n-1)(1 - \frac{\sqrt{3}}{2})d$$

where v_n represents the in-plane amplitude during the n^{th} layer.

When the rope exits from the cross-over region, its total displacement is half a rope diameter in the out-of-plane lateral direction, relative to the entry position. Thus the magnitude of the lateral out-of-plane displacement is:

$$w = \frac{d}{2}$$

The magnitude of the displacement in the u direction can be calculated by considering the geometric properties of the cross-over region as illustrated in figures A.3,A.2. During a cross-over the axial velocity of the rope increases to accommodate the difference between the arc length traversed through a cross-over, and that which would be traversed in the absence of a cross-over. Thus relative to the nominal axial displacement due to the winding velocity, this difference represents the additional axial displacement applied to the system. This difference is calculated as:

$$u = R_d\beta[1 + (\frac{d}{2R_d\beta})^2 + (\frac{2v_n}{R_d\beta} \qquad - R_d\beta$$

$$u \approx (0.125 + 0.018(n-1)^2)\frac{d^2}{R_d\beta}$$

Figure A.4 illustrates the physical motion of the rope in the u, v, w directions for one rotation of the drum[1]. The motion in the u direction illustrates that the average winding velocity is slightly larger than that of the peripheral velocity of the drum. This is reflected by the dotted line in figure A.4 (a). The periodic component of the longitudinal motion is consequently the motion relative to this line, as presented in figure A.5 (a). The lateral in-plane displacement v due to the rope rising over an underlying coil is presented in figure A.4 (b). This motion consists of periodic pulses. Figure A.4 (c) presents the

[1]The physical parameters employed reflect those of the Kloof mine winder - $V_e = 15m/s, R_d = 2.14m, d = 48mm, \beta = 0.2rad$, where V_e, R_d, d, β represent the nominal winding velocity, the drum radius, the rope diameter and the cross over arc respectively. Note that these plots reflect the displacement amplitudes for an upwind on the second layer ie. u is negative whilst the rope is traversing in the positive v direction. The displacement profile u is calculated continuously with respect to the cross-over arc β, via $u(\theta) = [(R_d\theta)^2 + (\frac{d\theta}{2\beta})^2 + (\frac{2v_n\theta}{\beta})^2]^{\frac{1}{2}} - R_d\theta \qquad 0 \leq \theta \leq \beta/2$, and a similar relationship for $\beta/2 \leq \theta \leq \beta$. The displacement profile v is calculated as a triangular pulse of magnitude $(1 - \sqrt{3}/2)d$. The displacement profile w is calculated as a ramp of magnitude $d/2$.

lateral out-of-plane displacement w, and reflects the total lateral displacement for one revolution. This displacement comprises of both the average traverse velocity (reflected by the dotted line) and the periodic displacement at the coil cross-over, as presented in Figure A.5.

The Fourier spectra of the periodic wave-forms presented in figure A.5 are presented in figure A.6. Figure A.7 presents the periodic wave forms and their reconstruction from the first and second harmonics of the Fourier spectrum. The periodic displacement functions are:

$$u(t) = \sum_{n=1}^{2} Re(U_n e^{jn\Omega t})$$

$$v(t) = \sum_{n=1}^{2} Re(V_n e^{jn\Omega t})$$

$$w(t) = \sum_{n=1}^{2} Re(W_n e^{jn\Omega t})$$

The harmonic amplitudes U_n, V_n, W_n are complex and contain both amplitude and phase information. For a 180^o Lebus liner, the excitation frequency Ω is related to the nominal winding velocity V_e and the drum diameter R_d by:

$$\Omega = 2V_e / R_d$$

It is evident from the spectra presented in figure A.6 that the most significant excitation occurs in the out-of-plane lateral direction (w), and is an order of magnitude larger than the first harmonic of the in-plane lateral excitation v. Although the longitudinal excitation is small, the axial stiffness is high and consequently significant periodic axial forces can be generated[2].

The displacement profiles presented in figures A.4,A.5 were constructed numerically. A Fourier transform of the displacement profiles provided the amplitude and phase information of each wave form. In this way, both the magnitude and phase relationships between the longitudinal and lateral excitations can be assessed for use in either the stability analysis, or the numerical simulation[3].

[2]Dimitriou and Whillier [1973] estimate the axial forces due to the longitudinal excitation to be of the order of 5KN.

[3]This definition was applied in the non-linear normal mode simulation. An alternative definition, as applied by Mankowski, was applied to the quasi-static model, and is defined in section A.4

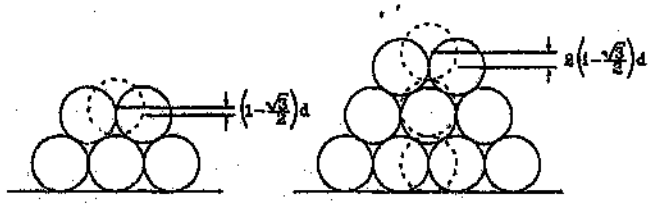

Figure A.2: Geometry of rope layers

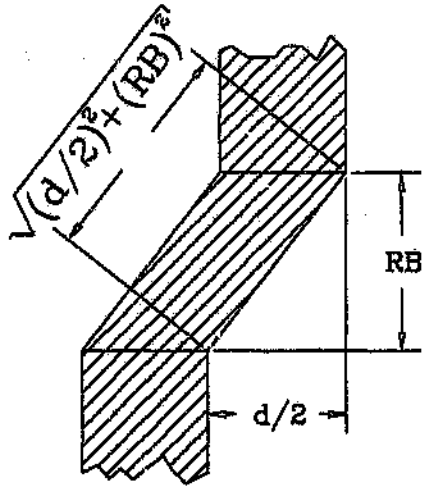

Figure A.3: Cross-over geometry

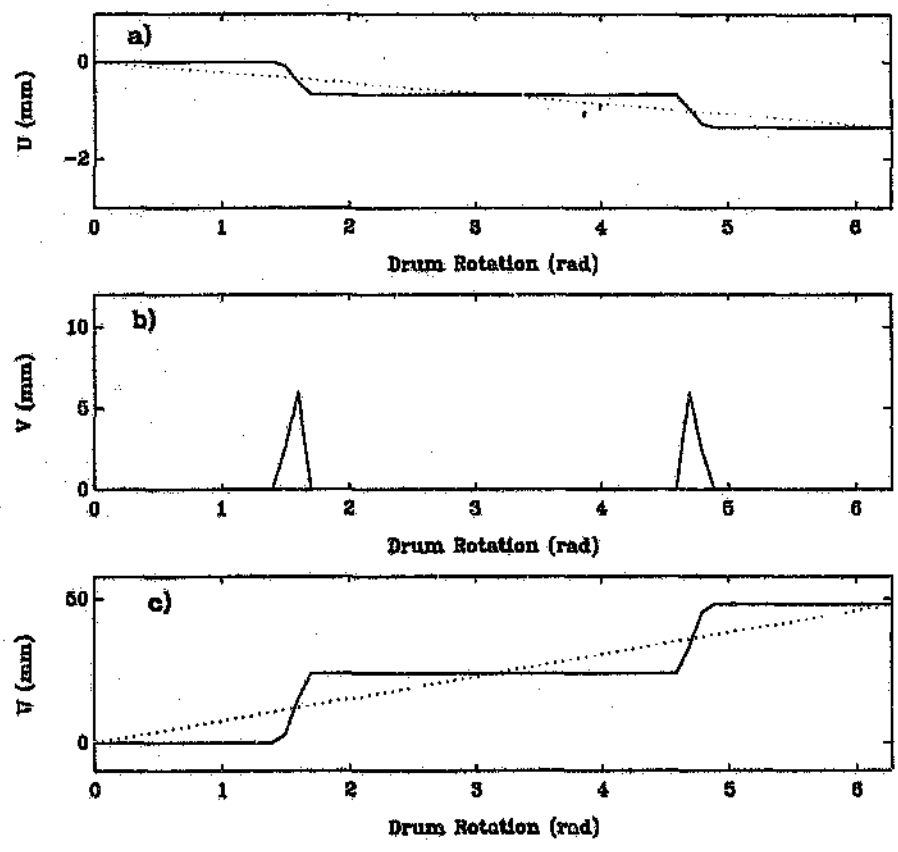

Figure A.4: Physical rope motion per drum revolution

(a) Longitudinal Motion u
(b) In-plane Lateral Motion v
(c) Out-of-plane Lateral Motion w

$V = 15m/s$, $\beta = 0.2rad.$, $d = 48mm$, $R_d = 2.14m$.

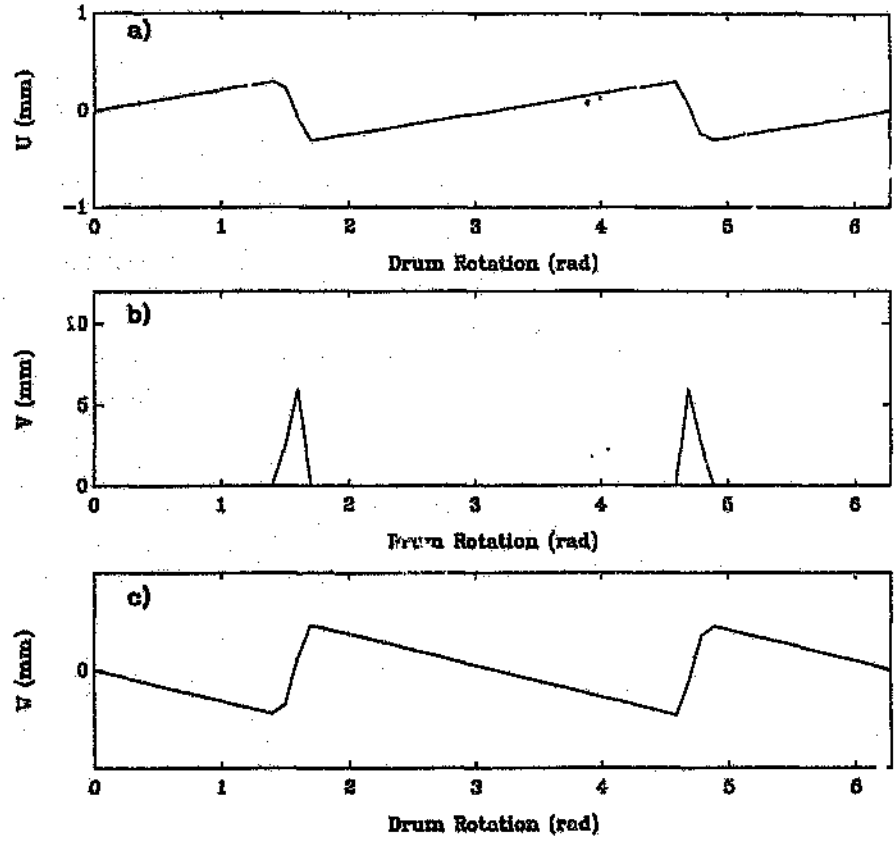

Figure A.5: Periodic motion per drum revolution

(a) Longitudinal Motion u
(b) In-plane Lateral Motion v
(c) Out-of-plane Lateral Motion w

$V = 15m/s$, $\beta = 0.2rad.$, $d = 48mm$, $R_d = 2.14m$.

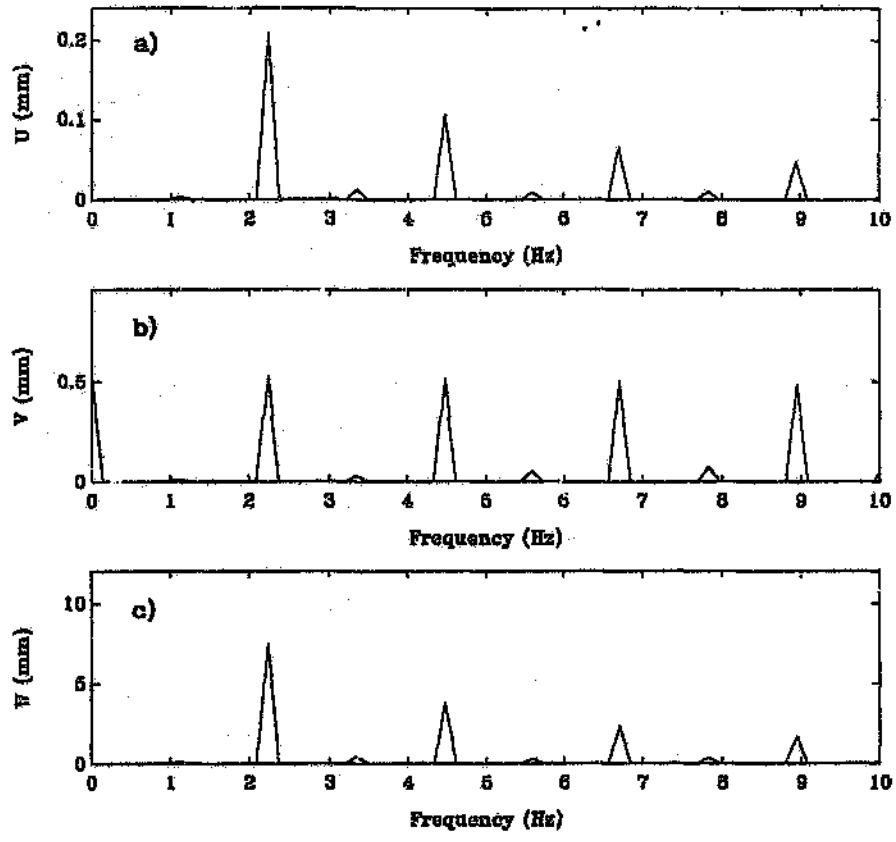

Figure A.6: Displacement spectra

(a) Longitudinal Spectrum u
(b) In-plane Lateral Spectrum v
(c) Out-of-plane Lateral Spectrum w

$V = 15m/s$, $\beta = 0.2rad.$, $d = 48mm$, $R_d = 2.14m$.

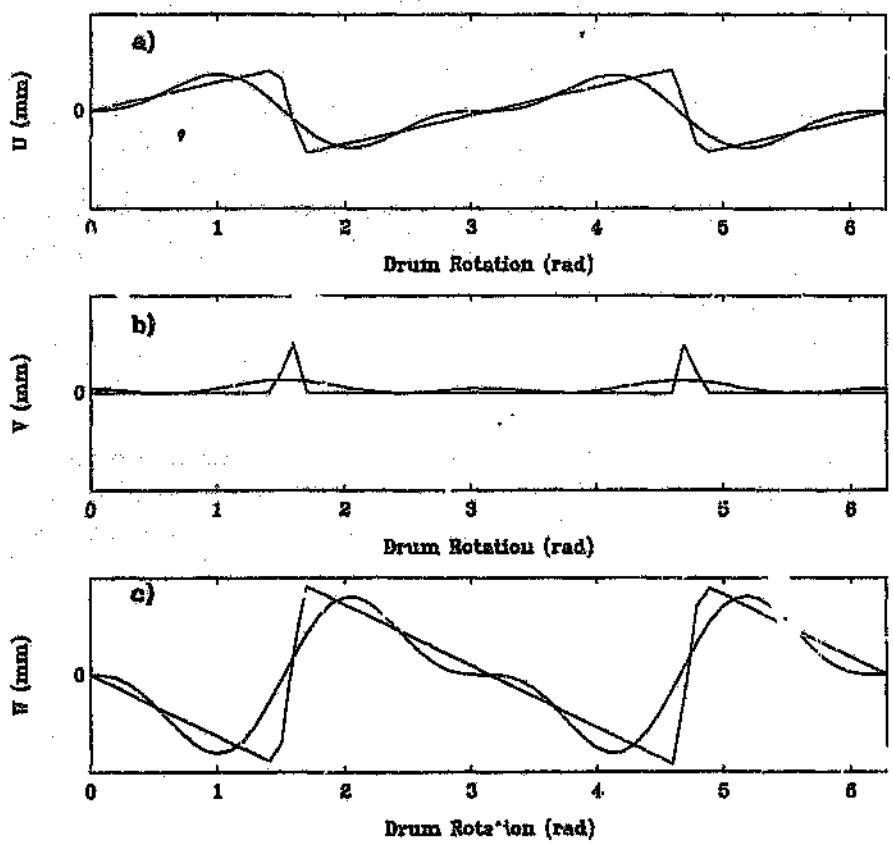

Figure A.7: Simulated Fourier vs. physical excitation - 2 Harmonics

(a) Longitudinal Motion u
(b) In-plane Lateral Motion v
(c) Out-of-plane Lateral Motion w

$V = 15m/s$, $\beta = 0.2rad.$, $d = 48mm$, $R_d = 2.14m$.

A.2 Acceleration/Deceleration Excitation

The longitudinal transient response of the system due to the initial acceleration or deceleration profile is commonly viewed as the most significant aspect of the dynamic response. Consequently many studies in the mining industry have focussed on longitudinal oscillations such as Vaughan[1903, 1917], Pollock and Alexander[1951], Perry and Smith[1932], Greenway[1989], whilst neglecting the coupled dynamics of the catenary. The inertial loading due to the acceleration and deceleration profile is significant and is modelled in modal space by applying a co-ordinate transformation to the system. Considering the inertial term in the longitudinal equation of motion $[1 + \zeta\delta(l_c) + \eta\delta(l_v)]u_{tt}$, where $\zeta = I/\rho AR^2$ and $\eta = M/\rho A$, and applying a co-ordinate transformation:

$$u = u + \overline{u}(t)$$

where u represents the dynamic motion at any point along the rope relative to an axial rigid body motion $\overline{u}(t)$. Since the rigid body motion is not a function of the spatial variable, the equivalent inertial load applied to the system is:

$$F(s,t) = -[1 + \zeta\delta(l_c) + \eta\delta(l_v)]\ddot{\overline{u}}(t)$$

This load is evaluated in modal space as:

$$P_i(t) = -\frac{1}{m_{ii}^u}\int_0^{l_c+l_v}[1 + \zeta\delta(l_c) + \eta\delta(l_v)]\ddot{\overline{u}}(t)\phi(s)ds$$

where $P_i(t)$ represents the equivalent modal force applied to the i^{th} mode; $\ddot{\overline{u}}(t)$ represents the acceleration or deceleration of the system; m_{ii}, ϕ_i represent the modal mass and mode shape of the i^{th} longitudinal mode respectively, as defined in Appendix C for the normal mode model.

A.3 Layer Change Excitation

At a layer change the effective radius of the drum increases/decreases by one rope diameter (d) over the cross-over arc, during the up or down wind respectively. Immediately after this, the rope reverses its direction of traverse. The reversal of the transverse motion causes the lateral out-of-plane excitation to change in phase by 180°. If the winder is treated as an ideal energy source, with a constant drum speed, then in order to accommodate the effective change in diameter at a layer change, the rope experiences a velocity change in a direction tangential and normal to the drum surface. The change in velocity results in a longitudinal and in plane lateral acceleration of the system, and consequently longitudinal and lateral in plane transient response. Since the system is non-linear, these pulses may pre-empt a jump to an alternative dynamic state. For this reason, this excitation source has been included in the analysis. A simple approach is developed below to approximate the acceleration pulse induced by a layer change.

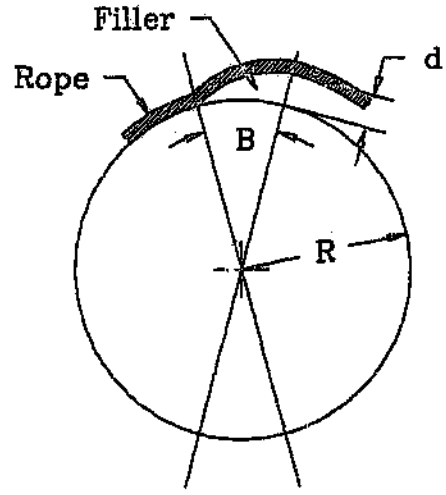

Figure A.8: Filler geometry

In figure . . the detail of a 180° Lebus liner is presented, whilst figure A.8 presents a section of the liner at the drum flange. A filler is positioned on the drum flange to achieve a layer change. In this figure, the layer change occurs over an arc length β. If it is assumed that the winder is an ideal energy source, then the angular velocity of the drum ω remains constant. During the layer change the rope changes its radial position by one rope diameter. If it is assumed that the radial profile is:

$$r(\theta) = dsin^2(\frac{\pi\theta}{2\beta})$$

For a constant angular velocity ω of the drum, $\theta = \omega t$:

$$r(t) = dsin^2(\frac{\pi\omega t}{2\beta})$$

The radial acceleration of the rope is given as:

$$\ddot{r}(t) = \frac{1}{2}d(\frac{\pi\omega}{\beta})^2 cos(\frac{\pi\omega t}{\beta})$$

The axial acceleration is determined from the change of the arc length s of the profile.

$$s(\beta) = \int_0^\beta [1 + \frac{1}{R_d^2}(\frac{dr}{d\theta})^2]^{\frac{1}{2}} R_d d\theta$$

Substituting for the profile $r(\theta)$ and simplifying:

$$s(\theta) = R_d\beta + \frac{1}{2R_d}(\frac{\pi d}{2\beta})^2 \int_0^\beta sin^2(\frac{\pi\theta}{\beta})d\theta$$

Converting to the time domain and carrying out the differentiation with respect to time:

$$\ddot{s}(t) = \frac{\omega}{2R_d}(\frac{\pi d}{2\beta})^2(\frac{\pi\omega}{\beta})sin(\frac{2\pi\omega t}{\beta})$$

In view of the previous section, the additional loading in the longitudinal modal co-ordinates, for the normal mode model, is given by:

$$P_i(t) = -\frac{1}{m_{ii}^w}\int_0^{l_c+l_v} \ddot{s}(t)[1+\zeta\delta(l_c+\eta\delta_{l_v}]\phi(s)ds$$

In the quasi-static model, the longitudinal excitation due to the layer change is applied through a displacement at the drum. Across the arc of the layer change, this displacement is given by:

$$u_l(\theta) = \frac{1}{2R_d}(\frac{\pi d}{2\beta})^2\int_0^{\beta} sin^2(\frac{\pi\theta}{\beta})d\theta$$

This displacement is held constant until the next layer change, where an additional displacement function is applied in a step-wise manner until the end of the wind.

A co-ordinate transformation is applied to account for the inertial loading in the in-plane lateral direction. Since the catenary is restrained in the lateral direction at the sheave end, the displacement varies from that at the drum, linearly to zero at the sheave. Thus the co-ordinate transformation applied is:

$$v = \overline{v} + (1-\frac{s}{l_1})r(t)$$

where $\overline{v}$ represents the dynamic motion of the cable with respect to the rigid body motion $r(t)$. Thus the distributed inertial loading is:

$$F_v(s,t) = -(1-\frac{s}{l_1})\ddot{r}(t)$$

This equivalent modal load applied to the i^{th} mode can be evaluated in the usual manner as:

$$Q_i(t) = -\frac{1}{m_{ii}^w}\int_0^{l_c} \ddot{r}(t)(1-\frac{s}{l_c})\Phi(s)ds$$

where m_{ti}, Φ_i represent the modal mass and mode shape of the i^{th} lateral mode respectively.

These loads are calculated at the appropriate time during the wind. It is interesting to note that since the layer change occurs over a short time interval, the radial acceleration is significant and is of the order of 30g, whilst that of the axial acceleration is of the order of 2g. Figure A.3 presents a plot of the physical rope displacement in the region of the layer change, and the associated axial and normal acceleration of the rope, as a function of drum rotation. It is pertinent to note that radial acceleration is inversely proportional to the square of the arc length, whilst the axial acceleration is inversely proportional to the cube of the arc length (β); thus the layer change transient can be significantly reduced by increasing the riser and cross-over arc[4].

[4]A long filler is undesirable since it leads to additional wear of the rope strands. Experience regarding the cross-over arc length is that the stability of the coiling pattern is adversely affected with an increase in the cross-over arc. Currently the maximum cross-over arc is of the order of 30°.

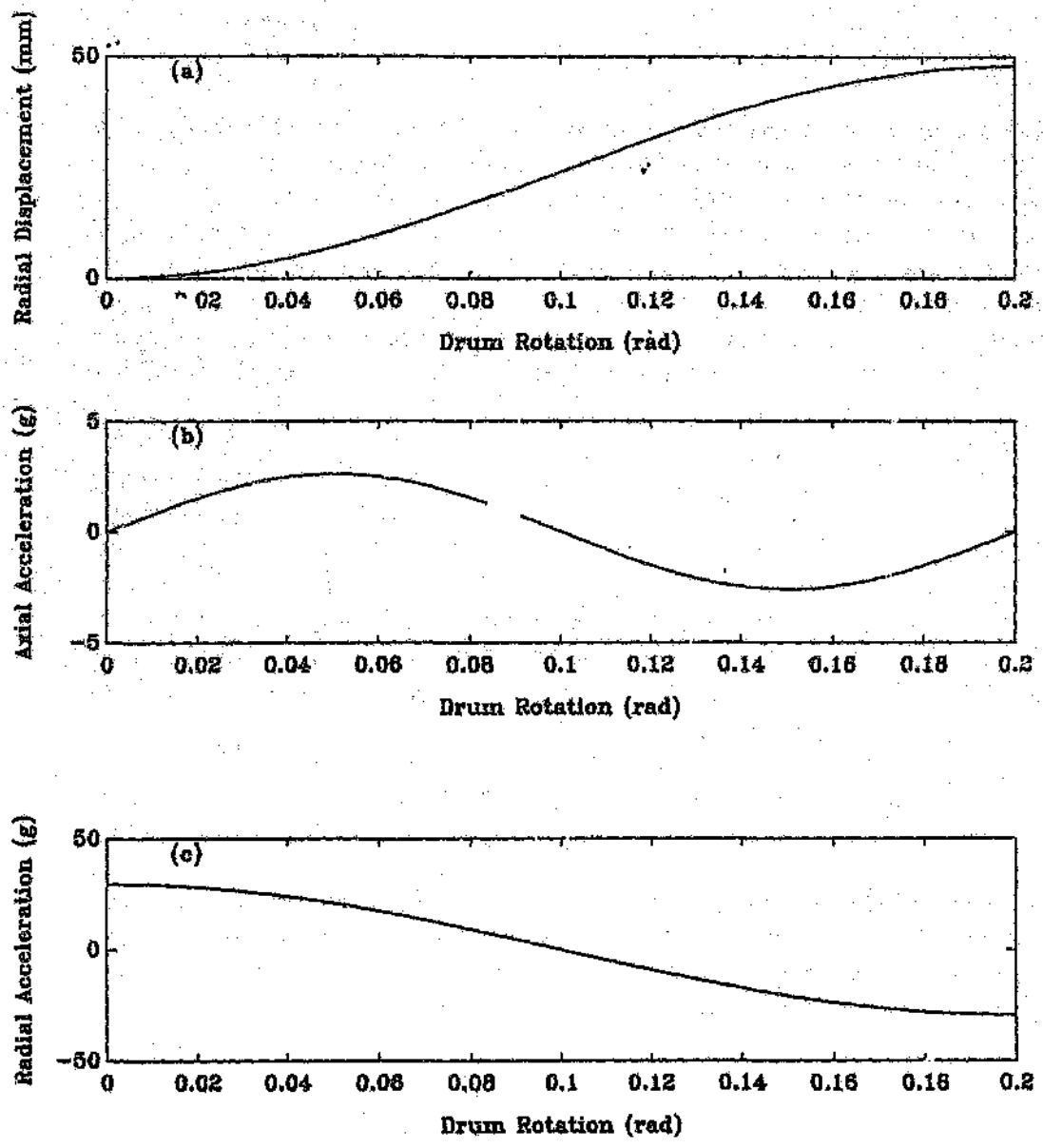

Figure A.9: Layer change transient excitation

(a) Radial Displacement (mm)
(b) Radial Acceleration $\ddot{r}(t)$ (g)
(c) Axial Acceleration $\ddot{s}(t)$ (g)

$V = 15m/s$, $\beta = 0.2rad.$, $d = 48mm$, $R_d = 2.14m$.

A.4 Excitation Definition for the Quasi-Static Model

In developing the quasi-static model with the Simulink software, it was possible to define the geometry of the coil cross over region by means of a look-up table. This is advantageous since the impulsive nature of the excitation is retained for little additional computational effort. Mankowski[1982] defined the coil cross over excitation by means of versine functions in terms of the period of the Lebus frequency τ the duration of the Lebus cross-over τ_β, and the delay time between two successive layer cross overs τ_d. The forcing function displacements are illustrated in figure (A.10). These functions are defined by:

$$\tau = \pi R_d / V_e$$
$$\tau_\beta = \tau\beta/\pi$$
$$\tau_d = \tau - \tau_\beta$$
$$\omega = \pi/\tau_\beta$$

$$u(0,t) = \tfrac{1}{2}\overline{U}[1 - cos(\omega t)] \quad 0 < t \leq \tau_\beta$$
$$v(0,t) = \tfrac{1}{2}\overline{V}[1 - cos(2\omega t)] \quad 0 < t \leq \tau_\beta$$
$$w(0,t) = \tfrac{1}{2}\overline{W}[1 - cos(\omega t)] \quad 0 < t \leq \tau_\beta$$

$$u(0,t) = \overline{U}[t - \tau_\beta]/\tau_d \quad \tau_\beta < t \leq \tau$$
$$v(0,t) = 0 \quad \tau_\beta < t \leq \tau$$
$$w(0,t) = d/2 \quad \tau_\beta < t \leq \tau$$

where $u(0,t)$, $v(0,t)$, $w(0,t)$ refers to the periodic forced displacement at the drum in the longitudinal, in-plane lateral, and out-of-plane lateral directions respectively; d refers to the rope diameter, β refers to the arc of the layer cross over region, V_e the surface speed of the drum, and R_d refers to the winder drum radius.

$$\overline{U} \approx (0.125 + 0.018(n-1)^2)d^2/R_d\beta$$
$$\overline{V} = (n-1)(1 - \sqrt{3}/2)d = 0.134(n-1)d$$
$$\overline{W} = d/2$$

where $\overline{U}, \overline{V}, \overline{W}$ are determined by considering the geometry of the layer cross-over region, and n represents the layer number. The lateral excitation is applied to the catenary by a co-ordinate transformation, which results in an equivalent inertial load being applied in the transformed reference frame. The versine function is easily differentiated in the cross-over region allowing the forcing function to be defined as a function of shaft depth for the in and out-of-plane lateral modes, and defined in a look-up table.

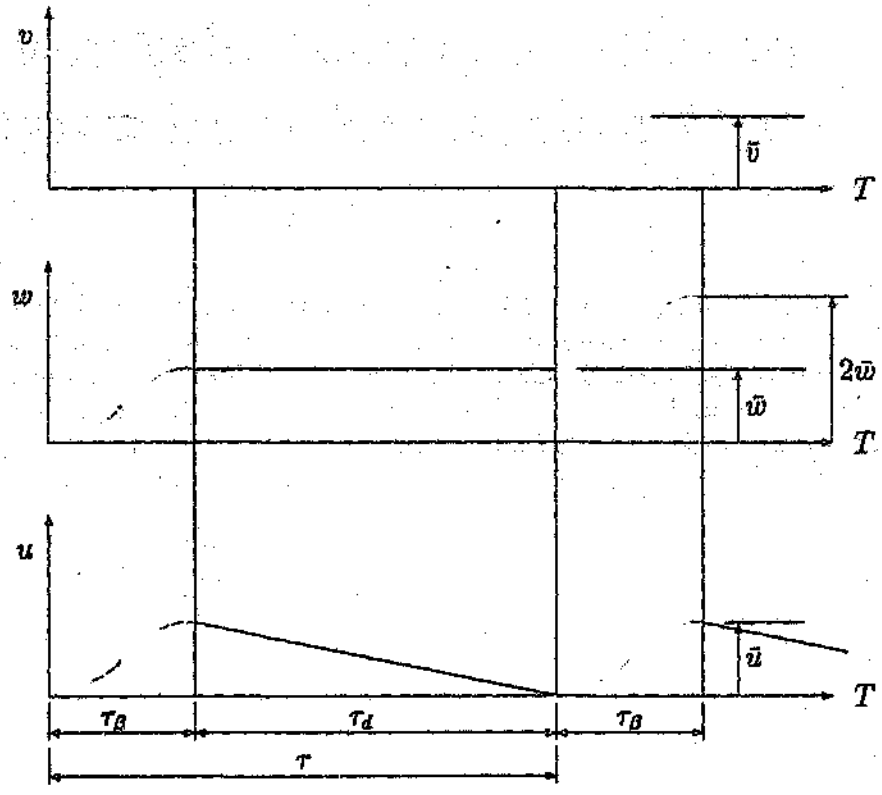

Figure A.10: Lebus coil-cross over excitation - Versine functions

Appendix B

Parametric Response due to Longitudinal Excitation Only

This appendix documents work carried out in the early stages of the study, where the lateral stability of the catenary was examined in the absence of cable curvature and axial transport velocity, due to stationary longitudinal excitation at the winder drum. The equations of motion developed in chapter 3, including relative proportional viscous damping and excluding cable curvature and axial transport velocity are:

$$\begin{aligned}(1+\zeta\delta(s-l_1)+\eta\delta(s-l_2))u_{tt} &= c^2u_{ss}+\mu u_{t,ss}\\ &+c^2(v_sv_{ss}+w_sw_{ss})[H(s)-H(s-l_1)]\end{aligned} \tag{B.1}$$

$$v_{tt} = \bar{c}^2v_{ss}+\mu_l v_{t,ss}+c^2\left[(u_sv_s)_s+\tfrac{3}{2}(v_s)^2v_{ss}+\tfrac{1}{2}(w_s^2v_s)_s\right] \tag{B.2}$$

$$w_{tt} = \bar{c}^2w_{ss}+\mu_l w_{t,ss}+c^2\left[(u_sw_s)_s+\tfrac{3}{2}(w_s)^2w_{ss}+\tfrac{1}{2}(v_s^2w_s)_s\right] \tag{B.3}$$

Where s refers to the axial co-ordinate measured along the rope from the drum to the suspended mass. l_1, l_2 refer to the length of the catenary and total length of the rope respectively. c^2, and $\bar{c}^2$ represent the longitudinal and lateral wave speeds. $\zeta = \frac{I}{\rho AR^2}, \eta = \frac{M}{\rho A}$, and I, R, M, E, A refer to the sheave inertia, sheave radius, conveyance mass, modulus of elasticity, and effective steel area of the rope respectively. μ, μ_l represent the longitudinal and lateral

damping mechanism respectively. Lateral damping is low, of the order of 0.02% of critical, and will consequently be discarded at this stage of the analysis. Longitudinal damping is more appreciable, and is of the order of 1.5% for the first mode, and is therefore retained. Damping is discussed in more detail in chapter 5[1].

In the absence of lateral excitation, the lateral motion may be assumed to be trivial, and hence the response of the rope is purely longitudinal. The purpose of the analysis was to examine where such a solution would be stable. In the absence of lateral motion, the longitudinal equation of motion reduces to:

$$(1 + \zeta\delta(s - l_1) + \eta\delta(s - l_2))u_{tt} = c^2 u_{ss} + \mu u_{t,ss} \tag{B.4}$$

This is a linear equation, and the steady state longitudinal response due to harmonic excitation at the winder drum, $u(0,t) = Re(\sum_{n=1}^{i} U_n e^{jn\Omega t})$, can be formulated in closed form[2]. The axial system response in the catenary section of the rope to such an excitation is presented in appendix C as:

$$u(s_1,t) = Re[\sum_{n=1}^{i}[A_n cos\lambda_n s + B_n sin\lambda_n s]e^{jn\Omega t}]$$

where $\lambda_n = \frac{n\Omega}{c}$, and A_n, B_n are defined in Appendix C.

On substituting the solution for the longitudinal response into equations (B.2),(B.3), the linearised form of the lateral variational equations of motion contain identical terms, and thus only one of the two need be considered. Instability of the trivial solution predicts departure from longitudinal motion to non-planar motion. The severity of this motion will depend on the nonlinear nature of the system, and whether internal resonance occurs, which would further promote the coupling between the lateral and longitudinal motion. The linearised variational equation governing the lateral stability of the catenary is:

$$v_{tt} = \bar{c}^2 v_{ss} + c^2 [u_s v_s]_s \tag{B.5}$$

[1]This model accounts for relative proportional viscous damping, and consequently the modal damping factor increases in proportion to the natural frequency, and the higher modes become successively more damped. On site drop test measurements are presented in appendix G, and indicate that a general proportional damping mechanism may be more appropriate.

[2]Ω represents the coil cross-over frequency.

This equation is converted to an ordinary differential equation with periodic coefficients by applying an eigenfunction expansion for $v(s,t)$ as:

$$v(s,t) = \sum_{i=1}^{n} \phi_i(s) q_i(t) \tag{B.6}$$

where the eigenfunction $\phi_i(s)$ which satisfies the boundary conditions is:

$$\phi_i(s) = sin(\frac{i\pi}{l_1} s)$$

Substitution of equation (B.6) into equation (B.5), and orthogonalising with respect to $\phi_i(s)$ results in a set of coupled ordinary differential equations with periodic coefficients:

$$\left\{ \ddot{q} \right\} + \left[\begin{array}{cc} \backslash & \\ & \omega_i^2 \\ & & \backslash \end{array} \right] + \sum_{n=1}^{i} \left[\left[\begin{array}{c} \\ D_{ij} \\ \\ \end{array} \right]_n cos(n\Omega t) \right] \left\{ q_i \right\} = \left\{ 0 \right\} \tag{B.7}$$

The parametric coupling matrix $[D_{ij}]_n cosn\Omega t$ is identical to that derived in Appendix F for $[W_{ww}(n\Omega t)]^1$, where the axial harmonics of the excitation $U_n e^{jn\Omega t}$ are in phase or 180° out of phase.

$$[D_{ij}]_n cosn\Omega t = Re([W_{ww}(n\omega t)])$$

B.1 Stability Analysis

The variational equations of motion governing the lateral stability of the system are linear equations with time varying coefficients. At this stage of the study, the lateral stability of the system due to longitudinal excitation was considered as a potential indicator for large amplitude catenary motion. Dimitriou and Whillier[1973], Mankowski[1982] and Backeberg[1984] were aware of the potential influence of parametric excitation and response, however no formal mathematical development was performed to examine this phenomenon. Intuitive criteria centred around the observation that regions of main parametric resonance[3] may exist where a lateral mode tunes to half the frequency of the Lebus coil cross-over frequency. This is often termed subharmonic resonance, as identified by Dimitriou and Whillier[1973], where lateral response occurs at a subharmonic of the axial excitation frequency. Dimitriou and Whillier[1973] discussed subharmonic resonance with regard to the experiment of Melde (1859), and the analysis of Lubkin and Stoker[1943]. In this discussion, It was proposed that subharmonic resonance would be amplified if a longitudinal mode was simultaneously resonant. Dimitriou and Whillier[1973] did not identify this condition with internal resonance, where the longitudinal mode tunes to twice the lateral mode, and consequently the nonlinear coupling which subsequently arises, where autoparametric resonance conditions develop. It was recognised that regions of combination resonance in mechanical systems had been reported in the literature, but as no formal analysis was performed proving their existence in the context of the mine hoist system, they were not considered.

The complexity of the mine rope problem is compounded by the fact that in reality the rope is moving with an axial transport velocity, and consequently the natural frequencies of the system are continuously changing. This effect is of considerable importance in the mine hoist system, since the travelling system may pass through a region of instability sufficiently rapidly to contain the growth of the lateral amplitude to an acceptable value. Thus in reality the importance of the region of instability is likely to be a function of both the transport velocity and the amplitude of the parametric excitation. This conforms to the case of a parametrically excited system with non stationary parameters, as discussed by by Nayfeh and Asfar[1988], Neal and Nayfeh[1990], and considered extensively by Mitropolskii[1965].

[3]Main parametric resonance occurs when $\Omega_p = 2\omega_i$.

B.2 Parametric Resonance of MDOF Systems

Hsu[1963] considered the primary regions of instability of a a multi-degree of freedom system subjected to periodic parametric excitation, where the periodic excitation was represented as a Fourier expansion containing an infinite series of harmonic functions. In his method, a perturbation approach was applied to analyse the size of the regions of parametric instability, when the parametric coupling terms are small. Nayfeh[1973a, 1992] reconsidered this and other problems related to parametrically excited linear and nonlinear systems, by applying the method of multiple scales . More recently Szemplinska-Stupnika[1978] and Takahashi[1981a] have extended the method of the generalised harmonic balance as proposed by Bolotin[1964], to include combination resonance regions. Unlike perturbation techniques, the harmonic balance methods are not limited to the concept of a small parameter. The use of ultraspherical polynomial approximation techniques, employing Floquet stability theory have also been proposed (Sinha et al.[1979], Srinivasan and Sankar[1974]. The latter methods are computationally intensive for any sizeable system. Hsu's[1963] method was initially applied to study the system. In retrospect, Nayfeh's[1973b] method of multiple scales is more convenient, as it results in a uniformly valid expansion, and does not require the averaging techniques applied by Hsu[1963].

Hsu's[1963] results may be applied directly to a system of equations of the form:

$$\{\ddot{x}\} + \left(\epsilon \sum_{s=1}^{S} [D^s] cos s\omega t + [\omega_i^2]\right) \{x\} = \{0\}$$

where $[D]^s$ represents the parametric coupling matrix of the s^{th} harmonic, which may be a non-symmetric full matrix, and $[\omega_i^2]$ is a diagonal matrix with its terms equal to the square of the linear natural frequencies of the system, which are assumed to be distinct, and s refers to the s^{th} harmonic of the excitation frequency ω.

B.2.1 Hsu's Perturbation Solution

In analysing the system, Hsu[1963] represented the equations of motion in first order form as:

$$\begin{aligned} \frac{dx_i}{dt} &= w_i \\ \frac{dw_i}{dt} + \omega_i^2 x_i &= f_i(x_i, \omega_i, t) \end{aligned} \tag{B.8}$$

where the solution $x_i(t)$ contains a component representing the free response of the linear solution, and a power series expansion in the perturbation term ϵ:

$$x_i(t) = A_i(t)cos\omega_i t + B_i(t)sin\omega_i t + \sum_{q=1}^{n} \epsilon^q x_i^{(q)} \tag{B.9}$$

$$w_i = \frac{dx_i}{dt} = \omega_i(\ -A_i(t)sin\omega_i t + B_i(t)cos\omega_i t) + \sum_{q=1}^{n} \epsilon^q \frac{dx_i^{(q)}}{dt} \tag{B.10}$$

The first two terms on the right hand side of these equations are termed the variational part of the solution, whilst the remaining term is the perturbation part of the solution. In essence the variational component of the solution represents the response of the system to an initial disturbance or a variation of the trivial solution. If this component of the solution is stable, then the disturbance remains bounded, and the response to the disturbance is essentially dictated by the free response of the system. However in a region of instability, the variational component of the solution grows without bound, indicating that the system is unstable if subjected to an arbitrarily small disturbance.

In equation (B.10) above, A_i, B_i are assumed to vary slowly with time, and consequently are assumed time independent, when differentiating with respect to time. However, since A_i, B_i may be functions of time, the condition of slowly varying parameters is satisfied only when:

$$\frac{dA_i}{dt}cos\omega_i t + \frac{dB_i}{dt}sin\omega_i t = 0$$

Substitution of the assumed solution (B.9), into the equation motion (B.8) results in:

$$\begin{aligned}\omega_i(-A_i' sin\omega_i t - \omega_i A_i cos\omega_i t &+ B_i' cos\omega_i t - \omega_i B_i sin\omega_i t) + \\ \omega_i^2(A_i cos\omega_i t + B_i sin\omega_i t) &+ \omega_i^2 \sum \epsilon^q \dot{x}_i^q + \sum \epsilon^q \frac{d^2 x_i^q}{dt^2} \\ &= -\epsilon \left\{ \sum_{s=1}^{S} \sum_{j=1}^{n} d_{ij}^s cos s\omega t x_j \right\} \end{aligned} \tag{B.11}$$

Considering only the first order powers[4] of ϵ and equating terms, the following system of equations are obtained; the solution of which determines the coefficients A_i, B_i:

$$\frac{dA_i}{dt} cos\omega_i t + \frac{dB_i}{dt} sin\omega_i t = 0 \tag{B.12}$$

$$\begin{aligned} -\omega_i \frac{dA_i}{dt} sin\omega_i t + \omega_i \frac{dB_i}{dt} cos\omega_i t &+ \epsilon(\frac{d^2 x_i^1}{dt^2} + \omega_i^2 x_i^1) = \\ &- \frac{\epsilon}{2} \sum_{s=1}^{S} \sum_{j=1}^{n} \{ d_{ij}^s A_j (cos(\omega_j + s\omega)t \\ &+ cos(\omega_j - s\omega)t) + d_{ij}^s B_j (sin(\omega_j + s\omega)t \\ &+ sin(\omega_j - s\omega)t)\} \end{aligned} \tag{B.13}$$

Hsu[1963] then proceeded by considering the variational and perturbation part of the solution separately. Those terms which result in small divisors are retained in the variational part of the solution, whilst the remaining terms are carried to the perturbation component of the solution. If one assumes that the system is tuned such that ω_i are distinct and $\omega_j \pm s\omega$ are not close to $\pm\omega_i$, then all the terms on the right hand side of equation (B.13) are retained in the perturbation part of the solution, which is bounded. The equations describing the variational part of the solution are:

[4]Expansions developed to higher order would define the second and subsequent regions of instability. These are known to be smaller and more difficult to enter than the primary region, and consequently only the primary parametric region is considered by Hsu[1963].

$$\begin{aligned} \frac{dA_i}{dt}cos\omega_i t + \frac{dB_i}{dt}sin\omega_i t = 0 \\ -\frac{dA_i}{dt}sin\omega_i t + \frac{dB_i}{dt}cos\omega_i t = 0 \end{aligned} \tag{B.14}$$

Solving for A_i, B_i leads to constant coefficients, and thus the solution is bounded and stable.

However in cases where $\omega_j \pm s\omega$ is close to $\pm\omega_i$, the stability of the system must be examined as small divisor terms occur in the perturbation part of the solution $x^{(q)}$, and are consequently carried to the variational part of the solution. The variational equations can be transformed into a set of autonomous equations by applying the Kryoloff-Bogoliuboff-Van der Pohl averaging technique, where it is assumed that A_i, B_i are slowly varying functions of time relative to the averaging period, and are therefore treated as constants. The stability of these autonomous equations, and consequently the stability of the variational solution, can then be determined by examining the characteristic roots of the autonomous equations.

Proceeding in this manner, Hsu[1963] determined that for an undamped system, the motion would be unstable and grow without bound if the following conditions were satisfied.

$\omega = \frac{2\omega_i}{s}$	Main parametric resonance
$\omega = \frac{1}{s}(\omega_i \pm \omega_j)$	Combination parametric resonance

Further analysis provides the regions of instability as a function of the perturbation coefficient ϵ. These regions are given by:

Main parametric resonance

$$\frac{2\omega_i}{s} - \frac{\epsilon|d_{ii}|^{(s)}}{2s\omega_i} < \omega < \frac{2\omega_i}{s} + \frac{\epsilon|d_{ii}|^{(s)}}{2s\omega_i}$$

Combination sum type parametric resonance:

$$\frac{\omega_i + \omega_j}{s} - \frac{\epsilon}{2s}\left(\frac{d_{ij}^{(s)}d_{ji}^{(s)}}{\omega_i\omega_j}\right)^{\frac{1}{2}} < \omega < \frac{\omega_i + \omega_j}{s} + \frac{\epsilon}{2s}\left(\frac{d_{ij}^{(s)}d_{ji}^{(s)}}{\omega_i\omega_j}\right)^{\frac{1}{2}}$$

Combination difference type parametric resonance

$$\frac{\omega_i - \omega_j}{s} - \frac{\varepsilon}{2s}\left(\frac{-d_{ij}^{(s)} d_{ji}^{(s)}}{\omega_i \omega_j}\right)^{\frac{1}{2}} < \omega < \frac{\omega_i - \omega_j}{s} + \frac{\varepsilon}{2s}\left(\frac{-d_{ij}^{(s)} d_{ji}^{(s)}}{\omega_i \omega_j}\right)^{\frac{1}{2}}$$

These regions are termed main and combination sum and difference type resonances respectively. These results confirm that in a coupled system, the diagonal terms of the parametric coupling matrix $d_{ii}^{(s)}$ govern the size of the main parametric resonance region, whilst the off diagonal terms $d_{ij}^{(s)}$ govern the size of the combination parametric resonance region. Difference type resonances can only occur if $d_{ij}^{(s)} d_{ji}^{(s)} < 0$ and conversely sum type can only occur if $d_{ij}^{(s)} d_{ji}^{(s)} > 0$. Thus only sum type combination resonances will occur if the coupling matrix is symmetric, whilst both may occur if the matrix is asymmetric.

B.3 Anomalous Cases

The results from Hsu's[1963] analysis confirm that if the parametric coupling matrix is diagonal, which results in a set of uncoupled Mathieu equations, then only main parametric resonances will occur. In the general case of a nonsymmetric coupling matrix, main as well as sum and difference type parametric resonances occur. In the mine hoist system, the parametric coupling matrix is always symmetric, and consequently parametric resonances of the difference type do not arise. Hsu[1963] notes that in the case where repeated natural frequencies of the system occur, or when different combinations of i, j, s overlay each other, then an anomalous situation arises, where more than one resonance is excited simultaneously, and a more detailed analysis is required. The former case of repeated natural frequencies has been analysed by Nayfeh[1983b] and Tezak et al[1982]. The later case of multi-frequency excitation of a two degree of freedom system is considered by Nayfeh[1983a].

The stability analysis presented considers the stability of the motion in the neighbourhood of the first order expansion. Consequently principal[5] regions of main and combination parametric resonance are considered. This follows Hsu's[1963] argument that although higher order regions may co-exist within the principal parametric regions, and therefore secular terms arise in the higher order expansion, for small parametric excitation the boundary of stability would be dictated by the principal region, and hence the stability of the first order expansion. In the case of the mine hoist system, anomalous conditions almost always arise since the natural frequencies of the catenary are related by integer multiples, or are commensurable. Thus if one harmonic of the excitation tunes to a region of parametric resonance, then other harmonics will simultaneously excite other resonances. These may be main or combination parametric resonances of the summed type. Thus it is possible to develop a number of anomalous cases, depending on the number of harmonics accounted for in the longitudinal excitation, and the number of lateral modes accounted for in the eigenfunction expansion[6]. Three conditions are examined for the mine hoist system, as presented in table B.1.

It is shown that the first two cases are in fact not anomalous, and Hsu's[1963] formulae can be applied directly. However in the last case, a stability criterion is derived which requires explicit solution to determine the span of the region

[5] For a multi-degree-of-freedom parametrically excited system, with a single excitation frequency Ω, regions of instability arise at $\Omega = \omega_i \pm \omega_j/n$; the principal region refers to $n = 1$, and is obtained by considering the first order expansion. Secondary regions occur at $n = 2, 3 \cdots$ as defined by the second order and higher expansions.

[6] Although the model is truncated to account for a finite number of lateral modes, the forced longitudinal response represents the complete solution, without modal truncation.

Table B.1: Anomalous regions of parametric resonance

Case	DOF	Harmonics	Resonance Condition
Case 1	2 DOF	$s = 1, 2$	$\omega \approx 2\omega_1, 2\omega \approx 2\omega_2$
Case 2	3 DOF	$s = 1$	$\omega \approx 2\omega_2 \approx \omega_1 + \omega_3$
Case 3	2 DOF	$s = 1, 2, 3$	$\omega \approx \omega_1, 2\omega \approx 2\omega_1, 3\omega \approx \omega_1 + \omega_2$

of instability. Nayfeh[1983a] presented results of an analysis of a two degree of freedom system to multi-frequency excitation. The third case considered here is identical to the fifth case presented by Nayfeh[1983a], where simultaneous main resonance and a summed combination resonance arises due to two different harmonics.

B.3.1 Case 1: 2 DOF - $s = 1, 2 \qquad \omega \approx 2\omega_1$

This case represents a two degree of freedom system excited by a periodic function with two harmonic components at a frequency ω and 2ω. It is assumed that ω is close to $2\omega_1$, and ω_2 since the natural frequencies of the system are related by integer numbers. Employing a detuning parameter $\lambda\epsilon$, the excitation frequency ω may be written as:

$$\omega = 2\omega_1 + \lambda\epsilon$$

$$\omega = \omega_2 + \lambda\epsilon$$

or as:

$$\begin{aligned} \omega - \omega_1 &= \omega_1 + \lambda\epsilon \\ 2\omega - \omega_2 &= \omega_2 + 2\lambda\epsilon \end{aligned} \tag{B.15}$$

Transferring small divisor terms in the perturbation part of the solution to the variational part, and expanding the variational part of equation(B.13) for the two degrees of freedom:

$$-\frac{dA_1}{dt}sin\omega_1 t + \frac{dB_1}{dt}cos\omega_1 t = -\frac{\epsilon}{2\omega_1}\sum_{s=1}^{2}\left\{\begin{array}{c} A_1 d_{11}^{(s)}(cos(\omega_1 + s\omega)t + cos(\omega_1 - s\omega)t) + \\ B_1 d_{11}^{(s)}(sin(\omega_1 + s\omega)t + sin(\omega_1 - s\omega)t) + \\ A_2 d_{12}^{(s)}(cos(\omega_2 + s\omega)t + cos(\omega_2 - s\omega)t) + \\ B_2 d_{12}^{(s)}(sin(\omega_2 + s\omega)t + sin(\omega_2 - s\omega)t) \end{array}\right\} \tag{B.16}$$

$$-\frac{dA_2}{dt}sin\omega_2 t + \frac{dB_2}{dt}cos\omega_2 t = -\frac{\epsilon}{2\omega_2}\sum_{s=1}^{2}\left\{\begin{array}{c} A_1 d_{21}^{(s)}(cos(\omega_1 + s\omega)t + cos(\omega_1 - s\omega)t) + \\ B_1 d_{21}^{(s)}(sin(\omega_1 + s\omega)t + sin(\omega_1 - s\omega)t) + \\ A_2 d_{22}^{(s)}(cos(\omega_2 + s\omega)t + cos(\omega_2 - s\omega)t) + \\ B_2 d_{22}^{(s)}(sin(\omega_2 + s\omega)t + sin(\omega_2 - s\omega)t) \end{array}\right\} \tag{B.17}$$

Substituting equations (B.15) into the above equations and retaining terms which would cause secular behaviour of the perturbation solution: ie any terms which result in frequencies close to ω_1 or ω_2 in equations (B.16),(B.17) respectively, results in:

$$-\frac{dA_1}{dt}sin\omega_1 t + \frac{dB_1}{dt}cos\omega_1 t = -\frac{\epsilon d_{11}^{(1)}}{2\omega_1}\{A_1 cos(\omega_1 + \epsilon\lambda)t - B_1 sin(\omega_1 + \epsilon\lambda)t\}$$

$$-\frac{dA_2}{dt}sin\omega_2 t + \frac{dB_2}{dt}cos\omega_2 t = -\frac{\epsilon d_{22}^{(2)}}{2\omega_2}\{A_2 cos(\omega_2 + 2\epsilon\lambda)t - B_2 sin(\omega_2 + 2\epsilon\lambda)t\}$$

$$\frac{dA_1}{dt}cos\omega_1 t + \frac{dB_1}{dt}sin\omega_1 t = 0$$

$$\frac{dA_2}{dt}cos\omega_2 t + \frac{dB_2}{dt}sin\omega_2 t = 0$$

These equations may be solved to determine[7] $\frac{dA_1}{dt}, \frac{dA_2}{dt}, \frac{dB_1}{dt}, \frac{dB_2}{dt}$. Applying the Kryoloff-Bogoliuboff-Van der Pohl averaging technique[8], and applying the transformation:

$$\begin{aligned} X_1 &= A_1 + iB_1 \\ X_2 &= A_1 - iB_1 \\ Y_1 &= A_2 + iB_2 \\ Y_2 &= A_2 - iB_2 \end{aligned}$$

Results in four first order equations:

$$\begin{aligned} \frac{dX_1}{dt} &= -\frac{i\epsilon d_{11}}{4\omega_1}X_2 e^{-i\epsilon\lambda t} \\ \frac{dX_2}{dt} &= \frac{i\epsilon d_{11}}{4\omega_1}X_1 e^{i\epsilon\lambda t} \\ \frac{dY_1}{dt} &= -\frac{i\epsilon d_{22}}{4\omega_2}Y_2 e^{-i2\epsilon\lambda t} \\ \frac{dY_2}{dt} &= \frac{i\epsilon d_{22}}{4\omega_2}Y_1 e^{i2\epsilon\lambda t} \end{aligned} \tag{B.18}$$

These equations can be converted into autonomous form[9], and consequently the stability of the equations can be examined by considering the roots of the characteristic equation.

---

[7]Where it is implied henceforth that d_{11} and d_{22} are the parametric components of the first harmonic and second harmonic respectively.

[8]This is accomplished by substituting $\Phi_i = w_i t$, and averaging the equations as $\frac{1}{2\pi}\int_0^{2\pi}\frac{dA_i}{dt}d\Phi_i$ where A_i, B_i are treated as constants.

[9]The autonomous form is obtained by applying the transformations $X_1 = \overline{X}_1 e^{-i\frac{\epsilon\lambda}{2}t}$, $X_2 = \overline{X}_2 e^{i\frac{\epsilon\lambda}{2}t}$, $Y_1 = \overline{Y}_1 e^{-i\epsilon\lambda t}$, $Y_2 = \overline{Y}_2 e^{i\epsilon\lambda t}$

Assuming a solution of the form:

$$\begin{aligned} X_1 &= \overline{X}_1 e^{pt - i\frac{\epsilon\lambda}{2}t} \\ X_2 &= \overline{X}_2 e^{pt + i\frac{\epsilon\lambda}{2}t} \\ Y_1 &= \overline{Y}_1 e^{qt - i\epsilon\lambda t} \\ Y_2 &= \overline{Y}_2 e^{qt + i\epsilon\lambda t} \end{aligned} \tag{B.19}$$

Substituting equations (B.19) into the equations (B.18), results in:

$$\begin{bmatrix} p - i\frac{\epsilon\lambda}{2} & \frac{i\epsilon d_{11}}{4\omega_1} & 0 & 0 \\ -\frac{i\epsilon d_{11}}{4\omega_1} & p + i\frac{\epsilon\lambda}{2} & 0 & 0 \\ 0 & 0 & q - i\epsilon\lambda & \frac{i\epsilon d_{22}}{4\omega_2} \\ 0 & 0 & -\frac{i\epsilon d_{22}}{4\omega_2} & q + i\epsilon\lambda \end{bmatrix} \begin{Bmatrix} \overline{X}_1 \\ \overline{X}_2 \\ \overline{Y}_1 \\ \overline{Y}_2 \end{Bmatrix} = \begin{Bmatrix} \vdots \\ 0 \\ \vdots \end{Bmatrix} \tag{B.20}$$

The characteristic equation is obtained by setting the determinant of equation (B.20) to zero:

$$(p^2 + \frac{\epsilon^2\lambda^2}{4} - \frac{\epsilon^2 d_{11}^2}{16\omega_1^2})(q^2 + \epsilon^2\lambda^2 - \frac{\epsilon^2 d_{22}^2}{16\omega_2^2}) = 0$$

Thus :

$$p = \pm\frac{\epsilon}{2}(\frac{d_{11}^2}{4\omega_1^2} - \lambda^2)^{\frac{1}{2}}$$

$$q = \pm\epsilon(\frac{d_{22}^2}{16\omega_2^2} - \lambda^2)^{\frac{1}{2}}$$

In order for the system to be neutrally stable, the roots p, q of the above equations must be imaginary.

Thus the stability region is given by:

$$\frac{d_{11}^2}{4\omega_1^2} - \lambda^2 < 0$$

$$\frac{d_{22}^2}{16\omega_2^2} - \lambda^2 < 0$$

Substituting $\epsilon\lambda$ from equation (B.15) into the above equations and simplifying results in the stability intervals:

$$2\omega_1 - \frac{\epsilon|d_{11}|}{2\omega_1} < \omega < 2\omega_1 + \frac{\epsilon|d_{11}|}{2\omega_1}$$

$$\omega_2 - \frac{\epsilon|d_{21}|}{4\omega_2} < \omega < \omega_2 + \frac{\epsilon|d_{22}|}{4\omega_2}$$

It is evident that these are the same as Hsu's[1963] regions, for $s = 1, 2$, and thus this case is not an anomalous case, although this would not be evident beforehand.

B.3.2 Case 2: 3 DOF - $s = 1$ $\quad \omega \approx 2\omega_2$

This case represents a three degree of freedom system excited sinusoidally at a frequency ω close to $2\omega_2$. In this case a main and combination parametric resonance is excited simultaneously ie. $\omega \approx 2\omega_2 \approx \omega_1 + \omega_3$. Employing a detuning parameter $\lambda\epsilon$, the excitation frequency ω may be written as:

$$\omega = 2\omega_2 + \lambda\epsilon$$

$$\omega = \omega_1 + \omega_3 + \lambda\epsilon$$

or as:

$$\begin{aligned} \omega - \omega_2 &= \omega_2 + \lambda\epsilon \\ \omega - \omega_1 &= \omega_3 + \lambda\epsilon \\ \omega - \omega_3 &= \omega_1 + \lambda\epsilon \end{aligned}$$

Proceeding in the same manner as the preceding section, and retaining secular terms of the perturbation solution in the variational part of the solution results in three equations.

$$-\frac{dA_1}{dt}sin\omega_1 t + \frac{dB_1}{dt}cos\omega_1 t = -\frac{\epsilon d_{13}}{2\omega_1}\{A_3 cos(\omega_1 + \epsilon\lambda)t - B_3 sin(\omega_1 + \epsilon\lambda)t\}$$

$$-\frac{dA_2}{dt}sin\omega_2 t + \frac{dB_2}{dt}cos\omega_2 t = -\frac{\epsilon d_{22}}{2\omega_2}\{A_2 cos(\omega_1 + 2\epsilon\lambda)t - B_2 sin(\omega_1 + 2\epsilon\lambda)t\}$$

$$-\frac{dA_3}{dt}sin\omega_3 t + \frac{dB_3}{dt}cos\omega_3 t = -\frac{\epsilon d_{31}}{2\omega_3}\{A_1 cos(\omega_3 + \epsilon\lambda)t - B_1 sin(\omega_3 + \epsilon\lambda)t\}$$

and:

$$\frac{dA_i}{dt}cos\omega_i t + \frac{dB_i}{dt}sin\omega_i t = 0 \qquad i = 1, 2, 3$$

The above six equations may be solved to determine $\frac{dA_i}{dt}, \frac{dB_i}{dt}$. Applying the Kryoloff-Bogoliuboff-Van der Pohl averaging technique, and applying the transformation:

$$\begin{aligned} X_1 &= A_1 + iB_1 \\ X_2 &= A_1 - iB_1 \\ Y_1 &= A_2 + iB_2 \\ Y_2 &= A_2 - iB_2 \\ Z_1 &= A_3 + iB_3 \\ Z_2 &= A_3 - iB_3 \end{aligned}$$

Result: in six first order equations:

$$\begin{aligned} \frac{dX_1}{dt} &= -\frac{i\epsilon d_{13}}{4\omega_1} Z_2 e^{-i\epsilon\lambda t} \\ \frac{dX_2}{dt} &= +\frac{i\epsilon d_{13}}{4\omega_1} Z_1 e^{i\epsilon\lambda t} \\ \frac{dY_1}{dt} &= -\frac{i\epsilon d_{22}}{4\omega_2} Y_2 e^{-i\epsilon\lambda t} \\ \frac{dY_2}{dt} &= +\frac{i\epsilon d_{22}}{4\omega_2} Y_1 e^{i\epsilon\lambda t} \\ \frac{dZ_1}{dt} &= -\frac{i\epsilon d_{31}}{4\omega_3} X_2 e^{-i\epsilon\lambda t} \\ \frac{dZ_2}{dt} &= +\frac{i\epsilon d_{31}}{4\omega_3} X_1 e^{i\epsilon\lambda t} \end{aligned} \tag{B.21}$$

Equations (B.21) can be conveniently transformed into two second order autonomous equations:

$$\ddot{X}_1 + i\lambda\epsilon\dot{X}_1 - \frac{\epsilon^2 d_{13} d_{31}}{16\omega_1\omega_3} X_1 = 0 \tag{B.22}$$

$$\ddot{Y}_1 + i\lambda\epsilon\dot{Y}_1 - \frac{\epsilon^2 d_{22} d_{22}}{16\omega_2^2} Y_1 = 0 \tag{B.23}$$

The solutions to equations (B.22),(B.23) are:

$$\begin{aligned} X_1 &= \overline{X}_1 e^{(a-i\frac{\epsilon\lambda}{2})t} \\ Y_1 &= \overline{Y}_1 e^{(b-i\frac{\epsilon\lambda}{2})t} \end{aligned}$$

$$a = \pm\left(\frac{\epsilon^2\lambda^2}{4} - \frac{\epsilon^2 d_{13}d_{31}}{16\omega_1\omega_3}\right)^{\frac{1}{2}}$$

$$b = \pm\left(\frac{\epsilon^2\lambda^2}{4} - \frac{\epsilon^2 d_{22}^2}{16\omega_2^2}\right)^{\frac{1}{2}}$$

These solutions are neutrally stable if a, b are imaginary. Thus the stability region is defined by:

$$\epsilon^2\lambda^2 > \frac{\epsilon^2 d_{13}d_{31}}{4\omega_1\omega_3}$$

$$\epsilon^2\lambda^2 > \frac{\epsilon^2 d_{22}^2}{4\omega_2^2}$$

Substituting $\epsilon\lambda$ from equation (B.21) into the above equations and simplifying, results in the stability intervals:

$$(\omega_1+\omega_3) - \frac{\epsilon}{2}\sqrt{\frac{d_{13}d_{31}}{\omega_1\omega_3}} < \omega < (\omega_1+\omega_3) + \frac{\epsilon}{2}\sqrt{\frac{d_{13}d_{31}}{\omega_1\omega_3}}$$

$$2\omega_2 - \frac{\epsilon|d_{22}|}{4\omega_2} < \omega < 2\omega_1 + \frac{\epsilon|d_{22}|}{4\omega_2}$$

It is evident that once again these regions are the same as Hsu's[1963] regions, and thus this case is not anomalous. The largest region would dictate the stability of the system, and thus the relative magnitudes of the coefficients are important.

B.3.3 Case 3: 2 DOF - $s = 1, 2, 3 \qquad \omega \approx \omega_1$

This case represents a two DOF system excited by a periodic function with three harmonic components at frequencies ω, 2ω, 3ω. In this case a main and combination parametric resonance is excited simultaneously by the second and third harmonic respectively, ie $2\omega \approx 2\omega_1, 3\omega \approx \omega_1 + \omega_2$. Employing a detuning parameter $\lambda\epsilon$, the excitation frequency ω may be written as:

$$\omega = \omega_1 + \lambda\epsilon$$

$$\omega = \frac{\omega_1 + \omega_2}{3} + \lambda\epsilon$$

or as:

$$\begin{aligned} 2\omega - \omega_1 &= \omega_1 + 2\lambda\epsilon \\ 3\omega - \omega_1 &= \omega_2 + 3\lambda\epsilon \\ 3\omega - \omega_2 &= \omega_1 + 3\lambda\epsilon \end{aligned}$$

Proceeding in the same manner as the preceding section, and retaining secular terms of the perturbation solution in the variational part of the solution results in the equations.

$$-\frac{dA_1}{dt}sin\omega_1 t + \frac{dB_1}{dt}cos\omega_1 t = -\frac{\epsilon}{2\omega_1}\left\{ \begin{array}{l} d_{11}^{(2)}(A_1 cos(\omega_1 + 2r\lambda)t - B_1 sin(\omega_1 + 2\epsilon\lambda)t \\ +d_{12}^{(3)}(A_2 cos(\omega_1 + 3\epsilon\lambda)t - B_2 sin(\omega_1 + 3\epsilon\lambda)t \end{array} \right\}$$

$$-\frac{dA_2}{dt}sin\omega_2 t + \frac{dB_2}{dt}cos\omega_2 t = -\frac{\epsilon d_{21}^{(3)}}{2\omega_2}\{A_1 cos(\omega_2 + 3\epsilon\lambda)t - B_1 sin(\omega_2 + 3\epsilon\lambda)t\}$$

$$\frac{dA_1}{dt}cos\omega_1 t + \frac{dB_1}{dt}sin\omega_1 t = 0$$

$$\frac{dA_2}{dt}cos\omega_2 t + \frac{dB_2}{dt}sin\omega_2 t = 0$$

These equations may be solved to determine $\frac{dA_1}{dt}$, $\frac{dA_2}{dt}$, $\frac{dB_1}{dt}$, $\frac{dB_2}{dt}$. Applying the Kryoloff-Bogoliuboff-Van der Pohl averaging technique, and applying the transformation:

$$
\begin{aligned}
X_1 &= A_1 + iB_1 \\
X_2 &= A_1 - iB_1 \\
Y_1 &= A_2 + iB_2 \\
Y_2 &= A_2 - iB_2
\end{aligned}
$$

Results in four first order equations:

$$
\begin{aligned}
\frac{dX_1}{dt} &= -\frac{i\epsilon}{4\omega_1}\left\{d_{11}^{(2)} X_2 e^{-i2\epsilon\lambda t} + d_{12}^{(3)} Y_2 e^{-i3\epsilon\lambda t}\right\} \\
\frac{dX_2}{dt} &= +\frac{i\epsilon}{4\omega_1}\left\{d_{11}^{(2)} X_1 e^{i2\epsilon\lambda t} + d_{12}^{(3)} Y_1 e^{i3\epsilon\lambda t}\right\} \\
\frac{dY_1}{dt} &= -\frac{i\epsilon}{4\omega_2}\left\{d_{21}^{(3)} X_2 e^{-i3\epsilon\lambda t}\right\} \\
\frac{dY_2}{dt} &= +\frac{i\epsilon}{4\omega_2}\left\{d_{21}^{(3)} X_1 e^{i3\epsilon\lambda t}\right\}
\end{aligned}
\tag{B.24}
$$

By applying successive differentiation and substitution, equations (B.24) are converted into two second order equations.

$$
\begin{aligned}
\ddot{Y}_1 + i\frac{3\gamma}{2}\dot{Y}_1 - cbY_1 &= -iaexp^{-2i\gamma t}\dot{Y}_2 \\
\ddot{Y}_2 - i\frac{3\gamma}{2}\dot{Y}_2 - cbY_2 &= +iaexp^{2i\gamma t}\dot{Y}_1
\end{aligned}
\tag{B.25}
$$

where:

$$
\begin{aligned}
a &= \frac{\epsilon d_{11}^{(2)}}{4\omega_1} \\
b &= \frac{\epsilon d_{12}^{(3)}}{4\omega_1} \\
c &= \frac{\epsilon d_{21}^{(3)}}{4\omega_2} \\
\gamma &= 2\epsilon\lambda
\end{aligned}
\tag{B.26}
$$

Assuming a solution of the form:

$$\begin{aligned} Y_1 &= \overline{Y}_1 e^{pt-i\gamma t} \\ Y_2 &= \overline{Y}_2 e^{pt+i\gamma t} \end{aligned} \tag{B.27}$$

Substitution into the equations (B.25) results in:

$$\begin{bmatrix} (p-i\gamma)^2 + i\frac{3\gamma}{2}(p-i\gamma) - cb & ia(p+i\gamma) \\ -ia(p-i\gamma) & (p+i\gamma)^2 - i\frac{3\gamma}{2}(p+i\gamma) - cb \end{bmatrix} \begin{Bmatrix} \overline{Y}_1 \\ \overline{Y}_2 \end{Bmatrix} = \begin{Bmatrix} \vdots \\ 0 \\ \vdots \end{Bmatrix} \tag{B.28}$$

The characteristic equation is obtained by setting the determinant of equation (B.28) to zero:

$$p^4 + (\frac{5\gamma^2}{4} - 2cb - a^2)p^2 + (\frac{\gamma^2}{2} - cb)^2 - a^2\gamma^2 = 0$$

thus the roots of p^2 are:

$$p^2 = -\frac{1}{2}(\frac{5\gamma^2}{4} - 2cb - a^2) \pm \frac{1}{8}\sqrt{(3\gamma^2 + 4a^2)^2 - 16cb(\gamma^2 + 4a^2)} \tag{B.29}$$

Which can be written as:

$$p^2 = -\Gamma \pm \sqrt{\Delta}$$

For neutral stability, the roots of p must be imaginary. Thus two situations may arise:

i) $\Delta = 0$ and $\Gamma > 0$

ii) $\Gamma \pm \sqrt{\Delta} < 0$ and real.

Thus this case is anomalous and does not reduce to Hsu's[1963] form. Equation (B.29) must be solved for various values of $\lambda\epsilon$ and the boundary of the stability region constructed, such that the roots for p are always imaginary.

The two limiting cases ie $a = 0$ and $b = c = 0$ are considered to illustrate that the stability condition conforms to known results.

Case 1: $b = c = 0$

This case is equivalent to removing the third harmonic from the excitation, thus Hsu's[1963] result should be obtained for main parametric resonance with $s = 2$:

In this case:

$$p^2 = \frac{1}{2}[-\frac{5\gamma^2}{4} + a^2 \pm \frac{1}{4}(3\gamma^2 + 4a^2)]$$

Thus:

$$p^2 = -\gamma^2, -\frac{\gamma^2}{4} + a^2$$

Thus for p to be imaginary:

$$\gamma^2 > 4a^2$$

$$\longrightarrow \lambda^2\epsilon^2 > (\frac{\epsilon d_{11}^{(2)}}{4\omega_1})^2$$

Substituting for $\lambda\epsilon$ confirms Hsu's[1963] result for $s = 2$.

$$\omega_1 - \frac{\epsilon|d_{11}^{(2)}|}{4\omega_1} < \omega < \omega_1 + \frac{\epsilon|d_{11}^{(2)}|}{4\omega_1}$$

Case 2: $a = 0$

This case is equivalent to removing the second harmonic from the excitation, thus Hsu's[1963] result should be obtained for combination parametric resonance with $s = 3$:

In this case:

$$\Delta = \gamma^2(9\gamma^2 - 16cb)$$

and

$$p^2 = \frac{1}{2}[(-\frac{5\gamma^2}{4} + 2cb) \pm \frac{1}{4}\sqrt{\Delta}]$$

It can be shown that the discriminant becomes complex before the root p becomes complex, thus the stability is governed by the discriminant:

$$\gamma^2 > \frac{16}{9}cb$$

$$\longrightarrow \lambda^2\epsilon^2 > (\frac{\epsilon d_{12}^{(3)} d_{21}^{(3)}}{36\omega_1\omega_2})$$

Once again substituting for $\lambda\epsilon$ confirms Hsu's[1963] result for $s = 3$.

$$\frac{(\omega_1 + \omega_2)}{3} - \frac{\epsilon}{6}\sqrt{\frac{d_{12}^{(3)} d_{21}^{(3)}}{\omega_1\omega_3}} < \omega < \frac{(\omega_1 + \omega_2)}{3} + \frac{\epsilon}{6}\sqrt{\frac{d_{12}^{(3)} d_{21}^{(3)}}{\omega_1\omega_3}}$$

B.4 Kloof Mine Observations

Observations performed at Kloof mine were well documented by Dimitriou and Whillier[1973] in the section *Dynamic behaviour of winding ropes at Kloof*, and will be discussed in light of the present analysis. Figure B.1 is reproduced from their paper, and represents the dynamic chafacteristics of the Kloof mine, in terms of the uncoupled linear transverse catenary natural frequencies (FTC_n), the transverse natural frequencies of the vertical rope (FVT_n), and the longitudinal natural frequencies of the vertical rope (FVL_n). Figure B.2 represents the lateral and longitudinal natural frequencies calculated according to appendix C. Note that the longitudinal natural frequencies calculated by Dimitriou and Whillier[1973], and presented in figure B.1, treated the vertical rope as if it were fixed end at the sheave. The longitudinal natural frequencies presented in figure B.2 include the catenary length and the inertia of the sheave.

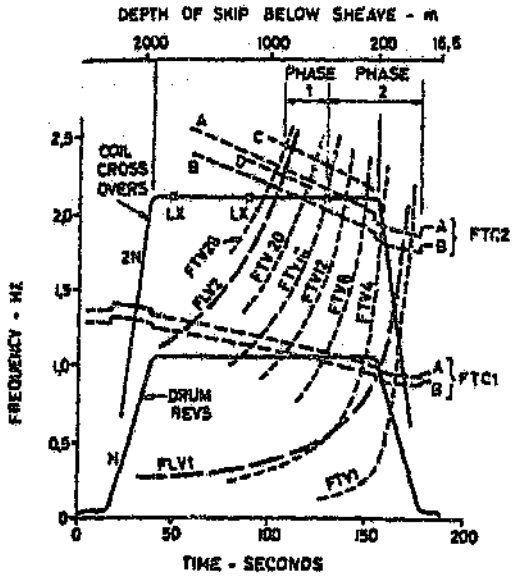

Fig 3 Variation of frequencies, full skip riding. $LS = 2\,071$ m
$FTCn$ = Frequency of Transverse vibrations in Catenary
$FTVn$ = Frequency of Transverse vibrations in Vertical rope
$FLVn$ = Frequency of Longitudinal vibrations in Vertical rope
LX = Layer cross-over

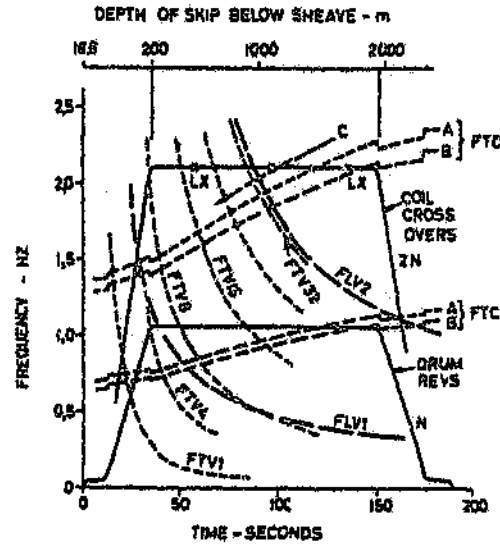

Fig 4 Variation of frequencies, empty skip descending. $LS = 1\,030$ m

Figure B.1: Dimitriou and Whillier (1973): Kloof Mine shaft dynamic characteristics

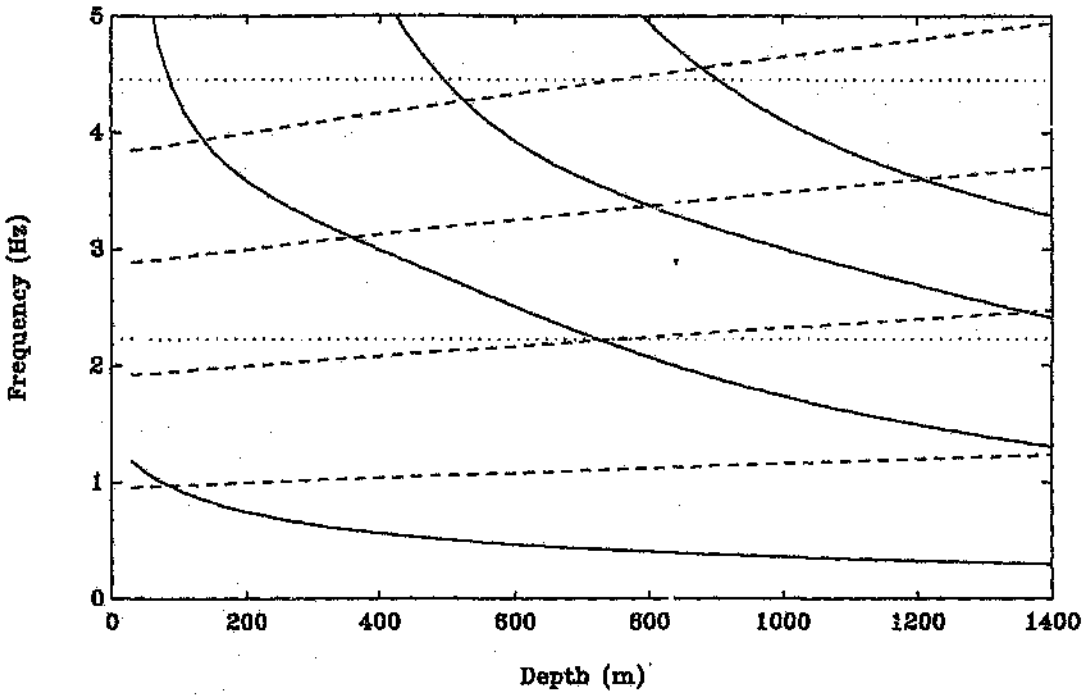

Figure B.2: Ascending Kloof Mine shaft dynamic characteristics
· · · · Lebus Drum Frequencies, —— Longitudinal Frequencies, - - Lateral Catenary Frequencies

Dimitriou and Whillier[1973] made the following observations regarding Kloof.

(1) Large catenary motion occurs, starting in phase 1, when the skip is approximately 900m below the head sheave during the rising cycle, however large motion is not observed when the skip is lowered.

(ii) During phase 1, the amplitude increases and the catenaries settle into a clearly defined second mode.

(iii) During phase 1, the vertical ropes start vibrating transversely at a similar wavelength to that of the catenary. This is not observed when the skip is lowered.

(iv) On occasions, at the beginning of phase 2, the vibrations develop a large vertical component in excess of 2m. One of the authors believes a first mode pattern was observed in the vertical component of the motion. This motion was termed whip.

(v) By reducing the speed of winding abruptly at the beginning of phase 1 from 15m/s to 14m/s, the amplitude of the vibrations was significantly reduced.

These observations contain much detail, confirming the potentially complex behaviour of the mine rope system. Considering figure B.1, the authors attributed the resonance and whip behaviour of the catenary to a combination of parametric response due to the longitudinal excitation at the drum, and autoparametric excitation due to parametric response of the lateral modes of the vertical rope, and consequently amplified parametric excitation of the catenary. Dimitriou and Whillier[1973] comment:

"At Kloof, at the beginning of phase 1, the catenaries are approaching the resonant condition $FTC2 = 2N$, due to the z-excitation (out-of-plane lateral excitation) and their amplitude is growing ...". "Therefore, the tension in the catenaries fluctuate with increasing magnitude, ϵ, at a frequency p close to $4N$, thus approaching the condition for subharmonic excitation of the vertical ropes."

"Another factor, which promotes subharmonic resonance in both the catenaries and vertical ropes, is the harmonic component at $p = 4N$ of the w-excitation (longitudinal excitation). The magnitude, ϵ, of this component is only of the order 10^{-4}. However at the beginning of phase 1, ϵ is amplified by resonance of the longitudinal mode of the ropes at $FLV3 = 4N$..". ..."The growth of the transverse vibrations of the vertical ropes provides increased parametric excitation of the catenaries..." "Eventually, the two ropes (catenary and vertical) mutually excite one another....".

Although this argument was constructed in an ad hoc manner, it succinctly describes the potential interactions which may arise. Dimitriou and Whillier[1973] note that for an appreciable rope length, at least one or more of the higher lateral frequencies of the vertical rope will tune closely to one or more of the natural frequencies of the catenary. In this sense, the system may maintain a state of autoparametric resonance for an appreciable period of the wind.

At the time of executing this phase of the study, it was realised that the aspect of autoparametric excitation via the forced lateral motion of the catenary would be important. However, it was decided that an appreciation of the linear stability of the system in the presence of longitudinal excitation only would represent a beneficial first step.

In the context of the Kloof system, the first and second harmonic of the longitudinal excitation frequency induces main parametric resonance of the first and second catenary modes simultaneously. As noted by Dimitriou and Whillier[1973], the effective amplitude of the parametric excitation depends on the proximity of the harmonic excitations to a condition of longitudinal resonance. It was determined in section B.3.1 that this condition of tuning is not

anomalous, and the size of the region of parametric resonance can be determined directly from Hsu's[1963] results. The resulting regions of instability[10] for main resonance of the first and second catenary modes are illustrated in figure B.3(a),(b) respectively. This figure represents a composite of three levels of longitudinal damping ranging from undamped to a maximum of 1.5% of critical in the first longitudinal mode. The lower part of the figure represents the absolute value of the difference between the longitudinal response at the sheave and winder drum, and is consequently related to the tension fluctuations occurring in the catenary. The parameter epsilon in the upper figure represents a scaling factor applied to the longitudinal excitation at the winder drum. Thus the actual excitation level for the Kloof winder is achieved when epsilon is unity.

It is clear from this figure that the regions of parametric instability are strongly influenced by the degree of longitudinal damping. The peak response in figure B.3(c),(d) relates to resonance of the second and fourth longitudinal modes respectively[11]. Since relative viscous proportional damping has been applied in the model, the modal damping factor applicable to the i^{th} longitudinal mode is related to that in the first mode by the ratio ω_i/ω_1. Consequently if the first mode is set to have a modal damping factor of 1.5%, the damping factors for the second third and forth modes would be of the order of 4%, 9% 14% respectively. The assumption of relative proportional damping by industry has led to the conclusion that the longitudinal behaviour of the system can be modelled by considering the fundamental mode only, as response in the higher modes is strongly attenuated. This is clearly evident in figure B.3(c),(d), where the resonant peak is quickly eroded with the inclusion of longitudinal damping. As a result the region of parametric resonance becomes dependent on the base level of excitation applied at the drum, rather than on the longitudinal tuning of the system. Figure B.4 presents a stability plot of the system, where the harmonic balance method proposed by Takahashi[1981a] has been applied to determine the regions of system stability. Identical parameters applied in figure B.3 have been used, and the stability plot represents a composite of three levels of damping. The predicted regions of instability via the perturbation result, and the harmonic balance method are identical. The harmonic balance method is however more general, since it does not require special considera-

[10]The longitudinal excitation amplitudes were calculated for the first and second harmonic of the Lebus excitation frequency in accordance with Appendix A.These are : $U_1 = 0.2mm, U_2 = 0.1mm$

[11]Dimitriou and Whillier neglected the sheave inertia in their calculation of the longitudinal natural frequencies; consequently in their calculation the natural frequency of the third longitudinal mode was higher and resonant at approximately 900m. Once the sheave inertia is accounted for, resonance of the third longitudinal mode is delayed and occurs at approximately 500m below the sheave, whilst the fourth longitudinal mode is resonant at approximately 900m.

tion when dealing with anomalous cases, and depending on the order of the Fourier expansion assumed, can identify the higher order or secondary regions of instability for both main and combination resonance. It is also not limited by the notion of a small parameter.

Although regions of parametric instability do occur, they do not occur over extended lengths of the shaft when epsilon is unity. The effect of these regions will be reduced due to the winding speed of the system, and consequently these regions are not viewed as sufficient to warrant the definition of a design criterion. Nevertheless, this exercise was useful in developing an understanding of the system stability and partly confirming the intuitive interpretation of Dimitriou and Whillier[1973] in a formal manner. It is likely that significant longitudinal response would occur due to the coupled lateral motion of the rope. This is a form of autoparametric excitation, where lateral response due to the lateral excitation at the winder drum, promotes longitudinal parametric excitation. This concept provided the basic incentive for developing the stability analysis of the coupled system, where both longitudinal and lateral excitation of the catenary is accounted for, as presented in chapter 4.

Finally, it is noted that this analysis provides evidence of main as well as combination parametric resonances, due to longitudinal excitation. Combination parametric resonance regions do not arise in a string with pinned end conditions, since the lateral eigenfunctions are orthogonal to the longitudinal eigenfunctions. With regard to the influence of rope curvature, Takahashi[1991] considered the regions of parametric resonance of a pinned cable with curvature, under axial excitation at one boundary. Takahashi[1991] reported the existence of regions of additive combination resonance, however, Perkins[1992b] corrected these findings, and demonstrated that only main parametric resonance regions existed, where in addition to being parametrically excited, the system was directly excited due to in-plane curvature coupling. It is surmised that in the present system, since the lateral eigenfunctions are not orthogonal to the longitudinal eigenfunctions, additive combination parametric resonance regions will arise in the presence of external excitation due to the catenary curvature. In practice the catenary curvature is small, and further analysis accounting for catenary curvature was not undertaken.

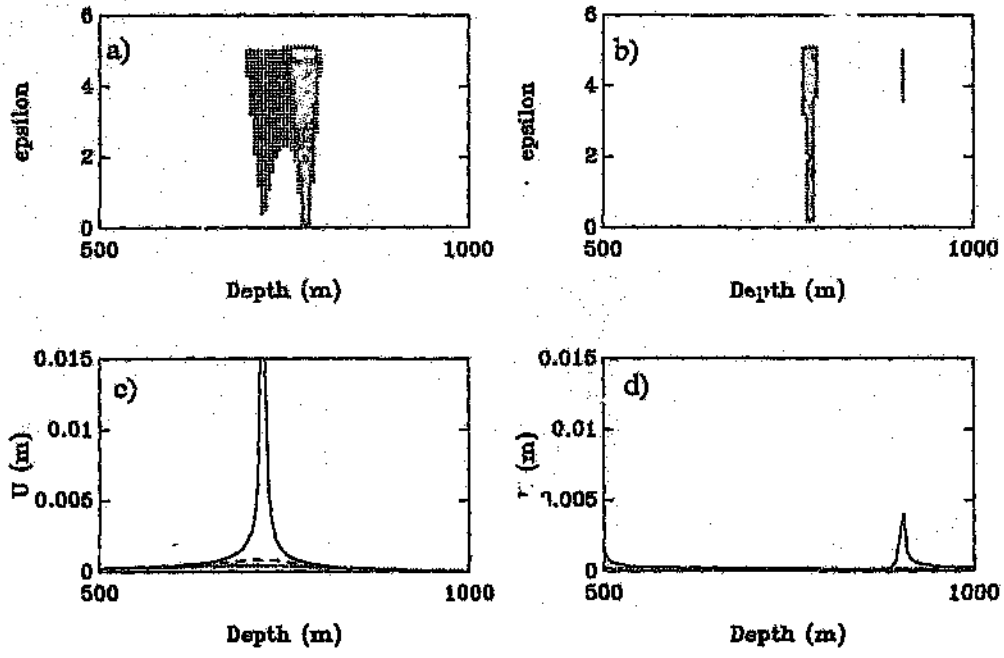

Figure B.3: Main parametric resonance regions - Case 1

(a) $\Omega = \omega_1$
(b) $2\Omega = 2\omega_2$

$V = 15m/s$, $\beta = 0.2rad.$, $d = 48mm$, $R_d = 2.14m$.
$-$ $\zeta_1 = 0$, $- -$ $\zeta_1 = 0.75\%$, $\cdots$ $\zeta_1 = 1.5\%$

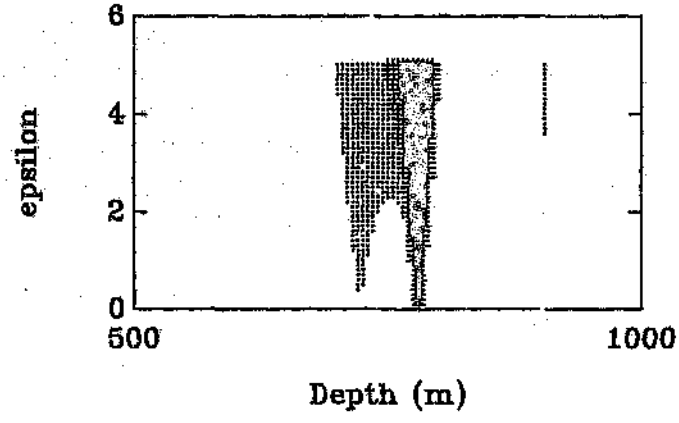

Figure B.4: Parametric resonance regions - Harmonic balance method

$V = 15m/s$, $\beta = 0.2rad.$, $d = 48mm$, $R_d = 2.14in.$
$\cdot - \zeta_1 = 0, + - \zeta_1 = 0.75\%, \times - \zeta_1 = 1.5\%$

Appendix C

Linear Longitudinal System Response

The purpose of this appendix is to present the eigenfunctions associated with the longitudinal linear system, in the absence of lateral catenary motion, for use in a normal mode analysis of the non-linear equations of motion. The solution of longitudinal steady state motion of the system, in the presence of relative and general proportional viscous damping, due to an harmonic axial excitation at the winder drum is subsequently presented.

Figure C.1 illustrates the system under consideration, which consists of a rope of material density ρ, cross sectional area A, and modulus of elasticity E. The system is split into two sub-systems denoted by displacement co-ordinates $u_1(s_1,t)$ and $u_2(s_2,t)$. The sub-systems are coupled by a sheave of mass moment of inertia I. The conveyance is represented by a mass M, which is suspended at the free end of the second system. The co-ordinates s_1, s_2 represent the position along the rope from the catenary end and the sheave end respectively.

The equations of motion and boundary conditions of the two systems are presented as:

<u>System 1</u>

$$\frac{\partial^2 u_1}{\partial t^2} = \mu \frac{\partial^3 u_1}{\partial s_1^2 \partial t} + c^2 \frac{\partial^2 u_1}{\partial s_1^2} \tag{C.1}$$

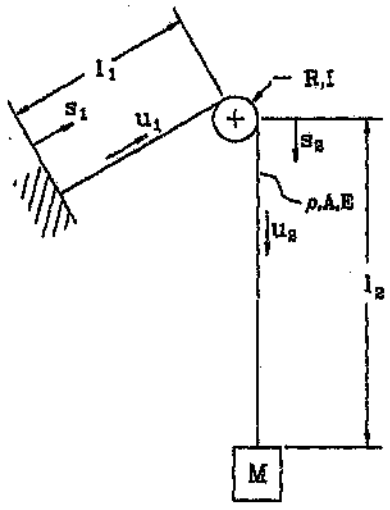

Figure C.1: The longitudinal system

where c represents the longitudinal wave speed $c = \sqrt{E/\rho}$, and μ represents the damping coefficient related to the intrinsic dissipation property of the wire rope. This particular form of damping mechanism represents a relative proportional damping model, where the damping action is orthogonal to the normal modes of the undamped system, and proportional to the stiffness properties.

The boundary conditions for the rope are given as:

$$u_1(0,t) = \sum Re(U_n e^{j\omega t}) \tag{C.2}$$
$$u_1(l_1,t) = u_2(0,t) \tag{C.3}$$

Where U_n is complex and contains the amplitude and phase of the n^{th} harmonic of the excitation applied at the drum due to the Lebus cross over excitation.

System 2

$$\frac{\partial^2 u_2}{\partial t^2} = \mu \frac{\partial^3 u_2}{\partial s_2^2 \partial t} + c^2 \frac{\partial^2 u_2}{\partial s_2^2} \tag{C.4}$$

The boundary conditions for the rope are given as:

$$u_2(0,t) = u_1(l_1,t) \tag{C.5}$$

$$(AE\frac{\partial u_2}{\partial s_2} + \rho\mu A\frac{\partial^2 u_2}{\partial s_2 \partial t})|_{(l_2,t)} = -M\frac{\partial^2 u_2}{\partial t^2}|_{(l_2,t)} \tag{C.6}$$

System Coupling

The coupling of the catenary system to the vertical section is achieved by ensuring continuity of the longitudinal displacement, as well as a momentum balance across the sheave wheel. These conditions are satisfied by:

$$u_2(0,t) = u_1(l_1,t)$$

$$\begin{aligned} \frac{I}{R^2}\frac{\partial^2 u_1}{\partial t^2}|_{(l_1,t)} &= AE\{\frac{\partial u_2}{\partial s_2}|_{(0,t)} - \frac{\partial u_1}{\partial s_1}|_{(l_1,t)}\} \\ &+ \rho A\mu\{\frac{\partial^2 u_2}{\partial s_2 \partial t}|_{(0,t)} - \frac{\partial^2 u_1}{\partial s_1 \partial t}|_{(l_1,t)}\} \end{aligned} \tag{C.7}$$

C.1 Undamped Natural Frequencies

Setting the damping factor $\mu = 0$, and the harmonics of the boundary excitation $U_n = 0$, the undamped natural frequencies of the system can be determined by assuming.

$$\begin{aligned} u_1(s_1,t) &= [A_1 cos\gamma s_1 + B_1 sin\gamma s_1]e^{j\omega t} \\ u_2(s_2,t) &= [A_2 cos\gamma s_2 + B_2 sin\gamma s_2]e^{j\omega t} \end{aligned} \tag{C.8}$$

where $\gamma = \frac{\omega}{c}$;

From equation (C.2):

$$u_1(0,t) = 0$$

$$\rightarrow A_1 = 0$$

Substituting the expressions (C.8) into equation (C.6) gives:

$$AE\frac{du_2}{ds_2}|_{(l_2,t)} = M\omega^2 u_2|_{(l_2,t)}$$

$$\frac{du_2}{ds_2}|_{(l_2,t)} = \Lambda^2 u_2|_{(l_2,t)} \tag{C.9}$$

where $\Lambda^2 = \frac{M\omega^2}{AE}$.

Use of relations (C.8) and equation (C.9) gives:

$$A_2[\Lambda^2 cos\gamma l_2 + \gamma sin\gamma l_2] + B_2[\Lambda^2 sin\gamma l_2 - \gamma cos\gamma l_2] = 0 \tag{C.10}$$

From equation (C.3):

$$u_1|_{(l_1,t)} = u_2|_{(0,t)}$$

which requires that:

$$B_1 sin\gamma l_1 = A_2 \tag{C.11}$$

Equation (C.7) requires:

$$-\omega^2 \frac{I}{R^2} u_1|_{(l_1,t)} + AE \frac{du_1}{ds_1}|_{(l_1,t)} = AE \frac{du_2}{ds_2}|_{(0,t)}$$

Substituting relations (C.8) into this equation results in:

$$B_1[\frac{\Gamma^2}{\gamma} sin\gamma l_1 - cos\gamma l_1] + B_2 = 0 \tag{C.12}$$

where $\Gamma^2 = \frac{\omega^2 I}{AER^2}$

Equations (C.10),(C.11),(C.12) can be written in matrix form as:

$$\begin{bmatrix} sin\gamma l_1 & -1 & 0 \\ (\frac{\Gamma^2}{\gamma} sin\gamma l_1 - cos\gamma l_1) & 0 & 1 \\ 0 & (\Lambda^2 cos\gamma l_2 + \gamma sin\gamma l_2) & (\Lambda^2 sin\gamma l_2 - \gamma cos\gamma l_2) \end{bmatrix} \begin{Bmatrix} B_1 \\ A_2 \\ B_2 \end{Bmatrix} = \begin{Bmatrix} 0 \\ 0 \\ 0 \end{Bmatrix}$$

In order for the coefficients B_1, A_2, B_2 to be non-trivial, the determinant must be equal to zero. This defines the frequency equation as:

$$\Delta(\omega) = sin\gamma l_1[\Lambda^2 cos\gamma l_2 + \gamma sin\gamma l_2] + [cos\gamma l_1 - \frac{\Gamma^2}{\gamma} sin\gamma l_1][\Lambda^2 sin\gamma l_2 - \gamma cos\gamma l_2] = 0$$

The roots of the frequency equation determine γ_i, and hence the i^{th} natural frequency of the system is $\omega_i = c\gamma_i$. The i^{th} eigenfunction coefficients $B_{1_i}, A_{2_i}, B_{2_i}$

are determined by scaling the coefficients such that $B_{1_i} = 1$, and solving for A_{2_i}, B_{2_i} from equations (C.11), (C.12).

$$B_{1_i} = 1$$

$$A_{2_i} = sin\gamma_i l_1$$

$$B_{2_i} = (-\frac{\Gamma^2}{\gamma_i} sin\gamma_i l_1 + cos\gamma_i l_1)$$

C.2 Forced Longitudinal Damped Response

The damped steady state longitudinal response due to the boundary excitation at the winder drum is determined in the absence of lateral catenary motion.

Since relative proportional viscous damping is included in the equations of motion, the eigenfunctions presented in relations (C.8) are complex. The complex eigenfunctions can be determined by considering the proportionally damped wave equation:

$$\frac{\partial^2 u}{\partial t^2} = \mu \frac{\partial^3 u}{\partial s^2 \partial t} + c^2 \frac{\partial^2 u}{\partial s^2}$$

This equation is variable separable ie:

$$u(s,t) = \phi(s)q(t)$$

and consequently:

$$\phi'' + \gamma^2 \phi = 0$$

$$\ddot{q} + \gamma^2 \mu \dot{q} + \gamma^2 c^2 q = 0$$

Assuming the response is harmonic:

$$q(t) = e^{i\omega t}$$

and solving for γ.

$$\gamma = \frac{\frac{\omega}{c}}{(1 + (\frac{\mu\omega}{c^2})^2)^{1/4}} e^{-i\alpha/2}$$

$$\alpha = tan^{-1} \frac{\mu\omega}{c^2}$$

Thus $\phi(s)$ may be presented in the form:

$$\phi(s) = A_1 cos\gamma s + B_1 sin\gamma s$$

where A_1, B_1, γ are complex.

Thus conveniently $\phi(s)$ is of the same form as that determined for the undamped response in relations (C.8), however it is now a complex function.

Applying the boundary conditions stated in equations (C.2),(C.3),(C.6),(C.7), and assuming that the excitation is represented by a single harmonic at frequency ω, then the forced response of the rope is given by:

$$u_1(s_1, t) = \phi_1(s_1) e^{i\omega t}$$

$$u_2(s_2, t) = \phi_2(s_2) e^{i\omega t}$$

where:

$$\phi_1(s_1) = A_1 cos\gamma s_1 + B_1 sin\gamma s_1$$

$$\phi_2(s_2) = A_2 cos\gamma s_2 + B_2 sin\gamma s_2$$

The following matrix equation for the coefficients A_1, B_1, A_2, B_2 may be defined.:

$$[\mathbf{A}]\{x\} = \{b\}$$

where.

$$[\mathbf{A}] =$$

$$\begin{bmatrix} 1 & 0 & 0 & 0 \\ cos\gamma l_1 & sin\gamma l_1 & -1 & 0 \\ (\frac{\Gamma^2}{\lambda} cos\gamma l_1 + sin\gamma l_1) & (\frac{\Gamma^2}{\lambda} sin\gamma l_1 - cos\gamma l_1) & 0 & 1 \\ 0 & 0 & (\Lambda^2 cos\gamma l_2 + \lambda sin\gamma l_2) & (\Lambda^2 sin\gamma l_2 - \lambda cos\gamma l_2) \end{bmatrix}$$

$$\{x\} = \begin{Bmatrix} A_1 \\ B_1 \\ A_2 \\ B_2 \end{Bmatrix}$$

$$\{b\} = \begin{Bmatrix} U \\ 0 \\ 0 \\ 0 \end{Bmatrix}$$

where:

$$\Lambda^2 = \frac{M\omega^2}{AE} \qquad \Gamma^2 = \frac{I\omega^2}{AER^2} \qquad \gamma = \frac{\frac{\omega}{c}}{(1+(\frac{\mu\omega}{c^2})^2)^{1/4}} e^{-i\alpha/2}$$
$$\alpha = tan^{-1}\frac{\omega\mu}{c^2} \qquad \zeta = \frac{\omega\theta\gamma}{AE} \qquad \lambda = \gamma + i\zeta$$
$$\theta = \rho A\mu \qquad c^2 = \frac{E}{\rho}$$

Due to the influence of damping, the longitudinal motion of the system will be phase shifted from the excitation, as expected. This can be demonstrated by considering the catenary motion $u_1(s_1, t)$.

$$u_1(s_1, t) = \phi_1(s_1, t)e^{i\omega t}$$

If the applied excitation is of the form $u_1(0, t) = Re(Ue^{i\omega t}) = |U|cos(\omega t + \phi)$, where ω is the excitation frequency, then the response is given by:

$$u_1(s_1, t) = Re(\phi_1(s_1)e^{i\omega t})$$

$$u_1(s_1, t) = (Re(\phi_1)cos\omega t - Im(\phi_1)sin\omega t) = A(s_1)cos(\omega t + \Phi)$$

$$A(s_1, t) = \sqrt{Re(\phi_1)^2 + Im(\phi_1)^2}$$

$$\Phi = tan^{-1}(\frac{Im(\phi_1)}{Re(\phi_1)})$$

The longitudinal response due to a periodic axial excitation at the winder drum can be determined for each harmonic of the excitation, and consequently the overall response can be determined via superposition of the forced harmonic responses.

C.2.1 Determination of the Modal Damping Coefficient

In order to select the material damping constant μ to achieve a prescribed relative proportional modal damping coefficient in the first mode ζ_1, the free response of the equation for $q(t)$ may be examined:

$$\ddot{q} + \frac{\omega_n^2}{c^2}\mu\dot{q} + \omega_n^2 q = 0$$

Thus:

$$2\zeta_n\omega_n = \frac{\omega_n^2\mu}{c^2}$$

If the material damping coefficient is selected on the basis of the modal damping ratio, then:

$$\mu = \frac{2c^2\zeta_1}{\omega_1}$$

and it follows that:

$$\zeta_n = \zeta_1\frac{\omega_n}{\omega_1}$$

This demonstrates that ζ_n is proportional to the ratio of the n^{th} natural frequency of the fundamental ω_1. Hence if μ is selected on the basis of the fundamental, the higher modes will become successively more damped and less significant in the response.

C.3 General Proportional Damping

Greenway[1989] provided a rudi nentary damping estimate regarding the damp- ıg coefficient extracted from free response data captured during deceleration tests at Deelkraal Mine. This estimate was obtained from the logarithmic decrement of first longitudinal mode; Greenway[1989] showed that if a relative proportional damping model was applied, a material damping coefficient μ could be defined. A viscous relative proportional damping model results in the higher modes becoming successively more damped. Since the damping factor is critical to the steady state stability analysis, further site tests were conducted to determine if the damping estimate related to the higher modes followed such a relationship. In that test it was found that the higher modes were more lightly damped than the fundamental, and that the damping estimate obtained for the fundamental was dependent on the mean rope tension. These results are presented and discussed in detail in Appendix G. Greenway[1993] demonstrated that if the dependence of the first mode on mean tension was neglected, a general proportional viscous damping model could be constructed, which accounts for the lower damping estimates measured in the higher modes.

The analysis presented regarding the relative proportional damped longitudinal response, can be readily modified to include the case of general viscous proportional damping. For general viscous proportional damping, two material damping coefficients are introduced, μ_a, μ_b, where the first relates to a damping force which is proportional to the mass properties of the system, whilst the second relates to a damping force which is proportional to the stiffness properties of the system. This is analogous to a Rayleigh damping form in a discrete system. The linear longitudinal equation of motion is governed by:

$$u_{tt} + \mu_a u_t = \mu_b u_{t,ss} + c^2 u_{ss}$$

For a forced response at frequency ω:

$$u(s,t) = \phi(s) e^{i\omega t}$$

Thus:

$$\phi'' + (\frac{\omega^2 - i\mu_a\omega}{c^2 + i\mu_b\omega})\phi = 0$$

Thus:

$$\phi(s) = A cos\gamma s + B sin\gamma s$$

where:

$$\gamma = (\frac{\omega^2 - i\mu_a\omega}{c^2 + i\mu_b\omega})^{\frac{1}{2}}$$

The modal damping factor can be obtained by applying a normal mode expansion, and considering the principal modes q_i.

$$\ddot{q}_i + (\mu_a + \mu_b(\frac{\omega_i}{c})^2)\dot{q}_i + \omega_i^2 q_i = 0$$

Thus it follows that:

$$\zeta_i = \frac{1}{2}(\frac{\mu_a}{\omega_i} + \frac{\mu_b}{c^2}\omega_i)$$

With reference to Appendix G, the material damping constants a, b would be related to μ_a, μ_b as:

$$\mu_a = a$$

$$\mu_b = c^2 b$$

The forced response for general proportional viscous damping can be obtained from the equations developed in section C.2 by appropriate substitution for γ.

C.4 Longitudinal Response - Kloof Mine

The steady state forced longitudinal response for the Kloof Mine is examined. This exercise demonstrates the difference between a relative proportional, and a general proportional damping model. Appendix G presents longitudinal damping factors extracted by Greenway[1989] from free decay results at Deelkraal Mine and by Constancon[1992] from free decay results obtained from Elandsrand Mine. Since no other data is available, this data will be utilised as being representative of the Kloof Mine rope damping properties.

C.4.1 Relative Proportional Damping Model

The relative proportional material damping co-efficient μ, is selected on the basis of the Deelkraal[1] data as presented in table G.1 of Appendix G. This data indicated that the material damping constant b increased roughly in proportion to the rope length. Thus the relative proportional damping coefficient μ is defined as:

$$\mu(s) = c^2 bs/l$$

where s represents the length of the rope.

The data tabulated in Appendix G table G.1 provides $b = 0.03sec$, at a rope length of $\frac{3}{4}l$ of the depth of the shaft, where $l = 2062m$. Thus

$$c = \sqrt{EA/m} = 3658m/s$$

$$\mu(s_2) = c^2 \frac{4 \times 0.03}{3 \times 2062} s_2 = 259 s_2$$

By selecting the damping constant μ, the modal damping factor of the n^{th} mode is set to $\zeta_n = \zeta_1 \frac{\omega_n}{\omega_1}$. The modal damping factors for the first four modes are presented in figure C.2. As is evident, in comparison to the fundamental, the second and higher modes are significantly damped.

[1]The data was recorded by Thomas et al.[1987], and the logarithmic decrement was extracted by Greenway[1989].

C.4.2 General Proportional Damping Model

A general proportional damping model is presented in Appendix G. This model was proposed by Greenway[1993], based on measurements captured by Constancon[1992] and Page[1992] at Elandsrand Gold Mine. Measurements were captured at 73 level, which represents an active rope length between the drum and skip of 2090m. Due to time limitations, further measurements were not obtained at a different level, and thus the variation of the damping constants with rope length could not be determined. However at 73 level, material damping coefficients of $\mu_a = 0.159$ and $\mu_b = 0.00164c^2$ were determined from the test data. As stated in Appendix G, this model provides a convenient fit to the measured data, rather than physical evidence of a general viscous damping mechanism. Further experimental results would be required to define the physical basis for such a model. Since the measurements at Deelkraal mine indicate that the damping coefficient b increases in proportion to rope length, a similar assumption with regard to the proportional damping coefficient μ_b. Thus the model proposed is:

$$\mu_a = 0.159$$

$$\mu_b(s_2) = 0.001644c^2 \frac{s_2}{2090} = 10.49 s_2$$

The modal damping coefficients based on this model are presented in figure C.3. It is evident in this figure that the fundamental mode is more damped than the higher modes. This emphasises the difference between the damping models, and consequently the need to accurately determine the damping mechanism.

C.4.3 Forced Longitudinal Response

The Kloof Mine system parameters are presented in table C.1. The natural frequencies of the first four modes, for a full ascending skip, are presented in figure C.4(a). In figure C.4(a), the horizontal lines represent the Lebus groove excitation frequencies at the first and second harmonic of the coil cross-over frequency.

The modulus of the longitudinal forced response at the sheave wheel due to the first and second harmonic excitation at the winder drum, is presented in figure C.4(b),(c) respectively. The response amplitude is dramatically affected by the damping model assumed. It is clear that the higher modes would be active if the general proportional viscous damping model applied. The damping models proposed have been formulated on the basis of extremely limited data, and as such are approximate. However, at this stage the general proportional damping model is the most representative model available, and will be utilised until further experimental studies provide a better description.

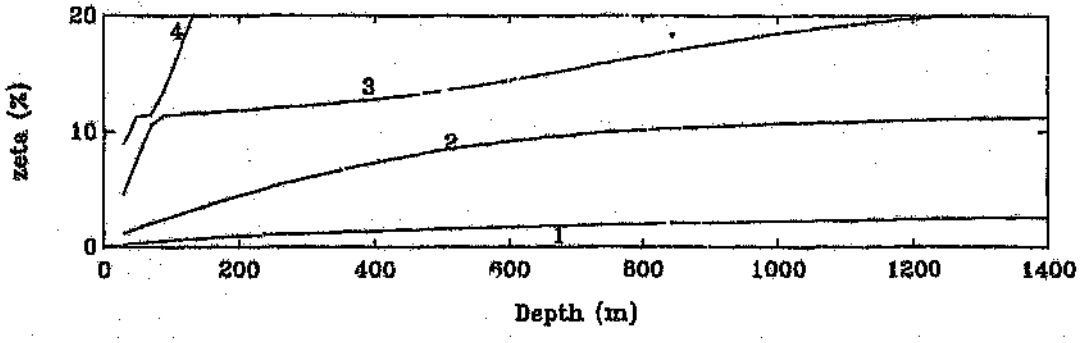

Figure C.2: Modal damping factors - Relative proportional damping

$$\zeta_n = \frac{1}{2}\frac{\mu}{c^2}\omega_n$$
$$\mu(s_2) = 259 s_2$$

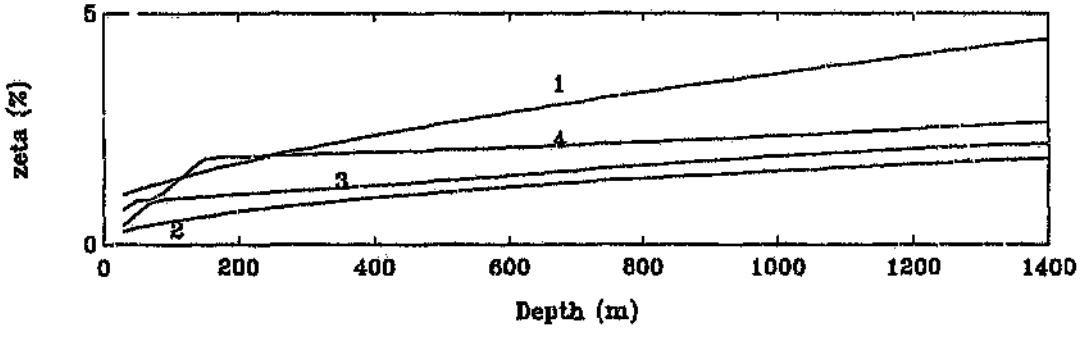

Figure C.3: Modal damping factors - General proportional damping

$$\zeta_n = \frac{1}{2}\left(\frac{\mu_a}{\omega_n} + \frac{\mu_b}{c^2}\omega_n\right)$$
$$\mu_a = 0.159 \qquad \mu_b = 10.49 s_2$$

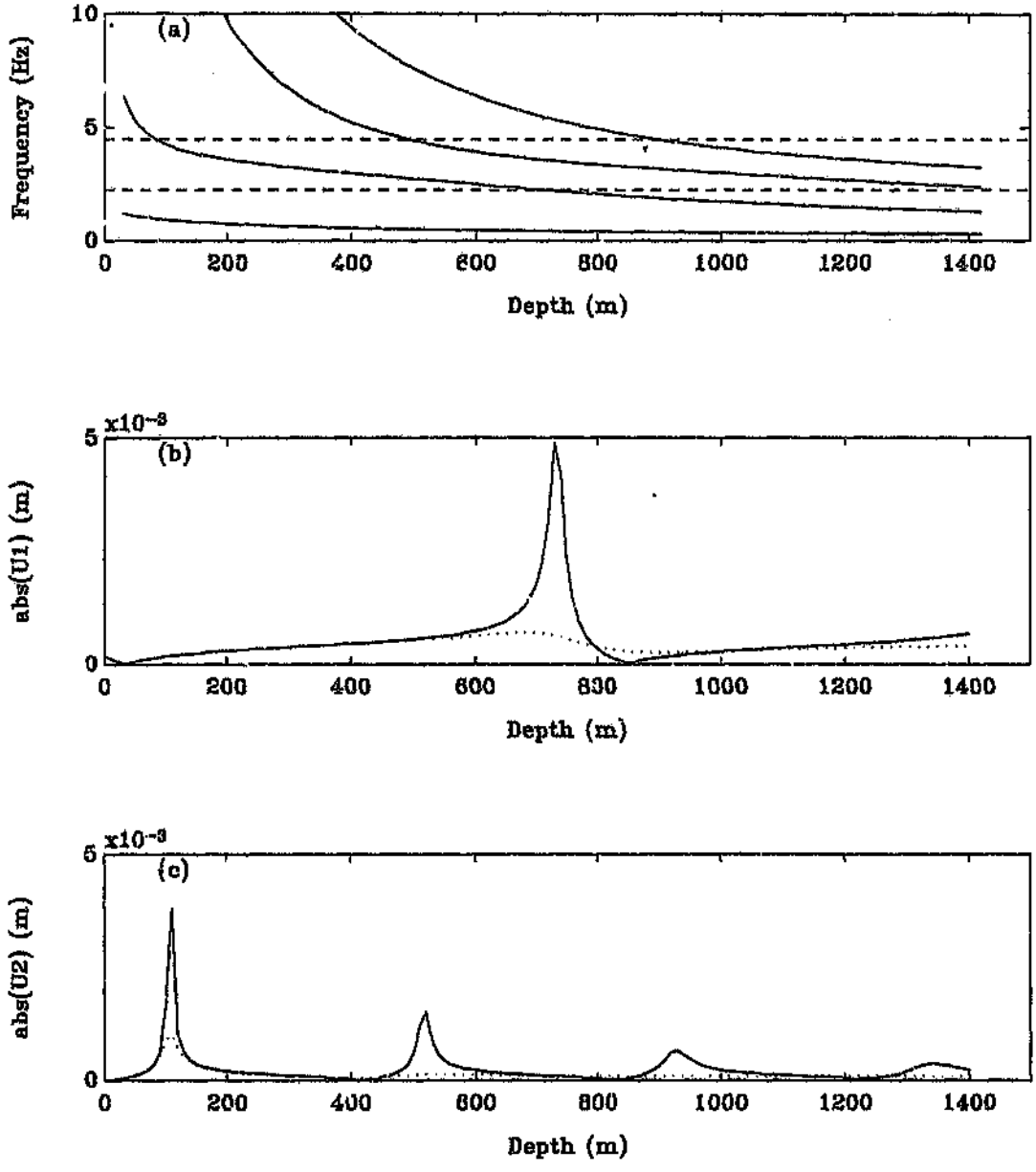

Figure C.4: Linear steady state forced response

(a) Longitudinal Natural Frequencies vs Shaft depth
(b) Forced Longitudinal Response at the Sheave Wheel - First Harmonic
(c) Forced Longitudinal Response at the Sheave Wheel - Second Harmonic
..... Relative proportional damping. — General proportional damping.

$$u(0,t) = 2.89 \times 10^{-4} cos(\Omega_l t + \phi_1) + 1.05 \times 10^{-4} cos(2\Omega_l t + \phi_2)$$

$$\Omega_l = \frac{4V_e}{Dd} = 14.01 rad/s, \quad \phi_1 = 1.669 rad, \quad \phi_2 = -1.374 rad$$

Table C.1: Kloof Mine - System parameters

J	Sheave Inertia.	15200 kgm^2
M	Skip Mass.	7920 kg
M0	Skip Pay-load.	9664 kg
m	Linear Rope density.	8.4 kg/m
V	Nominal Winding Speed.	15 m/s
De	Depth of wind.	2100m
Lc	Catenary Length.	74.95 m
E	Effective Youngs Modulus of the rope.	$1.1 \times 10^{11} N/m^2$
Ax	Effective steel area of the rope.	$0.001028 m^2$
β	Cross over arc.	0.2 rad
Dd	Drum Diameter.	4.28 m
Ds	Sheave Diameter.	4.26 m
Dr	Rope Diameter.	0.048 m

Appendix D

Linear Lateral Catenary Response

This appendix presents the linear analysis of the catenary, in the absence of curvature, and longitudinal coupling. In this context, the equation of motion governing the in and out-of-plane motion reduces to the linear wave equation associated with a taut string. It is well established that the undamped wave equation is variable separable, ie $v(s,t) = \sum \phi_i(s) q_i(t)$. The natural frequency of the i^{th} principal mode of a string with pinned end conditions is given by $\omega_i = i\frac{c_l}{2l_1}$ where c_l represents the lateral wave speed which is related to the tension T and linear mass density of the rope m, by $c_l = \sqrt{T/m}$, and l_1 represents the chord length between the pinned ends.

The eigenfunction for this configuration is given by:

$$\phi_i(s) = sin(\frac{i\pi}{l_1}s)$$

Since curvature is neglected, the in-plane and out-of-plane eigenfunctions and natural frequencies are identical.

D.1 Forced Response

The lateral response of the catenary to an out-of-plane harmonic boundary excitation $We^{i\omega t}$ at the drum end, in the presence of relative proportional viscous damping is presented[1]. The equation of motion has the same form as that presented in Appendix C, governing the damped longitudinal behaviour of the rope. ie.

$$\frac{\partial^2 w}{\partial t^2} = \mu_l \frac{\partial^3 w}{\partial s_1^2 \partial t} + c_l^2 \frac{\partial^2 w}{\partial s_1^2} \tag{D.1}$$

where μ_l represents the coefficient of lateral dissipation, and co-ordinate s_1 represents the distance measured along the rope from the drum to the sheave. This equation is variable separable, and thus the solution may be expressed as:

$$w(s_1, t) = \phi_l(s_1) q(t)$$

$$\phi_l(s) = A cos \gamma_l s_1 + B sin \gamma_l s_1$$

where:

$$\gamma_l = \frac{\frac{\omega}{c_l}}{(1 + (\frac{\mu_l \omega}{c_l^2})^2)^{1/4}} e^{-i\alpha_l/2}$$

$$\alpha_l = tan^{-1} \frac{\omega \mu_l}{c_l^2}$$

$$c_l^2 = \frac{T}{m}$$

The boundary conditions are:

$$w(0, t) = We^{i\omega t}$$

[1] W represents both phase and amplitude and is a complex entity

$$w(l_1, t) = 0$$

Under these boundary conditions, the solution can be shown to be:

$$w(s_1, t) = \frac{W}{sin\gamma_l l_1} sin(\gamma_l(l_1 - s_1))e^{i\omega t} = \phi_l(s_1)e^{i\omega t}$$

Since γ_l is complex, the response is phase shifted with respect to the excitation. Considering the first harmonic of the excitation as $w(0, t) = Re(We^{i\omega t})$, where ω is the excitation frequency, the response is:

$$w(s_1, t) = (Re(\phi_l)cos\omega t - Im(\phi_l)sin\omega t) = A_l(s_1)cos(\omega t + \Phi_l)$$

where:

$$A_l(s_1, t) = \sqrt{R \qquad + Im(\phi_l)^2}$$

$$\Phi_l = tan^{-1}(\frac{Im(\phi_l)}{Re(\phi_l)})$$

The forced lateral catenary response due to a periodic lateral excitation at the winder drum can thus be constructed via superposition of the forced response due to each harmonic in the periodic excitation.

Appendix E

Linear Coupled System Response

This appendix presents the solution to the linearised stationary steady state system response as proposed in Chapter 4. The equations of motion developed in Chapter 4, considered the stationary steady state solution, for small lateral amplitudes in the absence of curvature, such that nonlinear terms were neglected in the lateral equations of motion, but retained in the longitudinal equation of motion. The in-plane lateral excitation is significantly less than the out-of-plane lateral and longitudinal excitation, and is consequently neglected. Thus planar response occurs in the $u-w$ plane, and consequently the equations of motion under consideration for the catenary section are:

$$\frac{\partial^2 u_1}{\partial t^2} = \mu \frac{\partial^3 u_1}{\partial s_1^2 \partial t} + c^2 \frac{\partial^2 u_1}{\partial s_1^2} + c^2 \frac{\partial w}{\partial s_1} \frac{\partial^2 w}{\partial s_1^2} \tag{E.1}$$

$$\frac{\partial^2 w}{\partial t^2} = \mu_1 \frac{\partial^3 w}{\partial s_1^2 \partial t} + \bar{c}^2 \frac{\partial^2 w}{\partial s_1^2} \tag{E.2}$$

The vertical rope is laterally restrained and consequently the equation of motion describing longitudinal motion $u_2(s_2, t)$ is:

$$\frac{\partial^2 u_2}{\partial t^2} = \mu \frac{\partial^3 u_2}{\partial s_2^2 \partial t} + c^2 \frac{\partial^2 u_2}{\partial s_2^2} \tag{E.3}$$

where $c, \bar{c}$ represent the longitudinal and lateral wave speeds respectively, and s_1, s_2 represent the co-ordinates measured along the catenary from the drum end to the sheave, and along the vertical rope from the sheave to the conveyance respectively. $u_1(s_1,t), u_2(s_2,t)$ represent the longitudinal displacement in the catenary and vertical rope respectively.

Since the equation of motion for the lateral response is uncoupled from the longitudinal equation of motion, the lateral response due to forced boundary excitation $\sum W_n cos(n\omega t)$ can be derived in closed form[1], as presented in Appendix D. The lateral response couples independently to the longitudinal equation of motion, and consequently this coupling term may be viewed as a distributed forcing function over the catenary length.

The boundary conditions for the system, in the absence of longitudinal excitation at the drum end are:

$$u(0,t) = 0 \tag{E.4}$$

$$w(0,t) = \sum W_n cos(n\omega t) \tag{E.5}$$

$$\{AE\frac{\partial u_2}{\partial s_2} + \rho\mu A\frac{\partial^2 u_2}{\partial s_2 \partial t}\}|_{(l_2,t)} = -M\frac{\partial^2 u_2}{\partial t^2}|_{(l_2,t)} \tag{E.6}$$

In addition, since lateral motion exists, the inertial balance at the sheave is given as: :

$$\begin{aligned}[\frac{I}{R^2}\frac{\partial^2 u_1}{\partial t^2}]|_{l_1,t} &= [EA\frac{\partial u_2}{\partial s_2} + \rho\mu A\frac{\partial^2 u_2}{\partial s_2 \partial t}]|_{(0,t)} \\ &- [EA\{\frac{\partial u_1}{\partial s_1} + \frac{1}{2}\frac{\partial^2 w}{\partial s_1^2}\} + \rho\mu A\frac{\partial^2 u_1}{\partial s_1 \partial t}]|_{(l_1,t)}\end{aligned} \tag{E.7}$$

The quadratic nature of the coupling term $c^2\frac{\partial w}{\partial x}\frac{\partial^2 w}{\partial s_1^2}$ in the longitudinal equation of motion (E.1), and $\frac{1}{2}(\frac{\partial w}{\partial s_1})^2$ in equation (E.7) describing the inertial balance across the sheave, results in the generation and transmission of longitudinal excitation induced by the forced lateral catenary motion, to the catenary and

[1] In subsequent sections, subscript 1,2 will refer to terms evaluated at the first and second harmonic of the excitation frequency respectively

where $c, \bar{c}$ represent the longitudinal and lateral wave speeds respectively, and s_1, s_2 represent the co-ordinates measured along the catenary from the drum end to the sheave, and along the vertical rope from the sheave to the conveyance respectively. $u_1(s_1,t), u_2(s_2,t)$ represent the longitudinal displacement in the catenary and vertical rope respectively.

Since the equation of motion for the lateral response is uncoupled from the longitudinal equation of motion, the lateral response due to forced boundary excitation $\sum W_n cos(n\omega t)$ can be derived in closed form[1], as presented in Appendix D. The lateral response couples independently to the longitudinal equation of motion, and consequently this coupling term may be viewed as a distributed forcing function over the catenary length.

The boundary conditions for the system, in the absence of longitudinal excitation at the drum end are:

$$u(0,t) = 0 \tag{E.4}$$

$$w(0,t) = \sum W_n cos(n\omega t) \tag{E.5}$$

$$\{AE\frac{\partial u_2}{\partial s_2} + \rho\mu A\frac{\partial^2 u_2}{\partial s_2 \partial t}\}|_{(l_2,t)} = -M\frac{\partial^2 u_2}{\partial t^2}|_{(l_2,t)} \tag{E.6}$$

In addition, since lateral motion exists, the inertial balance at the sheave is given as: :

$$\begin{aligned}[\frac{I}{R^2}\frac{\partial^2 u_1}{\partial t^2}]|_{(l_1,t} &= [EA\frac{\partial u_2}{\partial s_2} + \rho\mu A\frac{\partial^2 u_2}{\partial s_2 \partial t}]|_{(0,t)} \\ &- [EA\{\frac{\partial u_1}{\partial s_1} + \frac{1}{2}\frac{\partial^2 w}{\partial s_1^2}\} + \rho\mu A\frac{\partial^2 u_1}{\partial s_1 \partial t}]|_{(l_1,t)}\end{aligned} \tag{E.7}$$

The quadratic nature of the coupling term $c^2\frac{\partial w}{\partial x}\frac{\partial^2 w}{\partial s_1^2}$ in the longitudinal equation of motion (E.1), and $\frac{1}{2}(\frac{\partial w}{\partial s_1})^2$ in equation (E.7) describing the inertial balance across the sheave, results in the generation and transmission of longitudinal excitation induced by the forced lateral catenary motion, to the catenary and

[1] In subsequent sections, subscript 1,2 will refer to terms evaluated at the first and second harmonic of the excitation frequency respectively

vertical rope. This excitation consists of a time independent component, and a dynamic component at multiples and beats of the lateral response frequency. This can be demonstrated by considering the case where the forced lateral response is comprised of two frequencies, namely at the fundamental and the second harmonic of the Lebus excitation frequency. Thus the lateral forced response could be represented by:

$$w(s,t) = |w_1(s,t)|cos(\omega t + \phi_1) + |w_2(s,t)|cos(2\omega t + \phi_2)$$

where $|w_1(s_1,t)|, |w_2(s_1,t)|$ represent the maximum value of the response at any point along the catenary, due to the first and second harmonic of the excitation spectrum respectively.

The longitudinal excitation induced via the lateral response $w(s,t)$ is:

$$\begin{aligned} c^2 \frac{\partial w}{\partial s_1}\frac{\partial^2 w}{\partial s_1^2} = \quad & \tfrac{1}{2}c^2\Big[(w_1' w_1'' + w_2' w_2'') + w_1' w_1'' cos(2\omega t + 2\phi_1) \\ & + (w_1' w_2'' + w_2' w_1'')\{cos(\omega t + \phi_2 - \phi_1) + cos(3\omega t + \phi_1 + \phi_2)\} + \\ & w_2' w_2'' cos(4\omega t + 2\phi_2)\Big] \end{aligned} \tag{E.8}$$

The first term on the right hand side of equation (E.8) is independent of time, and represents a static distributed force, which induces drift in the longitudinal response. Effectively this drift represents the mean displacement about which longitudinal motion occurs. The longitudinal excitation induced at frequencies $\omega, 2\omega, 3\omega, 4\omega$ demonstrates the autoparametric nature of the system, whereby the lateral motion induces longitudinal excitation.

The longitudinal system response due to the dynamic component of the excitation induced by the lateral motion follows, whilst the response due to the drift term is considered in section E.1.

Consider the longitudinal excitation induced by the linear lateral response of the catenary to the fundamental lateral excitation $W_1 cos(\omega t)$. The longitudinal excitation occurs due to the coupling term $\frac{\partial w_1}{\partial s_1}\frac{\partial^2 w_1}{\partial s_1^2}$ in the longitudinal equation of motion. Since:

$$w_1(s_1,t) = \mathcal{R}e\left[\frac{W_1}{sin\gamma_{l_1}} sin(\gamma_{l_1}(l_1 - s_1))e^{i\omega t}\right]$$

Thus it can be shown that[2].

$$Re(\frac{\partial w_1}{\partial s_1})Re(\frac{\partial^2 w_1}{\partial s_1^2}) = Re\left[\chi_1 sin2\gamma_{l_1}(l-s_1)e^{j(2\omega t)}\right] + D_1(s_1)$$

where $D_1(s_1)$ represents the static or drift excitation term. This term will be considered further in section E.1.

$$\chi_1 = \frac{W_1^2\gamma_{l_1}^3}{(2sin\gamma_{l_1}l_1)^2}$$

The longitudinal system response, considering the relevant boundary conditions described in equations (E.4),(E.6),(E.7) , is:

$$u_1(s,t) = Re\left[e^{2j\omega t}(Asin2\gamma_{l_1}(l_1-s_1) + A_1 cos\gamma_2 s_1 + B_1 sin\gamma_2 s_1)\right]$$

$$u_2(s,t) = Re\left[e^{2j\omega t}(A_2 cos\gamma_2 s_1 + B_2 sin\gamma_2 s_1)\right]$$

where[3] $A = \frac{c^2\chi_1}{4(\gamma_{l_1}^2c^2-\omega^2)+8i\mu\omega\gamma_{l_1}^2}$ and $u_1(s_1,t)$ and $u_2(s_2,t)$ represent the forced longitudinal motion of the catenary and vertical rope at frequency 2ω respectively.

The constants A_i, B_i are determined by the solution to the equations.

$$[\mathbf{A}]\{x\} = \{b\}$$

where:

---

2 $\frac{\partial Re(w_1)}{\partial s_1}\frac{\partial^2 Re(w_1)}{\partial s_1^2} = Re(\frac{\partial w_1}{\partial s_1})Re(\frac{\partial^2 w_1}{\partial s_1^2})$

3 In the case of general viscous damping, as introduced in Appendix G, $A = \frac{c^2\chi_1}{4(\gamma_{l_1}^2c^2-\omega^2)+j\omega(8\mu_a\gamma_{l_1}^2+\mu_a)}$.

$$[A] =$$

$$\begin{bmatrix} 1 & 0 & 0 & 0 \\ cos\gamma_2 l_1 & sin\gamma_2 l_1 & -1 & 0 \\ \frac{\Gamma^2}{\lambda} cos\gamma_2 l_1 + sin\gamma_2 l_1 & \frac{\Gamma^2}{\lambda} sin\gamma_2 l_1 - cos\gamma_2 l_1 & 0 & 1 \\ 0 & 0 & \Lambda^2 cos\gamma_2 l_2 + \lambda sin\gamma_2 l_2 & \Lambda^2 sin\gamma_2 l_2 - \lambda cos\gamma_2 l_2 \end{bmatrix}$$

$$\{x\} = \begin{Bmatrix} A_1 \\ B_1 \\ A_2 \\ B_2 \end{Bmatrix}$$

$$\{b\} = \begin{Bmatrix} -Asin2\gamma_{l_1} l_1 \\ 0 \\ (\frac{W_1\gamma_{l_1}}{2\lambda_2 sin\gamma_{l_1} l_1})^2 - \frac{2\gamma_{l_1} A}{\gamma_2} \\ 0 \end{Bmatrix}$$

where:

$$\Lambda^2 = \frac{4M\omega^2}{AE} \qquad \Gamma^2 = \frac{4I\omega^2}{AER^2} \qquad \gamma_2 = \frac{\frac{2\omega}{c}}{+(\frac{2\mu\omega}{c^2})^2)^{1/4}} e^{-i\alpha/2}$$

$$\alpha = tan^{-1}\frac{2\omega\mu}{c^2} \qquad \zeta_2 = \frac{2\omega\theta\gamma_2}{AE} \qquad \theta = \rho A_{fl}$$

$$\lambda_2 = \gamma_2 + i\zeta_2 \qquad \gamma_{l_1} = \frac{\frac{\omega}{c_l}}{(1+(\frac{\mu_{fl}\omega}{c_l^2})^2)^{1/4}} e^{-i\alpha_l/2} \qquad \alpha_{fl} = tan^{-1}\frac{\omega\mu_{fl}}{c_l^2}$$

$$c^2 = \frac{E}{\rho} \qquad c_l^2 = \frac{T}{m}$$

The longitudinal response induced by the forced lateral response due to the second harmonic of the lateral excitation $W_2 cos2\omega t$, is obtained by appropriate substitution into the above equations.

The longitudinal response due to the interaction of the first and second lateral harmonic motions is developed along the same lines below. In this case time independent terms do not arise, but rather dynamic terms at ω and 3ω arise.

$$Re(\frac{\partial w_1}{\partial s_1}) Re(\frac{\partial^2 w_2}{\partial s_1^2}) + Re(\frac{\partial w_2}{\partial s_1}) Re(\frac{\partial^2 w_1}{\partial s_1^2}) =$$

$$\frac{1}{4} Re\left[\left(\frac{\gamma_{l_1}^* \gamma_{l_2} W_1^* W_2}{sin\gamma_{l_1}^* l_1 sin\gamma_{l_2} l_1}\right) \{(\gamma_{l_2} + \gamma_{l_1}^*) sin[(\gamma_{l_2} + \gamma_{l_1}^*)(l_1 - s)] \cdot (\gamma_{l_2} - \gamma_{l_1}^*) sin[(\gamma_{l_2} - \gamma_{l_1})(l_1 - s)]\} e^{j\omega t}\right] +$$

$$\frac{1}{4} Re\left[\left(\frac{\gamma_{l_1} \gamma_{l_2} W_1 W_2}{sin\gamma_{l_1} l_1 sin\gamma_{l_2} l_1}\right) \{(\gamma_{l_2} + \gamma_{l_1}) sin[(\gamma_{l_2} + \gamma_{l_1})(l_1 - s)] + (\gamma_{l_2} - \gamma_{l_1}) sin[(\gamma_{l_2} - \gamma_{l_1})(l_1 - s)]\} e^{3j\omega t}\right]$$

where $\gamma_{l_1}^*, W_1^*$ refers to the complex conjugate of γ_{l_1}, W_1.

The longitudinal system response at $e^{j\omega t}$ is thus obtained as:

$$u_1(s,t) = Re\left[e^{j\omega t}(Asin(\gamma_{l_2}+\gamma_{l_1}^*)(l_1-s_1)+Bsin(\gamma_{l_2}-\gamma_{l_1}^*)(l_1-s_1)+A_1cos\gamma s_1+B_1sin\gamma s_1)\right]$$

$$u_2(s,t) = Re\left[e^{j\omega t}(A_2cos\gamma s_1+B_2sin\gamma s_1)\right]$$

where[4]:

$$A = \frac{c^2\gamma_{l_1}^*\gamma_{l_2}W_1^*W_2(\gamma_{l_1}^*+\gamma_{l_2})}{4sin\gamma_{l_1}^*l_1sin\gamma_{l_2}l_1[(\gamma_{l_2}+\gamma_{l_1}^*)^2(c^2+j\mu\omega)-\omega^2]}$$

$$B = \frac{c^2\gamma_{l_1}^*\gamma_{l_2}W_1^*W_2(\gamma_{l_2}-\gamma_{l_1}^*)}{4sin\gamma_{l_1}^*l_1sin\gamma_{l_2}l_1[(\gamma_{l_2}-\gamma_{l_1}^*)^2(c^2+j\mu\omega)-\omega^2]}$$

and the loading vector $\{b\}$ is:

$$\{b\} = \begin{Bmatrix} -Asin(\gamma_{l_2}+\gamma_{l_1}^*)l_1 - Bsin(\gamma_{l_2}-\gamma_{l_1}^*)l_1 \\ 0 \\ \frac{W_1^*\gamma_{l_1}^*W_2\gamma_{l_2}}{2\lambda_1 sin\gamma_{l_1}^*l_1 sin\gamma_{l_2}l_1} - \frac{(\gamma_{l_2}+\gamma_{l_1}^*)A+(\gamma_{l_2}-\gamma_{l_1}^*)B}{\gamma_1} \\ 0 \end{Bmatrix}$$

By appropriate substitution, the longitudinal response at the third harmonic of the Lebus excitation frequency can be obtained.

The total steady state longitudinal response may thus be obtained as a linear combination of that due to the longitudinal excitation at the winder drum,

[4]In the case of general viscous damping as described in Appendix G:

$$A = \frac{c^2\gamma_{l_1}^*\gamma_{l_2}W_1^*W_2(\gamma_{l_1}^*+\gamma_{l_2})}{4sin\gamma_{l_1}^*l_1sin\gamma_{l_2}l_1[(\gamma_{l_2}+\gamma_{l_1}^*)^2(c^2+j\mu_b\omega)+2j\omega\mu_a-\omega^2]}$$

$$B = \frac{c^2\gamma_{l_1}^*\gamma_{l_2}W_1^*W_2(\gamma_{l_2}-\gamma_{l_1}^*)}{4sin\gamma_{l_1}^*l_1sin\gamma_{l_2}l_1[(\gamma_{l_2}-\gamma_{l_1}^*)^2(c^2+j\mu\omega)+2j\mu_a\omega-\omega^2]}$$

as presented in Appendix C and that induced by the lateral response of the catenary[5].

Clearly, the direct longitudinal excitation at the winder drum results in axial response at integer multiples of the coil cross over frequencies $\omega, 2\omega$, whilst that due to lateral catenary coupling accentuates these components, and introduces additional excitation at $3\omega, 4\omega$, as well as a drift term.

The drift in the longitudinal response as derived above causes a change in the average tension in the rope. As a consequence of this, the natural frequencies related to the lateral modes of the the variational equations of motion presented in Chapter 4, increase.

[5]It is noted that the results presented consider the case where the lateral excitation harmonics have a zero phase angle. Different phase angles can easily be accommodated in the analysis by including the phase information in the harmonic amplitudes W_n. Thus in general W_n would be a complex number.

E.1 Longitudi al Drift Term

The drift induced in the longitudinal response due to the static component of the excitation $D(s_1)$, is examined in this section. This occurs as a result of the quadratic term $Re[w_{,s}]Re[w_{,ss}]$ in the longitudinal equation of motion. Consider the steady state lateral response w_1 due to the fundamental of the lateral excitation at the drum, $Re[W_1 e^{j\Omega t}]$. The static component of the excitation applied to the longitudinal system is:

$$D(s_1) = \frac{1}{2} Re[w_{1,s_1} w_{1,s_1 s_1}] = \frac{1}{4}[w_{1,s_1} w^*_{1,s_1}]_{,s_1}$$

The longitudinal response to the drift term is obtained by satisfying the equations:

$$\begin{aligned} \frac{\partial^2 u_1}{\partial s_1^2} &= -D(s_1) \quad 0 < s_1 < l_1 \\ \frac{\partial^2 u_2}{\partial s_2^2} &= 0 \qquad l_1 < s_2 < l_2 \end{aligned} \tag{E.9}$$

and the boundary conditions:

$$\begin{aligned} u_1(0,t) &= 0 \\ u_2(0,t) &= u_1(l_1,t) \\ \frac{\partial u_1}{\partial s_1} + \frac{1}{2}(\frac{\partial w}{\partial s_1})^2|_{(l_1,t)} &= \frac{\partial u_2}{\partial s_2}|_{(0,t)} \end{aligned}$$

The resulting drift in the longitudinal response is given by integrating equation (E.9) and satisfying the boundary conditions. This leads to:

$$u^D_{,ss} = -\frac{1}{4}[w_{,s} w^*_{,s}]_{,s} \tag{E.10}$$

$$u^D_{,s} = -\frac{1}{4}[w_{,s} w^*_{,s}] \tag{E.11}$$

$$u^D(s_1) = -\frac{1}{4}\int_0^{s_1} [w_{,s} w^*_{,s}] ds \tag{E.12}$$

Evaluating equation (E.12), and accounting for the first and second harmonic of the lateral response leads to:

$$u^D(s_1) = \chi_1 \left\{ \frac{1}{Re(\gamma_{l_1})^2} sin[2Re(\gamma_{l_1})(l-s_1)] cos\phi_1 + \frac{1}{Im(\gamma_{l_1})^2} sinh[2Im(\gamma_{l_1})(l-s_1)] sin\phi_1 \right\}$$
$$+\chi_2 \left\{ \frac{1}{Re(\gamma_{l_2})^2} sin[2Re(\gamma_{l_2})(l-s_1)] cos\phi_2 + \frac{1}{Im(\gamma_{l_2})^2} sinh[2Im(\gamma_{l_2})(l-s_1)] sin\phi_2 \right\}$$

$$\chi_1 = \frac{|\gamma_{l_1}|^3 |W_1|^2}{16 |sin\gamma_{l_1} l_1|^2}$$

$$\chi_2 = \frac{|\gamma_{l_2}|^3 |W_2|^2}{16 |sin\gamma_{l_2} l_1|^2}$$

The drift in the longitudinal response as derived above causes a change in the average tension in the rope. As a consequence of this, the natural frequencies related to the lateral modes of the the variational equations of motion presented in Chapter 4, increase. The drift induced by the lateral response due to the second harmonic of the lateral excitation at the winder drum can be evaluated by appropriate substitution. Thus the total longitudinal response of the system consists of a static drift to account for the lateral motion, and a dynamic component. The influence of the drift terms on the variational equations is considered further in Appendix F.3.

Appendix F

Parametric coupling Matrices

Chapter 4 presented a discussion which led to the proposition that the stability of the coupled linear steady state motion, as determined in appendices C,D,E, could serve as a criterion for determining design parameters so as to minimise the potential for nonlinear system behaviour. The homogeneous component of the linearised variational equations pertaining to the system are presented below, where the boundary conditions at the sheave and conveyance have been introduced with the use of the dirac delta function $\delta(s-l)$ and the Heaviside step function $H(s-l)$.

$$[1+\zeta\delta(s-l_1)+\eta(s-l_2)]\overline{u}_{,tt} = \mu\overline{u}_{,ss}+c^2\overline{u}_{,ss}+c^2\{w_{,s}\overline{w}_{,s}\}_{,s}[H(s)-H(s-l_1)] \quad \text{(F.1)}$$

$$\overline{v}_{,tt} = \mu_l\overline{v}_{,ss} + \overline{c}^2\overline{v}_{,ss} + c^2\{(\overline{v}_{,s}u_{,s})_{,s} + \frac{1}{2}(w_{,s}^2\overline{v}_{,s})_{,s}\} \quad \text{(F.2)}$$

$$\overline{w}_{,tt} = \mu_l\overline{w}_{,ss} + \overline{c}^2\overline{w}_{,ss} + c^2\{(\overline{w}_{,s}u_{,s})_{,s} + (w_{,s}\overline{u}_{,s})_{,s} + \frac{3}{2}(w_{,s}^2\overline{w}_{,s})_{,s}\} \quad \text{(F.3)}$$

$\zeta = I/\rho AR^2, \quad \eta = M/\rho A$

where c^2, $\overline{c}^2$ represent the longitudinal and lateral wave speeds respectively. $u(s,t)$ represents the total longitudinal steady state response due to the longitudinal excitation at the winder drum, and that induced by the lateral catenary motion, as derived in Appendices C, E respectively. $w(s,t)$ represents the steady state out-of-plane lateral catenary response as derived in Appendix D. $\overline{u},\overline{v},\overline{w}$ represents the variation of the motion about the steady state linear response in the longitudinal, in-plane lateral and out-of-plane lateral directions

respectively. l_1 represents the catenary length, whilst l_2 represents the total cable length. The longitudinal equation (F.1) is defined over the entire length of the rope $0 \leq s \leq l_2$, whilst the lateral equations (F.2),(F.3) are defined only over the catenary length $0 \leq s \leq l_1$.

By applying a normal mode technique, where:

$$\overline{u} = \sum \phi_i(s) p_i(t)$$

$$\overline{v} = \sum \Phi_i(s) q_i(t)$$

$$\overline{w} = \sum \Phi_i(s) r_i(t) \tag{F.4}$$

the equations of motion were reduced to a set of coupled linear parametrically excited ordinary differential equations of the form:

$$[I]\{\ddot{y}\} + [2\zeta_n \omega_n]\{\dot{y}\} + \left[[\omega_n^2] + [A_d] + \sum_{n=1}^{4}[P(n\Omega t)]\right]\{y\} = 0 \tag{F.5}$$

where:

$$\{y\}^T = (p_i, q_i, r_i)$$

$$\sum_{n=1}^{4}[P(n\Omega t)] = \begin{bmatrix} 0 & 0 & U_{uw}(\Omega t, 2\Omega t) \\ 0 & V_{vv}(\Omega t, 2\Omega t, 3\Omega t, 4\Omega t) & 0 \\ W_{uw}(\Omega t, 2\Omega t) & 0 & W_{ww}(\Omega t, 2\Omega t, 3\Omega t, 4\Omega t) \end{bmatrix}$$

Where $[A_d]$ represents an initial stress matrix. This matrix describes the change in the variational natural frequencies as a result in a change in the average tension in the catenary due to the forced excitation. $[A_d]$ is defined in section F.3.

The parametric coupling matrices are obtained on orthogonalising equations (F.1),(F.2),(F.3) with respect to the undamped longitudinal and lateral mode shapes $\phi_i(s), \Phi_i(s)$. It is evident from the above equation that parametric excitation occurs at multiples of the coil cross-over frequency Ω.

The submatrices $[U_{uv}(n\Omega t)], [V_{vv}(n\Omega t)], [W_{vu}(n\Omega t)], [W_{ww}(n\Omega t)]$ are derived in subsequent sections.

F.1 Longitudinal Parametric Coupling

In order to extract the submatrix $[U_{uv}(n\Omega t)]$ in the parametric coupling matrix $[P(n\Omega t)]$, a normal mode approximation is applied to the longitudinal equation of motion (F.1). This is accomplished by assuming:

$$\overline{u} = \sum \phi_i(s) p_i(t)$$

$$\overline{w} = \sum \Phi_i(s) r_i(t)$$

Where the undamped longitudinal and lateral mode shapes of the i^{th} longitudinal and lateral mode are $\phi_i(s), \Phi_i(s)$ respectively, where:

$$\begin{array}{ll} \phi_i(s) = sin\gamma_i s & 0 \le s \le l_1 \\ \phi_i(s) = sin\gamma_i l_1 cos\gamma_i(s-l_1) + (cos\gamma_i l_1 - \frac{\Gamma^2}{\lambda} sin\gamma_i l_1) sin\gamma_i(s-l_1) & l_1 \le s \le l_2 \\ \Phi_i(s) = sin\delta_i s & 0 \le s \le l_1 \end{array}$$

where $\delta_i = i\pi/l_1, \gamma_i^2 = w_i^2/c^2$, where ω_i is the i^{th} longitudinal natural frequency. Substituting the above equations into equation (F.1), and pre-multiplying by the i^{th} undamped longitudinal mode ϕ_i, and integrating over the domain of the rope leads to:

$$\begin{aligned} \int_0^{l_2} [1 + \zeta\delta(s-l_1) + \eta\delta(s-l_2)]\phi_i \sum \phi_j \ddot{p}_j ds &= c^2 \int_0^{l_2} \phi_i \sum \phi_j'' p_j ds \\ &+ c^2 \int_0^{l_1} \phi_i \left\{ \frac{\partial w}{\partial s} \sum \Phi_j'' r_j + \frac{\partial^2 w}{\partial s^2} \sum \Phi_j' r_j \right\} ds \\ &+ \lim_{l_{1-} \to l_{1+}} c^2 \int_{l_{1-}}^{l_{1+}} \phi_i \frac{\partial}{\partial s} \left\{ \frac{\partial w}{\partial s} \sum \Phi_j' r_j \right\} ds \end{aligned} \qquad \text{(F.6)}$$

The integrals $\int_0^{l_2}[1+\zeta\delta(s-l_1)+\eta\delta(s-l_2)]\phi_i\phi_j ds$ and $c^2 \int_0^{l_2} \phi_i\phi_j'' ds$ are orthogonal for the normal mode of a system by definition. These expressions are termed the modal mass and modal stiffness m_{ii}, k_{ii} respectively, where the ratio k_{ii}/m_{ii} is equal to the square of the undamped natural frequency ω_i^2. Thus it is only necessary to calculate the modal mass and the remaining integrals on the right side of equation of equation (F.6). ie:

$$m_{ii} = \int [1 + \zeta\delta(s-l_1) + \eta\delta(s-l_2)]\phi_i\phi_i ds$$

$$k_{ii} = c^2 \int \phi_i \phi_i'' ds = \omega_i^2 m_{ii}$$

The last integral on the right hand side of equation (F.6) accounts for the dirac delta function employed to represent the boundary condition at the sheave wheel, coupling the catenary to the vertical rope. This term may be integrated by parts as:

$$\lim_{l_{1-} \to l_{1+}} c^2 \int_{l_{1-}}^{l_{1+}} \phi_i \frac{\partial}{\partial s} \left\{ \frac{\partial w}{\partial s} \sum \Phi_j' r_j \right\} ds = -c^2 \phi_i \left\{ \frac{\partial w}{\partial s} \sum \Phi_j' \right\} |_{l_1} r_j$$

Thus the submatrix $[U_{uw}(n\Omega t)]$ is evaluated as:

$$[U_{uw}(n\Omega t)]_{i,j} = -\frac{c^2}{m_{ii}} \left[\int_0^{l_1} [\phi_i \Phi_j'' \frac{\partial w}{\partial s} + \phi_i \Phi_j' \frac{\partial^2 w}{\partial s^2}] ds - \frac{1}{2} \phi_i \left\{ \frac{\partial w}{\partial s} \Phi_j' \right\} |_{l_1} \right]$$

$$\begin{aligned} m_{ii} &= \frac{1}{2}(l_1 - \frac{1}{2\gamma_i} sin2\gamma_i l_1) + \frac{1}{2}(A_i^2 + B_i^2) l_2 + \frac{1}{4\gamma_i}(A_i^2 - B_i^2) sin2\gamma_i l_2 + \frac{A_i B_i}{\gamma_i} sin^2 \gamma_i l_2 \\ &\quad + \zeta \phi_i (l_1)^2 + \eta \phi_i (l_2)^2 \end{aligned}$$

$$A_i = sin\gamma_i l_1 \quad B_i = cos\gamma_i l_1 - \frac{\Gamma^2}{\gamma} sin\gamma_i l_1$$
$$\gamma_i = \omega_i / c \quad \eta = \frac{M}{\rho A} \quad \zeta = \frac{J}{\rho A R^2}$$

Where ω_i is the i^{th} undamped natural frequency of the longitudinal system.

If one considers the response due to the n^{th} lateral harmonic of the out-of-plane excitation at the winder drum, $W_n e^{jn\Omega t}$, where the response $w_n(s,t)$ in complex form is given by[1]:

$$w_n(s,t) = \frac{W_n}{sin\gamma_{l_n} l_1} sin(\gamma_{l_n}(l_1 - s)) e^{in\Omega t} \tag{F.7}$$

[1] W_n represents the amplitude and phase of the excitation and is generally a complex entity.

where

$$\gamma_{l_n} = \frac{\frac{n\Omega}{\bar{c}}}{(1+(\frac{n\mu_l l_n}{\bar{c}^2})^2)^{\frac{1}{4}}} e^{-\frac{\alpha_{l_n}}{2}}$$

$$\alpha_{l_n} = tan^{-1}\frac{\mu_l n\Omega}{\bar{c}^2}$$

Evaluation of the integral for $[U_{uw}(n\Omega t)]$ leads to:

$$[U_{uw}(n\Omega t)]_{i,j} = \frac{c^2}{m_{ii}}\left\{\frac{\delta_j\gamma_{l_n}W_n}{sin(\gamma_{l_n}l_1)}\left[\frac{\gamma_i\gamma_{l_n}sin(\gamma_{l_n}l_2)\{\delta_j^2+\gamma_i^2-\gamma_{l_n}^2\}-(-1)^j sin(\gamma_i l_2)\{\gamma_i^2(\delta_j^2+\gamma_{l_n}^2)-(\delta_j^2-\gamma_{l_n}^2)\cdot 1\}}{[(\delta_j+\gamma_i)^2-\gamma_{l_n}^2][(\delta_j-\gamma_i)^2-\gamma_{l_n}^2]}\right]\right.$$
$$\left.-\frac{1}{2}(-1)^j\gamma_{l_n}\delta_j W_n\frac{sin\gamma_i l_1}{sin\gamma_{l_n}l_1}\right\}e^{in\Omega t}$$

The parametric coupling matrix $[U_{uw}(n\Omega t)]$ is complex, hence the form of the matrix due to an excitation $Re\{W_n e^{in\Omega t}\}$ will be $Re([U_{uw}(n\Omega t)])$. If the first and second harmonic of the Lebus excitation frequency are considered, two sets of parametric coupling matrices arise, namely $Re\{[U_{uw}(\Omega t)]\}$, $Re\{[U_{uw}(2\Omega t)]\}$.

F.2 Lateral Parametric Coupling

This section presents the lateral parametric coupling matrices $[W_{uw}(n\Omega t)]$, $[W_{wu}(n\Omega t)]$, $[V_{vv}(n\Omega t)]$. The lateral out-of-plane equation of motion is:

$$\overline{w}_{,tt} = \mu_l \overline{w}_{,ss} + \overline{c}^2 \overline{w}_{,ss} + c^2\{(\overline{w}_{,s}u_{,s})_{,s} + (w_{,s}\overline{u}_{,s})_{,s} + \frac{3}{2}(w_{,s}^2\overline{w}_{,s})_{,s}\} \qquad \text{(F.8)}$$

Substituting the normal mode approximations (F.4) into equation (F.8), and pre-multiplying by the i^{th} undamped lateral mode Φ_i, and integrating the equation over the domain of the catenary[2] leads to:

$$\begin{aligned}
\int_0^{l_1} \Phi_i \sum \Phi_j \ddot{r}_j ds &= \overline{c}^2 \int_0^{l_1} \Phi_i \sum \Phi_j'' r_j ds \\
&+ c^2 \int_0^{l_1} \Phi_i \left\{ \frac{\partial w}{\partial s} \sum \phi_j'' p_j + \frac{\partial^2 w}{\partial s^2} \sum \phi_j' p_j \right. \\
&+ \left. \frac{\partial u}{\partial} \sum \Phi_j'' r_j + \frac{\partial^2 u}{\partial s^2} \sum \Phi_j' r_j \right\} ds \\
&+ \frac{3}{2} \int_0^{l_1} \{ (\frac{\partial w}{\partial s})^2 \sum \Phi_j' r_j \}_{,s} ds \qquad \text{(F.9)}
\end{aligned}$$

Since the normal modes of the catenary are orthogonal by definition and hence the integrals $\int_0^{l_1} \Phi_i \Phi_i ds = m_{ii}$, $\overline{c}^2 \int_0^{l_1} \Phi_i \Phi_i'' ds = k_{ii}$, where the terms m_{ii}, k_{ii} refer to the modal mass and stiffness of the catenary, and the ratio k_{ii}/m_{ii} is represents the square of the i^{th} undamped natural frequency of lateral vibration of the catenary $\overline{\omega}_i^2$. Thus it is necessary to calculate the modal mass and the remaining integrals in the last two terms on the right hand side of equation(F.9).

$$m_{ii} = \int_0^{l_1} \Phi_i \Phi_i ds = l_1/2$$

$$k_{ii} = \overline{c}^2 \int_0^{l_1} \Phi_i \Phi_i'' ds = \overline{\omega}_i^2 m_{ii}$$

[2]In this case, the domain reduces to the catenary length, as the lateral mode is only defined for the catenary

The remaining integrals are defined by:

$$[W_{uw}(n\Omega t)]_{i,j} = -\frac{c^2}{m_{ii}} \int_0^{l_1} \Phi_i \left\{ \frac{\partial w}{\partial s} \sum \phi_j'' + \frac{\partial^2 w}{\partial s^2} \sum \phi_j' \right\} ds$$

$$[W_{ww}(n\Omega t)]_{i,j} = -\frac{c^2}{m_{ii}} \int_0^{l_1} \Phi_i \left\{ \frac{\partial u}{\partial s} \sum \Phi_j'' + \frac{\partial^2 u}{\partial s^2} \sum \Phi_j' \right\} ds - \frac{3c^2}{2m_{ii}} \int_0^{l_1} \{(\frac{\partial w}{\partial s})^2 \sum \Phi_j'\}_{,s} ds$$

Parametric coupling matrix $[W_{uw}(n\Omega t)]$

Substituting the solution for the lateral out-of-plane response w_n from equation (F.7), due to the n^{th} harmonic of the lateral out-of-plane excitation at the Lebus drum, $W_n e^{in\Omega t}$, and carrying out the integration for the first integral above leads to:

$$[W_{uw}(n\Omega t)]_{j,i} = \frac{c^2 \delta_i \gamma_j \gamma_{l_n} W_n}{m_{ii} sin(\gamma_{l_n} l_1)} \left[\frac{(-1)^i \gamma_j sin(\gamma_j l_1)(\delta_i^2 - \gamma_j^2 + \gamma_{l_n}^2) + \gamma_{l_n} sin(\gamma_{l_n} l_1)(\delta_i^2 + \gamma_j^2 - \gamma_{l_n}^2)}{[\delta_i^2 - (\gamma_j - \gamma_{l_n})^2][\delta_i^2 - (\gamma_j + \gamma_{l_n})^2]} \right] e^{in\Omega t}$$

Parametric coupling matrix $[W_{ww}(n\Omega t)]$

The second integral above for $[W_{ww}(n\Omega t)]$ is simplified into two separate components. The integral depends on the forced response u due to the longitudinal excitation at the drum and as a result of the lateral catenary motion, and on the forced lateral response w.

Considering the first part of the integral which is due to the total longitudinal response u.ie:

$$[W_{ww}(n\Omega t)]_{i,j} = -\frac{c^2}{m_{ii}} \int_0^{l_1} \Phi_i \left\{ \frac{\partial u}{\partial s} \sum \Phi_j'' + \frac{\partial^2 u}{\partial s^2} \sum \Phi_j' \right\} ds$$

The total dynamic longitudinal response including the fundamental and the second harmonic longitudinal and lateral excitation at $\Omega, 2\Omega$ is:

$$\begin{aligned} u_l(s,t) \;=\; & Re\Big[R_1 e^{i\Omega t} + R_2 e^{2i\Omega t} + R_3 e^{3i\Omega t} + R_4 e^{4i\Omega t} + \\ & \{\mathcal{A}_1 sin[(\gamma_{l2} + \gamma_{l_1}^*)(l_1 - s) + \mathcal{B}_1 sin[(\gamma_{l2} - \gamma_{l_1}^*)(l_1 - s)\} e^{i\Omega t} \\ & + \mathcal{A}_2 sin 2\gamma_{l_1}(l_1 - s) e^{2i\Omega t} + \\ & \{\mathcal{A}_3 sin[(\gamma_{l2} + \gamma_{l_1})(l_1 - s) + \mathcal{B}_3 sin[(\gamma_{l2} - \gamma_{l_1})(l_1 - s)\} e^{3i\Omega t} + \\ & \mathcal{A}_4 sin 2\gamma_{l2}(l_1 - s) e^{4i\Omega t}\Big] \end{aligned}$$

where $\mathcal{A}_n, \mathcal{B}_n$ are determined from Appendix E as:

$$\mathcal{A}_1 = \frac{\gamma_{l_1}^* \gamma_{l_2} W_1^* W_2 (\gamma_{l_1}^* + \gamma_{l_2})}{4sin(\gamma_{l_1}^* l_1) sin(\gamma_{l_2} l_1)[(\gamma_{l_1}^* + \gamma_{l_2})^2 (c^2 + i\mu\Omega) - \Omega^2]} \qquad \mathcal{B}_1 = \frac{\gamma_{l_1}^* \gamma_{l_2} W_1^* W_2 (\gamma_{l_1}^* - \gamma_{l_2})}{4sin(\gamma_{l_1}^* l_1) sin(\gamma_{l_2} l_1)[(\gamma_{l_1}^* - \gamma_{l_2})^2 (c^2 + i\mu\Omega) - \Omega^2]}$$

$$\mathcal{A}_2 = \frac{\gamma_{l_1}^3 W_1^2 sin(2\gamma_{l_1}(l_1 - s)}{(2sin(\gamma_{l_1})^2[(2\gamma_{l_1})^2 (c^2 + 2i\mu\Omega) - 4\Omega^2]}$$

$$\mathcal{A}_3 = \frac{\gamma_{l_1} \gamma_{l_2} W_1 W_2 (\gamma_{l_1} + \gamma_{l_2})}{4sin(\gamma_{l_1} l_1) sin(\gamma_{l_2} l_1)[(\gamma_{l_1} + \gamma_{l_2})^2 (c^2 + 3i\mu\Omega) - 9\Omega^2]} \qquad \mathcal{B}_3 = \frac{\gamma_{l_1} \gamma_{l_2} W_1 W_2 (\gamma_{l_1} - \gamma_{l_2})}{4sin(\gamma_{l_1} l_1) sin(\gamma_{l_2} l_1)[(\gamma_{l_1} - \gamma_{l_2})^2 (c^2 + 3i\mu\Omega) - 9\Omega^2]}$$

$$\mathcal{A}_4 = \frac{\gamma_{l_2}^3 W_2^2 sin(2\gamma_{l_2}(l_1 - s)}{(2sin(\gamma_{l_2})^2[(2\gamma_{l_2})^2 (c^2 + 4i\mu\Omega) - 16\Omega^2]}$$

$$R_n = A_n cos\gamma_n s + B_n sin\gamma_n s$$

and A_n, B_n, γ_n are obtained from the solutions to the forced longitudinal system response as defined in Appendix E.

The parametric coupling matrix relating to the longitudinal response will be evaluated as two component matrices. ie

$$[W_{ww}(n\Omega t)]_{n=1,2,3,4} = [W_{ww}(n\Omega t)]^1_{n=1,2,3,4} + [W_{ww}(n\Omega t)]^2_{n=1,2,3,4}$$

Where $[W_{ww}(n\Omega t)]^1_{n=1,2,3,4}$ results from the terms $R_n e^{in\Omega t}$ in the longitudinal response, whilst $[W_{ww}(n\Omega t)]^2_{n=1,2,3,4}$ results from the remaining terms.

Considering the coupling matrix $[W_{ww}(n\Omega t)]^1$ due to the longitudinal response term $R_n e^{in\Omega t}$, the integral $[W_{ww}(n\Omega t)]^1$ is given by:

$$[W_{ww}(n\Omega t)]^1_{ij} = \delta_i \delta_j \gamma_n^2 \beta_n \frac{c^2}{m_{ii}} \left[\frac{\delta_i^2 + \delta_j^2 - \gamma_n^2}{[(\delta_i + \delta_j)^2 - \gamma_n^2][(\delta_i - \delta_j)^2 - \gamma_n^2]} \right] e^{in\Omega t}$$

$$\beta_n = A_n - (-1)^{i+j} \{A_n cos(\gamma_n l_1) + B_n sin(\gamma_n l_1)\}$$

The parametric coupling matrix $[W_{ww}(n\Omega t)]^2_{ij}$ is obtained by considering the term $\mathcal{A}_2 sin2\gamma_l(l_1 - s)e^{2i\omega t}$ separately. Carrying out the appropriate integration leads to:

$$[W_{ww}(2\Omega t)]^2_{ij} = 4\mathcal{A}_2 \delta_i \delta_j \gamma_{l_1}^2 sin(2\gamma_{l_1} l_1) \frac{c^2}{m_{ii}} \left[\frac{\delta_i^2 + \delta_j^2 - 4\gamma_{l_1}^2}{[(\delta_i + \delta_j)^2 - 4\gamma_{l_1}^2][(\delta_i - \delta_j)^2 - 4\gamma_{l_1}^2]} \right] e^{2i\Omega t}$$

The matrices $[W_{ww}(n\Omega t)]^2$ for $n = 1, 3, 4$ can be evaluated by appropriate substitution in the above equation.

The coupling matrix due to the forced lateral response w is defined by:

$$[W_{ww}(n\Omega t)]^3 = -\frac{3c^2}{2m_{ii}} \int_0^{l_1} \Phi_i \{(\frac{\partial w}{\partial s})^2 \sum \Phi_j'\}_{,s} ds \tag{F.10}$$

If one considers the forced lateral response due to the first and second harmonic of the Lebus frequency then:

$$w = Re(\sum_{n=1}^{2} \frac{W_n}{sin\gamma_{l_n} l_1} sin\gamma_{l_n}(l_1 - s)e^{in\Omega t}) = w_1 + w_2$$

Consequently dynamic[3] components of $(w_{,s})^2$ occur at $n\Omega$, $n = 1 \cdots 4$, given respectively as:

$$(w_{,s})^2 = \frac{1}{2}[2Re(\frac{\partial w_1}{\partial s}\frac{\partial w_2^*}{\partial s}) + Re(\frac{\partial w_1}{\partial s})^2 + 2Re(\frac{\partial w_1}{\partial s}\frac{\partial w_2}{\partial s}) + Re(\frac{\partial w_2}{\partial s})^2]$$

Consider the second component $Re(\frac{\partial w_1}{\partial s})^2$:

$$Re(\frac{\partial w_1}{\partial s})^2 = \frac{1}{2}Re((\frac{\gamma_{l_1} W_1}{sin\gamma_{l_1} l_1})^2 cos^2\gamma_{l_1}(l_1 - s)e^{2i\Omega t})$$

Substituting this expression into equation (F.10) and performing the integration:

$$[W_{ww}(2\Omega)]^3 = \frac{3c^2}{2m_{ii}}\{\frac{\gamma_{l_1} W_1}{sin\gamma_{l_1} l_1}\}^2 \left[\frac{\delta_i \delta_j \gamma_{l_1} sin2\gamma_{l_1} l_1}{[(\delta_i - \delta_j)^2 - (2\gamma_{l_1})^2][(\delta_i + \delta_j)^2 - (2\gamma_{l_1})^2]} - \Lambda\right] e^{i\Omega t}$$

where $\Lambda = \frac{l_1}{8}$ if $i = j$, and $\Lambda = 0$ if $i \neq j$.

[3]The static component of this term affects the lateral variational frequencies, and is considered further in section F.3.

The remaining matrices for $n = 1, 3, 4$ may be evaluated by appropriate substitution and integration of equation (F.10).

Thus the total parametric coupling matrix $[W_{ww}(n\Omega t)]$ is obtained from:

$$[W_{ww}(n\Omega t)] = \sum_{n=1}^{4} Re\{[W_{ww}(n\Omega t)]^1 + [W_{ww}(n\Omega t)]^2 + [W_{ww}(n\Omega t)]^3\}$$

The parametric coupling matrix $[V_{vv}(n\Omega t)]$ is obtained in an identical fashion. It is not identical to $[W_{ww}(n\Omega t)]$ since the term $(w_{,s}^2 \overline{v}_{,s})_{,s}$ in equation (F.2) is pre-multiplied by $\frac{1}{2}$, where as $(w_{,s}^2 \overline{w}_{,s})_{,s}$ in equation (F.3) is pre-multiplied by $\frac{3}{2}$. $[V_{vv}(n\Omega t)]$ can be constructed from the component matrices of $[W_{ww}(n\Omega t)]$ as:

$$[V_{vv}(n\Omega t)] = \sum_{n=1}^{4} Re\{[W_{ww}(n\Omega t)]^1 + [W_{ww}(n\Omega t)]^2 + \frac{1}{3}[W_{ww}(n\Omega t)]^3\}$$

Since the real part of the component matrices constitute the overall parametric coupling matrix, the parametric coupling matrix may be expanded to:

$$[P(n\Omega t)] = \sum_{n=1}^{4} \{[P_c]_n cos(n\Omega t) + [P_s]_n sin(n\Omega t)\}$$

Thus if the first two harmonics $\Omega, 2\Omega$ of the Lebus cross-over frequency are accounted for, the system is excited parametrically at $\Omega, 2\Omega, 3\Omega, 4\Omega$ by sine and co-sine functions. Thus the parametric matrices relating to each harmonic are impedance functions, and are phase shifted with respect to each other.

F.3 Drift Terms

This section considers the influence of the drift term in the longitudinal response $u^D(s)$, and the static component of $w_{,s}^2$ in equations (F.2),(F.3) on the lateral variational equations. The longitudinal drift $u^D(s)$ was determined in Appendix E.1 as[4]:

$$u^D_{,ss} = -\frac{1}{4}[w_{,s}w^*_{,s}]_{,s} \tag{F.11}$$

$$u^D_{,s} = -\frac{1}{4}[w_{,s}w^*_{,s}] \tag{F.12}$$

$$u^D(s_1) = -\frac{1}{4}\int_0^{s_1}[w_{,s}w^*_{,s}]ds \tag{F.13}$$

Considering the first harmonic of lateral response w_1, the static component of $Re(w_{1,s})Re(w_{1,s})$ is denoted $(w_{1,s})^2_D$:

$$(w_{1,s})^2_D = \frac{1}{2}[w_{1,s}w^*_{1,s}] \tag{F.14}$$

Drift terms do not affect the variational form of the longitudinal equation of motion (F.1). However they do effect the variational form of the lateral equations of motion (F.2-F.3). These equations are reproduced below, where only static or drift components of the linear steady state response are retained.

$$\overline{v}_{,tt} = \mu_l\overline{v}_{t,ss} + \overline{c}^2\overline{v}_{,ss} + c^2\{(\overline{v}_{,s}u^D_{,s})_{,s} + \frac{1}{2}((w_{1,s})^2_D\overline{v}_{,s})_{,s}\} \tag{F.15}$$

$$\overline{w}_{,tt} = \mu_l\overline{w}_{t,ss} + \overline{c}^2\overline{w}_{,ss} + c^2\{(\overline{w}_{,s}u^D_{,s})_{,s})_{,s} + \frac{3}{2}((w_{1,s})^2_D\overline{w}_{,s})_{,s}\} \tag{F.16}$$

Substituting equations (F.12),(F.14) into the above equations leads to:

$$\overline{v}_{,tt} = \mu_l\overline{v}_{t,ss} + \overline{c}^2\overline{v}_{,ss} \tag{F.17}$$

[4] w^* represents the complex conjugate of w

$$\overline{w}_{,tt} = \mu_l \overline{w}_{,ss} + \overline{c}^2 \overline{w}_{,ss} + c^2\{\frac{1}{2}(w_s w_s^* \overline{w}_{,s})_{,s}\} \qquad \text{(F.18)}$$

Since the lateral in-plane variational equation (F.17) reduces to its linear counterpart, the drift terms exert no influence on the natural frequencies of the in-plane variational modes. However, in the case of the out-of-plane variational equation, the drift terms do exert an influence. Effectively the final term in equation (F.18) modifies the linear lateral natural frequencies of the out-of-plane modes. This influence can be ascertained by applying a normal mode approximation for $\overline{w}$, and carrying out the appropriate integration. This results in a modified modal stiffness matrix with off diagonal terms, coupling the lateral out-of-plane modes.

This matrix is given by:

$$[k_{ij}] = -\frac{\overline{c}^2}{m_{ii}} \int_o^{l_1} \Phi_i \Phi_j'' ds - \frac{c^2}{m_{ii}} \int_o^{l_1} \Phi_i \{\frac{1}{2}(w_s w_s^* \Phi_j')_{,s}\} ds$$

where $\overline{c}, c, m_{ii}, \Phi$ represent the lateral wave speed, the longitudinal wave speed, the modal mass, and the i^{th} linear eigenfunction respectively, and Φ' represents differentiation of Φ with respect to s. The linear eigenfunction satisfying the boundary conditions is:

$$\Phi_i(s_1) = sin(\delta_i s_1) \qquad where \qquad \delta_i = i\pi/l_1$$

Performing the integration leads to:

$$[k_{ij}] = [\omega_i^2] + \sum [A_{ij}]_n$$

$$\begin{aligned}
[A_{ij}]_n \;=\; & \frac{c^2 \delta_i \delta_j}{2m_{ii}} \left\{ \frac{|W_n||\gamma_{l_n}|}{|sin(\gamma_{l_n} l_1)|} \right\}^2 \left\{ \frac{sin(\gamma_{l_n} - \gamma_{l_n}^*) l_1}{(\delta_i + \delta_j + \gamma_{l_n} - \gamma_{l_n}^*)} - \frac{sin(\gamma_{l_n} - \gamma_{l_n}^*) l_1}{(\delta_i - \delta_j - \gamma_{l_n} + \gamma_{l_n}^*)} \right. \\
& + \frac{sin(\gamma_{l_n} - \gamma_{l_n}^*) l_1}{(\delta_i - \delta_j + \gamma_{l_n} - \gamma_{l_n}^*)} - \frac{sin(\gamma_{l_n} - \gamma_{l_n}^*) l_1}{(\delta_i + \delta_j - \gamma_{l_n} + \gamma_{l_n}^*)} \\
& - \frac{sin(\gamma_{l_n} + \gamma_{l_n}^*) l_1}{(\delta_i - \delta_j - \gamma_{l_n} - \gamma_{l_n}^*)} + \frac{sin(\gamma_{l_n} + \gamma_{l_n}^*) l_1}{(\delta_i - \delta_j + \gamma_{l_n} + \gamma_{l_n}^*)} \\
& \left. - \frac{sin(\gamma_{l_n} + \gamma_{l_n}^*) l_1}{(\delta_i + \delta_j - \gamma_{l_n} - \gamma_{l_n}^*)} + \frac{sin(\gamma_{l_n} + \gamma_{l_n}^*) l_1}{(\delta_i + \delta_j + \gamma_{l_n} + \gamma_{l_n}^*)} \right\}
\end{aligned}$$

where $[w_i^2]$ represents a diagonal matrix containing the linear natural frequencies of the out-of-plane modes, and $[A_{ij}]_n$ represents additional stiffness coupling generated between the out-of-plane modes due to the n^{th} harmonic of the lateral response. Since this matrix is a function of the excitation amplitude, the stiffness of the variational system changes with the lateral response amplitude, and consequently the natural frequencies of the out-of-plane variational modes change and detune from the in-plane modes. The modified natural frequencies of the lateral variational modes are thus found by extracting the eigenvalues of $[k_{ij}]$.ie:

$$\left[\backslash\omega_w^2\backslash\right] = Eig[K_{ij}]$$

It is important to note that the detuning of the variational system is a consequence of the assumed linear solution, and is consistent only where this solution is valid. The variation in the natural frequency corresponds to the frequency at which the system would respond, to small disturbances about the linear solution. In constructing the linear steady state solution, it was assumed that the lateral response amplitude was small, and therefore terms of $o(w^3)$ were neglected. This is unlikely to be the case in a region of external lateral resonance.

Appendix G

Longitudinal Damping Estimates

G.1 Damping Mechanisms

A crucial step required in a dynamic simulation concerns the definition of an appropriate damping mechanism. Greenway[1989] examined the logarithmic decrement associated with the free response of the first longitudinal mode of a conveyance at Deelkraal Mine, due to emergency braking. The sheave support structure was strain gauged to measure rope load, providing time data for the event. The data was gathered by Thomas et al.[1987], as a part of a report for COMRO(1987). The logarithmic decrement was extracted from this data, for an empty and full conveyance, decelerated at stations at approximately quarter and three quarters of the shaft depth. The results of these tests are presented in table G.1. In interpreting the logarithmic decrement with respect to the longitudinal oscillations, Greenway[1989] considered the longitudinal equation of motion of the system in the principal modal co-ordinates as:

$$\ddot{q}_i + (a + b\omega_i^2)\dot{q}_i + \omega_i^2 q_i = 0 \tag{G.1}$$

where q_i represents the i^{th} principal mode; the damping coefficient a represents the material damping constant corresponding to a distributed damping force $u_{,t}$, which is proportional to the mass properties; b represents the material damping constant corresponding to the distributed damping force $u_{xx,t}$, which is proportional to the stiffness properties. The latter type of damping amounts to relative damping since it is associated with the relative velocities of the

displacement co-ordinates. Greenway[1989] considered relative damping to be appropriate, and thus set $a = 0$, whilst retaining the coefficient b.

Considering this equation in the form:

$$\ddot{q}_i + 2\zeta_i\omega_i\dot{q} + \omega_i^2 q = 0$$

where ζ_i represents the modal damping ratio associated with the i^{th} mode and ω_i represents the i^{th} natural frequency. Comparison of the equations leads to:

$$\zeta_i = \frac{b\omega_i}{2}$$

Thus for a constant damping coefficient b, the modal damping ratio in each principal mode is proportional to the undamped natural frequency of that mode. Although the data was limited, Greenway[1989] demonstrated that with respect to this data, the logarithmic decrement depended on the conveyance mass and the vertical length of the rope, whilst the material damping coefficient b was less sensitive to skip mass, but related to the rope length. Greenway[1989] non-dimensionalised the equations of motion, and derived a dimensionless damping parameter $\beta = bc/2l$ where c and l represent wave speed and rope length respectively. This accounted for the variation of the material damping coefficient as a function of rope length.

Proportional relative damping results in a relationship between the modal damping factor of the first mode, and higher modes, such that $\zeta_n = \zeta_1 \frac{\omega_n}{\omega_1}$. Thus the modal damping factor of the higher modes increases in proportion to the ratio of the undamped natural frequencies, and thus higher modes become successively more highly damped. This has lead to the assumption that the fundamental mode dominates the longitudinal response, whilst the higher modes are more strongly attenuated and consequently less important. Greenway[1989] notes that the assumption of proportional modal damping is implemented in his analysis since it appears to be *intuitively* correct. Dimitriou and Whillier[1973] briefly commented that data obtained regarding the free decay response of skips, exhibited a linear decay profile, which is associated with friction , and hence a Coulomb damping mechanism rather than a viscous damping mechanism. This confirmed experimental results of Vanderveldt et al.[1973] regarding the lateral dynamic characteristics of stranded wire rope. Dimitriou and Whillier[1973] concluded that Coulomb damping played a greater roli than viscous damping in mine hoist wire ropes. As is

evident, the aspect of damping in mine hoist ropes ha not been given a great deal of attention. It is surmised that this is due to the production losses which would be incurred if an adequate experimental program was instituted to measure and formulate a damping model for the rope. This model is likely to be a complex non-linear function reflecting the rope construction and mean tension. Nevertheless, if accurate simulations are to be performed, a more thorough experimental determination of the damping levels will be required.

It was decided that approximate damping factors would have to be applied due to the limited data available. However, the decision as to the application of a relative proportionally damped model, as opposed to a hysteretically damped model could be investigated. It was this aspect which provided the incentive for performing further site tests.

G.2 Drop Tests

Anglo American Corporation (AAC) was assessing a levelock system on a conveyance at Elandsrand Gold Mine. The levelock system is a hydraulically actuated device which clamps the conveyance or man cage between the guides during unloading and loading cycles. The device releases the clamping force so that the skip or man cage slides without overshoot to its new equilibrium position. As part of the test program, it was decided to assess the cage response due to a pre-load in the cage, followed by a rapid release in the clamping force. This was accomplished by clamping an empty cage in position at the station, inserting a dead weight, and subsequently releasing the clamping force. Once the cage had settled to its new equilibrium position, it was repositioned at the station and clamped; the load was removed and subsequently the clamping force was released. In this manner, the free decay of the longitudinal oscillations could be examined in the presence of a fixed rope length, with various mean tensions and cage mass. Six tests were performed, namely[1]:

- Seven ton drop.
- Seven ton lift.
- Seven ton drop.
- Seven ton lift.
- Three ton drop.

[1] 1 ton= 1000kg

- Three ton lift.

Three different transducers were monitored during the tests. An accelerometer and displacement LVDT were recorded by AAC personnel[2]. Strain gauges were applied to the draw bar structure by University personnel, providing measurement of the rope force at the conveyance. The data from the AAC transducers was recorded directly without any pre-filtering. In order to amplify the response of the higher longitudinal modes, the measurement from the draw bar load cell was filtered prior to amplification. An analogue high-pass filter with a frequency cut-off of 0.5Hz was used.

The time traces from the AAC accelerometer are presented in figure G.2. The repeatability of the data is reflected in figures G.2(a),(d) where two records from different tests are superimposed. Similar results were obtained for the LVDT and draw bar measurement. Frequency response functions were created by treating the time data as being representative of the unit impulse response of the longitudinal system. The frequency response functions were constructed by applying a Fourier transformation to the time data. The frequency response functions[3] for the AAC accelerometer records are presented in figure G.3. The I-Deas package was utilised to perform this task, where an exponential window was applied to the time data prior to performing the Fourier transformation. A circle fit method was applied to extract the natural frequency and corrected[4] damping factor for each FRF. The results from the analysis are presented in table G.2 for the AAC accelerometer. The first mode was curve fitted for the LVDT measurement, whilst the draw bar measurement provided damping estimates for the second and third modes. These results are presented in tables G.3 ,G.4.

[2]The purpose of the AAC test was to assess the gross motion of the conveyance. The processing of the data to achieve further damping estimates, was proposed as a result of the research carried out in this thesis, which indicated that relative proportional damping overestimated the modal damping factors in the higher modes.

[3]A spectral resolution of 0.02 Hz was achieved.

[4]The damping factor was corrected to account for the exponential window.

G.3 Discussion

The objective of the test was primarily aimed at determining if a relative proportional modal damping mechanism, as proposed by Greenway[1989] is appropriate to mine hoist ropes. Since the natural frequency of the second mode is approximately four times higher than the first, relative proportional modal damping would imply that the second mode should reflect approximately four times the modal damping ratio of the first mode. Clearly this did not occur. Although an adequate degree of repeatability was achieved with respect to the modal damping factor of the first mode, because the conveyance is close to a nodal point for the higher modes, and consequently the modal coupling is reduced, a higher signal-to-noise ratio occurs with regard to the measured response of the second and higher modes. As a result, difficulty was encountered in curve fitting the second and third modes, as reflected by the scatter of the damping estimates presented in tables G.2,G.4.

This form of test is crude, and one would not expect to achieve highly accurate damping estimates. Nevertheless, the test was useful in that it confirmed that significantly higher damping factors were not measured for the higher modes, and consequently a relative proportional damping mechanism alone would not be appropriate.

The damping factor measured for the first mode reflects a strong dependency on the initial rope tension, or the amplitude of the impulse. Figure G.1 presents a plot of the measured damping factor of the first mode verses skip load. The time traces of the response, and the estimated damping factor reflect that the damping effect is lower when the cage is dropped as opposed to when it lifts. This effect may be the result of a number of different mechanisms, and clearly more extensive and accurate testing techniques would be required to determine these. However, when the skip is dropped, the mean tension in the rope rises; as a result of the rope construction the strands lock more readily, preventing relative interstrand motion, and resulting in a lower damping coefficient. During the lift cycle, overshoot of the cage results in a drop in the mean rope tension, promoting interstrand movement and consequently higher damping factors. Since the higher modes are less strongly coupled to the impulsive force induced in the test, the mean tension changes related to the higher modes would be less significant, and hence have less effect on the modal damping factors[5]. The mechanism proposed would result in a dependence of the damping estimate on the magnitude of the initial impulse applied to the system and in this context the response would be nonlinear. Consequently the

[5]Aerodynamic effects may also be pertinent to the response of the first mode, as a downward forced draft of approximately 10m/s exists in the shaft.

technique adopted to extract the damping estimate would not be valid.

In practice, the disturbances applied to the system during the winding cycle are not as severe as those applied in the drop test[6]. It may be argued that although the damping mechanism may be nonlinear when considering large disturbances, a linear mechanism may apply for smaller disturbances. Figure G.1 illustrates that the damping ratio of the first mode is approximately linearly dependent on the load in the skip or the initial impulse. In this context, the intercept of a line fitted through the data, with the abscissa would represent a *linear* estimate for small disturbances of the fundamental mode. A least squares curve fit of the data provides a *linear* damping estimate of 4.65%, which is of the order of the measurements extracted by Greenway[1989] as presented in table G.1.

A number of options exist regarding a practical approach to deriving a damping model, which reflects to some degree the longitudinal dissipation of the rope. For analytical reasons it is convenient to apply proportional damping models, since the continuous solution can be extracted in closed form. A more flexible method results if the system response is analysed via the normal mode technique, since modal damping factors can be applied independently to each principal mode[7]; however the disadvantage of a normal mode approach is that it requires that sufficient modes are included in the analysis to prevent modal truncation.

The damping estimates can be examined in the context of a general proportional form, where the damping constants a, b in equation (G.1) are not equal to zero. This would require that the damping action is proportional to both the mass and stiffness properties of the rope. In this sense the modal damping coefficient would be:

$$\zeta_n = \frac{1}{2}(\frac{a}{\omega_n} + b\omega_n)$$

where a, b represent the material damping coefficients, and ω_n represents the natural frequency of the n^{th} mode.

The damping estimates related to the first mode were considered more repeatable than those of the higher modes. Thus the constants a, b were extracted

[6]With regard to the winding cycle, large motion does occur at the conveyance during the acceleration and deceleration phase, and thus one may expect stronger attenuation during a deceleration from the nominal winding speed and visa versa.

[7]A hysteretic damping model would necessitate this approach.

by considering the experimental damping estimates as a function of frequency, pertaining to the first mode only. The constants[8] were extracted by applying a least squares minimisation procedure. The experimental data and analytical curve fit are presented in figure G.4. Figure G.5 presents the curve fit together with the estimates extracted for the second and third modes. It is clear that although such a damping model may adequately account for the dependence of the modal damping estimate of the first mode on the mean tension, it does not simultaneously satisfy low damping estimates for the higher modes.

Greenway[1993] interpreted the data differently, by globally fitting the data to the damping model. This results in a damping model which neglects the dependence of the first modal damping estimate on the mean tension, whilst adequately accounting for lower damping factors in the higher modes. Figure G.6 presents a plot of the experimental data and curve fit. This approach provides a damping model which adequately describes the trends in an average manner. The advantage of this model is that it can be directly incorporated into existing analyses, and accommodates more correctly the lower damping in the higher modes. The justification for applying such a model would be its convenience rather than being physically correct.

Figure G.7 presents the data curve fitted such that the *linear* modal damping coefficient of the first mode is applied, thus eliminating the dependence of this coefficient on the mean tension.

[8] A negative coefficient was obtained for a, which is not physically sensible.

G.4 Conclusion

Although the test data is sparse, and an extensive test program would be required to assess the dependence of the modal damping estimates on rope length and mean tension, important observations regarding the data can be proposed.

- The assumption of proportional relative damping is not appropriate since it results in large modal damping factors for the higher modes.
- The modal damping estimate is dependent on the mean tension in the rope, which indicates that for large disturbances frictional effects are important. The linear decay of the response in figure G.2(a,b,c) confirms that hysteretic effects are evident.
- It is possible to propose a general proportionally damped model which adequately describes the modal damping estimates in the low as well as higher modes. This model is proposed for convenience in an analytical study, and is not intended to account for the actual damping mechanism.
- A substantial effort by the industry is required to correctly quantify the nature of the damping mechanism, which adequately accounts for mean tension and rope length.

The damping mechanism is complex; although general proportional damping may represent the damping mechanism in an average sense, interstrand friction and hence Coulomb effects are likely to play a roll. Thus it is possible that a more accurate *linear* model would result as a combination of general proportional and hysteretic damping action. These findings are based on limited data, and are not well substantiated. Clearly substantial scope exists for further work which would lead to a more accurate determination of the damping mechanism appropriate to mine hoist ropes.

Table G.1: Deelkraal Data - Greenway[1989]

Depth	LoadedUnloaded	$f_1(Hz)$	δ	b(s)	ζ_1 %
3/4 down	load	0.278	0.163	0.03	2.6
3/4 down	empty	0.388	0.230	0.03	3.7
1/4 down	empty	0.731	0.173	0.12	2.7

Table G.2: Elandsrand - Drop test measurements - AAC accelerometer

Depth	Load	$f_1(Hz)$	$f_2(Hz)$	ζ_1%	ζ_2 %
75level	+7 ton	0.289	1.05	2.90	1.81
75level	-7 ton	0.337	1.102	6.76	2.20
75level	+7 ton	0.289	1.074	2.50	1.29
75level	-7 ton	0.343	1.114	6.75	1.26
75level	+3 ton	0.329	1.105	4.86	1.42
75level	-3 ton	0.34	1.148	5.37	0.65

Table G.3: Elandsrand - Drop test measurements - AAC LVDT

Depth	Load	$f_1(Hz)$	ζ_1%
75lev	+7 ton	0.289	2.94
75level	-7 ton	0.337	7.43
75level	+7 ton	0.289	2.53
75level	-7 ton	0.345	6.97
75level	+3 ton	0.331	4.23
75level	-3 ton	0.338	4.07

Table G.4: Elandsrand - Drop test measurements - WITS load cell

Depth	Load	$f_2(Hz)$	$f_3(Hz)$	$\zeta_2\%$	ζ_3 %
75level	+7 ton	1.048	1.927	2.25	2.42
75level	-7 ton	1.066	1.908	0.22*	2.60
75level	+7 ton	1.091	1.947	1.282	1.85
75level	-7 ton	1.114	1.981	0.701*	1.94
75level	+3 ton	1.108	2.021	0.798	-
75level	-3 ton	1.118	-	0.951	-

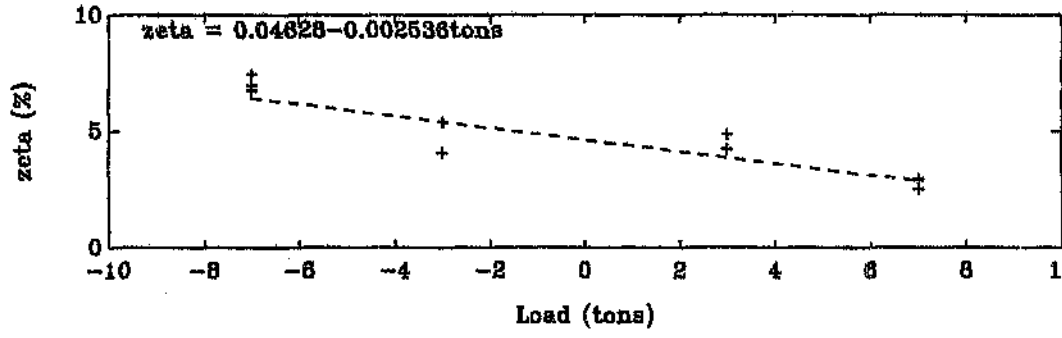

Figure G.1: Drop Test : Modal damping ratio ζ_1 verses conveyance load

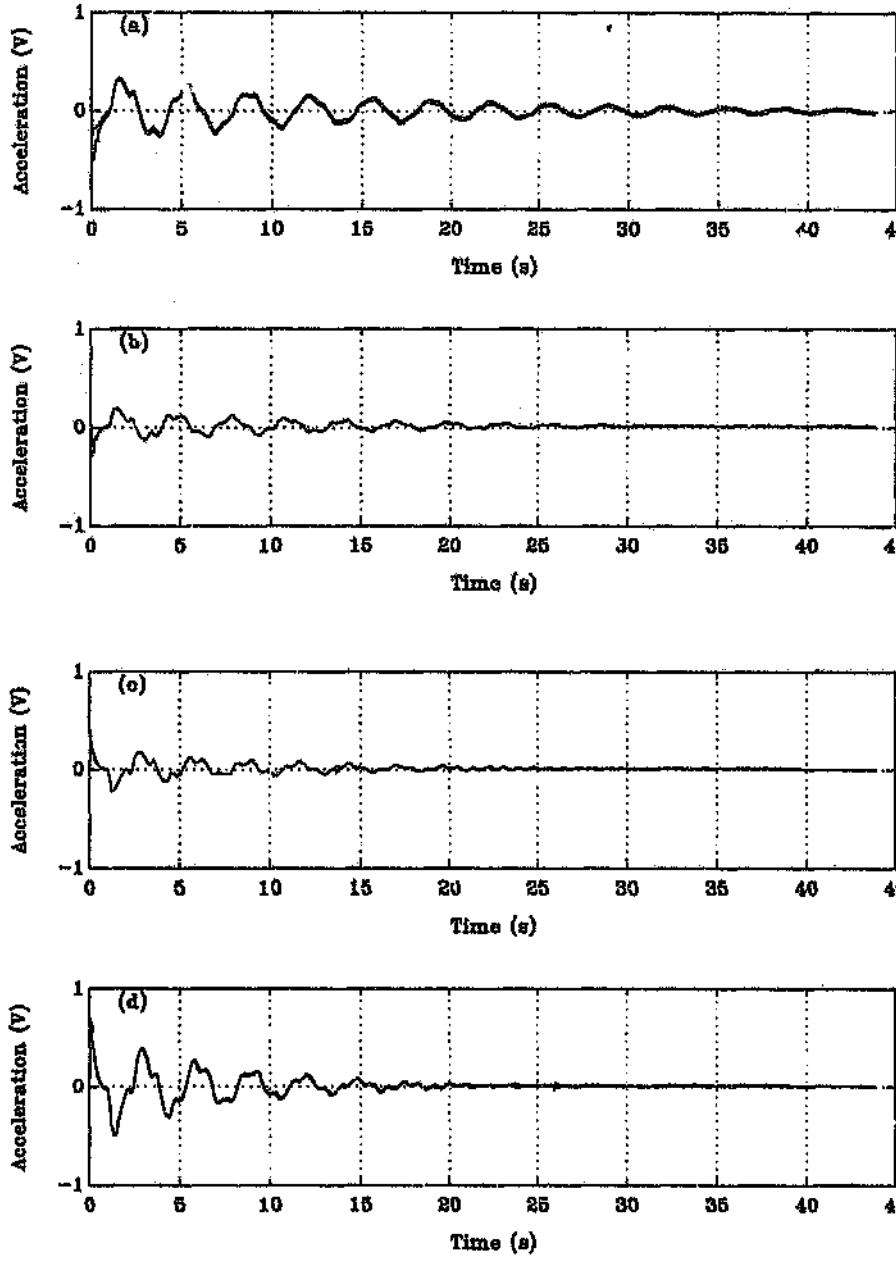

Figure G.2: Drop test free response: AAC accelerometer record

(a) 7 ton Drop (b) 3 ton Drop
(c) 3 ton Lift (d) 7 ton Lift

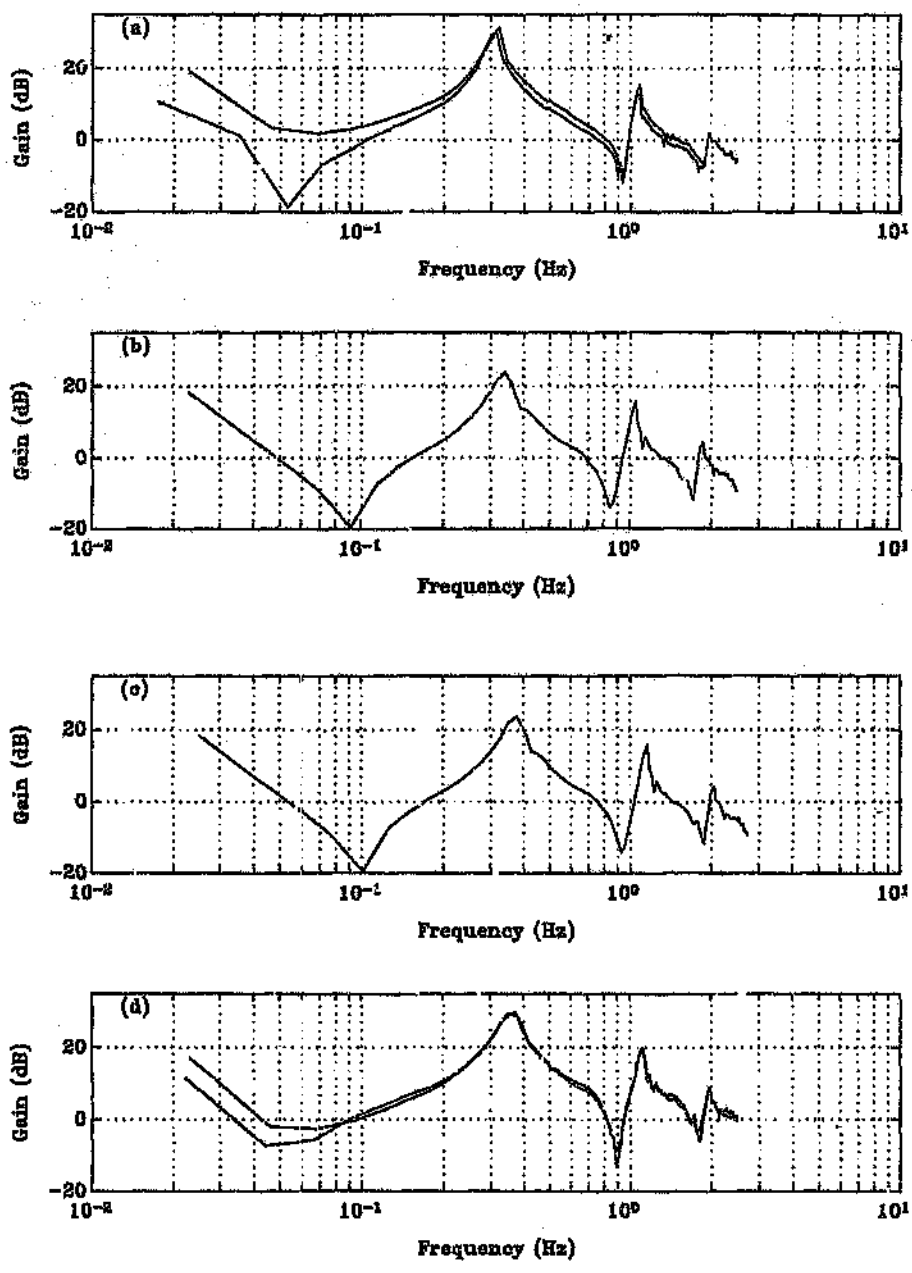

Figure G.3: Frequency response functions: AAC accelerometer record

(a) 7 ton Drop (b) 3 ton Drop
(c) 3 ton Lift (d) 7 ton Lift

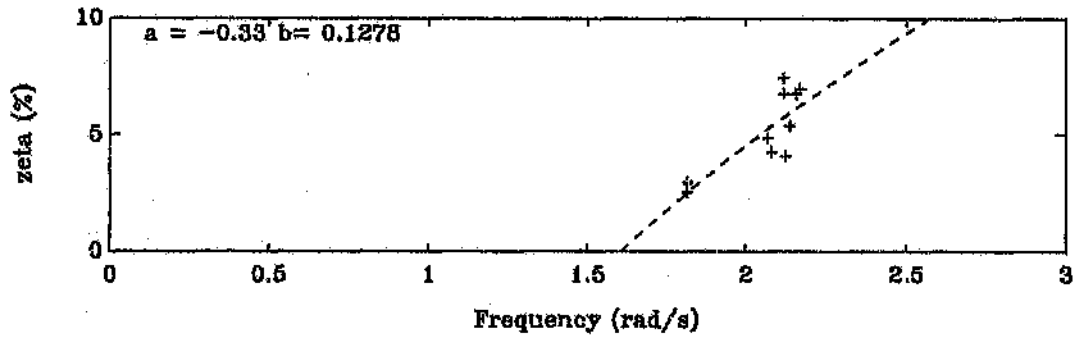

Figure G.4: Curve fitted data: Based on first modal damping estimates.

$$\zeta_1 = \frac{1}{2}\left(\frac{a}{\omega_1} + b\omega_1\right)$$

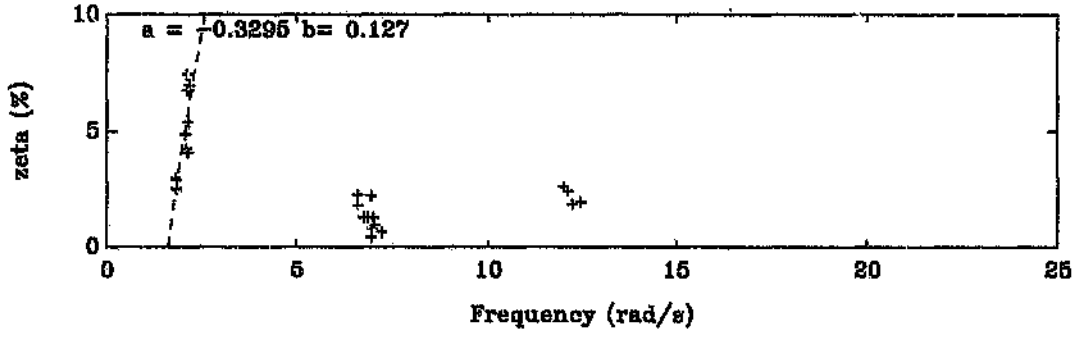

Figure G.5: Damping data and curve fit for the first longitudinal mode.

$$\zeta_1 = \frac{1}{2}\left(\frac{a}{\omega_1} + b\omega_1\right)$$

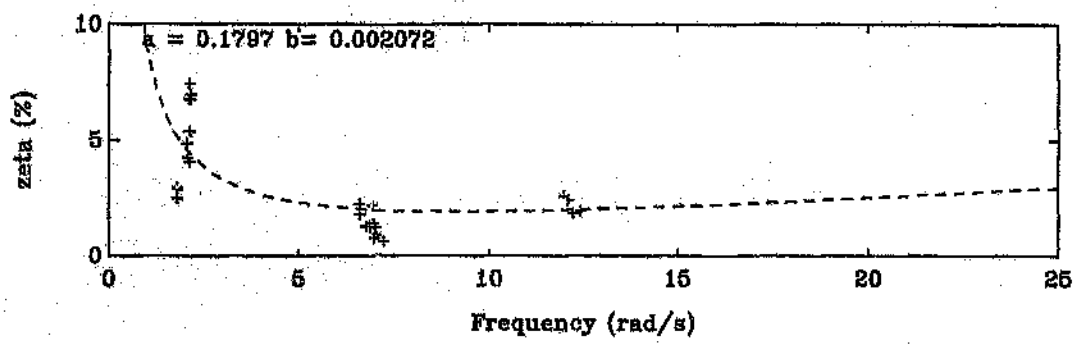

Figure G.6: Greenway (1993): Global longitudinal damping estimate

$$\zeta_n = \frac{1}{2}\left(\frac{a}{\omega_n} + b\omega_n\right)$$

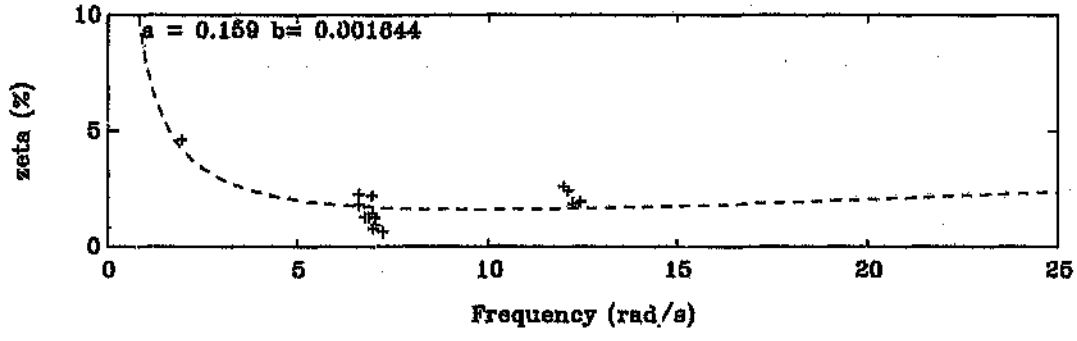

Figure G.7: Global longitudinal damping estimate based on *linear* ζ_1

$$\zeta_n = \frac{1}{2}\left(\frac{a}{\omega_n} + b\omega_n\right)$$

Appendix H

Lateral Damping of the Catenary

Information concerning the lateral damping coefficients applicable to mine hoist ropes is sparse. Vanderveldt et al [1973] examined the lateral damping coefficients obtained from a number of $\frac{3}{8}$-in diameter 65-inch long wire cables of different construction and material. The study concluded that:

- The dimensionless damping coefficient decreases with increasing axial load, and in the case of the cables tested, this coefficient varied between 0.05-0.15 % of critical.
- The major component of the damping mechanism is due to coulomb friction.
- The structural strength, heat treatment or alloy used is unrelated to the damping mechanism.
- The rope construction and geometry significantly influence the damping effort, however this is not strongly dependent on the number of wires, but rather as speculated, a feature of wire/strand interaction and hence construction geometry.

Although these results define broad dissipation characteristics of wire cable, mine hoist ropes are of larger diameter, experience higher tensions, and longer amplitude wavelengths than those tested by Vanderveldt et al. Mankowski [1988] experimentally simulated the energy loss of a typical mine hoist cable undergoing non-planar whirling motion. The experimental apparatus measured the power loss in a cable which was spun about its geometric axis, whilst

being deflected to induce curvature along its length. This was achieved by supporting a length of cable in thrust bearings, inclined so as to simulate cable sag. The rotation of the cable about its geometric centre effectively simulated the flexural effects of an irrotational cable undergoing non-planar whirl, and hence the power loss per cycle was directly related to the time rate of change of rope curvature[1]. Mankowski obtained an empirical relationship between power dissipation, rotational frequency, amplitude and catenary span empirically as:

$$P(n)_{Loss} = (2n)SSRF_nC_1(1 + C_2A_n) \qquad Watts$$

Where P_n is the internal power loss for the n^{th} mode, A_n is the amplitude of vibration of the n^{th} mode, F_n is the frequency of vibration (Hz), SSR is the sag to span ratio defined as $\frac{2nA_n}{span}$. Mankowski determined the coefficients C_1, C_2 for a cable which was of a similar construction and size to that employed at Kloof as $C_1 = 42.75J$ and $C_2 = 0.34m^{-1}$. The units of these coefficients were related to the damping capacity and curvature characteristic of the rope.

The energy losses achieved were small, as reflected in table H.1, where the calculated energy loss associated with the modal amplitudes observed at Kloof Mine are tabulated. Mankowski[1990] extended this work to investigate the effect of the power dissipation associated with a transverse kinetic shock travelling up the rope. Although the research provides valuable results, the experimental method is limited, since although various sag to span ratio's were achieved in the testing rig, the mean axial tension applied was significantly lower than that found in practice (the mean axial tension was varied between 1-30KN, whereas in practice the axial tension in the catenary varies between 120-300 KN). As it has been established that the dissipation mechanism is likely to be dominated by friction, the dissipation measured is likely to be dependent on the mean tension, which cannot be simulated correctly by the experimental apparatus. Furthermore, as is shown subsequently, it appears that aerodynamic drag may be as significant in practice as the damping mechanism associated with the time rate of change of curvature. Although Mankowski defines an empirical formula for the particular rope tested, relating power loss to the steady state amplitude and frequency of motion, this particular format would be difficult to apply in a non-stationary simulation of the system. However, the latter analysis of the power dissipation relating to transverse kinetic shocks may be valuable if a wave mechanics approach is adopted in the simulation.

[1]The time rate of chang of curvature is defined as $y_{xx,t}$, where y represents the amplitude of the lateral motion. This implies a damping mechanism which is proportional to the stiffness properties of the rope.

H.1 Aerodynamic Damping

Since the lateral damping mechanism in the rope is not well defined, and Mankowski's[1988] tests indicate that the energy dissipation related to the time rate of change of the rope curvature is low, it is likely that during rope whip, aerodynamic drag may be significant, and warrants consideration. The results of Mankowski's tests, which were conducted on a similar rope to that employed on the Kloof mine are tabulated in table H.1, together with an equivalent viscous modal damping coefficient[2].

The following relations were applied to convert Mankowski's results into an equivalent viscous and dimensionless damping coefficient:

$$P = \frac{1}{2}\omega_n^2 C_{eq} X_n^2$$

$$\zeta = \frac{C_{eq}}{2m\omega_n}$$

$$m = 0.5\rho_R l_c$$

where:

P represents the average power dissipation,X_n represents the modal amplitude, m represents the effective modal mass of the catenary, ρ_R represents the linear mass density of the rope, l_c represents the catenary length.

H.1.1 Aerodynamic Drag

Aerodynamic drag is proportional to the square of the rope velocity. Since the transport cable velocity is significant compared to the lateral velocity of the rope, the drag characteristic of the rope in the lateral direction is likely to be difficult to assess accurately. An upper bound to the modal drag force is estimated by neglecting the axial transport velocity of the rope, and treating the rope as a cylinder in steady state cross flow. Treating the rope as a cylinder,

[2]The purpose of presenting Mankowski's data in this form, is primarily to provide a comparative basis with respect to the equivalent aerodynamic dissipation, tabulated in table H.2.

with a drag coefficient of 1, the drag force per unit length of rope is calculated as:

$$F_d = \frac{1}{2}\rho d|V|^2 sign(V)$$

where V represents the absolute lateral velocity of the rope, $\rho \approx 1kg/m^3$ represents the air density, and d represents the rope diameter. The modelling of this drag force in modal space would be complex, as it would require the calculation of the absolute velocity, as well as a projection of the drag force onto the in and out of plane axes. For this reason, the following calculations are performed for motion in a single plane.

H.1.2 Planar Motion

In modal space the planar velocity of the rope is expressed as:

$$V(s)^2 = [\sum_{i=1}^{n}\sum_{j=1}^{n}\Phi_i(s)\Phi_j(s)\dot{q}_i\dot{q}_j]$$

$$\Phi_i(s) = sin(\frac{i\pi}{l_c}s)$$

Considering only direct coupling between the lateral catenary modes and the drag force, ie $i = j$, the drag force for the i^{th} mode is:

$$F_d^i(s) = \frac{1}{2}\rho d sin^2(i\pi s/l_c)\dot{q}_i^2 sign(\dot{q}_i)$$

where d represents the cross-sectional diameter of the rope.

The modal damping force is obtained by orthogonalising the drag force in modal space:

$$Q_d^i = i\int_0^{\frac{l_c}{i}} |F_d^i(s)|\Phi_i(s)ds$$

$$Q_d^i = \frac{1}{2}\frac{\rho d i}{m}\int_0^{\frac{l_c}{i}}[sin^3(\frac{i\pi s}{l_c})ds]\dot{q}_i^2 sign(\dot{q}_i)$$

$$Q_d^i = \frac{4\rho d}{3\pi\rho_R}\dot{q}_i^2 sign(\dot{q}_i)$$

The equivalent viscous damping coefficient and average power loss during a cycle are calculated as[3]:

$$C_{eq}^{Aero} = \frac{16\rho d l_c \omega_n X_n}{9\pi^2} \tag{H.1}$$

$$p^{Aero} = \frac{1}{2}\omega_n^2 C_{eq}^{Aero} X_n^2$$

$$\zeta^{Aero} = \frac{C_{eq}^{Aero}}{2m\omega_n} = \frac{16\rho d X_n}{9\pi^2\rho_R} \tag{H.2}$$

H.1.3 Non-Planar Motion

When the motion is non-planar, the absolute velocity vector of the rope is composed of motions in both planes. In this case the drag force is:

$$F_d = \frac{1}{2}\rho d|V|^2 sign(V)$$

where:

$$V(s)^2 = [\sum_{i=1}^{n}\sum_{j=1}^{n}\Phi_i(s)\Phi_j(s)(\dot{q}_i\dot{q}_j + \dot{r}_i\dot{r}_j)]$$

[3]For velocity squared damping, where the damping force is defined as $F_d = c_2\dot{X}^2 sign(\dot{X})$, it can be shown [1978] that the equivalent viscous damping coefficient is defined as $C_{eq} = \frac{8}{3\pi}\omega_n C_2 X$, where X is the amplitude at frequency ω_n

The drag force in the v, w plane would be obtained as:

$$F_d^v = F_d cos(\phi)$$

$$F_d^v = F_d sin(\phi)$$

$$\phi = tan^{-1}(\frac{V_w}{V_v})$$

If one considers single mode behaviour in both planes simultaneously ie $i = j$, the modal force in each plane would simplify to:

$$Q_d^i = \frac{4\rho d}{3\pi\rho_R}(\dot{q}_i^2 + \dot{r}_i^2)cos(\phi)$$

$$R_d^i = \frac{4\rho d}{3\pi\rho_R}(\dot{q}_i^2 + \dot{r}_i^2)sin(\phi)$$

$$\phi = tan^{-1}(\frac{\dot{r}_i}{\dot{q}_i})$$

where Q_d^i, R_d^i represent the modal components of the aerodynamic drag force in the v, w directions respectively.

If the the motion is circular ie $\dot{q} = \dot{r}$, then the relationships presented for the equivalent viscous and non-dimensional damping coefficients in the previous section would increase by $\sqrt{2}$.

H.2 Equivalent Aerodynamic Power Losses

Table H.2 represents the average aerodynamic power loss, for planar single mode motion ($C_d = 1$). The equivalent viscous and dimensionless damping coefficients are calculated via relations H.1,H.2 with the same parameters as used by Mankowski. For non-planar circular whirl, these values should be increased by $\sqrt{2}$.

It is likely that the drag coefficient is lower than 1 due to the axial transport velocity, and hence this calculation represents an upper bound to the aerodynamic dissipation. Nevertheless, even if a drag coefficient of 0.1 is assumed, dissipation through aerodynamic drag may be as significant as the mechanism proposed by Mankowski, especially in the fundamental mode.

Table H.1: Damping coefficients - Mankowski[1988] -Kloof Mine

Mode N0.	Frequency Hz	Amplitude m	Power Loss Watts	Equivalent Viscous Damping C_{eq} (N s m)	Equivalent Modal Damping ζ %
1	1.12	1	7.6	0.306	0.007
2	2.24	0.575	46.27	1.413	0.016
3	3.36	0.5	92.3	1.65	0.012
4	4.48	0.375	171.8	3.08	0.017

Table H.2: Damping coefficients - Aerodynamic -Kloof Mine

Mode No.	Frequency Hz	Amplitude m	Power Loss Watts	Equivalent Viscous Damping C_{eq} (N s m)	Equivalent Modal Damping ζ %
1	1.12	1	112.9	4.56	
2	2.24	0.575	171.8	5.25	0.06
3	3.36	0.5	381.3	6.84	0.05
4	4.48	0.375	381.3	6.84	0.04

H.3 Damping Model Applied in the Simulation

It is clear that in reality the damping mechanism is complex and falls beyond the realms of this study. It is commonly found in dynamic analyses that the most tenuous step an analyst can make is the assumption of one damping mechanism over another. An inappropriate damping mechanism may change the character of the response, as well as the amplitudes and consequently the correlation between simulation and reality dramatically. This issue is further complicated in this study, since the system is non-linear, and it is proposed that the mechanism leading to whip is related to the parametric stability of the system, which is known to be sensitive to damping effort. In fact, although viscous damping stabilises regions of simple parametric resonance, it can be shown to have the reverse effect on regions of combination parametric resonance (Nayfeh and Mook [1983]).

A numerical parametric study of damping would require substantial computational effort,which would be negated in the absence of an experimental research effort. For this reason, a relative proportional viscous damping mechanism is applied, where the aspect of the aerodynamic drag is left for future consideration.

Appendix I

Video Measurement System

Catenary vib ation on mine hoist · opes has received attention in the past through computer simulation and analytical modelling. However, due to instrumentation difficulties associated with the rope transport speed, measurements quantifying vibration levels or frequency content have not been performed. This appendix describes the video measurement system which was developed to measure the vibration of mine rope catenaries in situ.

I.1 Video System

Motion analysis methods have been introduced in recent years, through the development of frame grabber cards and high resolution CCD cameras (750×750 lines). The principle of operation is simple; the motion of the object is recorded via the video camera and recorder onto video tape. The recorded image is replayed through the frame grabber card, frame by frame, where the ' age is digitised and the object is tracked via a numerical algorithm. The resolution of the system is determined by the resolution of the recorder and frame grabber card. The frequency bandwidth of the system is dependent on the framing speed of the video equipment used. Standard video equipment is capable of a framing speed of 25 frames per second, or a bandwidth of 12.5 Hz. It is possible to double the framing speed at the cost of a lower frame resolution, by utilising a time lapse format video recorder, which formats the even and odd fields sequentially. Thus the bandwidth is increased to 25 Hz, at the expense of the effective image resolution (approximately 300×300 lines). This approach was applied, as a bandwidth of 25Hz was considered : dequate. Apart from its passive nature, this form of instrument has significant advantages over many other

methods when low frequency measurements with minimal drift are required. It is at a disadvantage when one considers its relatively small bandwidth and the possibility of aliasing the motion, which cannot be overcome. Thus it is crucial that the response bandwidth lies within the system bandwidth of 25Hz. Since catenary vibrations on mine hoist ropes lie well within this bandwidth, the video measurement system is ideally suited to this task.

I.2 Rope Tracking

This application requires the tracking of a travelling rope in a plane normal to its axial direction. Zoom lenses are utilised to magnify the image to obtain the maximum resolution. The rope is viewed against the sky, and by adjusting the contrast the rope appears as a black bar on a white background. Since it is possible to electronically superimpose two images from different cameras, it is possible to track the 2D motion of the rope in a plane normal to its axis. The set-up configuration, and resulting video image after mixing the two signals is illustrated in figure I.1,I.2. The tracking programme locates the vertical and horizontal edge of the combined image, as illustrated in figure I.2. The pixel co-ordinates are stored on disk, and provide a direct measurement of the rope motion.

I.3 Hardware Configuration

The hardware configuration of the the system developed is listed below. The measurement and recording equipment required on site consists of two CCD cameras, a camera synchronisation circuit, a signal mixer, a time lapse recorder and a video monitor. The site test work revealed that the set up time and measurement process was short and required no interference to normal mining operations. The analysis phase required the time base corrector unit, which is necessary to enhance the quality of the video synchronisation signal from the video recorder, to the quality required by the frame grabber card. This unit also compensates for signal drop out, thus providing a high quality freeze capability. Once the vertical and horizontal edges of the rope had been located via the frame grabber and software, the video recorder was automatically advanced one frame. This measurement was then stored in a data file and the process was repeated. Typically 20 000 frames were processed for a complete winding cycle.

(i) Two Pulnix TM-765 CCD high resolution black and white video cameras.

(ii) 70-300mm Zoom lenses.

(iii) Two channel video camera synchroniser.

(iv) Two Channel Video mixer.

(v) National Panasonic Time lapse Recorder AG-6720

(vi) National Panasonic Time Base Corrector

(vii) Data Translation DT2853 Frame grabber card.

(viii) IBM compatible PC 386

I.4 Dual Camera Measurement

It was originally envisaged that the system would measure the two dimensional motion of the rope, by focussing each camera at a point on the rope, and surveying the geometrical location of the cameras and their angle of inclination from the horizontal plane. During an on site commissioning test, it became apparent that although accurate measurements may be possible in a laboratory environment, the achievement of accurate geometrical positioning on site is unlikely. This is mainly due to the fact that in order to focus both cameras at the same point on the rope, the rope would have to be marked, wound out and held stationary whilst the cameras were focussed. Consequently the winding process would be interrupted, leading to a loss in production. It was also clear that triangulation of the geometrical location of the cameras and rope would require accurate surveying. In addition to this, it was also necessary to monitor a series of winding cycles, so that optimum zoom adjustment of the cameras was achieved to maintain the largest image within the field of view, maximising the sensitivity of the system. Since the zoom on each camera could be adjusted independently, a further variable would be introduced. Nevertheless, with these reservations in mind, it was found in fact that with little effort, the approximate two dimensional motion of the rope could be successfully obtained.

The two camera system was also applied to track the catenary motion and the lateral motion of the vertical rope at the shaft collar simultaneously. This measurement provided evidence of the autoparametric excitation of the vertical rope by the catenary.